UNIVERSITAT POLITÈCNICA DE VALÈNCIA

Doctorado en Automática, Robótica e Informática Industrial

PhD Dissertation

New contributions towards meal and exercise announcement-free artificial pancreas systems

Author: Iván Sala Mira

Supervisors: Prof. Jorge Bondia Company
Dr. José Luis Díez Ruano

Instituto de Automática e Informática Industrial

January 2023

This work was partially supported by: grant DPI2016-78831-C2-1-R funded by MCIN/AEI/10.13039/501100011033 and by "ERDF A way of making Europe"; grant PID2019-107722RB-C21 funded by MCIN/AEI/10.13039/501100011033; and grant ACIF/2017/021 funded by the Generalitat Valenciana through European Social Funds (FSE). Also, the grant BEFPI/2019/077, funded by the Generalitat Valenciana through FSE funds, supported a 7-month research stay at Physiological Controls Research Center of the Óbuda University (*Óbudai Egyetem*, Óbuda, Budapest, Hungary)

A todas las personas que me han ayudado, apoyado y aguantado. Muchas gracias.

To all the people who have helped, supported, and put up with me. Thank you very much.

Mindazoknak, akik segítettek, támogatottak és eltűrtek engem. Nagyon szépen köszönjük.

Iván Sala Mira

Abstract

English

Exogenous insulin infusions are vital for people with type 1 diabetes to partially make up for the inability of the pancreas to secrete insulin. However, current intensive therapies may restrict patients' quality of life. People with this disease have to constantly make decisions about insulin doses to bring glucose levels to a safe range. If unsuccessful, they may suffer from chronic and acute complications related to abnormally high and low glucose values. The automatic regulation of glucose with artificial pancreas systems promised to reduce patients' self-control burdens while improving time in normoglycemia and decreasing variability. However, these promises are fulfilled only partially. Although this technology outperforms the glycemic outcomes achieved by conventional therapies, meal intake and physical activity limit its daytime performance. Indeed, commercially available systems only can handle them with the support of the patients. For meals, patients must announce the carbohydrate content to the system. For exercise, they must notify the activity or take preventive actions like changing glucose setpoint or decreasing basal well ahead before exercise. These demands do not help reduce the patient's burden. They even can compromise the system performance when the patient misestimates the carbohydrate content, omits the meal announcement, or cannot plan the exercise event.

Hence, this thesis proposes new methods to eliminate the need for meal and exercise announcements, thus reducing patient intervention in artificial pancreas systems for a better quality of life. From a control perspective, meals and exercise

can be regarded as disturbances; therefore, this thesis exploits methods from the disturbance rejection and fault accommodation literature to achieve the thesis goal. Specifically, the following three applications must be highlighted: 1) a super-twisting-based residual generator has been developed to detect unannounced meals as the first step to their compensations; 2) a sliding-mode disturbance observer has been designed to estimate the glucose meal appearance, which is fed into a bolusing algorithm to compensate the meals; 3) the internal model principle is employed to mitigate the effects of meal intakes and exercise, supplementing insulin infusions with carbohydrate recommendations.

As a result, the contributions of this thesis pave the way for the development of announcement-free artificial pancreas systems, releasing patients from the burden of diabetes management.

Castellano

Las infusiones exógenas de insulina son vitales para las personas con diabetes tipo 1 para suplir parcialmente la incapacidad del páncreas de secretar insulina. Sin embargo, las terapias intensivas actuales pueden restringir la calidad de vida de los pacientes. Los pacientes con esta enfermedad tienen que tomar decisiones constantemente sobre las dosis de insulina que lleva a la glucosa a niveles seguros. Si no lo consiguen, pueden sufrir las complicaciones crónicas y agudas derivadas de los niveles anormalmente altos o bajos de glucosa. La regulación automática de glucosa con sistemas de páncreas artificial prometía reducir la carga del autocontrol de la enfermedad al mismo tiempo que se mejoraba el tiempo en normoglucemia y se reducía la variabilidad. Sin embargo, estas promesas sólo se han cumplido parcialmente. Aunque esta tecnología mejora el control glucémico que logran las terapias tradicionales, la ingesta de alimentos y la práctica de ejercicio limitan la eficiencia de los sistemas de páncreas artificial durante el día. De hecho, los sistemas comerciales sólo pueden hacerles frente con la ayuda de los pacientes. Para compensar las ingestas, los pacientes deben anunciar el contenido de carbohidratos al sistema. Para el ejercicio, deben anunciar el inicio de la actividad o tomar medidas preventivas como modificar la referencia de glucosa o reducir la basal con mucha antelación. Estas exigencias no sólo no ayudan a reducir la carga del paciente, sino que pueden comprometer la eficiencia del sistema cuando el paciente se equivoca al estimar los carbohidratos, omite el anuncio de la comida o no puede planificar el ejercicio.

Así pues, esta tesis propone nuevos métodos para eliminar el anuncio de ingestas y ejercicio lo que ayudaría a reducir la intervención del paciente en los sistemas

de páncreas artificial, y, en consecuencia, mejorar la calidad de vida. Desde un punto de vista de control, las ingestas y el ejercicio pueden considerarse perturbaciones. Esta tesis explota métodos de la literatura de rechazo de perturbaciones y acomodación de fallos para lograr el objetivo de la tesis. En concreto, hay que destacar tres aplicaciones: 1) se ha desarrollado un observador super-twisting para detectar comidas no anunciadas como primer paso para su compensación; 2) se ha diseñado un observador de modos deslizantes de primer orden para la estimación de la ratio de aparición de glucosa, la cual ha sido integrada en un generador de bolos para compensar las comidas; 3) se ha empleado el principio de diseño por modelo interno para mitigar el efecto de las ingestas de alimentos y ejercicio, añadiendo sugerencias de carbohidratos de rescate a la insulina.

Como resultado, las contribuciones de esta tesis allanan el camino para el desarrollo de sistemas de páncreas artificial sin anuncios, que liberen al paciente de la carga de la gestión de la diabetes.

Valencià

Les infusions exògenes d'insulina són vitals per a les persones amb diabetis tipus 1 per a suplir parcialment l'incapacitat del pàncrees de secretar insulina. No obstant, les teràpies intensives actuals poden restringir la qualitat de vida dels pacients. Les persones amb aquesta malaltia han de prendre decisions contínuament sobre la dosi d'insulina que fa que la glucosa estiga en valors segurs. Si no ho aconsegueixen, poden sofrir les complicacions cròniques i agudes derivades dels nivells anormalment alts o baixos de glucosa. La regulació automàtica de glucosa amb sistemes de pàncrees artificials prometia reduir la càrrega d'autocontrol de la malaltia al mateix temps que es millorava el temps en normoglucèmia i es reduïa la variabilitat. No obstant, aquestes promeses s'han complit només parcialment. Encara que aquesta tecnologia millora el control de la glucosa, la ingesta d'aliments i la pràctica d'exercici limiten l'eficiència dels sistemes de pàncrees artificials durant el dia. De fet, els sistemes comercials només poden fer-les front amb la ajuda dels pacients. Per a compensar les ingestes, el pacients han d'anunciar al sistema la quantitat de carbohidrats. Per al exercici, han d'anunciar l'inici de l'activitat o prendre mesures preventives com modificar la referència de glucosa o reduir la infusió basal d'insulina. Aquestes exigències no només no ajuden a reduir la càrrega al pacient, sinó que poden comprometre l'eficiència del sistema quan el pacient confon la estimació dels carbohidrats, omet l'anunciament de la ingesta o no pot planificar l'exercici.

Així doncs, aquesta tesi proposa nous mètodes per a eliminar l'anunciament d'ingestes i exercici permetent reduir així la intervenció del pacient, i, en conseqüència, millorar la qualitat de vida. Des del punt de vista de control, les ingestes i el exercici poden considerar-se pertorbacions. Aquesta tesi explota mètodes de la literatura de rebuig de pertorbacions i acomodament de fallades. En particular, es destaquen tres aplicacions: 1) s'ha desenvolupat un observador super-twisting per a detectar ingestes no anunciades com a primer pas per a la seua compensació; 2) se ha dissenyat un observador de modes lliscants per a estimar el rati d'aparició de glucosa de la ingesta, el qual s'ha integrat en un generador de bols d'insulina per compensar les ingestes; 3) se ha empleat el principi de disseny per model intern per a mitigar l'efecte de les ingestes i exercici, incorporant recomanacions de carbohidrats a la insulina.

Com a resultat, les contribucions d'aquesta tesi obren el camí per a desenvolupar sistemes de pàncrees artificial sense anunciaments, que alliberen al pacient de la càrrega de la gestió de la diabetis.

Contents

List of Figures

List of Tables

Acronyms

AP Artificial Pancreas.

ATP Adenosine triphosphate.

CGM Continuous Glucose Monitor.

DIY Do It Yourself.

ePID external Physiological Insulin Delivery.

FDA U.S Food and Drug Administration.

FN False Negative.

FOSMO First Order Sliding Mode Observer.

FP False Positive.

GLP-1A Glucagon-like peptide-1 receptor agonist.

GPC Generalized Predictive Controller.

IFB Insulin Feedback.

IVP Identifiable Virtual Patient.

KF Kalman Filter.

LPV Linear Parameter Varying.

LQG Linear Quadratic Gaussian.

MAE Median Absolute Error.

MaxAE Maximum Absolute Error.

MPC Model Predictive Controller.

NRMSE Normalized Root Mean-Squared Error.

OHSU Oregon Health and Science University.

PD Proportional-Derivative controller.

PID Proportional-Integral-Derivative controller.

qLPV Quasi Linear Parameter Varying.

RMSE Root Mean-Squared Error.

SGLT-2I Sodium–glucose co-transporter-2 inhibitor.

SMRC Sliding Mode Reference Conditioning.

T1DM Type 1 diabetes mellitus.

TP True Positive.

VO_2max Individual maximal oxygen consumption.

Chapter 1

Introduction

1.1 Scope and motivation

The following quote from a person with Type 1 diabetes mellitus (T1DM) illustrates the motivation of this dissertation:

> If you go out for a meal with friends that can be a big drama. It just requires guesstimates, em, buffets are clearly a nightmare: that's just, yeah. It's just pick a number [laughing], kinda correct later. (Participant of APCam11 trial, Lawton et al. 2019)

"Drama," "Nightmare," ... few people would use these words when describing their feelings towards going out for lunch or dinner. Unfortunately, the more than eight million people living with T1DM worldwide have reasons to feel like that (International Diabetes Federation 2021; Gregory et al. 2022): insulin replacement is essential to avoid the life-threatening complications of the disease, but current treatments demand a constant intervention and decision-making from the patient side, which affects their psychosocial health. This dissertation proposes control structures to alleviate the burdens related to the self-management of meals and exercise in the Artificial Pancreas (AP) context, aiming at automating insulin

delivery without patient intervention. Before detailing the dissertation's objectives, the context of T1DM and AP is presented in this section.

Cells need energy, in the form of Adenosine triphosphate (ATP), to sustain their metabolic processes. Human cells can obtain ATP by breaking down glucose, free fatty acids, and, to a lesser extent, amino acids from carbohydrates, fats, and proteins in meals, respectively. However, brain cells primarily rely on glucose as fuel, though ketones, a product of fatty acid oxidation, can be used as an alternative energy source after a long starvation period. Hence, the need to homeostatically regulate plasma glucose levels. In normal conditions, blood glucose levels remain between 70 mg/dL and 170 mg/dL, with a daily average of 100 mg/dL (Alsahli et al. 2017; Aronoff et al. 2004). This narrow range in plasma glucose is maintained by intricate coordination of tissues and organs (brain, pancreas, liver, kidneys, gut, muscle, adipose tissue, etc.) through hormones (insulin, glucagon, amylin, incretins, somatostatin, grown hormone, cortisol, etc.) and neurotransmitters (epinephrine, norepinephrine, etc.) that balances the glucose production and utilization (Alsahli et al. 2017; Aronoff et al. 2004).

Insulin and glucagon are the most important factors for plasma glucose regulation on a moment-to-moment basis. After meal ingestion (i.e., the postprandial period), the pancreatic β cells respond to the rise of glucose by secreting insulin. This hormone signals cells to use or store glucose, consequently reducing blood glucose levels. Specifically, insulin triggers the following actions: 1) increases glucose uptake in insulin-dependent tissues such as skeletal muscle and adipose tissue through the translocation (movement) of glucose transporters; 2) suppresses endogenous glucose production from the liver and kidneys, directly (activating or deactivating enzymes) and indirectly (inhibiting glucagon production or reducing fatty acids circulating levels); 3) promotes glucose storage in the form of glycogen; and 4) fosters glucose utilization as the preferred source of energy rather than fatty acids (Alsahli et al. 2017; Aronoff et al. 2004).

When plasma glucose level descends (i.e., post-absorptive period, exercise, etc.), insulin levels reduce while glucagon concentration increases. Glucagon is secreted by the pancreatic α cell. It acts on the liver, promoting the endogenous production of glucose from glycogen (glycogenolysis) and noncarbohydrate components such as pyruvate, glycerol, or lactate (gluconeogenesis) (Szablewski 2017).

The complex mechanism tightly regulating the plasma glucose in people without diabetes fails in T1DM due to the autoimmune destruction of the pancreatic insulin-producing β-cells triggered by a not well-known interplay of genetic, immunological, environmental, and gut microbiome determinants (DiMeglio et al. 2018; Gómez-Díaz 2019). The deficient secretion of this hormone in T1DM imbalances the tight

equilibrium between glucose production, uptake, and intestinal absorption, leading to an abnormal glucose increase known as hyperglycemia.

Persistent hyperglycemia can damage small blood vessels, eventually altering the function of the eyes, kidneys, and nervous system (DiMeglio et al. 2018; Díaz-Flores et al. 2019). Progression of these alterations can lead to other complications, such as ulcers and infections, increasing the risk of foot or limb amputation (Harkless et al. 2019). Hyperglycemia can also promote blood clots that block big vessels toward the heart or brain, raising acute complications like cardiomyopathy, myocardial infarction, or stroke (DiMeglio et al. 2018). These complications reduce the life expectancy of individuals with T1DM compared to people without it (Lieber et al. 2015; Livingstone et al. 2015). Furthermore, untreated hyperglycemia is related to an accumulation of ketones in the bloodstream (diabetes ketoacidosis) due to metabolizing fatty acids as a source of energy alternative to glucose. This condition can cause nausea, abdominal pain, weakness, and, in severe cases, lead to loss of consciousness, seizure, coma, or death (Orban et al. 2018).

Although promising treatments are under research (e.g., encapsulated β-cell transplantation, cell therapy, glucose-responsive insulins, etc; Domingo-Lopez et al. 2022; Seetharaman et al. 2022), exogenous insulin replacement is still paramount to circumvent hyperglycemia-related complications in people with T1DM. The most extended insulin replacement treatments (e.g., multiple daily injections, continuous insulin infusion, sensor-augmented pumps) infuse or inject insulin through the subcutaneous tissue since this route is more accessible for domiciliary use than other more physiological ones such as intraperitoneal or intravenous (Renard 2008). The subcutaneous route also allows more insulin bioavailability than non-invasive routes such as oral, intranasal, transdermal, or ocular (El Maalouf et al. 2022).

These subcutaneous insulin intensive regimes intend to mimic the pancreatic insulin secretion to lower the blood glucose, following a basal-bolus pattern. On the one hand, basal insulin covers the daily insulin demands for liver, adipose tissue, and muscle during starvation (Faradji et al. 2019a). To imitate this pattern subcutaneously, one or two shots of ultra-long or long-acting insulin are delivered in the multiple daily injection therapy, or a continuous delivery of rapid or fast insulin is infused for pump-based treatments. On the other hand, the bolus insulin reduces the postprandial (after meals) glucose increase by promoting glucose uptake and inhibiting endogenous production (Faradji et al. 2019a). The insulin boluses are delivered as peaks of rapid-acting insulin at mealtime, ideally 15-20 min earlier (Weinzimer et al. 2008). To calculate the insulin boluses, patients must estimate the carbohydrate meal content (Reiterer et al. 2019), which is a challenging and burdensome task.

Numerous studies have shown that intensive insulin therapies decrease the glycated hemoglobin (a measure of the average blood glucose in the last three months), which retards the progression of microvascular complications, reduces their appearance, and decreases the mortality risk (DCCT 1993; Virk et al. 2016; Orchard et al. 2015). However, intensive insulin therapies are also related to hypoglycemia (DCCT 1993), a condition of abnormally low plasma glucose level with a short-term impact, such as palpitations, trembling, anxiety, hunger, or concentration difficulties, and, if untreated, with potentially dangerous consequences like a seizure, cardiac arrest, cerebral ischemia, coma, or death (Orban et al. 2018; Faradji et al. 2019b).

Therefore, people with T1DM under intensive therapies must frequently check their glucose levels and modify the basal and bolus accordingly to steer the glucose to a safe range (a value between 70 mg/dL and 180 mg/dL is usually accepted as a coarse range; Battelino et al. 2019) or normoglycemia. Also, they need to have carbohydrate supplements handy and decide when to use them to correct glucose drops. But, despite being adherent to the therapy, external and internal factors (meals, exercise, illnesses, stress, etc.) may frustrate their attempts to be in normoglycemia. This substantial degree of self-management impacts patients' emotional health and social life. For instance, fear of hypoglycemia is behind the causes of mood changes, anxiety, or sleep disorders T1DM patients usually suffer, leading to a deliberate suboptimal treatment of the disease (Faradji et al. 2019b). In addition, this disease shapes the meal patient habits. Some patients prefer to stick to a regular meal pattern to simplify the insulin bolus calculation (Lawton et al. 2019). When these habits are perturbed (e.g., going out for lunch or dinner), the patient can feel doubtful and stressed; especially adolescent even may decide to skip the bolus to avoid revealing the disease (Bishop et al. 2009).

Fortunately, advances in technology in the last 50 years have helped patients to reduce their burden of the self-management: new calibration-free continuous glucose monitors (CGM) are predetermined to replace the annoying blood finger-pricking samples as a measure of glucose while providing a more detailed picture of the daily glucose profile; insulin pumps have made the basal selection more flexible compared to insulin shots, and sensor-augmented pumps have mitigated nocturnal hypoglycemia (and the fear of it) suspending the pump if reduced blood glucose is measured or predicted (Forlenza et al. 2020). In that technological quest for enhancing patients' life, the announcement of the U.S Food and Drug Administration (FDA) on the 28 September 2016 became a milestone: the Medtronic 670G (Medtronic, Northridge, CA, United States), the first day-and-night closed-loop system for glucose regulation, also known as AP, was approved for medical use. Since then, six APs systems have been available in the market, and more than 20 institutions worldwide have been researching on this topic (León-Vargas et al.

2022). Also, communities of people with T1DM, families, and care-providers have played an active role in the development of AP systems; they have created and promoted do-it-yourself (DIY) AP systems counting thousands of users worldwide despite being unregulated and unapproved for medical use (Jennings et al. 2020; Lum et al. 2021).

An AP system employs a control algorithm to calculate the insulin infusion delivered by the insulin pump from glucose readings provided by the CGM. Commercially available AP systems are based on Proportional-Integral-Derivative controller (PID), Model Predictive Controller (MPC), or fuzzy-logic-based controllers (Thomas et al. 2021). However, other techniques have been exploited to implement controllers in AP systems, such as sliding mode techniques, linear parameter varying systems, robust fixed point transformation approaches, or machine learning algorithms (Tašić et al. 2022).

Recent meta-analyses of randomized controlled clinical trials have shown the effectiveness of the AP systems: compared to open-loop intensive therapies, the AP systems increased the percentage time in 70-180 mg/dL (normoglycemia) by 7.91-17.85 %, reduced the percent time above 180 mg/dL (hyperglycemia) and below 70 mg/dL (hypoglycemia) by 0.67-8.89 % and 0.67-1.49 %, respectively, and decreased the glucose variability (Jiao et al. 2022; Fang et al. 2022; Pease et al. 2020; Karageorgiou et al. 2019; Bekiari et al. 2018). Observational studies of commercial AP systems in real-life experiences with follow-up periods exceeding the five months (Jacobsen et al. 2022; Pintaudi et al. 2022; Breton et al. 2021; Varimo et al. 2021; Da Silva et al. 2021) or with more than 800 individuals involved (Silva et al. 2022; Breton et al. 2021; Da Silva et al. 2021) confirm the results of the randomized controlled trials. With more time in normoglycemia and less variability, these improved glycemic outcomes foresees a reduction of the risk of acute complications with this technology (El Malahi et al. 2022; Yapanis et al. 2022). Regarding the psychosocial impact of AP systems, quantitative studies with surveys produce promising but still incongruous results: Beato-Víbora et al. (2021) show that the Minimed 780G improves the quality of life and sleep, but no statistically significant differences were demonstrated for satisfaction, distress, or fear of hypoglycemia. Conversely, Boscari et al. (2022) and Polonsky et al. (2022) reported a statistically significant improvement in fear of hypoglycemia and satisfaction, but not in the quality of life or sleep. Lastly, Jiao et al. (2022)'s meta-analysis unveils no improvement in distress, satisfaction, or quality of life. These inconsistencies may exist because the analyzed AP technologies were different or because of common disconformities in CGM and pumps (e.g., technical glitches, alarms, physical bulk, information overload, constant reminding of the disease, body image, etc.) counterpoise the benefits (Farrington 2018).

Although AP systems outperform the glycemic metrics of open-loop intensive therapies, the most noticeable differences occurred overnight. For instance, Jiao et al. (2022)'s meta-analysis reported that AP systems improved the time in normoglycemia of open-loop treatments by 16.22 % within the nocturnal period, while this difference decreased to 6.62 % within the diurnal period. Bekiari et al. (2018)'s meta-analysis, with involved more heterogeneous clinical trials than Jiao et al. (2022)'s, found that the improvement of time in range regarding open-loop treatments was five points larger overnight than within a 24-h period (15.15 % vs. 9.62 %); since the diurnal time in range contributes more to the overall time in range than the resulted from the nocturnal period, the difference regarding the diurnal period might be still more remarkable. AP systems outperform open-loop therapies just moderately during the daytime because the largest glycemic disruptors, i.e., meal intakes and exercise events, occur within this period. Indeed, like open-loop therapies, current systems mostly delegate the compensation of these disturbances to patients.

Most of the AP systems assessed in randomized controlled trials and all the commercialized ones so far are hybrid systems (Phillip et al. 2022). This means that users must estimate the carbohydrate meal content and provide it to the system to calculate a prandial bolus (Weinzimer et al. 2008). Prandial boluses advance the meal insulin coverage at mealtime; otherwise, the postprandial excursion may be intolerably elevated (Weinzimer et al. 2008; Dovc et al. 2020) due to the delayed insulin action, sensor lags, and the dysregulation of other hormones involved in the glucose homeostasis (e.g., amylin and glucagon). Albeit worthwhile, carbohydrate counting places a burden on subjects, and, if not provided timely and accurately, can degrade the AP performance (Boughton et al. 2019; De Bock et al. 2017).

Another disturbance that limits the performance of AP systems is physical activity. In T1DM patients, physical activity may lead to either hyperglycemia or hypoglycemia depending on the type (aerobic, anaerobic, or interval), duration, intensity, or circulating plasma insulin (Tagougui et al. 2019). Due to the shortcoming negative consequences of exercise-induced hypoglycemia, most patients abandon a regular exercise practice renouncing its positive effects on glycated hemoglobin control, body weight, blood lipid profile, and cardiorespiratory fitness (Riddell et al. 2017; Tagougui et al. 2019). Current hybrid AP systems require the patient to announce the activity for the system to reduce the insulin infusion or increase the glucose targets (Thabit et al. 2021; Fuchs et al. 2020). Insulin absorption delays and stacking do not guarantee an immediate reduction of circulating insulin levels. Therefore, exercise must be announced with anticipation of hours to reduce, albeit not eliminate, the risk of hypoglycemia (Tagougui et al. 2019; Zaharieva et al. 2020). This supposes another restriction on patients' life and

another discouraging factor to practicing exercise. Also, hyperglycemia may arise if the patient skips the announced exercise. Furthermore, some physical activities just cannot be planned (e.g., walking fast to reach a place on time).

Aware of the positive impact removing meals and exercise announcements would have on patients, the research group framing this dissertation targets integrating these features into the AP systems they have been developing for more than ten years. While one open research line in the group (Moscardó et al. 2019a; Moscardó et al. 2019b) is addressing this goal with a dual-hormone system (a system that includes glucagon to increase the glucose levels), this dissertation continues the works of Ramkissoon et al. (2019), Beneyto et al. (2018) that resort to a single-hormone system augmented by carbohydrate recommendations to handle unannounced exercise events. Although these works reduced the risk of exercise-hypoglycemia, the latter with success in a clinical trial (Viñals et al. 2021), they always considered announced meals. This dissertation intends to fill this gap.

1.2 Objectives

Therefore, the general goal of this dissertation is to **design new methods to reduce patient intervention by eliminating the need for meal intake and exercise event announcements** in AP systems. These methods should result in independent modules that can be integrated, with minimal modifications, into a wide range of hybrid AP systems; this would simplify its application into already designed hybrid AP systems. In addition, once integrated these modules in the AP, the overall system should perform similarly to the hybrid counterpart.

To address this general goal, three further specific objectives are pursued in this dissertation:

1. To identify the challenges of glycemic control against meals and exercise events with AP systems, especially when these events are not announced to the system.

2. To detect or estimate the effect of meal intakes and exercise events on glucose as a first step toward developing announcement-free AP systems.

3. To construct announcement-free AP systems integrating the estimation methods developed in the previous sub-objective.

1.3 Outline

This dissertation is structured as follows:

- Chapter 2 reviews the limitations of announcing meals and exercise. It also studies the strategies that have been applied in the literature to remove these announcements.
- Chapter 3 presents methods to estimate the effect of meals on glucose. Specifically, the performance of a first-order sliding mode observer and a Kalman filter will be compared with simulations. As a complement to this chapter, Chapter 4 illustrates the reconstruction of the meal disturbance with the sliding mode observer when the observer employs clinical data as input. Similarly, this chapter shows that the exercise effect on glucose can also be estimated from a clinical dataset with the observer.
- Chapter 5 designs an algorithm that detects when an unannounced meal starts affecting glucose. The algorithm, consisting of a super-twisting observer and a threshold-based decision logic, was assessed with simulation and clinical data.
- Chapter 6 develops the first strategy proposed in this thesis to deal with unannounced meals. The proposed module includes a bolusing algorithm that computes insulin bolus based on the meal estimation and detection information provided by the methods developed previously.
- Chapter 7 develops the second strategy proposed in this thesis to deal with unannounced meals, which also can deal with unannounced exercise events. The proposed module uses an internal model control approach with a switching logic to counteract the postprandial glycemic excursion with bolus-like insulin infusions or suggest carbohydrate intakes to avoid severe hypoglycemias.
- Finally, Chapter 8 closes the dissertation by discussing the results, the limitations, and future work.

Chapter 2

Announcement-free artificial pancreas systems: challenges and state of the art

Commercially available AP systems rely on patient actions (i.e., announcements) to compensate for meal intakes and exercise events. Releasing patients from the burden of meal and exercise announcements is challenging because of the limitations of the insulin administration route and glucose measurement, variability, and ineffectiveness of glucoregulatory hormones other than insulin, among others. This chapter describes the challenges of announcement-free AP to handle meal and exercise events. The chapter also presents a classification of the methods used in the literature to address these challenges.

2.1 Introduction

Up to six AP systems are commercially available (Domingo-Lopez et al. 2022; Phillip et al. 2022; Rodríguez-Sarmiento et al. 2022): the Medtronic 670G (Medtronic, Northridge, CA, USA), the Medtronic 780G (Medtronic, Northridge, CA, USA), the t:slim X2 pump with Control-IQ (Tandem, San Diego, CA, USA), the CamAPS FX (CamDiab, Cambridge, UK), the DBLG1 (Diabeloop, Grenoble, France), and the Insulet Omnipod 5 (Insulet, Billerica, MA, USA). All these systems include the three principal elements of a closed-loop system (Figure 2.1): a

sensor (the Continuous Glucose Monitor (CGM)), an actuator (the insulin pump), and a controller (a PID or an MPC, extended in some cases with fuzzy logic features). However, they are deemed "hybrid" since the patient is not only the controlled plant but must be involved in the control logic (Phillip et al. 2022). Due to the limitations of the subcutaneous route for insulin delivery and glucose measurement, manual interventions become paramount when handling disturbances with a significant impact on glucose, such as meals and physical activity.

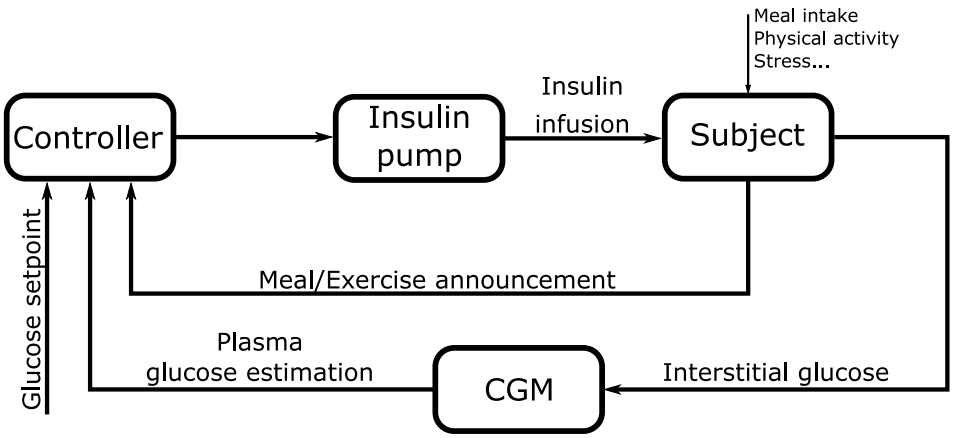

Figure 2.1: Basic hybrid artificial pancreas overview.

On the one hand, the system requires the patient to announce the carbohydrate meal content, ideally 15–20 min in advance, to calculate a prandial insulin bolus. This prandial insulin bolus effectively reduces the postprandial excursion (Weinzimer et al. 2008). However, carbohydrate counting hampers diabetes self-management, and patients would prefer simplifying it or discharging from it (Fortin et al. 2017). In addition, an accurate estimation of carbohydrates is challenging; patients tend to underestimate high-carbohydrate-content meals and overestimate low-carbohydrate-content meals (Kawamura et al. 2015; Roversi et al. 2020). Even though the meal carbohydrate content was accurately estimated, other macronutrients (e.g., fat, fiber, and proteins) or alcohol influence the glycemic postprandial response (Vetrani et al. 2022; García et al. 2021; Gingras et al. 2018a); consequently, other bolus amounts and patterns may be required (Bell et al. 2016; Keating et al. 2021). For instance, fat and proteins enlarge the postprandial duration; hence, wave-like boluses are preferable over a single prandial bolus (Bell et al. 2016). Faced with this complexity in estimating boluses, some patients stick to strict eating behaviors, and may feel unconfident or anxious when having lunch outside or eating more or less than anticipated (Lane et al.

2021). Furthermore, delays in the administration of boluses and omissions are frequent (Lane et al. 2021; Bishop et al. 2009). Indeed, patients prefer a mealtime bolus to the most recommended pre-meal bolus infused 15-20 min before the meal (Lane et al. 2021). Besides being a burdensome task, if the manual bolus is not delivered timely and accurately, the performance of the AP may decline. These systems usually tolerate carbohydrate underestimation better than open-loop therapies (Cherñavvsky et al. 2016; Grosman et al. 2016); however, overestimation and delays may cause hypoglycemia (Boughton et al. 2019; De Bock et al. 2017).

On the other hand, hybrid AP systems' users have to announce exercise start 30–90 min ahead (Thabit et al. 2021; Zaharieva et al. 2020). This way, the system can reduce the aggressiveness of the controller (e.g., increasing glucose target, reducing basal insulin, etc.) to mitigate the risk of hypoglycemia. Nevertheless, exercise announcement burdens patients since some physical activity is spontaneous, especially in children (Quirk et al. 2014). In addition, reducing controller aggressiveness may lead to hyperglycemia if the exercise is skipped.

Given the drawbacks of meal and exercise announcements mentioned above, several strategies have been developed in the literature to remove them. This chapter reviews the most relevant methods and the challenges of applying them.

2.2 Challenges of diurnal control

Before addressing the strategies for announcement-free AP systems, this section details the limitations of a system without announcement against meals and exercise events.

2.2.1 Postprandial control

Figure 2.2 illustrates the challenges and limitations of meal control. The first challenge is avoiding postprandial hyperglycemia (Gingras et al. 2018b). In a non-diabetic person, the pancreas releases insulin before glucose from meals reaches the bloodstream, stimulated by the sensory receptors in the oral cavity (Teff 2011). This early release contributes to reducing the postprandial glucose excursion since it prevents a rapid glucose increase and attenuates endogenous glucose production. A meal-announcement-free system cannot count on this anticipatory insulin release; the system needs to sense the glucose rise to start compensating for the meal intake. Therefore, the controller cannot react until, first, the plasma glucose begins to increase (on average, 10 min after the meal intake; American Diabetes Association 2001; Gingras et al. 2018b), and, second, the CGM acknowledges this

change in the interstitial fluid (a physiological lag between 5 and 10 min; Basu et al. 2015).

Besides a delayed reaction against the meal intake, insulin's slow pharmacokinetics/pharmacodynamics limit the compensation for the meal rise. The rapid-acting insulin analogs start lowering the glucose (i.e., onset action) 10–15 min after the subcutaneous administration, with an action peak at 60–120 min (Gingras et al. 2018b; Sharma et al. 2019). Thus, insulin lowers the glucose concentration at a slower rate than glucose appearing in the blood.

The subcutaneous route is also ineffective in inhibiting endogenous glucose production (Edgerton et al. 2021). In a non-diabetic person, the insulin secreted endogenously is absorbed into the hepatic portal vein; hence, the blood entering the liver contains more insulin than in the rest of the body. This liver-to-arterial insulin gradient is relevant to effectively reduce the hepatic glucose production (Edgerton et al. 2021). Since the subcutaneously-administered insulin is absorbed into the peripheral circulation, this higher concentration of insulin in the liver is no longer possible; thus, the suppression of the hepatic glucose production occurs later and with a lower magnitude than when insulin is secreted endogenously (Edgerton et al. 2021; Thomas et al. 2021). To aggravate this hyperglycemic situation, the auto-immune destruction of the β-cells also reduces the production of amylin (Infante et al. 2021). This hormone delays gastric emptying and suppresses glucagon release (Ling et al. 2019). Therefore, the postprandial glucose excursion in T1DM is more extensive and prolonged than in a non-diabetic person.

A meal-announcement-free AP system can mitigate hyperglycemia by increasing the controller's aggressiveness, for instance, delivering boluses or re-tuning the controller after detecting the meal, as seen later in Section 2.3. However, an excess of insulin can lead to late postprandial hypoglycemia; avoiding these hypoglycemia events is the second challenge of postprandial control (Figure 2.2). Insulin cannot be removed exogenously (negative control actions are not possible); thus, once the insulin reaches the bloodstream, its glucose-lowering effect may remain active up to 5 h later (Sharma et al. 2019). Besides the non-negativeness of the control action, the meal absorption has faster dynamics than the insulin action. As a result, any attempt to compensate for hyperglycemia would result in an undershoot (Goodwin et al. 2015). In addition, during the subcutaneous absorption, insulin can be stacked in depots in the subcutaneous tissue (Fathi et al. 2018). Then, it can reach the bloodstream when the meal has already been absorbed, and plasma glucose has started to decrease. An excess of this "insulin-on-board" explains many of hypoglycemic events occurring at the late postprandial (Fathi et al. 2018).

The third challenge in postprandial control is coping with the variability. The insulin absorption and action profiles vary considerably among people (Heinemann 2002). Furthermore, an individual's insulin demands can change daily, even during the day. For instance, a certain amount of carbohydrates for breakfast requires more insulin than the same amount at lunch or dinner (Hinshaw et al. 2013). In addition, the nutritional composition of meals influences the postprandial glucose excursion. For example, a meal rich in proteins or fat would lead to a more extended postprandial period than another meal with a lower content of these macronutrients even though both have the same amount of carbohydrates (García et al. 2021). Moreover, other factors such as emotional or physical stress, illness, hormonal changes, and microbiome shape the postprandial glucose excursion (Gingras et al. 2018a; Wilson et al. 2021). Thus, identical meals can result in different glucose levels between days or individuals (Rasmussen 1993; Dingena et al. 2020).

2.2.2 Post-exercise control

Regular practice of physical activity enhances cardiorespiratory fitness, muscular strength, endothelial function, and blood lipid profile. It is also related to better HbA1c levels and a lower risk for cardiovascular disease, stroke, or diabetes-related complications such as retinopathy (Riddell et al. 2017; Codella et al. 2017). However, physical activity has a complex impact on glucose; glucose may decrease or increase depending on the intensity and duration, hampering the physical activity management (Moser et al. 2020).

During exercise, contraction of skeletal muscle fibers promotes glucose uptake without the mediation of insulin (Rose et al. 2005); thus, the first endocrine response in individuals without T1DM is to reduce insulin secretion. An exercise-announcement-free AP system cannot reduce the circulating insulin levels in such a short time (Figure 2.3). The reasons are similar to the ones discussed in Section 2.2.1. On the one hand, the CGM may not sense timely a plasma glucose decrement because the change of temperature and blood flow following exercise onset, added to the plasma-to-interstitial diffusion lag, compromise its accuracy (Fabra et al. 2021). On the other hand, despite suspending the pump, insulin may remain active due to the prolonged action time of insulin (Zaharieva et al. 2019) and an accelerated insulin absorption rate from the subcutaneous depots induced by the physical activity (Zaharieva et al. 2020).

This inability to timely suppress circulating insulin levels may lead to a high concentration of insulin during physical activity that, in turn, enhances glucose uptake while diminishing the endogenous glucose production (Codella et al. 2017).

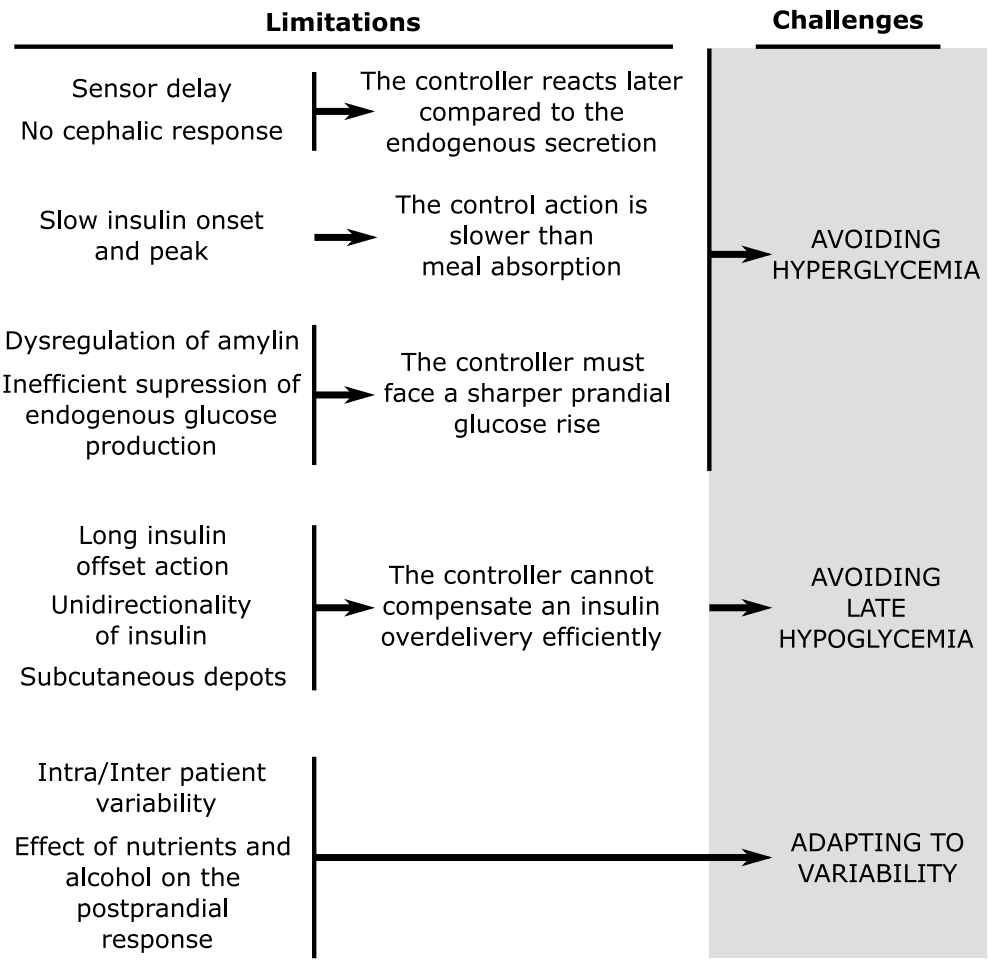

Figure 2.2: Summary of the limitations and challenges of postprandial control without meal announcement. The limitations of the insulin action (slow absorption and unidirectionality) with the dysregulation of other mechanisms involved in the homeostasis and the variability challenge the controller with recurrent hyperglycemia and hypoglycemia events.

This imbalance between glucose disposal and production results in a marked glucose drop during mild-to-moderate aerobic physical activity (Zaharieva et al. 2019; Moser et al. 2020). Avoiding the concomitant hypoglycemia is the main challenge for exercise-announcement-free AP systems. In a non-diabetic person, glucagon, a pancreatic hormone that stimulates hepatic glucose production from

glycogen, would be secreted to avoid hypoglycemia. Nevertheless, in T1DM, the progress of the disease and subsequent hypoglycemia events may blunt, and even suppress, the glucagon response to hypoglycemia (Tagougui et al. 2019). Other mechanisms to promote endogenous production, such as the secretion of epinephrine, are also attenuated (Codella et al. 2017). In addition, the risk of hypoglycemia can be extended more than 10 h after the exercise ends due to the increased insulin sensitivity and the still high glucose disposal rate to replenish glycogen stores (Tagougui et al. 2019).

Conversely, vigorous physical activity may result in a glucose rise due to the effect of catecholamines and cortisol that raises hepatic glucose production and attenuates glucose disposal (Codella et al. 2017). Similarly, an exercise involving intense and repetitive muscle contractions augments the lactate levels, promoting hepatic glucose production (Codella et al. 2017). Therefore, unless insulin increases, especially during the recovery, glucose production will excel glucose disposal, increasing the risk of hyperglycemia.

Once the principal challenges of announcement-free systems are described, the following sections review the most relevant research attempts to address them.

2.3 Strategies to remove meal announcements

A diverse set of techniques have been proposed to remove the need for carbohydrate counting. In general, they consist of *ad hoc* solutions involving multiple control paradigms (PID control, MPC, sliding mode techniques, observer-based disturbance rejection, etc.), evaluated in diverse conditions (from simulations to randomized clinical trials), and even addressing different goals (announcing a qualitative amount of carbohydrate, reporting only the time, or completely removing the announcement). Therefore, the comparison between them is challenging. To organize the exposition, this section groups the techniques into three broad, complementary strategies (Figure 2.4): 1) increasing the aggressiveness of the insulin control action once a meal or hyperglycemia is acknowledged, 2) overcoming the slow insulin absorption with new faster formulation or different administration routes, and 3) complementing insulin with other hormones or medications.

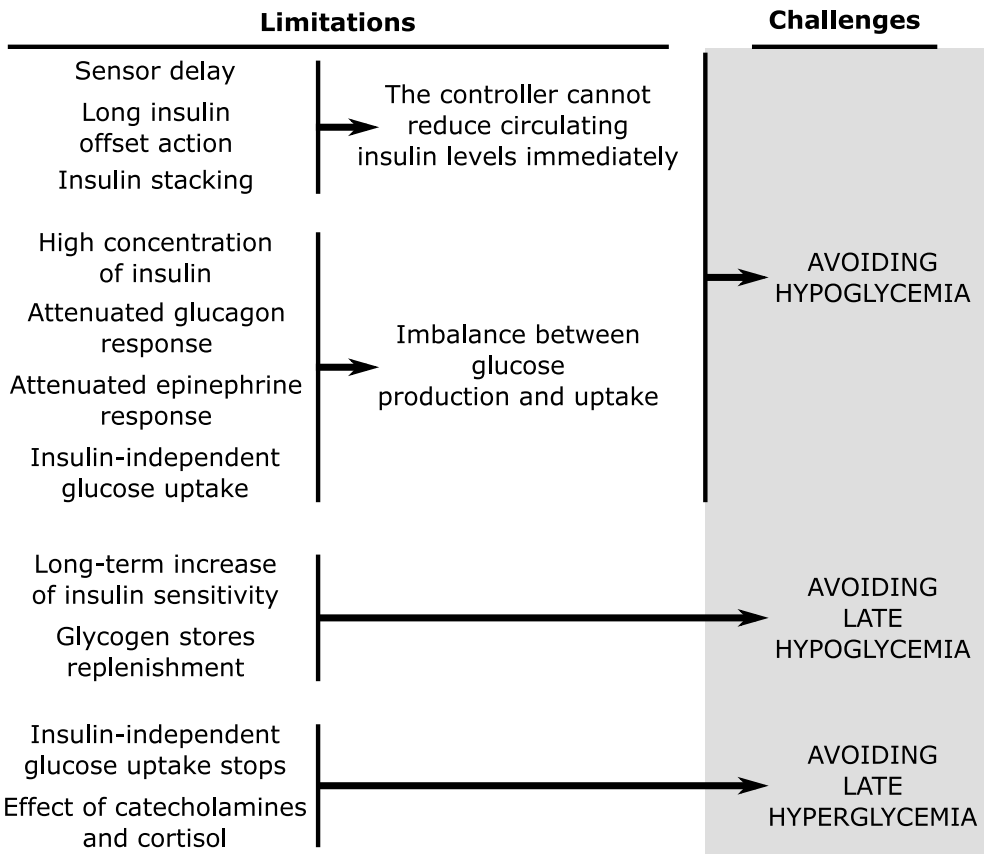

Figure 2.3: Summary of the limitations and challenges of post-exercise control without announcement. The controller cannot reduce the plasma insulin circulating levels readily. The subsequent high insulin concentration attenuates the effect of counterregulatory mechanisms, while insulin-independent mechanisms exist to uptake glucose during exercise resulting in a risk of hypoglycemia. The increased insulin sensitivity and the need to replenish the glycogen stores may lead to post-exercise hypoglycemia. In contrast, the secretion of catecholamines and cortisol induced by high-intensity exercise may lead to hyperglycemia.

2.3.1 Increasing the insulin control action aggressiveness during meals

Accurate carbohydrate-matched prandial insulin boluses are unbeatable for reducing postprandial hyperglycemia (Goodwin et al. 2015). In a broad sense, prandial boluses correspond to a high increase of insulin control action aggressiveness within a short time. Some techniques dealing with unannounced meals try to imitate this

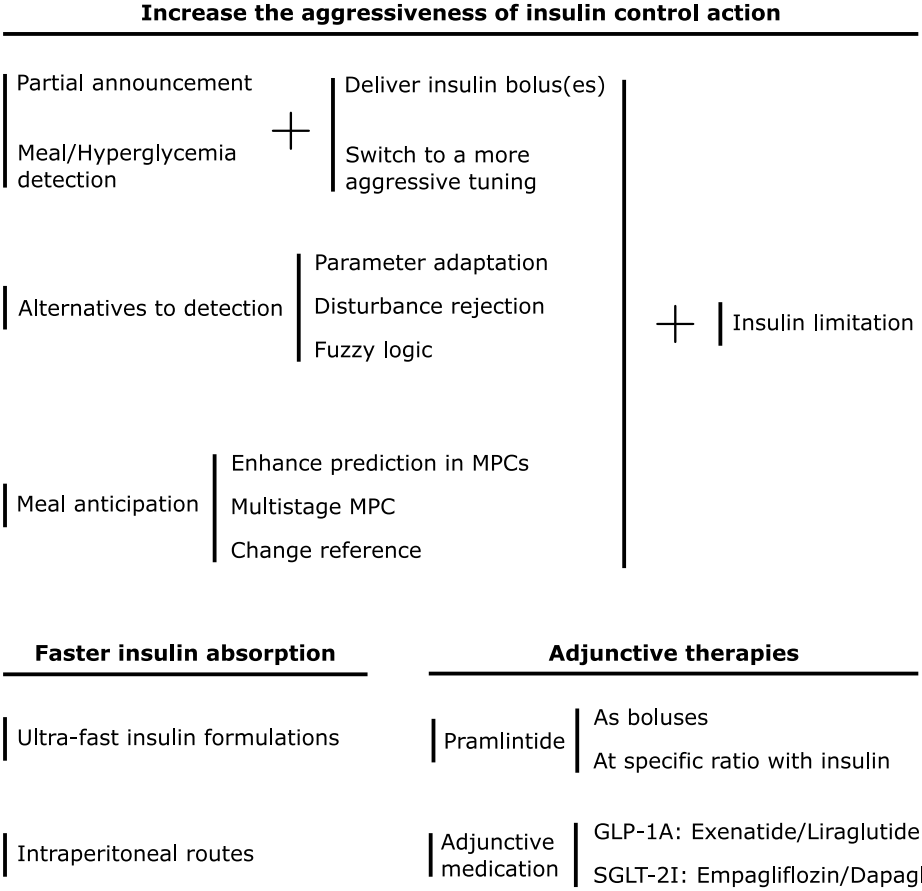

Figure 2.4: Strategies to remove carbohydrate counting. Three strategies can be identified to remove carbohydrate counting: increasing the aggressiveness of the insulin control action, speeding the insulin absorption up, or using adjunctive therapies. Three methods have been used to increase insulin aggressiveness: delivering boluses or switching to a more aggressive tuning at detection or partial announcement time, exploiting historical data to anticipate meals, or using alternative methods to detection. Insulin limitation methods are usually required in these techniques. To enhance the absorption dynamics, subcutaneous ultra-fast insulin or the intraperitoneal route has been utilized. Lastly, the adjunctive therapies that have been evaluated were the pramlintide and medications such as GLP-1A or SGLT-2I. *Notation.* MPC: Model Predictive Controller (MPC), GLP-1A: Glucagon-like peptide-1 receptor agonist (GLP-1A), SGLT-2I: Sodium–glucose co-transporter-2 inhibitor (SGLT-2I).

logic wherein a meal occurrence event (announced by the patient or detected by an algorithm) triggers a series of actions to increase the aggressiveness (insulin boluses, controller retuning, etc.). Another group of techniques replaces the need for an explicit meal event with a more continuous meal compensation using methods from the control engineering toolkit such as observer-based disturbance rejection or adaptive control. Lastly, other strategies learn food intake patterns from historical data, allowing them to confirm or anticipate meal events. Examples of these groups of techniques are reviewed in this subsection.

Partial announcement

A partial announcement, wherein the user provides the mealtime or a qualitative amount of carbohydrate content (e.g., small, regular, large), is a mid-way approach between carbohydrate announcement and no announcement. A representative example of this strategy is implemented in the iLet® Bionic Pancreas (Beta Bionics, Irvine, CA, USA). This investigational device, which admits glucagon delivery, included a partial announcement after undesirably large postprandial glucose excursions found in El-khatib et al. (2010) with a version of the system that relied only on the feedback controller (a Generalized Predictive Controller (GPC)) to compensate meals. In newer versions, the user only needs to announce the mealtime. The system then delivers an insulin bolus calculated from the body weight and previous infused insulin. In a more recent version of the algorithm (El-Khatib et al. 2017), the system incorporated the option to define the type of the meal (breakfast, lunch, or dinner) or grade its size (typical, more than typical, less than typical, or a small bite). The system was assessed in several clinical trials resulting in a satisfactory average %time in 70–180 mg/dL ranging from 65 % to 84.8 % (Russell et al. 2012; El-Khatib et al. 2014; Russell et al. 2014; El-Khatib et al. 2017; Russell et al. 2020; Castellanos et al. 2021; Russell et al. 2022).

Ahmad Haidar's group, from McGill University, adopted a similar approach to El-Khatib et al. (2017) for its MPC-based AP system. In this system, the user had to grade the meal carbohydrate content according to two levels (regular, large), in a preliminary version (Gingras et al. 2016b), or to four levels (snack, regular, large, or very large meal) in a more recent version (Gingras et al. 2016a). The system delivers an insulin bolus according to a fuzzy logic algorithm with this information. The related clinical trials show that both versions achieved comparable results to a system with carbohydrate counting, although large meals were more challenging for the two-level-grading-based algorithm.

Commercial hybrid AP systems with corrective boluses features, such as the Minimed 780G, have also evaluated partial announcement approaches with satisfactory results (Hirsh et al. 2022).

In the examples above, an insulin bolus was delivered when the user announced the meals. However, other strategies are possible. For instance, Colmegna et al. (2018) designed a switched Linear Quadratic Gaussian (LQG) that commutes to an aggressive controller when the user indicates the meal onset and glucose is rising. The system also includes an insulin over-delivery safety layer that attenuates the output of the switched LQG if the insulin-on-board exceeds a limit. This limit is piecewise and depends on a qualitative estimation of meal size (small, medium, large). In a 36-h inpatient trial, the system outperformed the open-loop therapy for the mean %time in 70–180 mg/dL (open-loop: 82.9 % vs. partial announcement: 88.6 %) and the mean %time above 180 mg/dL (open-loop: 33.3 % vs. partial announcement: 19.5 %). Still, no statistically significant differences were found for the %time below 70 mg/dL (Sánchez-Peña et al. 2018). In a 72-h outpatient trial, the controller also increased the %time in 70–180 mg/dL achieved by an open-loop therapy (50.9 % vs. 46.9 %), but the largest improvement occurred at nighttime (Garelli et al. 2022).

Detection-based meal compensation

Partial announcements can still place some burden on patients. Also, these approaches are sensitive to meal announcement skips. Research about meal detection algorithms has been intense for the last 15 years to avoid these drawbacks.

The design of a meal detector usually involves two stages: 1) to determine signals and features experiencing large deviations after meals and 2) to construct a detection logic allowing to acknowledge the meal occurrence from those signals and features. Most of the meal detector algorithms resort to CGM measurements (Weimer et al. 2016; Zheng et al. 2019; Villeneuve et al. 2020) or signals derived from it, such as

- glucose derivatives obtained by numerical approximations (Dassau et al. 2008; Harvey et al. 2014b; Samadi et al. 2017; Hajizadeh et al. 2019a) or state observers, namely, Kalman Filter (KF) variants (Dassau et al. 2008; Mahmoudi et al. 2019),
- deviations between the measured and estimated of glucose (Mahmoudi et al. 2017; Fathi et al. 2019; Staal et al. 2019; Xu et al. 2021; Alzate et al. 2022),

- or estimations of the meal rate of glucose appearance calculated from several methods like KF variants (Turksoy et al. 2016b; Xie et al. 2016; Ramkissoon et al. 2018; Fushimi et al. 2019) or moving horizon estimators (Kölle et al. 2017; Mahmoudi et al. 2018).

Other features combine glucose measurements in a more involved way than those mentioned above: Weimer et al. (2016) present two statistics that result from the projection of the CGM reading in a physiological-invariant parameter space; Ramkissoon et al. (2018) utilize the normalized cross-covariance between the CGM reading and the forward difference of the meal disturbance estimation as a feature; Samadi et al. (2017) use a qualitative description of the CGM signal; Mahmoudi et al. (2019) consider the cumulative sum of the error between CGM and the glucose estimated by a KF; Zheng et al. (2019) construct residuals from the predictions of multiple models; and Askari et al. (2022) combine CGM-derived features (product of derivatives, correlation between CGM and its derivatives, frequency of dominant peaks) with estimations of plasma concentration and gut absorption rate.

Besides CGM reading, other signals have been employed to detect meals, such as abdominal sound, head movement, or wrist movement. However, the proposed methods work as bolus reminders or, in general, medication reminders in other diseases (Ghosh et al. 2021). To the best of the author's knowledge, the only device applied in meal-announcement-free AP systems, though in a feasibility study, was the smartphone application Klue (Roy et al. 2022). This application translates the hand movement, registered with a smartwatch, to carbohydrate doses, which then are fed into a Medtronic 780G to calculate boluses (Roy et al. 2022).

Regarding the detection logic, a large variety of methods have been presented. Most of the methods apply *ad hoc* thresholds to the features (Dassau et al. 2008; Hyunjin et al. 2009; Bon et al. 2010; Wang et al. 2010; Harvey et al. 2014b; Turksoy et al. 2015; Colmegna et al. 2016; Mahmoudi et al. 2018). In some techniques, the threshold value roots in the statistics theory. For instance, Xie et al. (2017) determine a meal when the innovation of a switched KF exceeds a threshold determined by the chi-square test. Mahmoudi et al. (2017) calculate the threshold on the innovative term of a KF-like based on the T^2 statistic, while Fathi et al. (2019) and Palisaitis et al. (2021) use a generalized likelihood test. Other methods use information from behavioral meal patterns to confirm a meal occurrence (Cameron et al. 2012; Villeneuve et al. 2020). Lastly, classification algorithms have also been used to discern the meal events, such as logistic regression (Garcia-Tirado et al. 2021c; Garcia-Tirado et al. 2021b; Corbett et al. 2022), linear discriminant

analysis (Kölle et al. 2017; Kölle et al. 2020), extended isolation forest (Zheng et al. 2020), fuzzy logic (Samadi et al. 2017), or recursive neural networks (Askari et al. 2022).

Following meal detection, many works adopt some bolusing strategy to compensate for the meal. When the meal detector algorithm also estimates the meal content, the AP system typically computes a standard bolus (based on the insulin-to-carbohydrate ratio and the correction factor) but is attenuated to account for the detection delays (Fathi et al. 2019; Mahmoudi et al. 2019). Palisaitis et al. (2021) evaluated a Fathi et al. (2019)'s proposal in a 9-h feasibility trial with unannounced lunch. The proposed meal-announcement-free system reduces the %time above 180 mg/dL (calculated up to 4 h after lunch) achieved by the feedback controller, an MPC, without meal detection (58 % vs. 74.2 %). When the meal detector only provides the occurrence of a meal, the AP system can assume a fixed amount of carbohydrate to calculate the bolus (Harvey et al. 2014b; Majdpour et al. 2021). Alternatively, meal detection may trigger a series of bolus delivery. For instance, the Inreda AP (Inreda Diabetic BV, Goor, the Netherlands) infuses corrective boluses when glucose exceeds 117 mg/dL and another bolus when it exceeds 234 mg/dL (Bon et al. 2010; Blauw et al. 2021). Similarly, the multivariable AP of Ali Cinar's group, from Illinois Institute of Technology, delivers a bolus every time the estimated rate of glucose appearance exceeds a threshold, provided a specific time has elapsed from the last bolus (Turksoy et al. 2017). Hyunjin et al. (2009) devised a more elaborated logic, wherein a bolus is delivered depending on the glucose and the two first derivatives. A different approach is adopted in Garcia-Tirado et al. (2021a) to design a priming bolus strategy for the RocketAP system. The bolus magnitude is proportional to the total daily insulin; the meal occurrence probability, estimated by a logistic regression, modifies the degree of proportionality such that the AP system delivers larger boluses for meals with a higher chance.

Other actions triggered by detecting a meal (or hyperglycemia) can be found in the literature besides delivering a bolus. Fushimi et al. (2019) replaces the partial announcement required in Colmegna et al. (2018) to switch to a more aggressive LQG controller. Since this controller includes a safety layer to limit the insulin-on-board, the upper limit of the insulin-on-board is also modified to allow a more aggressive behavior right after the detection though decreasing after (Fushimi et al. 2020). The idea of switching to a more aggressive controller has also been adopted by Bhattacharjee et al. (2019) in the context of internal model control.

Lastly, Alzate et al. (2022) use the estimation of the meal-carbohydrate content as an input to an impulsive zone MPC to handle unannounced meals.

Methods not requiring meal detection

Adapting the controller parameters can also enhance the postprandial control without requiring an explicit meal detection event. For example, for the adaptive MPC of Ali Cinar's group, Hajizadeh et al. (2019a) relax the plasma insulin constraint of the optimization problem according to the predicted glucose and the trend of the CGM signal. Like the modification of the insulin-on-board in Fushimi et al. (2020), this allows a more aggressive reaction against meals. As an alternative for allowing more insulin during meals in the context of MPC controllers, Garcia-Tirado et al. (2021c) detune the control weight of the cost function depending on the insulin-on-board, the glucose, and its derivative. Similarly, Shi et al. (2019) add a new term in the cost function penalizing the glucose derivative when glucose levels are near hyperglycemia.

Adaptation can also be applied in PID-like controllers. Soylu et al. (2018) present a method to adapt the proportional gain according to a fuzzy logic whose inputs were the error and the glucose derivative. The adaptation rule favors aggressive gains when glucose is increasing to hyperglycemic levels.

Fuzzy logic has also been used to design controllers rather than just modifying a gain. The (DreaMed Diabetes, Petah Tikva, Israel) was one of the pioneer systems using this technique. It includes a Mamdani-type fuzzy logic controller that provides percentage change for the basal and bolus doses to bring the glucose to a range target based on the past and future glucose values and trends. In an 8-h feasibility trial with unannounced meals, the yielded a 73 % %time in 70–180 mg/dL. The algorithm was adquired by Medtronic (Northridge, CA, USA) and was embedded into the Medtronic 780G (Rodríguez-Sarmiento et al. 2022). However, the later commercial artificial pancreas system still requires meal announcements.

Meal compensation have also been tackled from the perspective of disturbance rejection. Sanz et al. (2020) designed a system that handles unannounced meals through an extended state observer and a switched tracking controller. Similary, Cai et al. (2020) present a non-linear active disturbance rejection controller. The system includes heuristic rules either in the controller or in the disturbance observer to increase the aggressiveness of the insulin control action without leading to hypoglycemia. Nath et al. (2020) design a robust observer through attractive ellipsoid methods to estimate the states and a disturbance term used to construct guaranteed-cost robust output feedback control. The disturbance can be estimated with other approaches besides observers. For instance, MohammadRidha et al. (2018) estimate a disturbance term by algebraic methods, in the so-called model-free control.

Meal anticipation from historical data

Food intake usually follows daily patterns (Askari et al. 2022). Some prediction-based controllers, namely MPC, have exploited this property to enhance the prediction quality against unannounced meals and consequently improve the control performance. Cameron et al. (2012) presented a multiple-model probabilistic approach to address this purpose. In each iteration, multiple models predict, independently, the state of insulin-glucose dynamics; each model assumes a different meal start time. Then, the predictions of the local models are integrated by weighting each prediction with the probability that the individual model explains the current data. The forecast of local models includes future meals by considering meal intake behavior derived from a nutritional survey. The multi-model probabilistic prediction approach has been integrated into an MPC. The controller achieved an average %time in 70–180 mg/dL of 63–78 % in several clinical trials with unannounced meals and mild or moderate exercise (Cameron et al. 2014; Cameron et al. 2017; Forlenza et al. 2018).

Another technique featured with meal anticipation capabilities was presented in Corbett et al. (2020) and extended later in Corbett et al. (2022). The core of the system is a multistage MPC. In each iteration, the control action results from an optimization problem involving multiple MPC concurrently executed; each MPC is fed with a different daily disturbance signal profile. To calculate the disturbance profiles, the daily disturbances were estimated retrospectively from individual data using a KF and then clusterized. The consensus of MPC problems in the optimization depends on the probability that the specific disturbance profile represents the actual disturbance. In silico validations of the system with the full version of the UVa/Padova simulator showed a %time in 70–180 mg/dL higher than 70 % (Corbett et al. 2022). However, compared with a single MPC that delivers bolus after detecting meals, the multistage MPC led to slight inferior results (Corbett et al. 2022). Therefore, Corbett et al. (2022) eventually incorporated both, detection and anticipatory capabilities, into the controller.

Like Corbett et al. (2022), Paoletti et al. (2020) consider the estimated disturbance in the optimization problem of an MPC. However, the authors applied a data-driven envelope of disturbances rather than a disturbance profile. Specifically the MPC selects the minimum insulin infusion at each time step, ensuring that the largest disturbance within the prediction horizon (estimated by a moving horizon estimator) belongs to the envelope.

Finally, Hajizadeh et al. (2019b) proposed a markedly different approach to responding to meals with anticipation: a meal detector identifies, retrospectively, the time windows where meals were ingested on previous days. Then, a glucose

target of 80 mg/dL is set to each time window. Lastly, the glucose target for the next day is configured by averaging the previously assigned glucose targets.

Insulin limitation

A meal-announcement-free system should reduce hyperglycemia, but not at the expense of larger hypoglycemia. Late postprandial hypoglycemia namely occurs because of an insulin over-delivery (see Section 2.2.1). Thus, most of the systems presented hereinabove consider somehow the active insulin or insulin-on-board to attenuate the control action. MPC-based systems usually adopt some of the following mechanisms to avoid insulin over-delivery:

- adding estimations of the plasma insulin or insulin-on-board to the hard constraints of the optimization problem (Hyunjin et al. 2009; Hajizadeh et al. 2019a),
- modifying the control action-related weight of the cost function based on some heuristic depending on the insulin-on-board or plasma insulin (Hajizadeh et al. 2019a; Shi et al. 2019),
- modifying the target-related weight of the cost function based on some heuristic depending on the insulin-on-board or plasma insulin (Paoletti et al. 2020; Garcia-Tirado et al. 2021c; Shi et al. 2019),
- expanding the cost function (soft constraint) with a new term penalizing estimated insulin concentration (El-khatib et al. 2010)

For systems not relying on receding horizon principles, Insulin Feedback (IFB) is a straightforward approach to reducing the risk of insulin over-delivery (Steil et al. 2011; Palerm 2011). The method subtracts from the control action (calculated, for instance, by a PID) an infusion proportional to the estimated plasma insulin (or other insulin-related states). In the context of meal-announcement-free systems, the IFB was implemented, for instance, in Huyett et al. (2015), Sanz et al. (2020), and Dovc et al. (2020).

To avoid insulin over-delivery, some researchers opted for adding an upper bound to the insulin-on-board and reducing the control action accordingly for the current insulin-on-board to be below the upper bound. This purpose can be achieved by directly saturating or suspending the insulin infusion rate if the calculated insulin within a sampling period exceeds the insulin-on-board limit (Cai et al. 2020). Revert et al. (2013) propose an alternative approach based on sliding

mode principles: the controller set-point is modified according to a switching logic designed to attain an invariance set in the difference between the upper bound and the estimated insulin-on-board. Thus, whenever the insulin-on-board exceeds the upper bound, the switching logic starts commuting between 0 and a high set-point value at a high rate, leading, after being filtered, to a new reference higher than the nominal reference. Consequently, the control action decreases. Colmegna et al. (2018) present a closely related methodology, wherein the switching logic attenuates the control output through a discontinuous gain rather than increasing the reference.

2.3.2 Accelerating insulin absorption

The 10–15 min onset action delay in subcutaneously-administered rapid-acting insulin formulations greatly restricts the controller performance against unannounced meals. Lee et al. (2013) and Colmegna et al. (2021b) show in silico that insulins with faster absorption improve performance against unannounced meals for PID and MPC control, respectively, without resorting to *ad-hoc* methodologies like in Section 2.3.1. Two alternatives enable more rapid insulin absorption: ultra-fast-acting insulin formulation and the intraperitoneal route for insulin administration.

Ultra-fast-acting formulations of insulin

Recent ultra-fast-acting formulations, such as the Fiasp® (Novo Nordisk, Bagsvaerd, Denmark), with an onset time of 2–4 min (Lee et al. 2021), have been validated in clinical trials. Unfortunately, the promising results shown in silico have not been found in these clinical trials: Russell et al. (2020) found no significant improvement of the Fiasp®, compared to standard rapid-acting insulin, when used in the insulin-only iLet system, even though qualitative carbohydrate counting was required. Tsoukas et al. (2021b) evaluated an MPC system with Fiasp® in a 12-day clinical trial. The system required the mealtime to calculate a meal bolus based on a 25-g meal. Despite this partial announcement, it yields a %time above 180 mg/dL of 32.7 %, higher than the guidelines recommend (Battelino et al. 2019). Lastly, Dovc et al. (2020) assessed the system (Atlas et al. 2010), a fully meal-announcement-free system, with Fiasp® in a 27-h trial; no benefit of Fiasp® was found over a rapid-acting insulin formulation. These unsatisfactory results arise because most evaluated systems were not specifically tuned for an ultra-fast insulin formulation (Dovc et al. 2020). Albeit with proper tuning, these new formulations' long action duration (3–5 h from the injection; Lee et al. 2021) would likely hinder the improvements.

Intraperitoneal route

Another approach to circumvent the delays related to subcutaneous absorption is to use alternative routes to administer insulin. Indeed, the initial developments of an AP system in the 1970's resorted to intravenous insulin administration and glucose sensing. The almost immediate insulin action enabled tight glucose control using simple Proportional-Derivative controller (PD) algorithms. However, those systems' high invasiveness and size circumscribed them to research applications in hospital settings (Renard et al. 2019). A more feasible alternative is the intraperitoneal route. In this route, insulin is infused into the abdominal cavity; thus, it reaches the portal vein before reaching the peripheral system (Chakrabarty et al. 2019). This allows enhanced pharmacokinetics and pharmacodynamics characteristics compared to the subcutaneous administration. For instance, intraperitoneal insulin action peaks 15 min after injection, almost six times more rapid than the subcutaneous route (Lal et al. 2019). Moreover, this route regulates hepatic glucose production more effectively, given the larger circulating levels in the portal vein.

During 2000-2002, the first closed-loop system with the intraperitoneal route, Long-Term Sensor System® (MiniMed-Medtronic, Northridge, CA, USA), was evaluated in a dozen of clinical trials up to 48 h in length. This system combines a fully implantable pump with an implantable intravenous glucose sensor (Renard et al. 2006). The initial trials run a PD without meal announcement. However, the delays in the intravenous glucose reading caused recurrent hypoglycemia episodes. These delays were attributed to the sensor composition (the glucose oxidase pad was larger than the subcutaneous sensor pad to enable a duration greater than a year) and signal processing (Renard et al. 2006; Steil et al. 2004). As a result, pre-meal boluses eventually had to be adopted to reduce the hypoglycemia events (Renard et al. 2006).

Conversely, the meal-announcement-free MPC presented in Jones et al. (2017) outperformed its subcutaneous hybrid counterpart under a nominal scenario with the Hovorka model as a virtual patient. Doyle's group, from Harvard University, also validated in silico its meal-announcement-free intraperitoneal zone MPC, albeit in more exigent simulations than Jones et al. (2017), including the 100-adult cohort of the UVa/Padova simulator. This zone MPC increases by more 15 % of the time spent in normoglycemia regarding its subcutaneous counterpart (Lee et al. 2012); compared to the subcutaneous case with prandial boluses, the zone MPC yields non-inferior results (Lee et al. 2014). The same zone MPC was assessed in a 24-h inpatient study with ten individuals with unannounced meals. The zone MPC spent 20 % more time in 70–180 mg/dL than the subcutaneous administration while reducing the time in hypoglycemia (Dassau et al. 2017).

The same group developed a PID for intraperitoneal insulin delivery and glucose reading; the PID was designed with a second-order transfer function following the internal model control principle and only contains an IFB and an anti-windup as safety mechanisms to avoid hypoglycemia. In a 27-h simulation with medium-sized unannounced meals, this system achieved a %time in 80–140 mg/dL larger than 70 % without hypoglycemia events (Huyett et al. 2015). Chakrabarty et al. (2019) upgraded Huyett et al. (2015)'s controller with an enhanced internal model and new tuning; the achieved %time in 70–180 mg/dL exceeded, in an in silico study, 90 % using either a subcutaneous or intraperitoneal glucose sensor. The interest in intraperitoneal systems goes beyond academia. Indeed, Chakrabarty et al. (2019)'s proposal belongs to the project line of PhysioLogic Devices. This company plans to develop a fully automatic and fully implantable AP system (the ThinPump^{TM}) shortly (JDRF 2020). The EU-funded project FORGETDIABETES is also developing a system with similar features (FORGETDIABETES 2020). Hence, the intraperitoneal route is appealing for developing meal-announcement-free AP systems. However, its invasiveness – a surgical procedure is required to implant the entire pump or, at least, the catheter in the abdominal cavity – and the risk of catheter obstructions (He et al. 2021) still discourage its use.

2.3.3 Complementing insulin with other hormones or medication

Insulin plays a crucial role in glucose homeostasis. However, other hormones, such as glucagon, amylin, or incretins, also intervene in this process. Thus, integrating adjunctive hormones or medication in the AP system can potentially improve postprandial response such that meal announcements would no longer be required. The adjunctive therapies that have been evaluated with AP against unannounced meals are the analogs of amylin and glucagon; medications usually addressed for treating type 2 diabetes such as exenatide, liraglutide, dapagliflozin, or empagliflozin, have also been tested.

Pramlintide

As indicated in Section 2.2.1, amylin action is also deficient in T1DM. This hormone retards meal absorption from the gut by delaying gastric emptying and diminishes glucagon release. To take advantage of these positive benefits of amylin in glycemic control, several trials evaluated the use of an amylin analog, i.e., pramlintide, in closed-loop therapies.

The preliminary trials of Weinzimer et al. (2012), Renukuntla et al. (2014), and Sherr et al. (2016) considered the effect of a fixed dose of pramlintide (30 or

60 µg) injected manually at mealtime (or 15 min earlier) replacing a carbohydrate-matched insulin bolus. The employed controller for the latter three trials was the external Physiological Insulin Delivery (ePID) algorithm consisting of a PID extended with an IFB. The addition of pramlintide reduced the %time above 180 mg/dL in 4–17 % of the ePID without pramlintide and the %time below 70 mg/dL in 1–4 %, but no statistically significant improvement was shown in all the studies Renukuntla et al. (2014). Furthermore, the need for manual injection of pramlintide does not suit well in a meal-announcement-free system.

Alternatively, Haidar's group considered a second pump to deliver a continuous infusion of pramlintide in a ratio of 10 µg of pramlintide per unit of Fiasp®, wherein an MPC calculated the insulin infusion. This was an experimental setting emulating an insulin-pramlintide co-formuation currently in development by a pharmaceutical companies (Andersen et al. 2021). An initial trial of 24 h and seven subjects evaluated the feasibility of replacing carbohydrate counting with a mealtime announcement. At the time of the announcement the system delivers a bolus corresponding to 25 g (Tsoukas et al. 2021a). The exploratory analysis revealed that the system with pramlintide and partial announcement halved the median time in hypoglycemia of the system without pramlintide and full announcement. Both achieved similar %time in 70–180 mg/dL and %time above 180 mg/dL. These results were confirmed in a 12-day outpatient trial also reported in Tsoukas et al. (2021a). This latter trial also showed (without a statistical analysis) the superior performance of the pramlintide-extended system with a partial announcement over a Fiasp-alone system with partial announcement in terms of %time in 70–180 mg/dL (70 % vs. 60 %) and %time above 180 mg/dL (28 % vs. 38 %), with only a slight increase of hypoglycemia (1.4 % vs. 0.5 %).

Given the potential benefits of pramlintide in alleviating carbohydrate counting observed in the previous trials, Haidar's group went a step away, substituting the partial announcement with Fathi et al. (2019)'s meal detector. This meal detector estimates the carbohydrate amount of meals; hence, at detection time, the controller delivers an insulin bolus (and the pramlintide dose corresponding to the ratio 10 µg:1 U) calculated with the estimated carbohydrates. After the positive results of this configuration in a feasibility trial (Majdpour et al. 2021), Tsoukas et al. (2021b) underwent a 24-h inpatient trial involving 24 individuals. This configuration yielded a desirable %time in 70–180 mg/dL of 74.3 %, with a zero median time spent in hypoglycemia. Nevertheless, statistical tests do not show non-inferiority over the Fiasp-alone hybrid counterpart in terms of percentage in normoglycemia. Since pramlintide is related to adverse effects like nausea, vomiting, bloating, or heartburn, further experiments with longer duration and a larger number of participants need to evaluate if pramlintide-based

meal announcement-free systems counterpose these adverse effects by significantly improving glycemic control.

Antihyperglycemic medications

Specific medications targeting hyperglycemia avoidance may be a suitable alternative for pramlintide, at least, until insulin-pramlintide co-formulations were available. Unlike pramlintide, these medications are not continuously delivered, but administered once or twice a day.

Glucagon-like peptide-1 receptor agonist (GLP-1A) is a group of medications that, like pramlintide, delays gastric emptying and suppresses glucagon secretion (Seetharaman et al. 2022). Renukuntla et al. (2014) considered a short-acting GLP-1A, the exenatide, as adjunctive therapy for the ePID system in an 11-h feasibility trial without carbohydrate-matched insulin boluses. The addition of exenatide turns into a statistically significant reduction of %time above 180 mg/dL regarding the insulin-only ePID without announcements (16 % vs. 30 %), without increasing hypoglycemia episodes. However, some individuals experienced nausea or vomiting.

Exenatide had to be administered subcutaneously at mealtime, detracting from a meal-announcement-free system. To partially alleviate this drawback, Ilkowitz et al. (2016) assessed the feasibility of a single daily subcutaneous injection of liraglutide, a long-acting GLP-1A. Adjuvant liraglutide, administered at breakfast time, yielded a statistically significant reduction of glucose excursion after breakfast and lunch compared to the insulin-only system, without increasing hypoglycemia. The reduction after dinner was less remarkable, showing a declining effect of this medication throughout the day. In addition, some individuals experienced nausea, vomiting, and headache as adverse effects of liraglutide.

Another family of antihyperglycemic agents is the Sodium–glucose co-transporter-2 inhibitors (SGLT-2Is). These agents inhibit glucose reabsorption from the kidneys, promoting its elimination through urine (Seetharaman et al. 2022). Haidar's group assessed whether a two-daily oral administration of empagliflozin, a type of SGLT-2I, could remove meal announcements from their insulin-only MPC algorithm (Haidar et al. 2021). The results showed that empagliflozin could not replace the prandial insulin bolus totally. Still, it did allow a partial announcement configuration wherein the user announces mealtime for the system to deliver an insulin bolus corresponding to a carbohydrate intake of 25 g. This latter configuration achieved comparable (not statistically significant) %time in 70–180 mg/dL, %time above 180 mg/dL, and %time below 70 mg/dL than the

hybrid insulin-only counterpart. Another SGLT-2I is dapagliflozin. Biester et al. (2021) show that adding 10 mg of this antihyperglycemic agent twice a day outperforms (with statistical significance) the %time in 70–180 mg/dL and %time above 180 mg/dL achieved by the system without increasing hypoglycemia.

Despite the positive results with adjunct SGLT-2Is, these agents increase the ketone levels (Haidar et al. 2021) and may eventually lead to diabetic ketoacidosis at excessive doses. No ketoacidosis cases were reported in the above studies, but its limited duration (9–24 h) impeded foreseeing the long-term effects of SGLT-2Is.

Glucagon: its role in postprandial hypoglycemia mitigation

Glucagon increases blood glucose levels. Hence, it might allow a more aggressive insulin reaction against meals, potentially counteracting any hypoglycemia induced by an insulin over-delivery. Fushimi et al. (2022) showed that an extension of Fushimi et al. (2019)'s LQG controller with glucagon removes hypoglycemic events in a simulation study. However, clinical trials did not show clear benefits of glucagon during the postprandial period (Peters et al. 2018; Infante et al. 2021). In an exploratory trial with a tri-hormonal system (insulin, pramlintide, and glucagon) against unannounced meals, Majdpour et al. (2021) reported that glucagon was used sparsely. In a second iteration, insulin and pramlintide aggressiveness were increased to exploit glucagon action more. Nonetheless, glucagon failed to avoid hypoglycemia events and eventually was removed from the system (Majdpour et al. 2021). Other studies also found that glucagon did not wholly remove hypoglycemic events after unannounced meals (Bon et al. 2010; El-khatib et al. 2010; Gingras et al. 2016a). This difficulties of glucagon to avoid hypoglycemic episodes in the postprandial period seem to be related to an inefficient stimulation of glucose production when circulating insulin levels are elevated (Infante et al. 2021), as is the case for postprandial periods.

In addition, several side effects arise after glucagon administration, such as nausea, vomiting, and headache (Ranjan et al. 2021). Furthermore, dual insulin-glucagon AP systems require more complex hardware (two pumps or double chamber pumps) and, therefore, an increased cost.

2.4 Strategies to remove exercise announcements

Physical activity may result in hyperglycemia or hypoglycemia depending on the intensity, type, and duration (see Section 2.2.2). However, hypoglycemia can lead to severe complications in a shorter time; fear of these complications is one of the main reasons people with T1DM abandon an active lifestyle (Riddell et al. 2017; Tagougui et al. 2019). Thus, as in most of the articles in the literature, this dissertation will only address hypoglycemia avoidance. Two complementary strategies are identified to address this goal (Figure 2.5): 1) reducing the insulin aggressiveness (e.g., pump suspension) and 2) supplementing insulin with the infusion of glucagon or the suggestion of rescue carbohydrates.

2.4.1 Reducing the insulin aggressiveness during exercise

The immediate reaction to imminent hypoglycemia is to suspend the insulin infusion. The most direct method is detecting or predicting a hypoglycemic event or exercise and then reducing or stopping the basal infusion. Other techniques do not use explicit exercise detection but rely on adaptive rules or integrate physical activity information in the feedback controller. Lastly, anticipating regular exercise patterns from historical data has been applied too. Some examples of these methodologies are described herein.

Detection/prediction-based methods

A simple approach to reduce the aggressiveness of the controller is to shut the basal infusion off when the glucose goes below a lower bound. This is the case, for example, of one of the preliminary versions of the Inreda AP (Van Bon et al. 2012). Similarly, low-glucose-suspend method implemented in Herrero et al. (2017) reduces the pump infusion a 50 % when the CGM reading is below 100 mg/dL and suspends it if it is below 80 mg/dL. Instead of directly suspending the pump infusion, systems counting with an insulin-on-board limitation can reduce the insulin-on-board limitation whenever hypoglycemia is detected or predicted (Garelli et al. 2022).

An estimated disturbance can also be used to detect the exercise. For instance, Ramkissoon et al. (2019) utilizes an unscented KF to estimate the glucose disappearance rate due to exercise. If this disturbance overpasses a certain lower threshold, the insulin infusion is suspended and the upper bound of the insulin-on-board reduced. These modifications expire when a risk of hyperglycemia or infusion under-delivery is detected based on the glucose level and its first derivative.

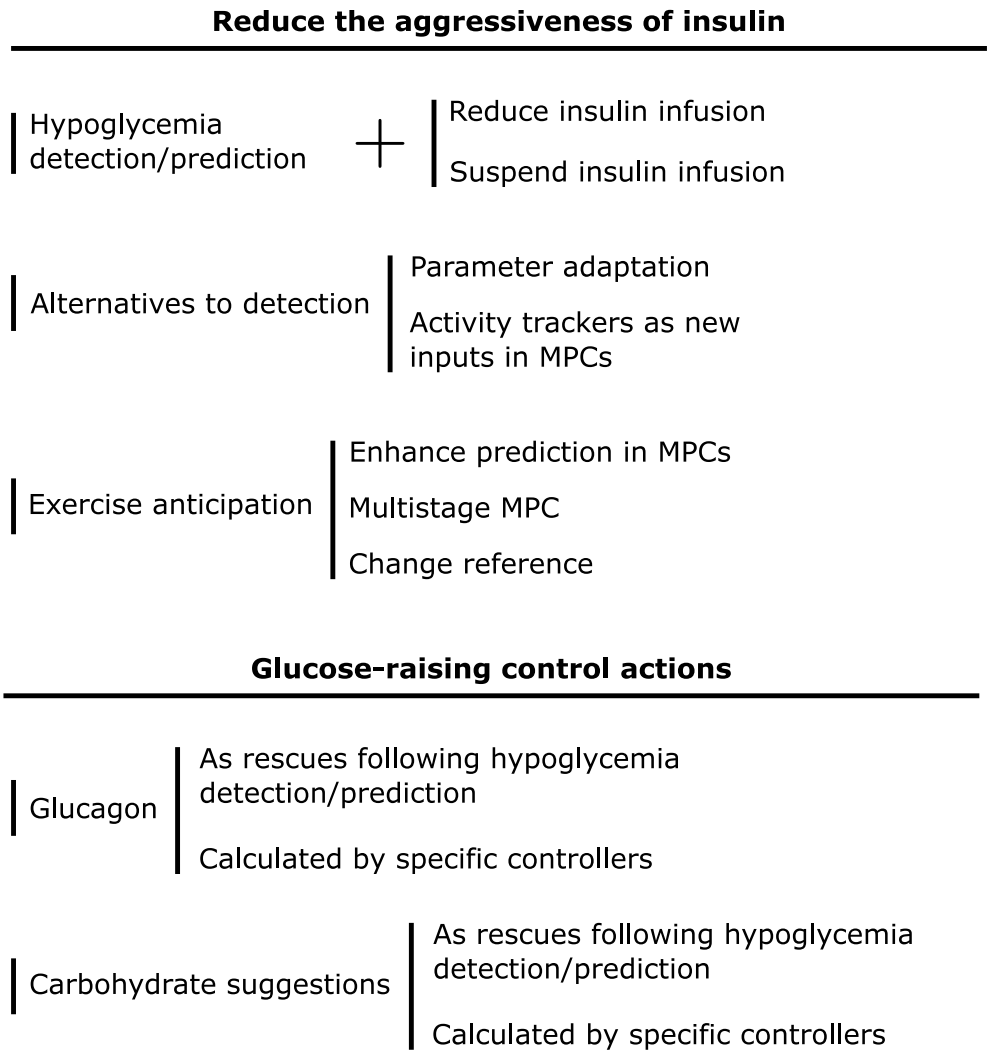

Figure 2.5: Strategies to remove exercise announcements. Two strategies can be identified to remove carbohydrate counting: reducing the aggressiveness of the insulin control action or using glucose-raising control actions. Three methods have been used to reduce insulin aggressiveness: insulin reduction or suspension hypoglycemia detection or prediction time, exploiting historical data to anticipate exercise or using alternative methods to detection. The glucose-raising control actions are glucagon and carbohydrates. Both can be delivered as rescues after detection or prediction or calculated from a specific controller. *Notation.* MPC: Model Predictive Controller (MPC).

Unlike in the meal detection problem, physiological signals different from glucose have been extensively applied to detect an exercise period and even grade its intensity or infer its type (Sevil et al. 2020; Cescon et al. 2021; Sawaryn et al. 2021). In Breton et al. (2014), the core controller changes to a less aggressive mode when the heart rate exceeds 125 %. This heart-rate informed controller reduces the glucose drop rate during exercise but without significantly reducing hypoglycemia (Breton et al. 2014). Likewise, a recent version of the Inreda AP reduces the insulin dose when the heart rate overpasses a certain threshold (Blauw et al. 2016). Jacobs et al. (2015) also measured the heart rate, but combined with accelerometry, to estimate the energy expenditure; whenever the estimated energy expenditure exceed 4 kcal/min, insulin infusion is suspended for 30 min, and after then, reduced a 50 % for 60 min.

Alternatives to detection/prediction-based exercise compensation

Detecting an exercise event is not strictly necessary to reduce the aggressiveness of the insulin control action. Hughes et al. (2010) adopted a more continuous approach wherein the insulin infusion was attenuated based on a predicted hypoglycemic risk. This strategy significantly reduced the %time below 70 mg/dL achieved by sensor-augmented therapy without increasing hyperglycemia in outpatient studies with young children where exercise was practiced more frequently and intensively than on regular days (Ly et al. 2016; Breton et al. 2017). Nonetheless, carbohydrate rescues were required.

Furthermore, just as MPCs can adapt their parameters to make the insulin response more aggressive (Section 2.3.1), they can also adapt them to reduce their aggressiveness facing hypoglycemia. For instance, Shi et al. (2019) modify the control weights of a zone MPC so that the deviations of the insulin infusion above the basal are penalized more than the those below the basal when the predicted glucose decreases. Hajizadeh et al. (2019b) change the target weight instead of the control; the deviations from the glucose target are penalized more for increasing hypoglycemia risk than hyperglycemia risk. Garcia-Tirado et al. (2019) follow a similar logic but modify the predicted set-point rather than the associated weight.

Lastly, MPCs can integrate activity-related physiological signals (e.g., energy expenditure, galvanic skin impedance, etc.) as inputs to the internal model to enhance the prediction. In silico trials with data-driven models (Turksoy et al. 2013; Hajizadeh et al. 2019a) or physiological models (Resalat et al. 2016) have shown that the integration of theses additional inputs results in a quicker reduction of insulin infusion, and, ultimately, a reduced %time below 70 mg/dL when compared with the case where only insulin is used as input of the internal model.

Exercise anticipation from historical data

For regular exercise, behavioral patterns can be learned from historical data to anticipate exercise onset and prospectively reduce insulin infusion. Some researchers that proposed methods to anticipate meals have an equivalent method for exercise. Garcia-Tirado et al. (2019) is the counterpart of Corbett et al. (2020) to anticipate the exercise periods based on multistage MPC: instead of a meal disturbance, each MPC, running concurrently, is fed with a different disturbance profile representing the glucose uptake caused by a moderate aerobic exercise. The disturbance profiles result from the clusterization of daily disturbances, each extracted by the convolution of the dynamics of the glucose uptake with a rectangular signal representing the exercise duration. To mitigate the risk of hypoglycemia induced by unexpected exercise, the system also can detect the exercise with activity trackers. Garcia-Tirado et al. (2021a) evaluated the system in a 48-h clinical trial. On the first day, the patient undertook an exercise session in the similar schedule used to tune the controller, whereas, on the second day, no exercise was practiced. Compared with a single MPC, the proposed system significantly reduced the hypoglycemic events during the exercise day, with only a slight increase in time in hyperglycemia during the sedentary day.

The data-driven robust MPC of Paoletti et al. (2020) also can deal with exercise. To this end, the authors estimated, besides the meal disturbance, two states related to exercise, i.e., the percentage of active muscular mass and the percentage of maximum oxygen consumption. Then, the same procedure explained to anticipate meals is applied: estimation of the disturbance envelope and calculation of the minimum insulin infusion that guarantees that the disturbance is inside the envelope.

Finally, the anticipatory modification of the glucose set-point presented in Hajizadeh et al. (2019b) for meals can be combined with exercise information. The idea is to retrospectively detect exercise periods of previous days with activity trackers. Then, the set-point is set to 160 mg/dL for each detected period. Lastly, the mean of the daily, retrospectively-defined glucose set-points defines the set-point for the next day.

2.4.2 Counteracting insulin unidirectionality with glucose-raising control actions

An insulin-alone AP may avoid physical activity-induced hypoglycemia without announcements if exercise patterns can be learned and anticipated (Garcia-Tirado et al. 2021a). However, when these patterns are less clear, e.g., unstructured physical activity, the best that an insulin-alone AP can do is to shut the pump off at exercise detection. Even in the unlikely case that no detection delay exists, suspending the pump at this time may be insufficient to avoid the hypoglycemia due to the long insulin offset time (Zaharieva et al. 2019). Moreover, the exercise causes a long-term increase in insulin sensitivity and increased mobility of insulin from subcutaneous depots to plasma; thus, hypoglycemia may occur hours after the exercise end (Tagougui et al. 2019). To avoid hypoglycemia in these situations, two glucose-rising control actions have been integrated into AP systems: glucagon and carbohydrate suggestions.

Glucagon

Dual glucagon-insulin AP systems have integrated glucagon following two not mutually exclusive policies (Jones 2019): 1) as rescue doses to recover from hypoglycemia or prevent an imminent one, and 2) as more frequent doses delivered with dedicated control algorithms.

On the one hand, glucagon rescues have been delivered when the glucose or the predicted glucose falls below a certain threshold, as is the case, respectively, of the Inreda AP (Van Bon et al. 2014) and the fading-memory PD-based system developed by the Oregon Health and Science University (OHSU) (Wilson et al. 2020).

On the other hand, dedicated glucagon-insulin controllers usually combines two independent loops, one for each controller output, which commute following certain threshold-based rules. This is the case for the iLet system (an MPC for the insulin and a PD for the glucagon; Russell et al. 2012), the BiAP of the Imperial College (a PID-like for insulin and a PD for glucagon; Herrero et al. 2013), the Inreda AP (two PDs; Van Bon et al. 2014), the DH-MPC of the OHSU (two MPCs; Resalat et al. 2016 or Boiroux et al. 2018), or the fading-memory PD-based system of the OHSU (two PD-like controllers; Jacobs et al. 2015). Since two independent loops of control actions with different signs (decreasing or increasing glucose) may cause oscillations, some of the latter systems incorporate *ad hoc* coordination mechanisms based on heuristical rules (Jacobs et al. 2015) or feedback inhibitions (Herrero et al. 2017). Moscardó et al. (2019b) presented a more systematic approach to

coordinating insulin and glucagon. The system consists of two elements: a master controller that calculates a virtual control action and a divisor that routes the control effort to the insulin channel or the glucagon channel based on a certain logic. This way, insulin and glucagon are inherently coordinated delivering the control effort as computed by the main controller.

Unlike in the meal compensation case, more evidence exists that dual glucagon-insulin AP systems outperform insulin-alone AP in clinical trials with hypoglycemic exercise periods by reducing the time spent in hypoglycemia (Haidar 2019; Infante et al. 2021; Zeng et al. 2022). Nevertheless, glucagon does not always mitigate hypoglycemia. Although without a total agreement among researchers, it has been observed that glucagon loses its effectiveness when glucose drops at a high rate, when insulin concentration is elevated, or when glycogen depots are empty after prolonged exercise or repetitive glucagon doses (Ranjan et al. 2021).

Carbohydrate supplementation

Fast-acting carbohydrate intake arises as a natural action to correct and, if applied on time, prevent hypoglycemia induced by an unannounced exercise (Tagougui et al. 2019; Patel et al. 2016). Unlike glucagon infusion, carbohydrates require patient intervention. In guidelines for the open-loop therapy, the time and amount of carbohydrate supplementations depend on elaborated rules involving the CGM value and trend. To overcome this potential burden for patients, several AP systems have included carbohydrate recommender modules that notify the user of the amount of carbohydrates needed to ingest to prevent or avoid hypoglycemia. Carbohydrate recommenders do not increase the hardware complexity of the system yet rely on fluid patient responsiveness. A dual insulin-glucagon system may be a better alternative when carbohydrate ingestion is not feasible (e.g., patients with frequent nocturnal hypoglycemia after exercise or during professional sports competition). Also, carbohydrate supplementation may deem unappealing for people aiming for weight loss by exercising.

Many carbohydrate recommenders included in AP are based on heuristical rules. The Inreda AP system recommends an intake of 12 g or 18 g when the glucose falls below 70 mg/dL or 54 mg/dL respectively (Blauw et al. 2016). Since during exercise the glucose may abruptly drop, some recommenders incorporate glucose predictions as in Harvey et al. (2012), which was later integrated in a zone-MPC AP and validated in clinical trials (Harvey et al. 2014a; Huyett et al. 2017). Turksoy et al. (2016a) add information on exercise-related physiological signals to enhance the 30-min-ahead prediction further and suggest a rescue whose amount depends on the measured glucose and the speed of the predicted glucose decrease.

In Turksoy et al. (2018), the recommender module was incorporated into a GPC-based AP system and validated in a clinical trial involving multiple types of exercise.

Other researchers have proposed specific control loops to suggest the carbohydrate amounts. Beneyto et al. (2018) extend an insulin loop based on a PD with an independent PD for carbohydrate rescues calculation. Mutual inhibitions coordinate both loops. In addition, glucose predictions at 5 min, 10 min, 15 min, and 20 min are fed to the carbohydrate controller to estimate future continuous actions. Finally, the recommender suggests 15 g doses according to a quantization logic depending on the past and predicted continuous control actions. The system was validated in a clinical trial, yielding satisfactory results against unannounced exercise (Viñals et al. 2021).

Moscardó et al. (2019a) also rely on feedback laws to calculate a rescue suggestion. Instead of an independent loop, Moscardó et al. (2019a) exploit the master-plus-divisor architecture of Moscardó et al. (2019b) to coordinate rescue suggestions with insulin and glucagon infusions. The continuous carbohydrate suggestion was quantized in 15-g doses for patient adherence.

2.5 Conclusion

The sensor lags, the long time of insulin onset and offset, and the dysregulation of other hormones involved in the glucose homeostasis limit the performance of AP systems against meals and exercise events. Hybrid AP sytems partially counteract these limitations with meal and exercise announcements but at the expense of a heavy burden for patients.

Three broad, complementary strategies were identified to remove meal announcements: 1) increasing the aggressiveness of the insulin control action while applying some mechanism to avoid insulin over-delivery; 2) using ultra-fast insulin formulations or the intraperitoneal route; or 3) complementing the insulin infusion with pramlintide, glucagon, or adjunctive medications. The last two strategies yield positive results in enhancing postprandial control against unannounced meals (albeit with unclear conclusions for using Fiasp or glucagon). However, they have associated drawbacks too. For instance, some cases still require patient intervention (exenatide, empagliflozin). Also, other methods imply an increased technological complexity (pramlintide pump) or are more invasive (intraperitoneal pump). Lastly, some adjunctive therapies are related to gastric adverse effects (pramlintide, liraglutide) or increased ketone levels (SGLT-2I). Thus, this dissertation will focus on the first strategy. Among the techniques that have been identified in this

strategy, the methods presented in this dissertation to remove meal announcement will rely on meal detection (Chapter 5), bolus delivery (Chapter 6), disturbance rejection (Chapter 3 and Chapter 7), or parameter adaptation (Chapter 6 and Chapter 7).

Regarding unannounced exercise compensation, the long insulin offset and insulin stacking hampers avoiding exercise-induced hypoglycemia with only insulin. Clinical trials have shown that dual insulin-glucagon AP systems reduce hypoglycemia in unannounced hypoglycemic exercise periods. However, the limitations of these systems (unclear effectiveness of glucagon to alleviate hypoglycemia in certain situations, glucagon side effects, and increased complexity) may question the cost-effectiveness. Thus, in this dissertation, carbohydrate supplementation, besides other strategies to reduce insulin aggressiveness (e.g., pump suspension, reduction of insulin-on-board limit), will be used instead of glucagon to mitigate the risk of exercise-induced hypoglycemia (Chapter 7).

Chapter 3

Meal disturbance estimation

Estimating how meals impact glucose may be valuable to design meal-announcement-free artificial pancreas systems. This chapter shows that this estimation is possible with state and disturbance observers. Two observers – a first-order sliding mode observer and a Kalman filter – are designed with two models of different complexity (the Identifiable Virtual Patient model and the Hovorka model). The influence on the estimation accuracy of the observer structure and the model complexity is assessed by simulations.

Authored publications related to this chapter:

- Sala-Mira, I.; Díez, J.-L.; Ricarte, B., et al. (2019). "Sliding-mode disturbance observers for an artificial pancreas without meal announcement". In: *Journal of Process Control (JCR 2019: Q2)* 78, pp. 68–77. ISSN: 09591524. DOI: 10.1016/j.jprocont.2019.03.008.

- Sala-Mira *, I.; Siket *, M.; Eigner, G., et al. (2020). "Kalman filter and sliding mode observer in artificial pancreas: an in-silico comparison". In: *21th IFAC World Congress. IFAC-PapersOnLine.* Vol. 53. 2. Berlin (Germany): Elsevier Ltd, pp. 16227–16232. DOI: 10.1016/j.ifacol.2020.12.617.

- Sala-Mira *, I.; Siket *, M.; Kovacs, L., et al. (2021). "Effect of Model, Observer and their Interaction on State and Disturbance Estimation in Artificial Pancreas: an In-Silico Study". In: *IEEE Access (JCR 2021: Q2)*, pp. 1–15. ISSN: 2169-3536. DOI: 10.1109/ACCESS.2021.3120880.

* *denotes equal contribution.*

3.1 Introduction

Carbohydrates in a meal are digested and absorbed to the bloodstream (Dalla Man et al. 2006). This glucose flux (also known as meal rate of glucose appearance) can be regarded as a disturbance in the context of the AP. Its real-time monitoring is appealing to handle unannounced meals either for detecting them or compensating them. However, no direct measurements of the rate of glucose appearance are possible.

In the gold standard estimation, glucose infusions or meals are enriched with multiple isotope tracers. The rate of glucose appearance (and other glucose fluxes) is reconstructed through dilution measurements (Basu et al. 2003). This technique is valuable for modeling (Dalla Man et al. 2006), but its complexity, cost, and degree of invasiveness make it unfeasible for real-time control.

State and disturbance observers are a suitable real-time alternative. Although its accuracy is lower than the gold standard method, they have been successfully applied for either meal detection (Kölle et al. 2017; Ramkissoon et al. 2018; Chen et al. 2019) or compensation of unannounced meals (Kovacs et al. 2019; Ullah et al. 2020; Sanz et al. 2020). The Kalman Filter (KF) is the prevalent observer option in the artificial pancreas literature; however, tuning the covariance matrix is not straightforward. Sliding mode observers feature robustness properties (insensitivity to matched disturbances) and have a simpler structure, thereby being an appealing alternative. The first goal of this chapter is to determine how relevant is the observer structure in the accuracy of the estimation of the meal rate of glucose appearance. To this end, a Kalman Filter (KF) that can estimate disturbances by augmenting the state is compared with a First Order Sliding Mode Observer (FOSMO).

The second goal is to study the influence of the glucose-insulin model used to construct the observer. The estimation of the meal disturbance may be coupled with other sources of uncertainty caused by model deficiencies. For example, other glucose fluxes, such as endogenous glucose production, would be indistinguishable from the meal disturbance. Therefore, complex models accurately describing these glucose fluxes are expected to improve the estimation of meal disturbance. In contrast, identifying complex models is challenging because of the increased number of parameters and their correlations. As a result, an inaccurate model individualization might hide the benefits of a better representation of the glucose flux, degrading the estimation of the meal disturbance. To analyze these factors, the two observers were designed with the Hovorka model (Hovorka et al. 2004) and the Identifiable Virtual Patient (IVP) model (Kanderian et al. 2009), two examples of medium-complexity and low-complexity models, respectively.

3.2 Disturbance estimation

This section describes the necessary background to estimate disturbances with the KF and the FOSMO. Table 3.1 includes the parameters and variables used in the definition of the observers.

Table 3.1: Description of the variables defining the observers

Variable	Description
General	
I_j	Identity matrix of dimension j
$0_{i\times j}$	Matrix of zeros with dimension $i \times j$
n_x	Number of states
n_y	Number of outputs
n_d	Number of disturbances
$x(t)\,, x[k]$	State variable in continuous and discrete representation ($\in \mathbb{R}^{n_x}$)
$u(t)\,, u[k]$	Control (known) input variable in continuous and discrete representation ($\in \mathbb{R}^{n_u}$)
$d(t)\,, d[k]$	Disturbance (unkown) input variable in continuous and discrete representation ($\in \mathbb{R}^{n_d}$)
$y(t)\,, y[k]$	Output variable in continuous and discrete representation ($\in \mathbb{R}^{n_y}$)
$A(t), A[k]$	State matrix in continuous and discrete representation ($\in \mathbb{R}^{n_x \times n_x}$)
$B(t), B[k]$	Input matrix in continuous and discrete representation related to the known input ($\in \mathbb{R}^{n_x \times n_u}$)
$D(t), D[k]$	Input matrix in continuous and discrete representation related to the unknown input or disturbance ($\in \mathbb{R}^{n_x \times n_d}$)
$C(t), C[k]$	Output matrix in continuous and discrete representation ($\in \mathbb{R}^{n_y \times n_x}$)
Kalman filter	
$n_{\overline{x}}$	Size of the augmented state, $n_{\overline{x}} \coloneqq n_x + n_d$
$\overline{x}[k]$	Augmented system state, $\overline{x}[k] \coloneqq \operatorname{col}(x[k], d[k])$ ($\in \mathbb{R}^{n_{\overline{x}}}$)

Table 3.1: (continued)

Variable	Description
$w[k]$	White zero-mean uncorrelated process noise ($\in \mathbb{R}^{n_x}$)
$v[k]$	White zero-mean uncorrelated output noise ($\in \mathbb{R}^{n_y}$)
$\overline{Q}[k]$	Covariance of $w[k]$ ($\in \mathbb{R}^{n_{\overline{x}} \times n_{\overline{x}}}$)
$\overline{R}[k]$	Covariance of $v[k]$ ($\in \mathbb{R}^{n_y \times n_y}$)
$\hat{\overline{x}}[k]$	Mean of augmented system state estimated by the KF, $\hat{\overline{x}}[k] = E\left[\overline{x}[k] \middle\vert y[1], \cdots, y[k]\right]$ ($\in \mathbb{R}^{n_{\overline{x}}}$)
$\overline{P}[k]$	Covariance matrix of the estimation error estimated by the KF, $\overline{P}[k] = E\left[(\overline{x}[k] - \hat{\overline{x}}[k])(\overline{x}[k] - \hat{\overline{x}}[k])^T\right]$ ($\in \mathbb{R}^{n_{\overline{x}} \times n_{\overline{x}}}$)
$\hat{\overline{x}}^-[k], \overline{P}[k]^-$	Approximation of $\overline{x}[k]$ and $\overline{P}[k]$ without the knowledge of the measurement
$K[k]$	KF matrix gain ($\in \mathbb{R}^{n_{\overline{x}} \times n_y}$)
Sliding mode observer	
$\phi(x, u, t)$	System non-linear term ($\in \mathbb{R}^{n_x}$)
L_ϕ	Lipschitz constant of $\phi(x, u, t)$ regarding $x(t)$
$\rho(y(t), u(t), t)$	Bound of the disturbance $d(t)$
$\bar{q}$	Rank of D
$\bar{x}(t) = \left[\begin{array}{c} x_1(t) \\ \hline x_2(t) \end{array}\right]$	Transformed state after the first coordinate change: $x_1(t) \in \mathbb{R}^{n_x - n_y}$ and $x_2(t) \in \mathbb{R}^{n_y}$
$\left[\begin{array}{c\|c} A_{11} & A_{12} \\ \hline A_{21} & A_{22} \end{array}\right]$	Transformed A matrix after the first coordinate change: $A_{11} \in \mathbb{R}^{(n_x - n_y) \times (n_x - n_y)}$, $A_{12} \in \mathbb{R}^{(n_x - n_y) \times (n_y)}$, $A_{21} \in \mathbb{R}^{(n_y) \times (n_x - n_y)}$, $A_{22} \in \mathbb{R}^{(n_y) \times (n_y)}$
$\left[\begin{array}{c} \phi_1(x, u, t) \\ \hline \phi_2(x, u, t) \end{array}\right]$	Transformed $\phi(\bar{x}, u, t)$ term after the first coordinate change: $\phi_1(x, u, t) \in \mathbb{R}^{(n_x - n_y)}$ and $\phi_2(\bar{x}, u, t) \in \mathbb{R}^{n_y}$
$\left[\begin{array}{c} 0_{(n_x - n_y) \times n_y} \\ \hline C_2 \end{array}\right]$	Transformed C matrix after the first coordinate change: $C_2 \in \mathbb{R}^{n_y \times n_y}$
$D_2 = \left[\begin{array}{c} 0_{(n_x - \bar{q}) \times n_d} \\ \hline D_{22} \end{array}\right]$	Transformed D matrix after the first coordinate change: $D_{22} \in \mathbb{R}^{\bar{q} \times n_d}$

Table 3.1: (continued)

Variable	Description
T	Transformation matrix for the second coordinate change, see (3.15)
$L = \left[L^0 \;\middle|\; 0_{(n_x-n_y)\times n_d}\right]$	Matrix to stabilize the linear part of the error dynamics with $L_0 \in \mathbb{R}^{(n_x-n_y)\times(n_y-n_d)}$
$\bar{z}(t) = \left[\frac{z_1(t)}{z_2(t)}\right]$	Transformed state after the second coordinate change: $z_1(t) \in \mathbb{R}^{n_x-n_y}$ and $z_2(t) \in \mathbb{R}^{n_y}$
$\bar{z}(t) = \left[\frac{\hat{z}_1(t)}{\hat{z}_2(t)}\right]$	State estimated by the FOSMO: $\hat{z}_1(t) \in \mathbb{R}^{n_x-n_y}$ and $\hat{z}_2(t) \in \mathbb{R}^{n_y}$
$\hat{d}(t)$	Disturbance estimated by the FOSMO
K	Gain of the linear correction term, see (3.17) ($\in \mathbb{R}^{n_y}$)
$\nu(t)$	Discontinuous feedback error term ($\in \mathbb{R}^{n_y}$)
$\nu_{eq}(t)$	Equivalent output error injection term ($\in \mathbb{R}^{n_y}$)
$k(t)$	Function building the term $\nu(t)$ ($\in \mathbb{R}$)

The notation $a[k]$ is the short form to represent a discrete variable $a[T_s k]$ where T_s is the sampling time and $k = \{0, 1, 2, ...\}$ the discrete iteration.

3.2.1 Kalman filter

Consider the following perturbed continuous-time system given by

$$\begin{cases} \dot{x}(t) = A(t)x(t) + B(t)u(t) + \\ \qquad\quad + D(t)d(t) \quad , \\ y(t) = C(t)x(t) \end{cases} \tag{3.1}$$

where $x(t) \in \mathbb{R}^{n_x}$, $y(t) \in \mathbb{R}^{n_y}$, $u(t) \in \mathbb{R}^{n_u}$, $d(t) \in \mathbb{R}^{n_d}$ are, respectively, the system states, the measured output, the deterministic known input and the deterministic unknown input (or disturbance) at time t. A widespread method to estimate the disturbance $d(t)$ with Kalman-like observers consists to augment the state with the equation

$$\dot{d}(t) = 0, \tag{3.2}$$

which assumes that the disturbance is constant or slowly-varying within the sampling time. Note that, although real disturbances will unlikely be constant, this is a widespread assumption in the disturbance estimation literature (Li et al. 2012). Taking $\overline{x}[k] := \mathrm{col}\,(x[k], d[k])$, the resulted augmented system is given by (Friedland 1969; Linder et al. 1997):

$$\begin{cases} \dot{\overline{x}}(t) = \overline{A}(t)\overline{x}(t) + \overline{B}(t)u(t) \\ y(t) = \overline{C}(t)\overline{x}(t) \end{cases} \tag{3.3}$$

where the overline symbol, e.g., $\overline{x}$, denotes a vector or a matrix that corresponds to the augmented system. The extended system matrices are the following:

$$\begin{aligned} \overline{A}(t) &= \begin{bmatrix} A(t) & D(t) \\ 0_{n_d \times n_x} & I_{n_d \times n_d} \end{bmatrix} \quad \overline{B}(t) = \begin{bmatrix} B(t) \\ 0_{n_d \times n_x} \end{bmatrix} \\ \overline{C}(t) &= \begin{bmatrix} C(t) & 0_{n_y \times n_d} \end{bmatrix} \end{aligned} \tag{3.4}$$

Since the standard KF presupposes a stochastic discrete system, the augmented system (3.3) has to be converted to:

$$\begin{cases} \overline{x}[k] = \overline{A}[k-1]\overline{x}[k-1] + \overline{B}[k-1]u[k-1] + w[k-1] \\ y[k] = \overline{C}[k-1]\overline{x}[k] + v[k] \end{cases} \tag{3.5}$$

resulting from the discretization of the system and the addition of the stochastic inputs $w[k]$ (process noise) and $v[k]$ (output noise). The stochastic inputs are considered white noises, zero-mean, uncorrelated (among them and among $x[k]$), and with known covariance matrices $\overline{Q}[k]$ and $\overline{R}[k]$, respectively (Simon 2006, Chapter 5). The argument $[k]$ in the variables refers to the sample iteration $t = kT_s$, where k is a positive integer (discrete iteration) and T_s is the sampling time.

A standard KF can be designed for the augmented dynamical system (3.5) provided the pair $\left(\overline{A}[k], \overline{C}[k]\right)$ is observable. The KF estimates the mean of $\overline{x}[k]$ in (3.5), $\hat{\overline{x}}[k] = E\left[\overline{x}[k] | y[1], \cdots, y[k]\right]$, and the covariance matrix of the estimation error, $\overline{P}[k] = E\left[(\overline{x}[k] - \hat{\overline{x}}[k])(\overline{x}[k] - \hat{\overline{x}}[k])^T\right]$. The estimation process involves the following two stages (Simon 2006, Chapter 5):

1. *Mean and covariance propagation before the output measurement.* Consider that $\hat{\overline{x}}[k-1]$ and $\overline{P}[k-1]$ are available (e.g., the filter is initialized in $\hat{\overline{x}}[0]$ and $\overline{P}[0]$, and $k=1$). The discrete-time model (3.5) is used to approximate the mean and the covariance matrix without the knowledge of the measurement $y[k]$ as follows:

$$\begin{aligned}\hat{\overline{x}}^{-}[k] &= E[x[k]|y[1],\cdots,y[k-1]] = \\ &= \overline{A}[k]\hat{\overline{x}}[k-1] + \overline{B}[k]u[k-1]\end{aligned} \tag{3.6}$$

$$\begin{aligned}\overline{P}^{-}[k] &= E\left[(\overline{x}[k]-\hat{\overline{x}}^{-}[k])(\overline{x}[k]-\hat{\overline{x}}^{-}[k])^T\right] = \\ &= \overline{A}[k]\overline{P}[k-1]\overline{A}^T[k] + \overline{Q},\end{aligned} \tag{3.7}$$

where $\hat{\overline{x}}^{-}[k]$ is the a priori estimation of the mean and $\overline{P}^{-}[k]$, the covariance matrix of the estimation error $(\overline{x}[k]-\hat{\overline{x}}^{-}[k])$. To deduce the above expression, two properties of $w[k]$ are considered: $w[k]$ is uncorrelated with $(\overline{x}[k]-\hat{\overline{x}}^{-}[k])$ (i.e., $E\left[(\overline{x}[k]-\hat{\overline{x}}^{-}[k])w[k]^T\right] = E\left[w[k](\overline{x}[k]-\hat{\overline{x}}^{-}[k])^T\right] = 0$) and it is zero-mean (i.e., $E[w[k]]=0$).

2. *Mean and covariance correction for an unbiased estimation of the mean minimizing the total variance of the estimation error.* The a priori estimation of the mean, $\hat{\overline{x}}^{-}[k]$, can be recursively corrected with the actual measurement $y[k]$ as follows:

$$\hat{\overline{x}}[k] = \hat{\overline{x}}^{-}[k] + \overline{K}[k]\Big(\overline{y}[k] - \overline{C}[k]\hat{\overline{x}}^{-}[k]\Big) \tag{3.8}$$

where $\overline{K}[k]$ is the KF's gain and $\hat{\overline{x}}[k]$ is the a posteriori estimated of $\overline{x}[k]$ (after the measurement). Expression (3.8) is an unbiased estimator regardless $\overline{K}[k]$ since the expected value of the error $e_x[k] \coloneqq \overline{x}[k] - \hat{\overline{x}}[k]$ is zero for all k (i.e., $E[e_x[k]]=0$) if $E[e_x[k-1]]=0$ and $v[k]$ has a zero mean (i.e., $E[v[k]]=0$). The unbiasedness property means that, on average, $\hat{\overline{x}}[k]$ coincides with $\overline{x}[k]$ (Simon 2006, Chapter 3). The matrix gain $\overline{K}[k]$ is selected such that the total variance – the sum of the variances of the estimation errors – is minimized. This is equivalent to minimize the trace of the estimated error covariance $\overline{P}[k] = E[e_x[k]e_x[k]^T]$ (Simon 2006, Chapter 3). Since the noise $v[k]$ is independent of $e_x[k-1]$, the covariance matrix $\overline{P}[k]$ is simplified to:

$$\overline{P}[k] = (I - \overline{K}[k]\overline{C}[k])\overline{P}^{-}[k](I - \overline{K}[k]\overline{C}[k])^T + \overline{K}[k]\overline{R}[k]\overline{K}[k]^T \tag{3.9}$$

Lastly, the $\overline{K}[k]$ minimizing the trace of $\overline{P}[k]$ is given by:

$$\overline{K}[k] = \overline{P}^{-}[k]\overline{C}^{T}[k]\big(\overline{C}[k]\overline{P}^{-}[k]\overline{C}^{T}[k] + \overline{R}\big)^{-1} \tag{3.10}$$

The expected value of the errors $\overline{x}[k]-\hat{\overline{x}}^{-}[k]$ and $\overline{x}[k]-\hat{\overline{x}}[k]$ are exponentially stable provided $\|\overline{A}[k]\|$ and $\|\overline{C}[k]\|$ are bounded, the pair $(\overline{A}[k], \overline{C}[k])$ is uniformly completely observable and $(\overline{A}[k], \overline{Q}[k]^{\frac{1}{2}})$ is uniformly completely controllable (Moore et al. 1980; Zhang et al. 2021). Hence, the augmented state can be estimated recursively by applying the above two stages.

Remark that augmenting the state to estimate the disturbance is not exclusive for KFs (e.g., Lin et al. (1995), Fan et al. (2010), and Kim et al. (2017)). For example, this method has been applied for Luenberger-like observers in the so-called Generalized Extended State observers (Kurtz et al. 1998; Li et al. 2012; Kotta et al. 2020). Moreover, if the exogenous system generating the disturbance is known (i.e., the internal model of the disturbance), it can replace the equation $d[k] = d[k-1] + w[k-1]$ when extending the state (Sanz et al. 2018).

3.2.2 Sliding mode observer

Sliding mode observers include a discontinuous output error injection ensuring the asymptotically convergence of the state error to zero despite matched disturbances (disturbance whose distribution matrix is in the range of the distribution matrix of the discontinuous injection; Sira-Ramírez et al. 1994). These observers can also reconstruct disturbances with only the information of their bound. This feature is exploited in this chapter to estimate the rate of glucose appearance. In particular, this chapter uses the First Order Sliding Mode Observer (FOSMO) proposed by Yan et al. (2007), which extends the design of Edwards et al. (1994) for non-linear systems. The theoretical framework supporting how this observer can be used for state and disturbance estimation is shown below.

The observer applies for the semi-linear system given by (Yan et al. 2007; Shtessel et al. 2014, Section 3.5):

$$\begin{cases} \dot{x}(t) = Ax(t) + \phi(x, u, t) + Dd(y, u, t) \\ y(t) = Cx(t) \end{cases} \tag{3.11}$$

where $y(t) \in \mathbb{R}^{n_y}$ is the measurable output, $x(t) \in \mathbb{R}^{n_x}$ is the system state, and $u(t) \in \mathbb{R}^{n_u}$ is the known input. The function $\phi(x, u, t) \in \mathbb{R}^{n_x}$ represents the

nonlinear term, Lipschitzian with respect to $x(t)$ with the Lipschitz constant L_ϕ. The disturbance (or other unknown inputs, such as parameter uncertainty) is $d(t) \in \mathbb{R}^{n_d}$, which is assumed to be bounded by the known term $\rho(y(t), u(t), t)$. A, C, and D are constant matrices of proper dimensions, with D and C both full rank.

Two nonsingular state transformations are applied to (3.11) to design the observer. Under the assumption

$$\operatorname{rank}(CD) = \operatorname{rank}(D) = \tilde{q} \tag{3.12}$$

a coordinate change exists such that the system (3.11) becomes (Yan et al. 2007, Lemma 1; Shtessel et al. 2014, Section 3.5):

$$\begin{cases} \dot{x}_1(t) = A_{11}x_1(t) + A_{12}x_2(t) + \phi_1(\bar{x}, u, t) \\ \dot{x}_2(t) = A_{21}x_1(t) + A_{22}x_2(t) + \\ \qquad\quad + \phi_2(\bar{x}, u, t) + D_2 d(t) \\ y(t) = C_2 x_2(t) \end{cases} \tag{3.13}$$

where $\bar{x}(t) := \operatorname{col}(x_1(t), x_2(t)) \in \mathbb{R}^{n_x}$ represents the transformed states where $x_2(t)$ are the last n_y elements of $\bar{x}(t)$, $A_{11} \in \mathbb{R}^{(n_x - n_y)\times(n_x - n_y)}$, $C_2 \in \mathbb{R}^{n_y \times n_y}$ is nonsingular and

$$D_2 = \begin{bmatrix} 0_{(n_y - \tilde{q})\times n_d} \\ D_{22} \end{bmatrix} \tag{3.14}$$

with $D_{22} \in \mathbb{R}^{\tilde{q}\times n_d}$ is of full rank. This special form for D_2 simplifies the observer design, circumventing the solution of the constrained Lyapunov equation proposed by Walcott et al. (1988). The term $\bar{\phi}(\bar{x}, u, t) := \operatorname{col}(\phi_1(\bar{x}, u, t), \phi_2(\bar{x}, u, t))$ represents the transformed nonlinearities where $\phi_2(\bar{x}, u, t)$ are the last n_y components of $\bar{\phi}(\bar{x}, u, t)$.

In the second coordinate change, the following transformation is applied to (3.13),

$$T := \begin{bmatrix} I_{n_x - n_y} & L \\ 0_{n_y \times (n_x - n_y)} & I_{n_y} \end{bmatrix} \quad , \quad L := \begin{bmatrix} L^0 & 0_{(n_x - n_y)\times n_d} \end{bmatrix} \tag{3.15}$$

leading to

$$\begin{cases} \dot{z}_1(t) = (A_{11} + LA_{21})\, z_1(t) + (A_{12} + LA_{22}\,(A_{11} + LA_{21})\, L)\, z_2(t) + \\ \qquad\quad + \begin{bmatrix} I_{n_x - n_y} & L \end{bmatrix} \phi(T^{-1}z, u, t) \\ \dot{z}_2(t) = A_{21} z_1(t) + (A_{22} - A_{21}L)\, z_2(t) + \\ \qquad\quad + \phi_2(T^{-1}z, u, t) + D_2 d(t) \\ y(t) = C_2 z_2(t) \end{cases} \tag{3.16}$$

where $z \coloneqq \mathrm{col}\,(z_1, z_2)$ are the transformed states and I is the identity matrix. The matrix L has the structure of (3.15), with $L^0 \in \mathbb{R}^{(n_x - n_y)\times(n_y - n_d)}$, to verify $LD_2 = 0$, otherwise the transformation to obtain (3.13) will be meaningless.

The observer for the system (3.16) reads as:

$$\begin{cases} \dot{\hat{z}}_1(t) = (A_{11} + LA_{21})\, \hat{z}_1(t) + (A_{12} + LA_{22}\,(A_{11} + LA_{21})\, L)\, C_2^{-1} y(t) + \\ \qquad\quad + \begin{bmatrix} I_{n_x - n_y} & L \end{bmatrix} \phi(T^{-1}\hat{z}, u, t) \\ \dot{\hat{z}}_2(t) = A_{21} \hat{z}_1(t) + (A_{22} - A_{21}L)\, \hat{z}_2(t) + \\ \qquad\quad + \phi_2(T^{-1}\hat{z}, u, t) - K e_y(t) + \nu(t) \\ \hat{y}(t) = C_2 \hat{z}_2(t) \end{cases} \tag{3.17}$$

where K is the gain of the linear error correction ($e_y(t) \coloneqq y(t) - \hat{y}(t)$) term to be designed. The term $\nu(t)$, defined as

$$\nu(t) \coloneqq \begin{cases} k(t) C_2^{-1} \frac{e_y(t)}{\|e_y(t)\|}, & \text{if } e_y(t) \neq 0 \\ 0, & \text{otherwise} \end{cases}, \tag{3.18}$$

is the discontinuous feedback error term allowing the state error ($e_1 \coloneqq z_1 - \hat{z}_1$) to reach the sliding surface $S \coloneqq \{(e_1(t),\, e_y(t)) | e_y(t) = 0\}$ and remain there afterwards provided the scalar function $k(t)$ is chosen sufficiently larger than $\rho(y(t), u(t), t)$.

The dynamics of the observer errors reads as:

$$\begin{aligned} \dot{e}_1(t) &= (A_{11} + LA_{21})\, e_1(t) + \\ &\quad + \begin{bmatrix} I_{n_x - n_y} & L \end{bmatrix} \left(\phi(T^{-1}z, u, t) - \phi(T^{-1}\hat{z}, u, t)\right) \qquad (3.19) \\ \dot{e}_y(t) &= C_2 A_{21} e_1(t) + \left((A_{22} - A_{21}L)\, C_2^{-1} + C_2 K\right) e_y(t) + \\ &\quad + C_2 D_2 d(t) - C_2 \nu(t) + C_2 \left(\phi_2(T^{-1}z, u, t) - \phi_2(T^{-1}\hat{z}, u, t)\right) \qquad (3.20) \end{aligned}$$

For the observer to estimate the disturbance, the error $e_1(t)$ and $e_y(t)$ must converge to the origin, asymptotically and in finite time, respectively. On the one hand, the error dynamics $\dot{e}_1(t)$ is asymptotically stable if the following condition – calculated using $V = e_1(t)^T P e_1(t)$ as Lyapunov candidate – holds (Shtessel et al. 2014, Proposition 3.2):

$$\bar{A}^T \bar{P}^T + \frac{1}{\epsilon} \bar{P} \bar{P}^T + \epsilon L_\phi^2 I_{n_x - n_y} + \alpha P < 0 \tag{3.21}$$

for $P = P^T > 0$, $\bar{P} \coloneqq \begin{bmatrix} I_{n_x - n_y} & L \end{bmatrix}$, $\bar{A} \coloneqq \mathrm{col}(A_{11}, A_{21})$ and the positive constants ϵ and α.

Condition (3.21) requires designing L^0 in (3.15) to stabilize $A_{11} + LA_{21}$ (the linear part of the error dynamics $e_1(t)$ in sliding mode). Hence, the pair (A_{11}, A_{21}) must be at least detectable, or equivalently, the invariant zeros of (A,D,C) in (3.11) must be stable (Shtessel et al. 2014, Lemma 3.2).

On the other hand, the output error $e_y(t)$ is driven to the origin in finite time if the following conditions are verified (Shtessel et al. 2014, Proposition 3.3):

$$\left(C_2 \left(A_{22} - A_{21} L\right) + C_2^{-1} K\right)^T + C_2 \left(A_{22} - A_{21} L\right) + C_2^{-1} K \leq 0 \tag{3.22}$$

$$k(t) \geq \left(\|C_2 A_{21}\| + \|C_2\| L_\phi\right) w(t) + \|C_2 D_2\| \rho(y, u, t) + \eta \tag{3.23}$$

where $\|\cdot\|$ denotes the Euclidean norm, the term η is a positive constant related to the convergence time, and $w(t)$ is an upper bound of $\|e_1(t)\|$ given by the solution of $\dot{w}(t) = \frac{1}{2}\alpha w(t)$ provided $\|e_1(0)\| \leq \|w(0)\|$. Expressions (3.22) and (3.23) determine K and $k(\cdot)$ to guarantee the reachability condition, that is, $\dot{\bar{V}} < -2\eta \bar{V}^{1/2}$ with $\bar{V} = e_y^T e_y$ a Lyapunov function.

If condition (3.23) holds, during the sliding mode regime $e_y(t) = \dot{e}_y(t) = 0$, hence the output error dynamics become

$$0 = -\nu_{eq}(t) + D_2 d(t) + \left(\phi(T^{-1} z, u) - \phi(T^{-1} \hat{z}, u)\right) + C_2 A_{21} e_1(t) \tag{3.24}$$

where $\nu_{eq}(t)$ is the so-called equivalent output error injection term (Edwards et al. 2000). This term can be interpreted as the average effect of the high-frequency correction in (3.18) that maintains the error trajectories in the surface S (Edwards et al. 2000; Yan et al. 2007). Because of (3.21), the terms $C_2 A_{21} e_1(t)$ and $(\phi(T^{-1} z, u) - \phi(T^{-1} \hat{z}, u))$ will vanish. As a result,

$$\nu_{eq} \approx D_2 d(t) \tag{3.25}$$

The actual value of $\nu_{eq}(t)$ is unknown since it depends on the disturbance. However, an estimation of $\nu_{eq}(t)$, $\hat{\nu}_{eq}(t)$, is possible by either filtering ν (Edwards et al. 2006; Zak et al. 2017) or approximating (3.18) with sigmoid functions (Edwards et al. 2000; Veluvolu et al. 2009).

Once $\hat{\nu}_{eq}(t)$ is computed, the estimated disturbance $\hat{d}(t)$ can be reconstructed from

$$\hat{d}(t) = (D_2^T D_2)^{-1} D_2 \hat{\nu}_{eq}(t) \tag{3.26}$$

Note that, unlike the KF, the FOSMO does not require the assumption of constant disturbance.

3.3 Models

Models are required to design the observers in Section 3.2. This chapter also studies the effect of the model structural complexity on the accuracy of the disturbance estimation. Thus, the observers were designed with two glucose-insulin models of different complexity: the Identifiable Virtual Patient (IVP) model (Kanderian et al. 2009) and the Hovorka model (Hovorka et al. 2004). A description of these models is provided in this section. In addition, the parameters and variables of the Identifiable Virtual Patient (IVP) model and the Hovorka model are summarized in Table 3.2 and Table 3.3, respectively.

The performance of the observers will be assessed in silico because, as indicated in the introduction of this chapter, measuring the meal rate of glucose appearance is challenging. Therefore, this section also presents the identification of the models with the simulator used for the in silico evaluation: the UVa/Padova simulator (Dalla Man et al. 2014). This simulator received the approval for the Food and Drug Administration to be a substitute for pre-clinical trial with animals. In this dissertation, a modified version of this simulator was utilized. This modified version is built upon the academic version with 30 virtual patients (10 adults, 10 adolescents, and 10 children). The academic version did not consider variability or exercise. Hence, to simulate under more challenging conditions, the research group this thesis belongs to has extended the simulator with multiples sources of variability (e.g., circadian variability, insulin absorption, and meal absorption) and exercise.

3.3.1 The Identifiable Virtual Patient Model

The IVP model is a trade-off between the Bergman model (Bergman et al. 1985) and the Hovorka model in terms of complexity: it expands the Bergman model by modeling the subcutaneous insulin administration. However, it describes with minor detail than Hovorka et al. (2004) the non-insulin-dependent glucose fluxes or the hepatic glucose production. In addition, the IVP model is less spread in the literature compared to the Hovorka model, yet its applications are numerous: observer design (Boiroux et al. 2017; Sala et al. 2018), controller design (Enright 2021), meal detection (Mahmoudi et al. 2019; Zheng et al. 2020), simulator for in silico studies (Meneghetti et al. 2021) or for training people with diabetes (Stocker et al. 2006), among others.

The equations of the IVP model read as:

$$\dot{I}_{SC}(t) = -\frac{1}{\tau_1} \cdot I_{SC}(t) + \frac{1}{\tau_1 C_I} \cdot u(t) \tag{3.27}$$

$$\dot{I}_{P}(t) = -\frac{1}{\tau_2} \cdot I_{P}(t) + \frac{1}{\tau_2} \cdot I_{SC}(t) \tag{3.28}$$

$$\dot{I}_{EFF}(t) = -p_2 \cdot I_{EFF}(t) + p_2 \cdot S_I \cdot I_P(t) \tag{3.29}$$

$$\begin{aligned} \dot{G}(t) = &-(GEZI + I_{EFF}(t)) \cdot G(t) + \\ &+ EPG + R_A(t) \end{aligned} \tag{3.30}$$

The expressions (3.27) and (3.28) model the absorption of the insulin infusion $u(t)$ (µU/min) with two compartments (modeling element assuming homogenous mass or concentration of a drug): one for the subcutaneous concentration $I_{SC}(t)$ (µU/L), and other for the plasma insulin concentration $I_P(t)$ (µU/L), respectively. The parameters τ_1 and τ_2 define the absorption time (min), and C_I is the insulin clearance (mL/min). Equation (3.29) describes the insulin effect on glucose disposal, $I_{EFF}(t)$(1/min), where p_2 is the kinetic rate for insulin action (1/min) and S_I is the insulin sensitivity (mL/(µU min)). Lastly, equation (3.30) models the fluctuations in plasma glucose concentration $G(t)$ (mg/dL) due to $I_{EFF}(t)$, non-insulin dependent uptake represented with the glucose effectiveness at zero insulin ($GEZI$ in 1/min), the hepatic glucose production (EGP in mg/(dL min)) and, finally, the meal rate of glucose appearance ($R_A(t)$ in mg/(dL min)), the disturbance to be estimated in this chapter. The parameters and variables describing the IVP model are listed in Table 3.2.

Table 3.2: Variables and parameters of the Identifiable Virtual Patient model

Symbols	Description	Units
Variables		
$u(t)$	Subcutaneous insulin infusion	µU/min
$I_{SC}(t)$	Insulin concentration in the subcutaneous compartment	µU L
$I_P(t)$	Insulin concentration in the plasma compartment	µU L
$I_{EFF}(t)$	Insulin effect on glucose	min
$G(t)$	Plasma glucose	mg/dL
$R_A(t)$	Meal rate of glucose appearance	mg/(dL min)
Parameters		
τ_1 , τ_2	Absorption time constants related to the insulin movement between the delivery site and the plasma	min
C_I	Insulin clearance gain	mL/min
p_2	Kinetic rate for insulin action	1/min
S_I	Insulin sensitivity	mL/(µU min)
EGP	Hepatic glucose production	mg/(dL min)
$GEZI$	Glucose effectiveness at zero insulin	1/min

3.3.2 The Hovorka model

The Hovorka model is a medium complexity model. It employs more compartments to describe the subcutaneous absorption, plasma glucose concentration, and insulin effect than the IVP model. Also, the degree of nonlinearity is more considerable, including, for example, two piecewise algebraic relations to model the non-insulin-dependent glucose and the renal glucose clearance. However, other simulation-oriented models, such as the model integrated into the UVa/Padova simulator (Dalla Man et al. 2014), provide more detailed descriptions of endogenous glucose production and meal absorption or include a glucagon subsystem model.

The Hovorka model is widely used in the literature: Wilinska et al. (2010) construct a simulator with this model to compare closed-loop control algorithms. In addition, some of the subsystems of the model are used to form new models, for example, to describe glucagon pharmacokinetics (Wendt et al. 2016; Furió-Novejarque et al. 2022) or exercise (Resalat et al. 2016). Indeed, Kanderian et al. (2009) describes the $R_A(t)$ in (3.30) with the bicompartimental model of Hovorka et al. (2004). The Hovorka model is also utilized to design state observers (Orozco-Lopez et al. 2018; Kölle et al. 2017), especially for Kalman-like filters (Ramkissoon et al. 2019;

Hajizadeh et al. 2018; Kovacs et al. 2019). The most explicit example of the relevant role of this model is that two of the five commercially available hybrid artificial pancreas systems implement this model: the CamAPS FX (CamDiab Ltd, Cambridge, UK; Hovorka et al. 2010) and the DBLG1 (Diabeloop, Grenoble, France; Hanaire et al. 2020).

The dynamic equations are the following (Hovorka et al. 2004):

$$\dot{S}_1(t) = u(t) - \frac{S_1(t)}{\tau_S}, \tag{3.31}$$

$$\dot{S}_2(t) = \frac{S_1(t)}{\tau_S} - \frac{S_2(t)}{\tau_S} \tag{3.32}$$

$$\dot{I}(t) = \frac{S_2(t)}{\tau_S V_I} - k_e I(t), \tag{3.33}$$

$$\dot{x}_1(t) = -k_{a1} x_1(t) + k_{b1} I(t), \tag{3.34}$$

$$\dot{x}_2(t) = -k_{a2} x_2(t) + k_{b2} I(t), \tag{3.35}$$

$$\dot{x}_3(t) = -k_{a3} x_3(t) + k_{b3} I(t), \tag{3.36}$$

$$\begin{aligned} \dot{Q}_1(t) = &-F_{01c}(t) - F_R(t) - x_1(t) Q_1(t) + k_{12} Q_2(t) \\ &+ EGP_0(1 - x_3(t)) + R_A(t), \end{aligned} \tag{3.37}$$

$$\dot{Q}_2(t) = Q_1(t) x_1(t) - (k_{12} + x_2(t)) Q_2(t), \tag{3.38}$$

The equations (3.31) and (3.32) model the absorption of the insulin infusion $u(t)$ (mU/(kg min)) through two compartments. $S_1(t)$(mU/kg) and $S_2(t)$(mU/kg) are the amounts of insulin, and τ_S is (min) the insulin absorption time constant. The plasma insulin concentration $I(t)$ (mU/L) is described by (3.33), where k_e(1/min) is the insulin clearance and V_I is the distribution volume (L/kg). The expressions (3.34), (3.35), (3.36) model the insulin effect on glucose distribution ($x_1(t)$ in 1/min), glucose disposal ($x_2(t)$ in 1/min) and glucose production in the liver ($x_3(t)$ (1)), where $k_{a1,2,3}$(1/min), $k_{b1,2}$(L/(mU min^2)) and k_{b3}(L/(mU min)) define the individual insulin sensitivities $S_{i1} = k_{b1}/k_{a1}$, $S_{i2} = k_{b2}/k_{a2}$, and $S_{i3} = k_{b3}/k_{a3}$. The expressions (3.37) and (3.38) represent the glucose kinetics where $Q_1(t)$(mmol/kg) and $Q_2(t)$(mmol/kg) are the glucose masses in the accessible (measurable) and non-accessible compartment. Besides the insulin actions, the glucose masses are affected by the exchange between compartments, defined by the transfer rate k_{12} (1/min), the R_A to be estimated (mmol/kg), the endogenous glucose production EGP_0 (mmol/(kg min)) affected by the insulin, and the following two algebraic expressions:

$$F_{01c}(t) = \begin{cases} F_{01}, & \text{if } G(t) \geq 4.5 \text{ mmol/L} \\ F_{01}G(t)/4.5, & \text{otherwise} \end{cases}, \tag{3.39}$$

$$F_R(t) = \begin{cases} F_{R0}V_G(G(t) - 9), & \text{if } G(t) \geq 9 \text{ mmol/L} \\ 0, & \text{otherwise} \end{cases}, \tag{3.40}$$

$$G(t) = \frac{Q_1(t)}{V_G}, \tag{3.41}$$

where F_{01c} (mmol/(kg min)) is the glucose consumption of the central nervous system, while F_{01} represents the consumption at ambient glucose concentration, F_R(mmol/(kg min)) is the renal excretion of glucose in the kidneys. The output of the model is the blood glucose concentration $G(t)$ (mmol/L), where V_G(L/kg) is the glucose distribution volume (Hovorka et al. 2004).

The parameters and variables defining the Hovorka model are described in Table 3.3.

Table 3.3: Variables and parameters of the Hovorka model

Symbols	Description	Units
Variables		
$u(t)$	Subcutaneous insulin infusion	mU/(min kg)
$S_1(t)$	Insulin amount in the first subcutaneous compartment	µU kg
$S_2(t)$	Insulin amount in the second subcutaneous compartment	µU kg
$I(t)$	Insulin concentration in the plasma insulin compartment	mU L
$x_1(t)$	Insulin effect on glucose distribution	1/min
$x_2(t)$	Insulin effect on glucose disposal	1/min
$x_3(t)$	Insulin effect on hepatic glucose production	1/min
$Q_1(t)$	Glucose amount in the accessible compartment	mmol/kg
$Q_2(t)$	Glucose amount in non-accessible compartment	mmol/kg
$G(t)$	Plasma glucose concentration	mmol/L
$R_A(t)$	Meal rate of glucose appearance	mmol/(kg min)
$F_{01_c}(t)$	Glucose consumption of the central nervous system	mmol/(kg min)
$F_R(t)$	Renal glucose clearance	mmol/(kg min)
Parameters		

Table 3.3: (continued)

Symbols	Description	Units
τ_S	Absorption time constants related to the insulin movement between insulin compartments	min
k_e	Insulin clearance rate	1/min
V_I	Distribution volume	L/kg
k_{aj}	Deactivation rate constants ($j = \{1, 2, 3\}$)	1/min
k_{bj}	Activation rate constants ($j = \{1, 2\}$)	L/(mU min^2)
k_{b3}	Activation rate constant	L/(mU min)
k_{12}	Transfer rate of the glucose exchanged between the accessible and non-accessible compartment	1/min
EGP_0	Endogenous glucose production extrapolated to zero insulin concentration	mmol/(kg min)
F_{01}	Glucose consumption of the central nervous system at ambient glucose concentration	mmol/(kg min)
F_{R0}	Renal glucose clearance rate	1/min
V_G	Glucose distribution volume	L/kg

The model can be reparametrized in terms of the insulin sensitivities (Hovorka et al. 2002): $S_{i1} = \frac{k_{b1}}{k_{a1}}$, $S_{i2} = \frac{k_{b2}}{k_{a2}}$, and $S_{i3} = \frac{k_{b3}}{k_{a3}}$

3.3.3 Models identification

The simulation study included in this chapter was performed with UVa/Padova simulator; thus, the Hovorka and IVP model parameters must be identified for the virtual cohort of this simulator.

Two parameter sets were determined to analyze the influence of personalizing models: a population-based parameter set (or average model) and an individualized parameter set. The population value parameter set was identified from the average virtual adult in the simulator. The individualized parameter sets were obtained by identifying two of the most sensitive parameters for each of the ten virtual adults in the simulator. The remaining parameters of the personalized model were fixed to their corresponding values in the population-based parameter set. The identification method followed the guidelines of Garcia-Tirado et al. (2018): study the structural identifiability, rank the parameters according to their global sensitivity, and identify the parameters.

Analysis of the structural identifiability

The structural identifiability of a parameter determines if the available inputs and outputs of the system suffice to find a solution for the parameter under ideal conditions, namely, absence of noise, use of continuous-time data, and structural match between the process and the model (Walter et al. 1982; Chis et al. 2011). If a unique solution exists, then the parameter is structurally globally identifiable; if a finite number of different solutions exist, then the parameter is structurally locally identifiable; and, if infinite solutions are available, the parameter is structurally unidentifiable (Chis et al. 2011).

The concept of structural identifiability can also be extended to the full model (Walter et al. 1982): the model is structurally globally identifiable if, and only if, all its parameters are structurally globally identifiable, and the model is structurally locally identifiable if at least one of its parameters is structurally locally identifiable.

The structural identifiability analysis was performed with the software GenSSI 2.0 (Ligon et al. 2018). This software implements the Generating Series Approach (Walter et al. 1982) combined with the identifiability tableaus (Balsa-Canto et al. 2010) to carry out the analysis; the combination of these methods is a trade-off between computational cost, complexity, and information provided regarding other methods in the literature (Chis et al. 2011).

The Generating Series Approach considers the following non-linear system affine in the inputs:

$$\begin{cases} \dot{x}(t) = f(x(t), \theta) + g(x(t), \theta)u \\ y(t) = h(x(t), \theta) \end{cases} \tag{3.42}$$

where $\theta \in \mathbb{R}^{n_\theta}$ is the set of unknown parameters, $y(t) \in \mathbb{R}^{n_y}$ is the measurable output, $u(t) \in \mathbb{R}^{n_u}$ is the input, and $x(t) \in \mathbb{R}^{n_x}$ is the system state with $x_0(\theta)$ its initial condition ($x(t = 0)$). The terms $f(x(t), \theta)$, $g(x(t), \theta)$ and $h(x(t), \theta)$ are vector fields defined anywhere (Walter et al. 1982). Note that both the Hovorka and IVP models can be expressed as (3.42). The Generating Series Approach method computes the successive Lie derivatives of $h(x(t), \theta)$ along the fields $f(x(t), \theta)$ and $g(x(t), \theta)$ – e.g., $L_f h(x(t), \theta)$, $L_g h(x(t), \theta)$, $L_f L_f h(x(t), \theta)$, $L_g L_g h(x(t), \theta)$, $L_f L_g h(x(t), \theta)$, etc. — where the Lie derivative is defined as:

$$L_f h(x(t), \theta) = \sum_{i=1}^{n_x} f_i(x(t), \theta) \frac{\partial h(x(t), \theta)}{\partial x_i} \tag{3.43}$$

with f_i the i-th component of vector $f(\cdot)$.

Then, the successive Lie derivatives, evaluated at $t = 0$, are compared with the same successive Lie derivatives for a hypothetical system with known parameters (θ^*), resulting in the following non-linear system of equations:

$$\begin{cases} h(x(t),\theta)|_{t=0} = h(x(t),\theta^*)|_{t=0} \\ L_f h(x(t),\theta)|_{t=0} = L_f h(x(t),\theta^*)|_{t=0} \\ L_g h(x(t),\theta)|_{t=0} = L_g h(x(t),\theta^*)|_{t=0} \\ L_f L_f h(x(t),\theta)|_{t=0} = L_f L_f h(x(t),\theta^*)|_{t=0} \\ \vdots \end{cases} \tag{3.44}$$

where the right hand of each equation is assumed to be a known scalar since depends only on θ^*.

The compatibility of the system of equations (3.44) determines the structural identifiability of the system (Balsa-Canto et al. 2010; Chis et al. 2011). If the rank of the Jacobian of the successive Lie derivatives equals the number of parameters, then the system is at least locally identifiable. Since the minimum order of the required Lie derivative is unknown beforehand and depends on the knowledge of the initial condition, the rank condition is only sufficient. Of note, the described rank condition is very similar to the rank condition used to check the observability of non-linear systems, evincing the relationship between observability and identifiability (Villaverde et al. 2016).

The rank condition only determines the local identifiability of the model. To give insight into the global identifiability and the identifiability properties of each parameter, the non-linear system of equations must be solved. The identifiability tableau is a visual tool to reduce the complexity involved in the solution of this system of equations (Balsa-Canto et al. 2010). The tableau represents in a table the non-zero elements of the Jacobian of the Lie derivatives (rows) with respect to the considered parameters (columns), simplifying the detection of unidentifiable parameters (empty columns) and the selection of the most straightforward relations between parameters (rows with the lowest number of non-zero elements; Balsa-Canto et al. 2010).

Regarding the identifiability study of the Hovorka and IVP model, the considered measurements were the glucose and the plasma insulin, and the known input, the insulin infusion. The meal disturbance was deemed available to this analysis; hence parameters related to the carbohydrate absorption model were excluded from

the study. Note that the plasma insulin and meal disturbance are not available in a domiciliary setting, but they are considered in this analysis to compare the models under ideal conditions. In addition, the value of the body weight BW in the Hovorka model is known; thus, it was not considered in the analysis. The parameters included in the identifiability analysis were:

$$\theta^0_{IVP} = \{\tau_1,\, \tau_2,\, C_I,\, p_2,\, S_I,\, GEZI,\, EGP\}$$
$$\theta^0_{HOV} = \{F_{01},\, k_{12},\, EGP_0,\, \tau_S,\, V_i,\, k_e,\, k_{a1},\, S_{i1},\, k_{a2},\, S_{i2},\, k_{a3},\, S_{i3},\, V_G\}$$

The initial condition of the states, calculated using parameters from the literature (Kanderian et al. 2009; Hovorka et al. 2004), are given by

$$x_{0_{IVP}} \coloneqq \mathrm{col}\,(I_{SC}(0), I_P(0), I_{EFF}(0), G(0)) = \mathrm{col}\,(17.42, 15, 0.01, 119.59)$$
$$x_{0_{HOV}} \coloneqq \mathrm{col}\,(S_1(0), S_2(0), x_1(0), x_2(0), x_3(0), Q_2(0), Q_1(0)) =$$
$$= \mathrm{col}\,(1.066,\, 0.42,\, 5.4166,\, 0.0277,\, 0.0044,\, 0.2817,\, 4.933,\, 4.933)$$

and are expressed in the appropriate units described in Section 3.3.1 and Section 3.3.2 or Table 3.2 and Table 3.3.

Taking the above considerations, the GenSSI 2.0 determines that the parameters in θ^0_{IVP} are structurally globally identifiable; hence the model is also structurally globally identifiable. Figure 3.1 (left panel) represents the reduced-order identifiability tableau. All the columns contain at least a non-zero element (black rectangles), confirming that all the parameters are identifiable. Note, however, that the structural identifiability analysis is sensitive to the initial conditions. For example, if $I_P(0) = I_{SC}(0)$, then τ_1 and τ_2 were only locally identifiable (same column in the identifiability tableau). The right panel of Figure 3.1 illustrates this feature since, unlike the $I_P(0) \neq I_{SC}(0)$ (left panel), the parameter τ_2 cannot be solved directly from a unique coefficient of the generating series. The analysis of the identifiability also depends on which inputs are considered known. If the meal disturbance is excluded (and $I_P(0) \neq I_{SC}(0)$), then GenSSI 2.0 showed that only the subset $\{\tau_1,\, \tau_2,\, C_I\}$ was structurally globally identifiable while the remaining parameters were only locally identifiable.

The more significant number of parameters in the Hovorka model makes the structural identifiability analysis more challenging. The rows of the identifiability tableau (Figure 3.2) involved, in general, many parameters; hence solving this complex non-linear system was computationally expensive. Indeed, the execution had to be halted after 12 h in an Intel(R) Core(TM) i7-7700 CPU with two cores of 3.60 GHz and 12 GB of RAM running on MATLAB 2021b. As a result, the

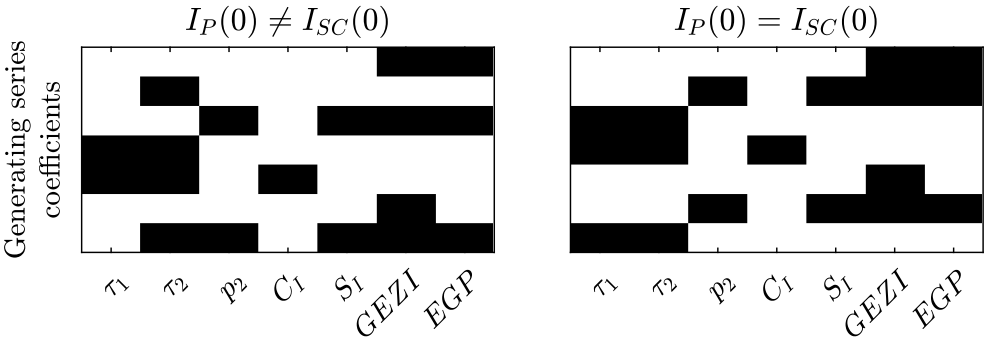

Figure 3.1: Reduced-order identifiability tableau for IVP model. The black rectangles represent a non-zero element in the Jacobian of the Lie derivatives, i.e., the corresponding parameter in the columns appears in the Lie derivative associated with the corresponding coefficient in the row. The analysis considered the meal disturbance, the plasma insulin, the insulin infusion, and the glucose as known variables. Two cases are studied: (left) the subcutaneous and plasma insulin have different initial conditions (right) the subcutaneous and plasma insulin have equal initial conditions.

software only computed the rank but it could not solve the complete system of equations, a step needed to assess the global identifiability. The software only showed that V_G is globally identifiable (the only parameter directly related to a coefficient in Figure 3.2 without depending on other parameters). The remaining parameters are structurally locally identifiable since the rank of the Jacobian of the Lie derivatives coincides with the number of parameters in θ^0_{HOV} (no empty columns in Figure 3.2). Therefore, the Hovorka model is only structurally locally identifiable.

Global sensitivity and parameters ranking

For local structural identifiable or unidentifiable systems, the structural global identifiability property can be recovered by fixing parameters to values in the literature (Balsa-Canto et al. 2010). It seems logical to fix those parameters influencing the outputs the least. Studying the influence of the parameters is precisely the goal of the sensitivity analysis.

The most widely used approach for sensitivity analysis is to numerically compute the derivative of the output regarding the parameters at a specific location of the parameter space, i.e., $\hat{\theta}$, and a given discrete-time t_s, that is (Garcia-Tirado et al. 2018; Balsa-Canto et al. 2010):

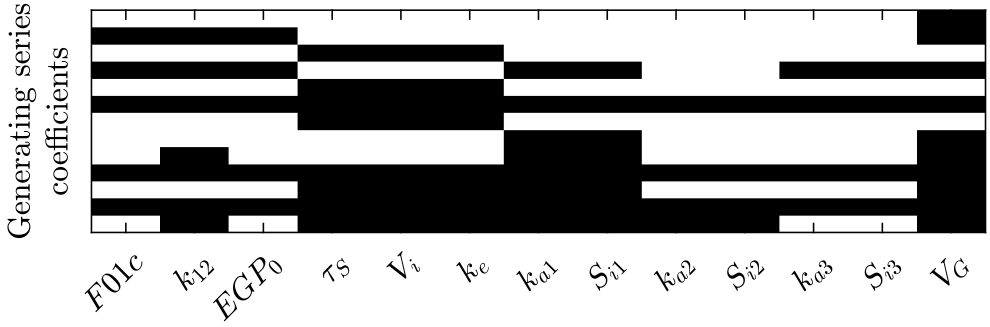

Figure 3.2: Reduced-order identifiability tableau for Hovorka model. The black rectangles represent a non-zero element in the Jacobian of the Lie derivatives, i.e., the corresponding parameter in the columns appears in the Lie derivative associated with the corresponding coefficient in the row. The analysis considered the meal disturbance, the plasma insulin, the insulin infusion, and the glucose as known variables.

$$S_p^o(t_s) = \left.\frac{\partial y_o}{\partial \theta_p}\right|_{\theta=\hat{\theta}, y_o=y_o(t,\hat{\theta})} \tag{3.45}$$

for $p = \{1, \cdots, n_\theta\}$ and $o = \{1, \cdots, n_y\}$. To avoid differences of magnitude in the parameters impacting the analysis, the sensitivities in (3.45) were normalized with the actual parameter value $\hat{\theta_p}$ and the actual output $y_j o(t_s)$ at the corresponding discrete time, as follows:

$$s_p^o(t_s) = \frac{\hat{\theta}_p}{y_j(t_s)} S_p^o(t_s) \tag{3.46}$$

The sensitivities in (3.46) already characterizes the influence of the parameters on the outputs; thus, they can be used, for example, to rank the parameters (Brun et al. 2001). However, the resulting ranking is only valid in the neighborhood of $\hat{\theta}$ (local sensitivity analysis). To expand the validity to the feasible space of θ, the analysis must be repeated for different $\hat{\theta}$. Balsa-Canto et al. (2010) suggested using the Latin hypercube (Iman et al. 1981) to sample $\hat{\theta}$ because it generally requires fewer samples than Monte Carlo sampling to explore the overall parameter space.

Besides $\hat{\theta}$, the value of the model inputs may also impact the sensitivities in (3.46) and, consequently, the parameter ranking. Balsa-Canto et al. (2010) suggested repeating the sensitivity analysis with different input profiles or experiments to

reduce the influence of the model inputs on the ranking. Therefore, the global parameter ranking must consider the relative sensitivities at n_{ts} discrete times, for n_{ps} samples of the parameters $\hat{\theta}$, and for n_e experiments. Balsa-Canto et al. (2010), which expanded the initial proposal of Brun et al. (2001), summarized this information in the mean square sensitivity measure (δ_p^{msqr}) defined as follows:

$$\delta_p^{msqr} = \frac{1}{n_e n_{ps} n_{ts} n_y} \sqrt{\sum_{ps=1}^{n_{ps}} \sum_{e=1}^{n_e} \sum_{o=1}^{n_y} \sum_{ts=1}^{n_{ts}} \left(s_p^{e,o,ps}(t_s^{e,o,ps})\right)^2} \tag{3.47}$$

where $s_p^{e,o,ps}(t_s^{e,o,ps})$ corresponds to the relative parametric sensitivity of the observable y_o under the experiment e and the parameter sampling ps at the discrete-time $t_s^{e,o,ps}$.

The above methodology (calculation of sensitivities, normalization, parameter sampling, and ranking metric) is applied to rank the parameters of the Hovorka and IVP models through the AMIGO2 MATLAB toolbox (Balsa-Canto et al. 2016). The glucose was the only considered measurable ($n_y = 1$), whereas the insulin infusion and the meal disturbance were the inputs. Seven input profiles ($n_e = 7$) were considered in the analysis as in Garcia-Tirado et al. (2018); they were generated from 1-day simulations ($n_{ts} = 288$ 5-min samples) of three meals with the modified version of the UVa/Padova simulator. The analysis included the same parameters considered in the structural identifiability. The bounds of the parameters required for the Latin hypercube sampling were calculated from values provided in the literature (Kanderian et al. 2009, Table 1; Hovorka et al. 2002, Table 1); they are shown in Table 3.4 and Table 3.5. The number of samples in the Latin hypercube was 100 000 ($n_{ps} = 100\,000$). Combination of parameters within previous bounds may lead to unfeasible glucose trajectories; thus, all samples resulting in a glucose value lower than 32 mg/dL and greater than 450 mg/dL were discarded when calculating δ^{msqr}.

Table 3.4: Nominal parameters and bounds of the IVP model used in the global sensitivity analysis and identification

Parameter	Nominal value	Lower bound	Upper bound
τ_1 (min)	$7.05 \cdot 10^1$	0	$2.103 \cdot 10^2$
C_I (mL/min)	$1.267 \cdot 10^3$	0	$3.894 \cdot 10^3$
τ_2 (min)	$4.44 \cdot 10^1$	0	$1.448 \cdot 10^2$
p_2 (min)	$1.145 \cdot 10^{-2}$	0	$3.418 \cdot 10^{-2}$
S_I (mL/(µU min))	$5.503 \cdot 10^{-4}$	0	$2.483 \cdot 10^{-3}$
$GEZI$ (1/min)	$2.346 \cdot 10^{-3}$	0	$1.340 \cdot 10^{-2}$
EGP (mg/(dL min))	1.152	0	5.046

Table 3.5: Nominal parameters and bounds of the Hovorka model used in the global sensitivity analysis and identification

Parameter	Nominal	Lower bound	Upper bound
F_{01} (mmol/(kg min))	$9.7 \cdot 10^{-3}$	$9.7 \cdot 10^{-4}$	$1.843 \cdot 10^{-2}$
F_{R0} (1/min)	$3 \cdot 10^{-3}$	$3 \cdot 10^{-4}$	$3 \cdot 10^{-2}$
k_{12} (1/min)	$6.6 \cdot 10^{-2}$	$6.6 \cdot 10^{-3}$	$1.254 \cdot 10^{-1}$
EGP_0 (mmol/(kg min))	$1.61 \cdot 10^{-2}$	$1.61 \cdot 10^{-3}$	$3.059 \cdot 10^{-2}$
τ_S (min)	$5.5 \cdot 10^1$	5.5	$1.045 \cdot 10^2$
V_I (L/kg)	$1.2 \cdot 10^{-1}$	$1.2 \cdot 10^{-2}$	$2.28 \cdot 10^{-1}$
k_e (1/min)	$1.38 \cdot 10^{-1}$	$1.38 \cdot 10^{-2}$	$2.622 \cdot 10^{-1}$
k_{a1} (1/min)	$6 \cdot 10^{-3}$	$6 \cdot 10^{-4}$	$1.14 \cdot 10^{-2}$
k_{a2} (1/min)	$6 \cdot 10^{-2}$	$6 \cdot 10^{-3}$	$1.14 \cdot 10^{-1}$
k_{a3} (1/min)	$3 \cdot 10^{-2}$	$3 \cdot 10^{-3}$	$5.7 \cdot 10^{-2}$
S_{i1} (L/(mU min))	$5.12 \cdot 10^{-3}$	0	$5.326 \cdot 10^{-2}$
S_{i2} (L/(mU min))	$8.2 \cdot 10^{-4}$	0	$1.258 \cdot 10^{-2}$
S_{i3} (L/mU)	$5.202 \cdot 10^{-2}$	0	$5.113 \cdot 10^{-1}$
V_G (L/kg)	$1.6 \cdot 10^{-1}$	$1.6 \cdot 10^{-2}$	$3.04 \cdot 10^{-1}$

The result of the global ranking is shown in Figure 3.3. Garcia-Tirado et al. (2018) classify the first parameters accumulating more than 80 % of δ^{msqr} (green bars in Figure 3.3) as sensitive parameters, the last parameters with less than 1 % (red bars) as insensitive parameters, and the remaining parameters (blue bars) as mildly sensitive.

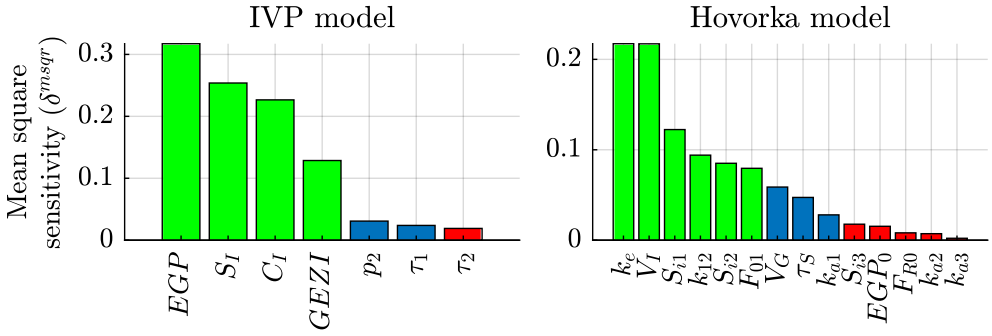

Figure 3.3: Global ranking of parameters in decreasing order of mean square sensitivity measure ($\delta^{\mathbf{msqr}}$). Green bars refer to the first parameters gathering more than the 80 % (sensitive parameters), red bars correspond to the last parameters summing less than 1 % (insensitive parameters), and blue bars are related to the mildly sensitive parameters.

Identification

The union of sensitive and mildly sensitive subsets, that is,

$$\theta^1_{IVP} = \{\tau_1,\, C_I,\, p_2,\, S_I,\, GEZI,\, EGP\}$$
$$\theta^1_{HOV} = \{F_{01},\, k_{12},\, \tau_S,\, V_I,\, k_e,\, k_{a1},\, S_{i1},\, S_{i2},\, V_G\}$$

results in a suitable parameter selection for average model identifications since it contains the parameters most impacting the glucose (Garcia-Tirado et al. 2018). The insensitive parameters were fixed to the nominal values in Table 3.4 and Table 3.5. Recall that analysis of the structural identifiability for subset θ^0_{HOV} resulted in locally structurally identifiability. Since θ^1_{HOV} is a subset of θ^0_{HOV}, more chances exist that the subset θ^1_{HOV} was globally structurally identifiable. Therefore, the structural identifiability analysis was repeated for the above subsets, θ^1_{HOV}, concluding globally structurally identifiability. Since the θ^0_{IVP} already was globally structurally identifiable, the subset θ^1_{IVP} also is.

Regarding the parameters for the personalized models, the subsets $\{S_I,\, C_I\}$ (IVP model) and $\{V_i,\, S_{i1}\}$ (Hovorka model) were selected because they are the most sensitive gains of the corresponding models.

The identification consisted of two optimizations. First, the parameters related to the insulin subsystem were identified by minimizing the Normalized Root Mean-Squared Error (NRMSE) of the plasma insulin, taking the insulin infusion as an

input. Then, the parameters of the insulin effect and glucose-related states were identified by minimizing the NRMSE of the glucose measurement, taking the meal disturbance, i.e., the meal rate of glucose appeareance, and the plasma insulin as inputs. The NRMSE is defined by:

$$NRMSE = \left(\sqrt{\frac{\sum_{i=1}^{N} \left(x^i_{model} - x^i_{UVa} \right)^2}{N}} \right) \cdot \left(\frac{1}{x^{i,max}_{UVa} - x^{i,min}_{UVa}} \right), \tag{3.48}$$

where x^i_{UVa} represents the actual measurement at sample i, whereas the superscripts max and min refer to the maximum and minimum values of these measurements, respectively. x^i_{model} denotes the glucose or plasma insulin obtained by the IVP or Hovorka models. This two-step optimization procedure allows more accurate identification of the insulin pharmacokinetics compared to a single optimization considering insulin and glucose as measurable signals (Kanderian et al. 2009). The inputs for the optimization problems – glucose, plasma insulin, insulin infusion, and meal rate of glucose appearance – were simulated with the UVa/Padova simulator under a 1-day scenario with three meals using the average adult to identify the average model and the corresponding virtual adult in the cohort to identify the personalized models. Of note, the full knowledge of these inputs is impractical for real applications, but they were used in this study to ensure accurate identification of the parameters and, consequently, reduce the influence of the identification error over the effect of the model structure on the observer performance. In addition, the meal rate of glucose appearance has been chosen as an input to avoid identifying the parameters of a meal model.

The optimization problems were solved with the genetic algorithm of the MATLAB Global Optimization Toolbox (MathWorks 2022). The algorithm was configured with its default settings. The bounds of the parameters required for the optimization algorithm coincide with those of the sensitivity analysis (Table 3.4 and Table 3.5).

Table 3.6 and Table 3.7 include the identified parameters for the IVP and the Hovorka models, respectively. A new 3-meal scenario was simulated for the average subject and the ten adults in the simulator cohort to assess the identification accuracy. The simulation with the average adult reveals that both average models fit moderately well the glucose and the plasma insulin: the Hovorka model

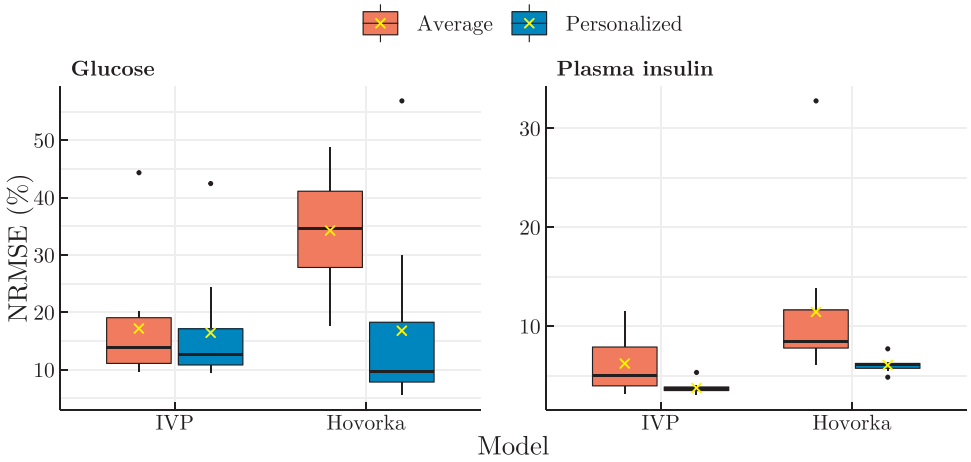

Figure 3.4: Results of the Normalized Root Mean-Squared Error (NRMSE) for the average and personalized models within the ten virtual adults.

outperforms the NRMSE compared to the IVP model (6.32 % vs. 9.87 %), but its accuracy is lower in the plasma insulin fit (6.38 % vs. 3.69 %).

However, the fit of the average models worsens when these models are used to predict the behavior of the ten virtual adults in the simulator (Figure 3.4). The most remarkable degradation observed in the Hovorka model may be because of an over-parametrization of the insulin effect. The Hovorka model considers a third compartment to model the insulin effect – the insulin effect on glucose transport x_1 –, absent in the simulator used to generate the virtual data (Dalla Man et al. 2014). Indeed, this compartment is related to S_{i1}, a sensitive parameter that was chosen to be individualized. This over-parametrization might lead to overfitting problems and, consequently, more sensitivity against inter-patient variability.

Model individualization reduces the variability of the glucose fit. It also dilutes the differences between both models for the glucose prediction: the difference in means, estimated by a paired t-test, is only -0.0036 (-0.0504, 0.0432) % (mean (95%-interval confidence)), a negligible discrepancy that neither proved to be statistically significant.

The individualization also outperforms the average models in the plasma insulin fit, reducing the mean value and the variability.

Table 3.6: Identified parameters of IVP model

Parameter	Average patient	Individual
S_I (mL/(µU min))	$7.03 \cdot 10^{-4}$	$6.95 \cdot 10^{-4}$ $6.19 \cdot 10^{-4}$ $6.34 \cdot 10^{-4}$ $7.88 \cdot 10^{-4}$ $7.25 \cdot 10^{-4}$ $4.59 \cdot 10^{-4}$ $6.77 \cdot 10^{-4}$ $6.79 \cdot 10^{-4}$ $7.35 \cdot 10^{-4}$ $7.74 \cdot 10^{-4}$
EGP (mg/(dL min))	1.49	1.49
C_I (mL/min)	$1.11 \cdot 10^3$	$1.16 \cdot 10^3$ $1.13 \cdot 10^3$ $1.28 \cdot 10^3$ $1.02 \cdot 10^3$ $9.31 \cdot 10^2$ $1.15 \cdot 10^3$ $1.09 \cdot 10^3$ $1.09 \cdot 10^3$ $9.06 \cdot 10^3$ $1.18 \cdot 10^3$
$GEZI$ (1/min)	$3.03 \cdot 10^{-8}$	$3.03 \cdot 10^{-8}$
τ_1 (min)	52.71	52.71
p_2 (1/min)	$2.85 \cdot 10^{-2}$	$2.85 \cdot 10^{-2}$

The values of the fixed parameters are in Table 3.4.

Table 3.7: Identified parameters of the Hovorka model

Parameter	Average patient	Individual
τ_s (min)	43.00	43.00
k_e (1/min)	$1.36 \cdot 10^{-1}$	-
V_i (L/kg)	$1.18 \cdot 10^{-1}$	$1.09 \cdot 10^{-1}$ $1.04 \cdot 10^{-1}$ $1.36 \cdot 10^{-1}$ $1.16 \cdot 10^{-1}$ $1.05 \cdot 10^{-1}$ $1.19 \cdot 10^{-1}$ $1.74 \cdot 10^{-1}$ $8.41 \cdot 10^{-2}$ $1.00 \cdot 10^{-1}$ $1.09 \cdot 10^{-1}$
V_G (L/kg)	$2.22 \cdot 10^{-2}$	$2.22 \cdot 10^{-2}$
k_{12} (1/min)	$9.11 \cdot 10^{-2}$	$9.11 \cdot 10^{-2}$
S_{i1} (L/(mU min))	$2.13 \cdot 10^{-3}$	$2.20 \cdot 10^{-3}$ $1.65 \cdot 10^{-3}$ $1.84 \cdot 10^{-3}$ $3.02 \cdot 10^{-3}$ $2.62 \cdot 10^{-3}$ $9.45 \cdot 10^{-4}$ $1.90 \cdot 10^{-3}$ $2.52 \cdot 10^{-3}$ $2.42 \cdot 10^{-3}$ $2.35 \cdot 10^{-3}$
S_{i2} (L/(mU min))	$1.02 \cdot 10^{-3}$	$1.02 \cdot 10^{-3}$
k_{a1} (1/min)	$2.35 \cdot 10^{-3}$	$2.35 \cdot 10^{-3}$
F_{01} (mmol/(kg min))	$1.28 \cdot 10^{-2}$	$1.28 \cdot 10^{-2}$

The values of the fixed parameters are in Table 3.5.

Given the superiority of the personalized models, the observers described in Section 3.2 were designed with these models.

3.4 Design and tuning of the observers

The observers described in Section 3.2 are applied to the models of Section 3.3 to estimate the rate of glucose appearance. Details about their design, tuning, and implementation are given in this section.

3.4.1 Kalman filters

As stated in Section 3.2.1, a simple approach to estimate a disturbance $d[k]$ with a KF is to extend the state with $d[k] = d[k-1] + w_d[k]$, where $w_d[k]$ is a white, median-zero noise. In the application considered in this chapter, i.e., the estimation of the meal rate of glucose appearance, this assumption of slowly varying disturbance may be inappropriate, especially in the surroundings of the meal onset. An alternative would be to augment the state with a model describing meal absorption. Nevertheless, current meal models (see a review by Fathi et al. (2018)) ignore the significant effects of macronutrients other than carbohydrates on meal absorption dynamics. Furthermore, augmenting the state with a meal model would increase the dimensions of the covariance matrices, making their tuning more challenging. Therefore, in this chapter, the states have been extended with $d[k] = d[k-1] + w_d[k]$ to design the KFs.

Since the IVP and Hovorka models contain nonlinearities, the Kalman Filter might be unsuitable for them. Although one could linearize the augmented model (3.5) or apply more advanced Kalman filters (such as Extended Kalman Filter or Unscented Kalman Filter; Szalay et al. 2014), in this chapter, the nonlinearities are hidden in a Quasi Linear Parameter Varying (qLPV) representation, which allows applying the classical KF described in Section 3.2.1 directly. LPV systems have the form of a classical linear time invariant system but with time-dependent matrices (Kovács 2017) as represented in:

$$\begin{cases} \dot{\overline{x}}(t) = \overline{A}(\mathbf{p}(t))\overline{x}(t) + \overline{B}(\mathbf{p}(t))u(t) \\ y(t) = \overline{C}(\mathbf{p}(t))\overline{x}(t) \end{cases} \tag{3.49}$$

where the parameter vector $\mathbf{p}(t) = [p_1(t) \dots p_R(t)]$ consists of the scheduling parameters $p_i(t)$. $\mathbf{p}(t) \in \mathbf{\Omega}^R \subset \mathbb{R}^R$ is an R-dimensional real vector within the set $\mathbf{\Omega} = [p_{1,min}, p_{1,max}] \times [p_{2,min}, p_{2,max}] \times \ldots \times [p_{R,min}, p_{R,max}]$. When the scheduling

parameters depend on states of the model, the system is referred as qLPV. Either the IVP or the Hovorka model admit the qLPV representation; the corresponding state matrices are given as follows:

- **IVP model**. Selecting $\mathbf{p}(t) = [p(t)] = [G(t)]$ as scheduling parameter leads to the following qLPV representation:

$$\overline{A}(\mathbf{p}(t)) = \begin{bmatrix} -GEZI + \frac{EGP}{p(t)} & -p(t) & 0 & 0 & 1 \\ 0 & -p_2 & p_2 S_I & 0 & 0 \\ 0 & 0 & -\frac{1}{\tau_2} & \frac{1}{\tau_2} & 0 \\ 0 & 0 & 0 & -\frac{1}{\tau_1} & 0 \\ 0 & 0 & 0 & 0 & 0 \end{bmatrix}, \tag{3.50}$$

$$\overline{B} = \begin{bmatrix} 0 & 0 & 0 & \frac{1}{\tau_1 C_I} & 0 \end{bmatrix}^T, \tag{3.51}$$

$$\overline{C} = \begin{bmatrix} 1 & 0 & 0 & 0 & 0 \end{bmatrix}, \tag{3.52}$$

  where the 5th state variable is the $d(t) \coloneqq R_A(t)$, with $\dot{R}_A(t) = 0$

- **Hovorka model**. Taking:

$$\mathbf{p}(t) = \begin{bmatrix} \frac{EGP_0 - F_{01c}(t) - F_R(t)}{Q_1(t)} & Q_1(t) & Q_2(t) \end{bmatrix}$$

  the qLPV representation is as follows:

$$\overline{A}(\mathbf{p}(t)) = \begin{bmatrix} p_1(t) & k_{12} & 0 & -p_2(t) & 0 & -EGP_0 & 0 & 0 & 1 \\ 0 & -k_{12} & 0 & p_2(t) & -p_3(t) & 0 & 0 & 0 & 0 \\ 0 & 0 & -k_e & 0 & 0 & 0 & 0 & \frac{1}{\tau_S V_I} & 0 \\ 0 & 0 & k_{b1} & -k_{a1} & 0 & 0 & 0 & 0 & 0 \\ 0 & 0 & k_{b2} & 0 & -k_{a2} & 0 & 0 & 0 & 0 \\ 0 & 0 & k_{b3} & 0 & 0 & -k_{a3} & 0 & 0 & 0 \\ 0 & 0 & 0 & 0 & 0 & 0 & -\frac{1}{\tau_S} & 0 & 0 \\ 0 & 0 & 0 & 0 & 0 & 0 & \frac{1}{\tau_S} & -\frac{1}{\tau_S} & 0 \\ 0 & 0 & 0 & 0 & 0 & 0 & 0 & 0 & 0 \end{bmatrix}, \tag{3.53}$$

$$\overline{B} = \begin{bmatrix} 0 & 0 & 0 & 0 & 0 & 0 & 1 & 0 & 0 \end{bmatrix}^T, \tag{3.54}$$

$$\overline{C} = \begin{bmatrix} \frac{1}{V_G} & 0 & 0 & 0 & 0 & 0 & 0 & 0 & 0 \end{bmatrix}, \tag{3.55}$$

where the 9th state variable corresponds to the $R_A(t)$. Note that the selected scheduling parameters $\mathbf{p}(t)$ depends on the unmeasurable state $Q_2(t)$; hence the estimations given by the KF would be used instead.

To implement the KFs, the system (3.49) must be discretized. The explicit Euler discretization of the (3.49) is given by:

$$\overline{A}\big[\mathbf{p}[k]\big] = I + T_s\overline{A}\big(\mathbf{p}(kT_s)\big), \tag{3.56}$$

$$\overline{B}\big[\mathbf{p}[k]\big] = T_s\overline{B}\big(\mathbf{p}(kT_s)\big), \tag{3.57}$$

$$\overline{C}\big[\mathbf{p}[k]\big] = \overline{C}\big(\mathbf{p}(kT_s)\big), \tag{3.58}$$

where the parentheses indicate the continuous LPV representations of state-space matrices, while the brackets are the discretized ones of the corresponding model.

The matrices (3.56)–(3.58) form the augmented system described in (3.5); thus, the KF can be applied to estimate the states and the meal disturbance.

Observability of the augmented systems

Recall from Section 3.2.1 that the pair $\big(\overline{A}\big[\mathbf{p}[k]\big], \overline{C}\big[\mathbf{p}[k]\big]\big)$ observability is required for the observers convergence (Zhang et al. 2021). Given the time-varying characteristics of the A matrices, the standard observability rank condition from linear time invariant systems must hold for every iteration, i.e., the pair $\big(\overline{A}\big[\mathbf{p}[k]\big], \overline{C}\big[\mathbf{p}[k]\big]\big)$ is observable if the condition

$$\operatorname{rank}\left(\mathcal{O}_k\right) = n_{\overline{x}}\,, \tag{3.59}$$

with

$$\mathcal{O}_k = \begin{bmatrix} \overline{C}\big[\mathbf{p}[k]\big] \\ \overline{C}\big[\mathbf{p}[k+1]\big] \cdot \overline{A}\big[\mathbf{p}[k] \\ \overline{C}\big[\mathbf{p}[k+2]\big] \cdot \overline{A}\big[\mathbf{p}[k+1] \cdot \overline{A}\big[\mathbf{p}[k] \\ \vdots \\ \overline{C}\big[\mathbf{p}[k+n_{\overline{x}-1}]\big] \cdot \overline{A}\big[\mathbf{p}[k+n_{\overline{x}-2}] \cdots \overline{A}\big[\mathbf{p}[k+1]\overline{A}\big[\mathbf{p}[k] \end{bmatrix} \tag{3.60}$$

holds for every $k \geq 0$ (Witczak et al. 2017). Hence, the two KFs – one for the IVP model and the other for the Hovorka model – were simulated with the UVa/Padova

simulator. For each discrete iteration, the (3.59) was evaluated. In all the iterations, the observability condition hold. Therefore, the pair $(\overline{A}[\mathbf{p}[k]], \overline{C}[\mathbf{p}[k]])$ was observable for the two augmented models.

Optimization-based tuning [1]

The two parameters to tune in the KFs are the variance of the CGM reading noise, $\overline{R}$, and the covariance matrix of the process noise, $\overline{Q}$. The parameter $\overline{R}$ can be directly computed from the glucose measurement. In this chapter, this parameter is set to $\overline{R} = 20\,(\mathrm{mg/dL})^2$ corresponding to the approximated variance observed within the steady-state of a simulation of the average subject in the academic version of the UVa/Padova simulator (Dalla Man et al. 2014).

Unlike $\overline{R}$, $\overline{Q}$ cannot be directly related to a measurable feature. Therefore, this parameter is usually tuned by trial and error (e.g., Kovacs et al. 2019). To lessen the human factor and homogenize the tuning method among the two KFs –a KF designed for the IVP model and another designed for the Hovorka –, an optimization-based tuning has been employed instead. As in similar works in the field using Kalman-like filters (e.g., Patek et al. 2007; Toffanin et al. 2013; Pereda et al. 2016; Xu et al. 2021; Acharya et al. 2022), the $\overline{Q}$ covariance matrix was considered diagonal. Although selecting a diagonal $\overline{Q}$ implies that the process noises are independent, it helps simplify the optimization tuning in two aspects: 1) reducing the number of parameters (with respect to a $\overline{Q}$ matrix where all its elements are non-zero) and 2) avoiding explicitly checking if the eigenvalues are positive to ensure the positiveness of $\overline{Q}$ (it suffices to ensure that the elements are positive if Q is diagonal). The non-zero elements of $\overline{Q}$ have been tuned using the MATLAB genetic algorithm (MathWorks 2022). The lower bounds of the diagonal elements were set to zero. The upper bound of each diagonal element corresponds to the lowest value that makes the filter converge to the Continuous Glucose Monitor (CGM) reading when the remaining elements of the diagonal are zero. The cost functions were specific for each model; they are given by:

[1] The content of this chapter resulted from a research stay at the Óbuda University (Budapest). In the research stay, another PhD candidate, Máté Siket, participated in the work, being the tuning of the KFs his main contribution. Therefore, in this section, I have only included a summary of the tuning procedure and more information can be found in a joint article (Sala-Mira et al. 2021).

$$J_{IVP} = k_{osc}(e_G + e_{I_{EFF}} + e_{I_p} + e_{I_{sc}} + e_{R_A}) \tag{3.61}$$

$$\begin{aligned} J_{Hovorka} = k_{osc}\Big(&\frac{9}{5}(e_G + e_{I_P} + e_{R_A}) \\ &+ \frac{3}{5}(e_{Q_2} + e_{x_1} + e_{x_2} + \\ &+ e_{x_3} + e_{S_1} + e_{S_2})\Big) \end{aligned} \tag{3.62}$$

where e denotes the NRMSE between the estimated state and the simulated state. The subscripts represent the corresponding states of the models. The weights $\frac{9}{5}$ and $\frac{3}{5}$ are set so that the error in $G(t)$, $I_P(t)$, and $R_A(t)$ yields a similar cost value in the Hovorka and the IVP model independently of their corresponding system order. Moreover, the coefficient k_{osc} reduces the overfitting by penalizing the oscillations. It is defined as:

$$x_{osc} = \sum_{i=3}^{n} \mid sgn(x[i] - x[i-1]) - sgn(x[i-1] - x[i-2]) \mid, \tag{3.63}$$

$$k_{osc} = \begin{cases} 10, & \text{if } x_{osc} > threshold \\ 1, & \text{otherwise} \end{cases} \tag{3.64}$$

where x is the state vector of the applied models, n is the number of samples, and the thresholds were dependent on the direction changes of the reference trajectory.

The simulated states in the above cost functions were simulated from IVP and the Hovorka models with an increment of 30 % in the model parameters of the observer. The tuning scenario was of 24 h with three meals: 45 g at 7 h, 70 g at 14 h, and 60 g at 21 h. The insulin delivery corresponded to an insulin-bolus (open-loop) therapy. No sensor noise was considered.

A summary of the KFs parameters is summarized in Table 3.8. Remark that the glucose and the meal rate of glucose appearance are expressed in different units between the models, which explains the magnitude discrepancies in the covariance matrices.

Table 3.8: Parameters of the Kalman Filters

Model	Q	R
IVP	$\mathrm{diag}\left(18.0 \cdot 10^3, 2.9 \cdot 10^{-6}, 5.0, 50.0, 18.0 \cdot 10^3\right)$	20 mg/dL
Hovorka	$\mathrm{diag}\left(581.4 \cdot 10^{-3}, 183.1 \cdot 10^{-3}, 12.5 \cdot 10^{-6}, 5.0 \cdot 10^{-3}, 0, 18.6 \cdot 10^{-3}, 996.7 \cdot 10^{-6}, 915.0 \cdot 10^{-6}, 10.0\right)$	1.1 mmol/L

$\mathrm{diag}(\cdot)$ denotes a diagonal matrix construction, e.g., $\mathrm{diag}(a, b) = \begin{bmatrix} a & 0 \\ 0 & b \end{bmatrix}$.

3.4.2 Sliding mode observers

For both models, the IVP model and the Hovorka model, the number of outputs ($n_y = 1$, the glucose) coincides with the number of disturbances ($n_d = 1$, the rate of glucose appearance); thus, the rank condition in (3.12) holds, and the models admit the system given by (3.13). The transformation only reorders the state variables hence preserving their physiological meaning. The resulting transformation is shown below:

- **IVP model**. Taking $\bar{x}(t) \coloneqq \mathrm{col}\left(I_{SC}(t), I_P(t), I_{EFF}(t), G(t)\right)$, $d(t) \coloneqq R_A(t)$, and $y(t) \coloneqq G(t)$ the equations of the IVP model can be expressed as (3.13) with the following matrices:

$$\begin{gathered} A_{11} := \begin{bmatrix} -1/\tau_1 & 0 & 0 \\ 1/\tau_2 & -1/\tau_2 & 0 \\ 0 & p_2 S_I & -p_2 \end{bmatrix}, \begin{matrix} A_{12} = A_{21}^T := 0_{3\times 1} \\ A_{22} := -GEZI \end{matrix} \\ \phi_1(t) := \begin{bmatrix} \frac{u(t)}{\tau_1 C_I} \\ 0_{2\times 1} \end{bmatrix}, \phi_2(t) := EGP - G(t) I_{EFF}(t), \\ C_2 = D_2 = 1 \end{gathered} \tag{3.65}$$

- **Hovorka model.** For $d(t) := R_A(t)$, $y(t) := G(t)$, and $x(t) \coloneqq \mathrm{col}\left(S_1(t), S_2(t), x_1(t), x_2(t), x_3(t), Q_2(t), Q_1(t)\right)$, the equations of the Hovorka model can be converted into (3.13) with:

$$
\begin{aligned}
A_{11} &= \begin{bmatrix}
-\frac{1}{\tau_s} & 0 & 0 & 0 & 0 & 0 & 0 \\
\frac{1}{\tau_s} & -\frac{1}{\tau_s} & 0 & 0 & 0 & 0 & 0 \\
0 & \frac{1}{\tau_s V_I} & -k_e & 0 & 0 & 0 & 0 \\
0 & 0 & k_{b1} & -k_{a1} & 0 & 0 & 0 \\
0 & 0 & k_{b2} & 0 & -k_{a2} & 0 & 0 \\
0 & 0 & k_{b3} & 0 & 0 & -k_{a3} & 0 \\
0 & 0 & 0 & 0 & 0 & 0 & -k_{12}
\end{bmatrix} \\
A_{21} &:= \begin{bmatrix} 0_{1\times 5} & -EGP_0 & k_{12} \end{bmatrix}, A_{12} := 0_{7\times 1}, A_{22} := 0 \\
\phi_1(t) &:= \begin{bmatrix} u(t) \\ 0_{5\times 1} \\ x_1(t)Q_1(t) - x_2(t)Q_1(t) \end{bmatrix}, C_2 := 1/V_G, D_2 := 1 \\
\phi_2(t) &:= -F_{01}^c(t) - x_1(t)Q_1(t) - F_R(t) + EGP_0
\end{aligned}
\tag{3.66}
$$

Another consequence of $n_y = n_d = 1$ is that L^0 in (3.15) is undefined, i.e., $L^0 \in \emptyset$. As a result, the matrix L is defined as $L = 0_{1\times n_x}$ ($n_x = 4$ for the IVP model and $n_x = 8$ for the Hovorka model), which results in an identity transformation matrix T in (3.15). Since the eigenvalues of A_{11}, which coincide with the invariant zeros of (A, D, C), lie in the left half plane, $A_{11} + LA_{21}$ is stable and the inequality (3.21) holds. The drawback is that no degree of freedom exists to modify the dynamics of the error in the sliding mode, i.e., $e_1(t)$, being exclusively imposed by A_{11}.

The design of the terms K and $k(u(t), z(t), \hat{z}(t))$ must ensure that $e_y(t)$ converges to zero in finite time. About K, plugging $L = 0_{1\times n_x}$ and the corresponding A_{21} and A_{22} of the models into the condition (3.22) results in the following criteria to design K:

$$
\begin{aligned}
K &\leq GEZI \quad \text{for the IVP model} \\
K &\leq 0 \quad\quad\;\; \text{for the Hovorka model}
\end{aligned}
\tag{3.67}
$$

Thus, $K = 0$ is a suitable value for this parameter.

Regarding $k(t)$, the expression (3.23) would motivate an adaptive $k(t)$ depending on $w(t)$, an upper bound for $\|e_1\|$, and $\rho(y, u, t)$, an upper bound of the disturbance. An adaptive $k(t)$ is appealing because it would alleviate the problem of chattering – oscillations in the observed states occurring after discretization because of a limited sampling rate (see Section 3.4.2) – by reducing the amplitude of the oscillations when the uncertainty size is small. Unfortunately, the adaptive $k(t)$ inspired

from (3.23) could not be implemented directly since no straightforward method to set $w(0)$ appears in Yan et al. (2007) or Shtessel et al. (2014). Although other examples of gain adaptation appear in the literature (Li et al. 2010; Huangfu et al. 2017; Nguyen et al. 2018), the chattering problem has been addressed in Section 3.4.2 through a particular discretization method (Kikuuwe et al. 2019). Therefore, $k(t)$ has been set to a constant. This constant must be larger than the highest rate of change of $e_y(t)$ caused by $e_1(t)$ and $d(t)$ on the output. Since theoretically deciding this maximum rate of change is not straightforward, $k(t)$ was tuned through exhaustive simulations using the same scenario used for the KFs tuning. A summary of the FOSMO parameters is provided in Table 3.9.

Table 3.9: Parameters of the sliding mode observer

Model	$\boldsymbol{L}$	$\boldsymbol{K}$	$\boldsymbol{k(t)}$
IVP	$0_{1\times4}$	0	18.7 mg/(dL min)
Hovorka	$0_{1\times8}$		0.916 mmol/(kg min)

Chattering and discretization

The chattering is an undesirable behavior of sliding mode controllers and observers occurring when the system trajectory does not attain the sliding manifold (the surface $S \coloneqq \{(e_1(t),\, e_y(t))|e_y(t) = 0\}$ in the case of the FOSMO), but oscillates around its vicinity (Utkin et al. 2006). As a result, the controlled output or the estimated states suffer from oscillations of finite frequency and amplitude, degrading the performance of the control or observation, respectively. In control applications, chattering occurs because the discontinuous control action excites some fast unmodeled dynamics of the actual plant, or the switching frequency of the control action is constraint by the finite sampling rate of the digital system. For sliding mode observers, exciting fast dynamics is less likely unless the model includes these dynamics; hence the chattering arises mainly because of the numerical implementation. Explicit discretization methods destroy the invariance property of the continuous sliding mode leading to chattering (Yu 2006; Galias et al. 2007; Wang et al. 2011; Qu et al. 2014; Wang et al. 2015). Figure 3.5 illustrates the issue of chattering for the glucose and rate of glucose appearance estimation in the IVP model (simulation and observer share model structure and parameters) when the designed FOSMO is discretized using the Euler explicit method, that is:

$$\begin{cases} \hat{I}_{SC}[k] = \left(1 - \dfrac{T_s}{\tau_1}\right)\hat{I}_{SC}[k-1] + \dfrac{T_s}{\tau_1 C_I}u[k-1] \\ \hat{I}_P[k] = \left(1 - \dfrac{T_s}{\tau_2}\right)\hat{I}_P[k-1] + \dfrac{T_s}{\tau_2}\hat{I}_{SC}[k-1] \\ \hat{I}_{EFF}[k] = (1 - T_s p_2)\hat{I}_{EFF}[k-1] + T_s p_2 S_I \hat{I}_P[k-1] \\ \hat{G}[k] = (1 - T_s GEZI - T_s \hat{I}_{EFF}[k-1])\hat{G}[k] + T_s EGP + T_s \nu[k-1] \end{cases} \tag{3.68}$$

where $T_s = 5\,\text{min}$. As shown in Figure 3.5, chattering affects the estimation of the glucose and also degrades the estimation of the rate of glucose appearance, obtained filtering $\nu[k]$ with a first order low pass filter of time constant equal to 10 min.

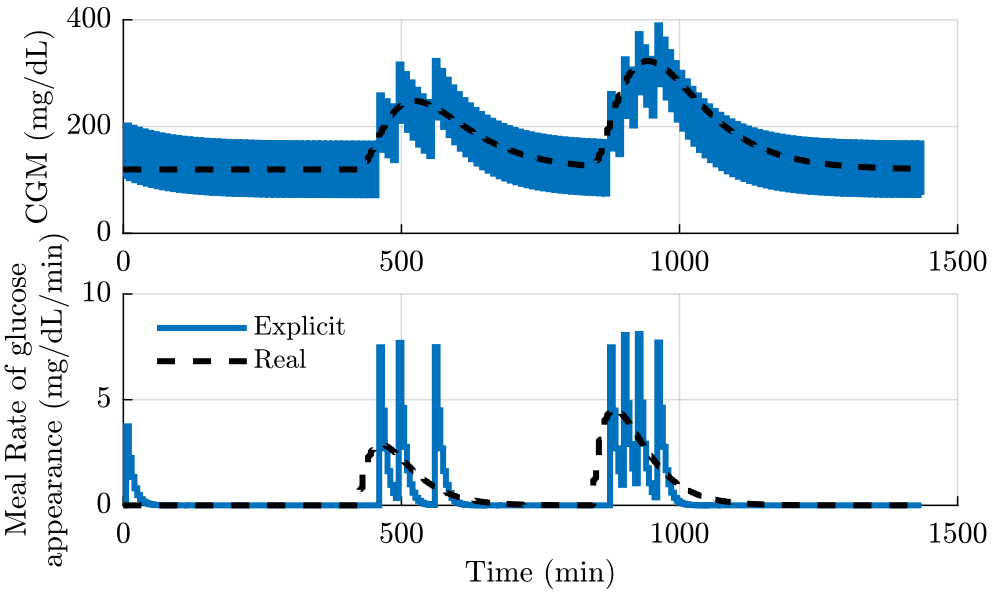

Figure 3.5: Example of chattering in the IVP model caused by the explicit discretization of the sliding mode observer. Solid blue lines represent the estimated glucose (top panel) and the estimated meal disturbance (bottom), while dashed lines are the actual values of these signals. Chattering avoids accurately estimating the glucose or the meal rate of glucose appearance. No mismatch between simulation and observer is considered. The initial condition of the estimated glucose is set 10% lower than the initial condition of the simulation.

A widespread method to reduce chattering is the boundary layer regularization (Slotine et al. 1983). In this method, the discontinuous injection $\nu[k]$ is approxi-

mated by a continuous function when the trajectories are in the vicinity of the sliding surface. Although the boundary layer regularization lowers the chattering, the method only guarantees that the error (the estimation error in case of observation) converges to a vicinity of the origin. To illustrate this behaviour, the injection term $\nu[k]$ in (3.68) is approximated to

$$\tilde{\nu}[k] := k\frac{e_y[k]}{|e_y[k]| + \delta} \tag{3.69}$$

with δ a positive constant. As illustrated in Figure 3.6, the chattering only is removed for $\delta = 50$. Although the errors in the estimated glucose are acceptable, the estimation of the disturbance for this δ is delayed and inaccurate.

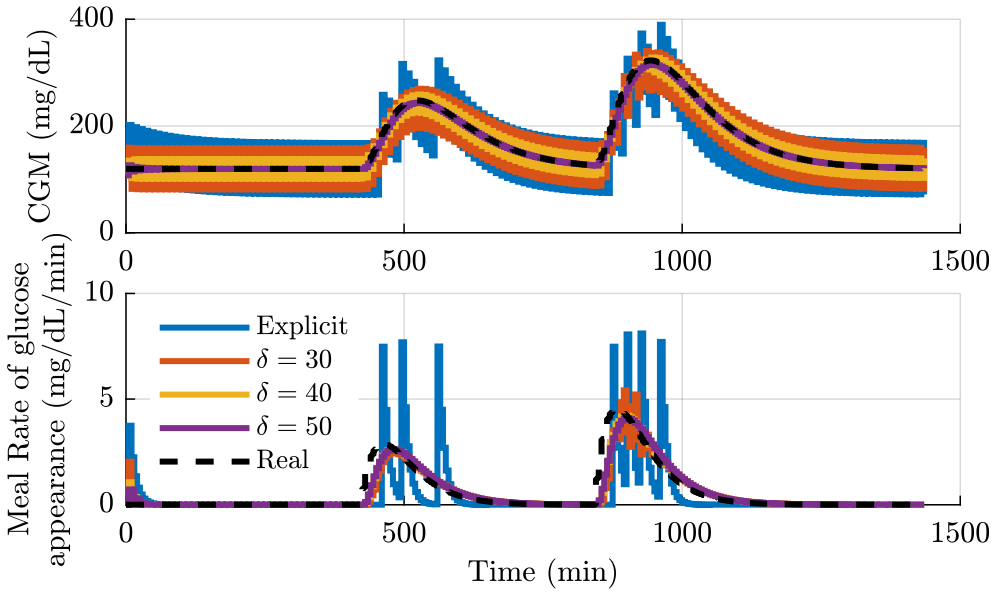

Figure 3.6: Explicit discretization with boundary layer regularization. Several values of the regularization parameter δ were tested. The estimated glucose (solid lines top panel) is acceptable for $\delta = 50$, but the estimated disturbance (solid lines bottom panel) is too delayed.

An alternative to explicit discretization with boundary layer regularization is implicit discretization (Acary et al. 2012; Kikuuwe et al. 2019). In this method, the discontinuous injection term defined in (3.18) is expressed as

$$\begin{cases} \nu(t) = k(t)C^{-1}\psi(t) \\ \psi(t) \in \text{msign}\,(y(t) - \hat{y}(t)) \end{cases} \tag{3.70}$$

where

$$\text{msign}\,(a) = \begin{cases} 1 & \text{if } a > 0 \\ -1 & \text{if } a < 0 \\ [-1,\, 1] & \text{if } a = 0 \end{cases} \tag{3.71}$$

is the multivalued signum function (Acary et al. 2012) for $a \in \mathbb{R}$; for $a \in \mathbb{R}^n$, consider the function element-wise. The implicit discretization given by (3.70) preserves the set-valueness of $\psi(t)$. As a result, $\nu(t)$ is inherently continuous in the vicinity of the sliding manifold, avoiding hence the chattering. To illustrate this property, the implicit discretization proposed by Kikuuwe et al. (2019) is applied to the FOSMO to estimate the glucose and the rate of glucose appearance of the IVP model. The implicit discretization counterpart of (3.68) is given by:

$$\frac{\hat{I}_{SC}[k] - \hat{I}_{SC}[k-1]}{T_s} = \frac{u[k]}{\tau_1 C_I} - \frac{\hat{I}_{SC}[k]}{\tau_1} \tag{3.72}$$

$$\frac{\hat{I}_{P}[k] - \hat{I}_{P}[k-1]}{T_s} = -\frac{\hat{I}_{P}[k]}{\tau_2} + \frac{\hat{I}_{SC}[k]}{\tau_2} \tag{3.73}$$

$$\begin{aligned} \frac{\hat{I}_{EFF}[k] - \hat{I}_{EFF}[k-1]}{T_s} &= -p_2 \cdot \hat{I}_{EFF}[k] + \\ &\quad + S_I p_2 \hat{I}_P[k] \end{aligned} \tag{3.74}$$

$$\begin{aligned} \frac{\hat{G}[k] - \hat{G}[k-1]}{T_s} &= EGP + k\psi[k] - \\ &\quad - (GEZI + \hat{I}_{EFF}[k])\hat{G}[k] \end{aligned} \tag{3.75}$$

with

$$\psi[k] \in \text{msign}\,(e_y[k]) \tag{3.76}$$

Although $e_y[k]$ appears on the right side of (3.76), the implicit discretization is causal. To obtain an explicit form for (3.76), the following manipulations are required:

- Solving the system of equations (3.72)–(3.75) and considering

$$\hat{y}[k] = C_2^{-1}(y[k] - e_y[k]),$$

with $y[k] = G[k]$ and $\hat{y}[k] = \hat{G}[k]$, leads to the following expression of the output error:

$$e_y[k] = e^*[k] - \beta[k]\psi[k] \tag{3.77}$$

with

$$e^*[k] = \frac{e_n^*[k]}{e_d^*[k]} \tag{3.78}$$

$$\begin{aligned}
e_d^*[k] = {} & (CI\,GEZI\,p_2 + SI\,p_2\,u[k])\;{T_s}^4 + \\
& + \Big(CI\,p_2 + CI\,GEZI + CI\,\hat{I}_{EFF}[k-1] + \\
& CI\,GEZI\,p_2\,\tau_1 + CI\,GEZI\,p_2\,\tau_2 + \\
& + CI\,\hat{I}_P[k-1]\,SI\,p_2\,\tau_2 + CI\,\hat{I}_{SC}[k-1]\,SI\,p_2\,\tau_1\Big)\;{T_s}^3 + \\
& + (CI + CI\,GEZI\,\tau_1 + CI\,GEZI\,\tau_2 + \\
& + CI\,\hat{I}_{EFF}[k-1]\,\tau_1 + CI\,\hat{I}_{EFF}[k-1]\,\tau_2 + CI\,p_2\,\tau_1 + \\
& + CI\,p_2\,\tau_2 + CI\,GEZI\,p_2\,\tau_1\,\tau_2 + \\
& + CI\,\hat{I}_P[k-1]\,SI\,p_2\,\tau_1\,\tau_2\Big)\;{T_s}^2 + (CI\,\tau_1 + CI\,\tau_2 + \\
& + CI\,GEZI\,\tau_1\,\tau_2 + CI\,\hat{I}_{EFF}[k-1]\,\tau_1\,\tau_2 + \\
& + CI\,p_2\,\tau_1\,\tau_2)\;T_s + CI\,\tau_1\,\tau_2
\end{aligned} \tag{3.79}$$

$$
\begin{aligned}
e_n^*[k] = (&CI\,GEZI\,G[k]\,p_2 - CI\,EGP\,p_2 + \\
&+G[k]\,SI\,p_2\,u[k])\;{T_s}^4 + (CI\,GEZI\,G[k] - \\
&-CI\,EGP + CI\,G[k]\,\hat{I}_{EFF}[k-1] + CI\,G[k]\,p_2 - \\
&-CI\,\hat{G}[k-1]\,p_2 - CI\,EGP\,p_2\,\tau_1 - CI\,EGP\,p_2\,\tau_2 + \\
&+CI\,GEZI\,G[k]\,p_2\,\tau_1 + CI\,GEZI\,G[k]\,p_2\,\tau_2 + \\
&+CI\,G[k]\,\hat{I}_P[k-1]\,SI\,p_2\,\tau_2 + \\
&+CI\,G[k]\,\hat{I}_{SC}[k-1]\,SI\,p_2\,\tau_1\Big)\;{T_s}^3 + (CI\,G[k] - \\
&-CI\,\hat{G}[k-1] - CI\,EGP\,\tau_1 - CI\,EGP\,\tau_2 + \\
&+CI\,GEZI\,G[k]\,\tau_1 + CI\,GEZI\,G[k]\,\tau_2 + \\
&+CI\,G[k]\,\hat{I}_{EFF}[k-1]\,\tau_1 + CI\,G[k]\,\hat{I}_{EFF}[k-1]\,\tau_2 + \\
&+CI\,G[k]\,p_2\,\tau_1 + CI\,G[k]\,p_2\,\tau_2 - CI\,\hat{G}[k-1]\,p_2\,\tau_1 - \\
&-CI\,\hat{G}[k-1]\,p_2\,\tau_2 - CI\,EGP\,p_2\,\tau_1\,\tau_2 + \\
&+CI\,GEZI\,G[k]\,p_2\,\tau_1\,\tau_2 + \\
&+CI\,G[k]\,\hat{I}_P[k-1]\,SI\,p_2\,\tau_1\,\tau_2\Big)\;{T_s}^2 + \\
&+\Big(CI\,G[k]\,\tau_1 + CI\,G[k]\,\tau_2 - CI\,\hat{G}[k-1]\,\tau_1 - \\
&-CI\,\hat{G}[k-1]\,\tau_2 - CI\,EGP\,\tau_1\,\tau_2 + \\
&+CI\,GEZI\,G[k]\,\tau_1\,\tau_2 + CI\,G[k]\,\hat{I}_{EFF}[k-1]\,\tau_1\,\tau_2 + \\
&+CI\,G[k]\,p_2\,\tau_1\,\tau_2 - CI\,\hat{G}[k-1]\,p_2\,\tau_1\,\tau_2\Big)\;T_s + \\
&+CI\,G[k]\,\tau_1\,\tau_2 - CI\,\hat{G}[k-1]\,\tau_1\,\tau_2
\end{aligned}
\tag{3.80}
$$

and

$$
\beta[k] = \frac{k\beta_n[k]}{\beta_d[k]} \tag{3.81}
$$

$$\begin{aligned}\beta_d[k] = &(CI\,GEZI\,p_2 + SI\,p_2\,u[k])\;{T_s}^4 + \\ &+ \Big(CI\,p_2 + CI\,GEZI + CI\,\hat{I}_{EFF}[k-1] + \\ &+ CI\,GEZI\,p_2\,\tau_1 + CI\,GEZI\,p_2\,\tau_2 + \\ &+ CI\,\hat{I}_P[k-1]\,SI\,p_2\,\tau_2 + CI\,\hat{I}_{SC}[k-1]\,SI\,p_2\,\tau_1\Big)\;{T_s}^3 + \\ &+ (CI + CI\,GEZI\,\tau_1 + CI\,GEZI\,\tau_2 + \\ &+ CI\,\hat{I}_{EFF}[k-1]\,\tau_1 + CI\,\hat{I}_{EFF}[k-1]\,\tau_2 + CI\,p_2\,\tau_1 + \\ &+ CI\,p_2\,\tau_2 + CI\,GEZI\,p_2\,\tau_1\,\tau_2 + \\ &+ CI\,\hat{I}_P[k-1]\,SI\,p_2\,\tau_1\,\tau_2\Big)\;{T_s}^2 + (CI\,\tau_1 + CI\,\tau_2 + \\ &+ CI\,GEZI\,\tau_1\,\tau_2 + CI\,\hat{I}_{EFF}[k-1]\,\tau_1\,\tau_2 + \\ &+ CI\,p_2\,\tau_1\,\tau_2)\;T_s + CI\,\tau_1\,\tau_2\end{aligned} \tag{3.82}$$

$$\begin{aligned}\beta_n[k] = &\;CI\,p_2\,{T_s}^4 + (CI + p_2\;(CI\,\tau_1 + CI\,\tau_2))\;{T_s}^3 + \\ &+ (CI\,\tau_1 + CI\,\tau_2 + CI\,p_2\,\tau_1\,\tau_2)\;{T_s}^2 + CI\,\tau_1\,\tau_2\,T_s\end{aligned} \tag{3.83}$$

- For $a \in \mathbb{R}$, $\text{msign}\,(a)$ is the subdifferential of $|a|$, which, in turn, is the indicator function of the closed non empty convex set $[-1,\,1] \subset \mathbb{R}$. As a result, the following property holds (Brogliato et al. 2021):

$$b \in \delta|a| = \text{msign}\,(a) \leftrightarrow a \in \mathcal{N}_{[-1,\,1]}(b) \tag{3.84}$$

  where $b \in \mathbb{R}$ and $\mathcal{N}_{[-1,\,1]}(b)$ is the normal cone onto $[-1,\,1]$ at point b. Applying the above property to (3.76) and (3.77), it turns out that

$$e^*[k] - \beta[k]\psi[k] \in \mathcal{N}_{[-1,\,1]}(\psi[k]) \tag{3.85}$$

- To solve the generalized equation (3.85), a second property of convex analysis is required: for a and $b \in \mathbb{R}$,

$$(b - a) \in -N_{[-1,\,1]}(b) \leftrightarrow b = \text{proj}\,([-1,\,1]; a) \tag{3.86}$$

  where $\text{proj}\,([-1,\,1]; a)$ is the orthogonal projection of a onto the set $[-1,\,1]$ (Brogliato et al. 2021). Applying the above property to (3.85), the following causal expression results to calculate $\psi[k]$:

$$\psi[k] = \text{proj}\left([-1,\, 1]; \frac{e^*[k]}{\beta[k]}\right) \tag{3.87}$$

Since the above projection is onto a scalar space, (3.87) can be expressed in terms of a saturation function as follows (Brogliato et al. 2021; Kikuuwe et al. 2019):

$$\psi[k] = \begin{cases} \frac{e^*[k]}{\beta[k]}, & \text{if } \frac{e^*[k]}{\beta[k]} \in [-1,\, 1] \\ 1, & \text{if } \frac{e^*[k]}{\beta[k]} > 1 \\ -1, & \text{if } \frac{e^*[k]}{\beta[k]} < -1 \end{cases} \tag{3.88}$$

from where it is clear that the set-valueness of $\text{msign}\,(e_y[k])$ is preserved. As a result, the chattering is avoided and, unlike explicit discretization, the disturbance can be estimated without filters or continuous approximation as follows:

$$\hat{d}[k] \approx \nu[k] = k\psi[k] \tag{3.89}$$

Figure 3.7 illustrates the benefits of implicit discretization: it removes chattering from the glucose estimation and the disturbance estimation is not delayed.

The same procedure to calculate $\psi[k]$ applies to the Hovorka model. Since the corresponding terms $e^*[k]$ and $\beta[k]$ are cumbersome, they are omitted here. Instead, the Appendix A prompts the MATLAB script used to calculate them.

3.5 Study of the effect of the model and observer structure on the estimation accuracy

In this section, an in silico study is performed to analyze the impact on the estimated meal disturbance accuracy of the following factors:

- "Model": the structure of the model was considered by comparing the IVP model with the Hovorka model.
- "Observer": the observers were assessed by comparing the FOSMO and the KF.

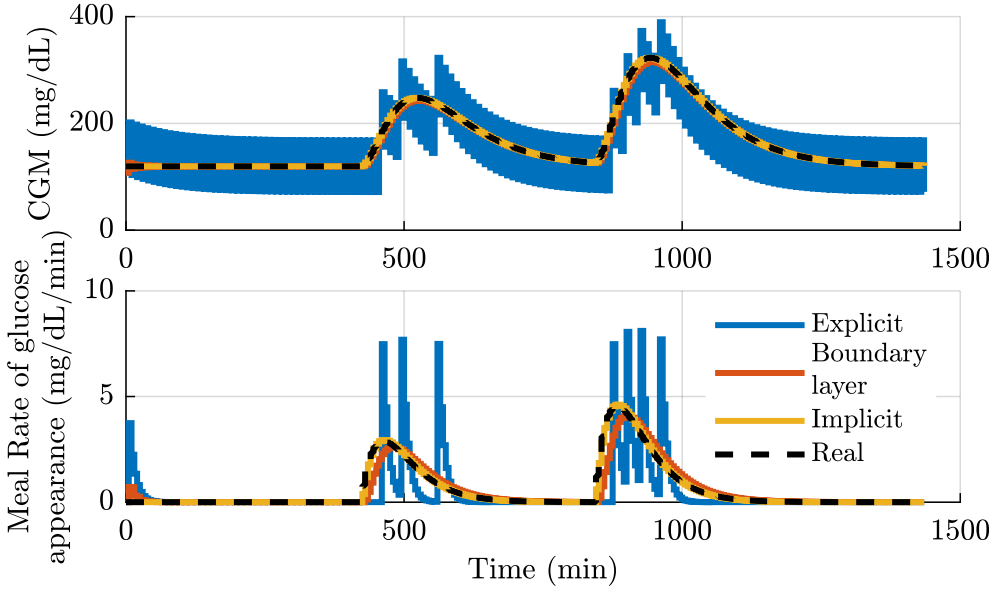

Figure 3.7: Comparison of implicit discretization with explicit discretization and boundary layer regularization ($\delta = 50$). The implicit discretization prevents the glucose estimation (top panel) from chattering. Also, the estimation of the disturbance (bottom panel) does not feature the delays of the filtering or boundary layer approach.

Thus, four cases were simulated: the KF designed with the IVP model (KF-FOSMO), the KF designed with the Hovorka model (KF-Hovorka), the FOSMO designed with the IVP model (FOSMO-IVP), and the FOSMO designed with the Hovorka model (FOSMO-Hovorka). Each of the four cases included a simulation of ten virtual adults, repeated three times with different instances of variability. All the simulations were carried out with the extended version of the academic UVa/Padova simulator. The simulated scenario was a 1-day length and included three meals (45 g at 7 h, 70 g at 14 h, and 60 g at 21 h). The scenario also considered variability in the insulin absorption (uniform distribution of ±30%), circadian insulin variability (of sinusoidal type with uniformly-distributed amplitude of ±30%), and CGM errors according to the default model in the simulator.

The accuracy of the estimated meal disturbance was assessed in terms of the Root Mean-Squared Error (RMSE), the Median Absolute Error (MAE), and the Maximum Absolute Error (MaxAE). Since the original units of the meal disturbance among models disagree, the Hovorka unit was converted to the IVP unit by the following change of units: $1\,(\text{mmol/kg min}) = 180/V_g\,(\text{mg/(dL min)})$.

To avoid the influence of the transient from the initial condition on the metrics, the first 30 min of the simulation were disregarded when computing the metrics.

A multifactorial ANOVA determined whether the factors "Model" and "Observer" and their interaction explained the variability found in the performance metrics. All the simulations shared the cohort of patients and the meals; hence the hypothesis of independence was unmet (Iversen 2011). To circumvent this issue, the factor "Subject" was considered as a covariate in the analysis. The significance level was 0.05.

The ANOVA conclusions were complemented with the Tukey honestly significant difference test (Tukey 1949). This test provides an estimate of the difference in means and the corresponding 95% confidence interval. This information does not only help to identify which level (or combination of levels in the interaction) causes the statistical significance, but it gives insight into the practical relevance of the difference (i.e., its effect size; Hand 2012). Another measure of the effect size employed in the analysis was the eta-squared (η^2, see e.g., Fritz et al. 2012), which informs about the proportion of variance related to each factor.

The statistical analysis was performed with R (R Core Team 2021).

3.5.1 Results

Figure 3.8 illustrates how noise and the model uncertainties degrade the estimation. The estimated values even reached negative values, an unphysiological behavior in the absence of exercise.

The statistical analysis is summarized in Figure 3.9, Figure 3.10, Table 3.10, and Table 3.11. The model is a statistically significant factor in explaining the variability of the RMSE (Table 3.10). Tukey's test reveals (Table 3.11) that observers designed with the Hovorka model reduce the RMSE of the observers designed with the IVP in 0.062 (0.020, 0.105) mg/(dL min). This difference in the RMSE might be because the observers designed with the IVP model overestimate the postprandial peak, slowly reaching the steady-state (Figure 3.8). The model is no longer a statistically significant factor regarding the other performance metrics (MAE and MaxAE), (Table 3.10). However, the observers designed with the Hovorka model still tend to improve those built upon the IVP model as concluded from the asymmetry of Tukey's confidence intervals (the lower limit of the model-related confidence intervals in Table 3.11 is closer to zero than the upper limit).

Despite the statistical significance of the improvement in the RMSE, its practical relevance is debatable. On the one hand, the magnitude of the improvement might be unimportant from the application point of view. On the other hand, as the η^2 shows (Table 3.10), the type of model explains less than 1% of the variability of the metrics, a negligible contribution compared to the more than 85% explained by the inter-patient variability (the "Subject" factor). Figure 3.10 evinces how the RMSE varies more within the subjects (see, for instance, the differences between subject 1 and subject 8) than within the models, illustrating the enormous impact of the inter-patient variability.

The contribution of the observer structure is even lower than that of the model. The size of the estimated difference in means among observers is one order of magnitude lower than for the model (Table 3.11), and the η^2 is less than $1 \cdot 10^{-5}$ %. In addition, the confidence intervals of the Tukey test are roughly symmetric, indicating that the variability caused by other factors hides any possible improvement of using a specific observer algorithm. This result is coherent with the ANOVA analysis concluding that the observer is not a statistically significant factor for any performance metrics (Table 3.10).

Note that differences in performance are negligible between the observers, even though the tuning of the KF is more cumbersome than tuning the FOSMO.

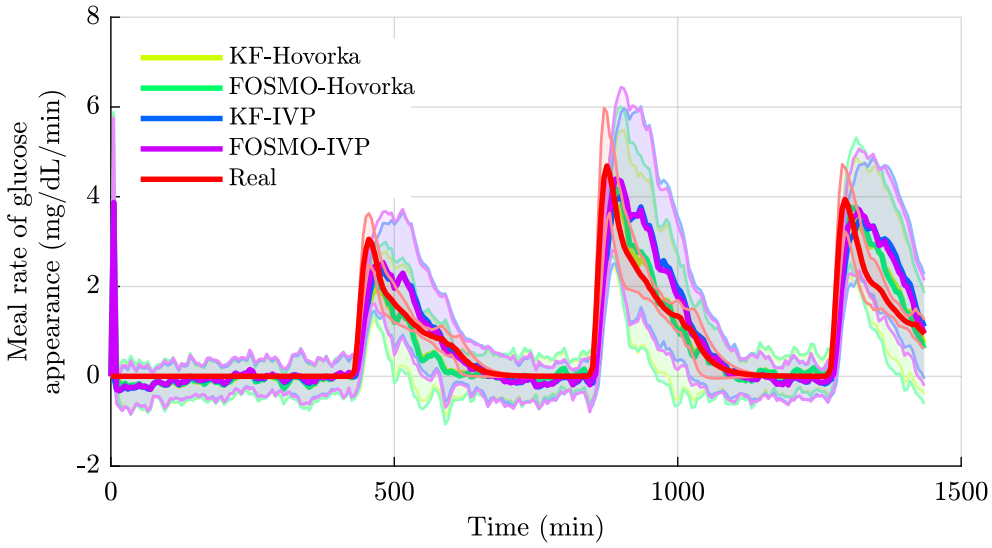

Figure 3.8: Comparison of the estimated meal disturbance. Thicker lines represented the median, and the shaded areas correspond to the interquartile range.

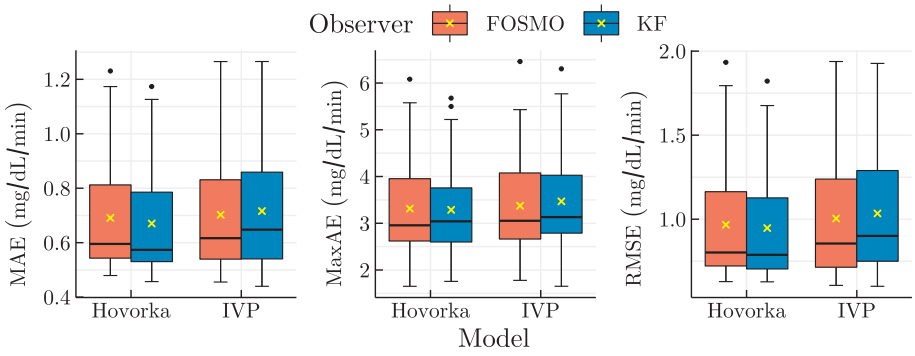

Figure 3.9: Performance metrics of the estimated meal rate of glucose appearance. The left panel shows the Median Absolute Error (MAE), the middle panel the Median Absolute Error (MAE), and the right panel the Root Mean-Squared Error (RMSE).

Table 3.10: Summary of ANOVA results of the meal disturbance estimation error

	RMSE		**MAE**		**MaxAE**	
	η^2	P	η^2	P	η^2	P
Model	0.70	0.01 *	0.40	0.06	0.30	0.11
Observer	0.00	0.81	0.00	0.81	0.00	0.66
Subject	89.90	0.00 *	88.00	0.00 *	87.70	0.00 *
Model:Observer	0.10	0.25	0.10	0.25	0.10	0.43

It summarizes three metrics: the root-mean-square error (RMSE), the mean absolute error (MAE) and the maximum absolute error (MaxAE). Terms "η^2" and "P" denote the eta squared effect size measurement and the P-value of the ANOVA F-statistics, respectively. The notation "Model:Observer" refers to the interaction of the factors "Model" and "Observer". The asterisk (*) indicates a statistically significant difference at 0.05 level.

3.6 Conclusion

Two observers were designed (Kalman filter and first-order sliding mode observer) to estimate the meal rate of glucose appearance. Two models of different complexity (IVP and Hovorka models) were also considered to build the observers. The influence of the structure of the models and observers was analyzed in an in silico comparison.

Table 3.11: Summary of the Tukey test

Metric	Contrast	Diff	CI	
RMSE	IVP-Hovorka	$6.205 \cdot 10^{-2}$	$[\ 1.96{\cdot}10^{-2},\ 1.05{\cdot}10^{-1}]$	*
	KF-FOSMO	$5.19 \cdot 10^{-3}$	$[-3.73{\cdot}10^{-2},\ 4.77{\cdot}10^{-2}]$	
MAE	IVP-Hovorka	$2.858 \cdot 10^{-2}$	$[-6.0{\cdot}10^{-4}\ ,\ 5.78{\cdot}10^{-2}]$	
	KF-FOSMO	$-3.56 \cdot 10^{-3}$	$[-3.27{\cdot}10^{-2},\ 2.56{\cdot}10^{-2}]$	
MaxAE	IVP-Hovorka	$1.221 \cdot 10^{-1}$	$[-2.79{\cdot}10^{-2},\ 2.72{\cdot}10^{-1}]$	
	KF-FOSMO	$3.356 \cdot 10^{-2}$	$[-1.16{\cdot}10^{-1},\ 1.84{\cdot}10^{-1}]$	

Tukey's test for the Root Mean-Squared Error (RMSE), the Median Absolute Error (MAE), and the Maximum Absolute Error (MaxAE). It estimates the difference in mean (Diff) within the levels of the "Model" and "Observer" factors, including the corresponding 95%-confidence intervals (CI). The asterisk "*" indicates a statistically significant difference.

All the observers reconstructed the meal disturbance, but the uncertainty was severely coupled to the estimation. In addition, the inter-patient variability was the most noticeable factor impacting the estimation accuracy, diluting the influence of the model structure and the observer algorithm. This evinces the importance of model individualization over the observer algorithm. Individualizing a model is challenging due to identifiability issues (e.g., the correlation between parameters or inputs), especially in a domiciliary setting where the only available signals are insulin and glucose. Therefore, the IVP will be preferred over the Hovorka model in the following chapters because its individualization is more reachable given its lower number of parameters.

Finally, the differences in performance between the two observer algorithms were negligible. As a result, the next chapters will use the FOSMO since it has a more straightforward tuning procedure, provided the discretization is correctly addressed.

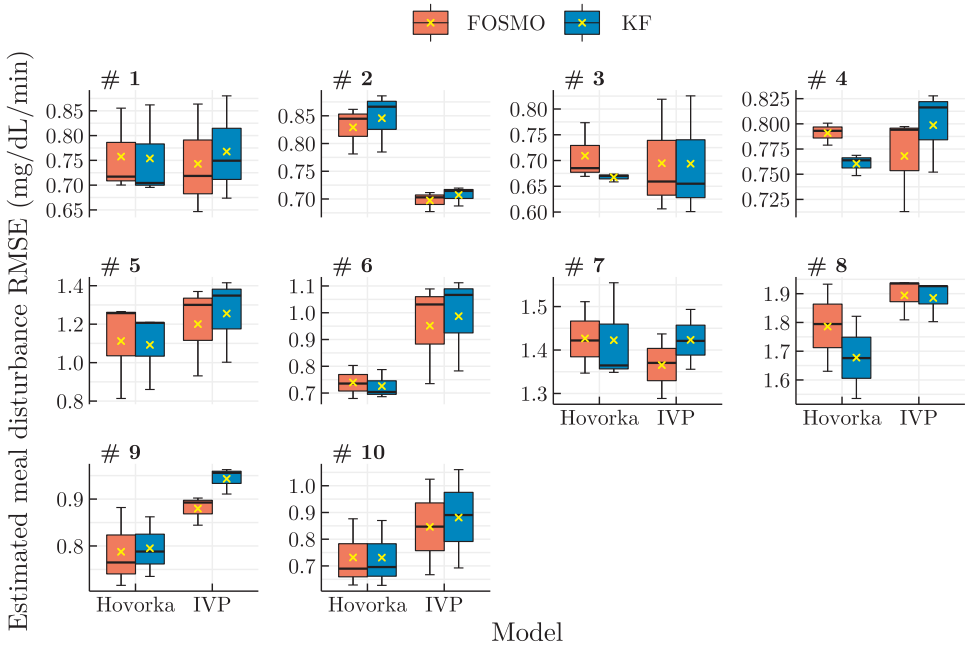

Figure 3.10: Root Mean-Squared Error (RMSE) of the meal disturbance estimation per subject.

Chapter 4

Disturbance reconstruction from clinical datasets

Real data suffers from many sources of variability (noise, metabolic changes, etc.), affecting the estimation of the meal disturbance. Indeed, any mismatch between the model embedded in the observer and the real subject will be coupled to the disturbance signal. This chapter illustrates how challenging is to estimate the meal disturbance when the FOSMO designed with the IVP model in previous chapter is fed with clinical data. In addition, the same observer is applied to a dataset of exercise periods to illustrate whether the observer can reconstruct the expected changes in the glucose fluxes caused by exercise.

4.1 Introduction

The observers evaluated in Chapter 3 managed to reconstruct the meal disturbance, though distorted because of the variability in the simulator. Since this variability is expected to be richer in real-life data, the consequent distortion will also be more notable. The first goal of this chapter is to illustrate the estimated meal disturbances when real data from a clinical study were fed to the observer (Rossetti et al. 2012).

Besides meals, exercise alters the input and output glucose fluxes in the bloodstream. Specifically, low-to-moderate aerobic exercise will likely reduce plasma

glucose, while intense anaerobic exercise may increase glucose levels due to catecholamines and cortisol secretion (Codella et al. 2017; Tagougui et al. 2019). Technically, glucose disturbances due to exercise can be dealt exactly in the same way as meals, since they can also be represented as an additive disturbance in the glucose derivative. The disturbance estimated by the observer will also be coupled with the changes in the glucose fluxes caused by exercises. Therefore, the second goal of the chapter is to illustrate whether the observer can reconstruct these glucose fluxes using a clinical dataset (Quirós et al. 2018).

4.2 Clinical datasets description

This chapter uses two clinical datasets to analyze the estimated disturbance with real data: Dataset A, which focuses on postprandial periods, and Dataset B, which collects exercise periods.

4.2.1 Dataset A

The postprandial data used in this chapter is related to the iBolus in-hospital clinical trial (Rossetti et al. 2012) under the scope of the SOLARE European project (id: FP7-PEOPLE-2009-IEF, ref 252085) and the National project CLOSED-LOOP4MEAL (ref: DPI2010-20764-C02-01). In particular, the data corresponds to an outpatient study undertaken before the in-home trial to identify the models of the 12 subjects involved in the study.

A total of 145 meals were registered in the outpatient trial. Meals were standardized, of sizes 40 g, 60 g, or 100 g. Meal boluses may be delivered before, at mealtime, or after the meal, depending on the glucose value and the meal carbohydrate content (Laguna et al. 2010). Insulin was infused with a pump Paradigm Veo - 554 (Medtronic Minimed, Northridge, CA, USA). Plasma glucose was monitored with two CGMs: the sensor integrated with the insulin pump and a Dexcom Seven Plus (Dexcom, San Diego, CA, USA).

4.2.2 Dataset B

The data was collected in an exploratory clinical trial at the Clinic University Hospital of Barcelona (Hospital Clínic Universitari, Barcelona, Spain) within the SAFE-AP national project (id: DPI2013-46982-C2-1-R) (Quirós et al. 2018). The clinical trial assessed the SAFE controller (Revert et al. 2013), without the insulin feedback term, for six patients with type 1 diabetes under six exercise sessions in about nine weeks per patient: three sessions of aerobic exercise (three series

of 15 min of static cycling at 60 % of individual maximum oxygen consumption (VO_2max) with 5 min between sets) and three sessions of anaerobic exercise (five sets of eight repetitions of several weightlifting exercises at 60 % of VO_2max with 90 s of rest between sets). Each subject was provided with two glucose sensors (Enlite-2, Medtronic Minimed, Northridge, CA, USA) and an insulin pump (Paradigm Veo, Medtronic Minimed, Northridge, CA, USA).

Besides the subcutaneous insulin infusion, the patients received an infusion of insulin or glucose intravenously, if required, to maintain comparable plasma glucose concentration at the exercise session onset (Quirós et al. 2018). In addition, patients ingested 23 g of carbohydrates before the exercise began and 15 g if hypoglycemia occurred (Quirós et al. 2018).

4.3 Preprocessing

The signals reported in the trials (CGM sensors, subcutaneous insulin infusion, and, if any, intravenous infusions) were synchronized at the 5-min sampling time of the primary CGM. In addition, missing data in the two CGM sensors were handled as follows. First, both CGM signals were merged, i.e., the missing values in the principal CGM were filled with the secondary CGM (if available). In the case that the resulting signal contained missing values, but the information loss affected up to six successive samples, the signal was interpolated with splines. For longer missed consecutive samples, the signal was cropped, and the slices not including the mealtime in Dataset A or the exercise time in Dataset B were discarded.

4.4 Application of the observer to real meal data

The FOSMO designed with the IVP model was selected for the analysis in this chapter since it is the most straightforward option of the ones analyzed in Section 3.5 while achieving acceptable results. The model parameters correspond to the "Average patient column" of Table 3.6, and the FOSMO tuning coincides with the described in Section 3.2.2.

48 out of 145 potential postprandial periods in Dataset A were discarded due to the following reasons: 25 postprandial periods have no CGM data, 6 have no insulin pump data, 5 have neither CGM nor pump data, and 12 have insufficient CGM data (less than 4 h) after discarding "long gaps" of missing data in the preprocessing stage. Therefore, 97 postprandial periods were eventually included in the analysis: 42 meals of 40 g, 16 of 60 g, and 39 of 100 g.

Figure 4.1 shows the populational evolution of the glucose and estimated disturbances, grouped by meal size. Overall, the median estimated disturbances (thick blue line) evolve similarly as in the simulations of Chapter 3: after mealtime (0 in the axis x), the disturbance starts to increase, it peaks after 100 min, approximately, and it eventually fades off. This expected profile of the meal disturbance can be also observed in individual responses such as those represented in Figure 4.2.

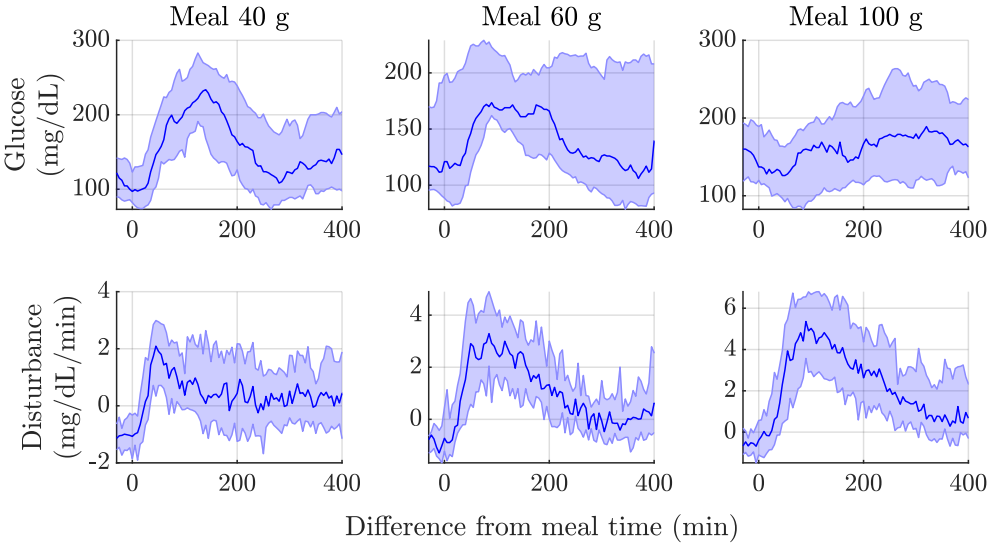

Figure 4.1: Meal disturbance estimation from clinical data grouped by meal size. Panels in the first row represent the glucose values, and panels in the second row, the estimated disturbances. Thick lines show the median and the shaded areas, the interquartile range. Each column summarizes the result of a given meal size. A total of 97 postprandial periods were considered: 42 meals of 40 g, 16 of 60 g, and 39 of 100 g. The 0 on the x-axis marks the meal announcement.

The differences in the estimated disturbance profiles between meal sizes are also coherent. Note that the median glucose profile of 100-g meals is flatter than for the other meal sizes in Figure 4.1. This is because the insulin bolus was administered 30 min before mealtime for these meals by protocol, while it was even delayed for the other meal sizes (Laguna et al. 2010). Despite this artifact introduced by the protocol, the median estimated disturbance of the meals with 100 g of carbohydrates (third column of Figure 4.1) has a more considerable peak than the median of the meals with 60 g or 40 g. A more representative example of this behavior is shown in the right panels of Figure 4.2. Although the glucose decreases after the meal as a result of the anticipated insulin bolus, the disturbance follows an evident meal-like shape. In Figure 4.1 (and also Figure 4.2), the estimated meal

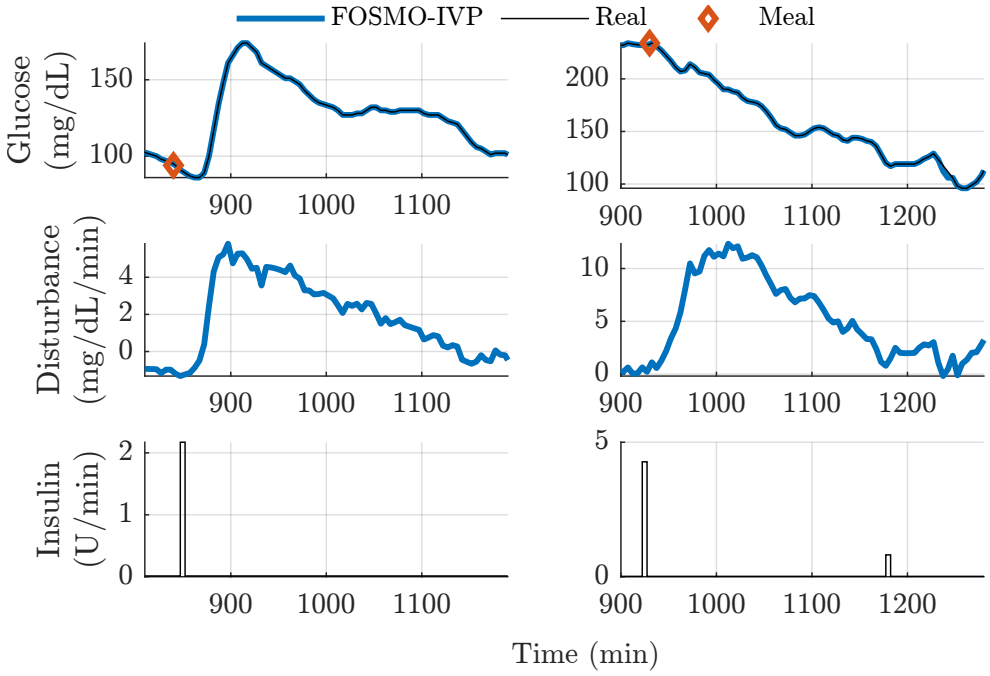

Figure 4.2: Example of estimated meal disturbances with coherent profiles. Panels in the first row represent glucose values (black: actual CGM, blue: estimated), panels in the second row depict the estimated disturbance, and panels in the third row correspond to the actual insulin infusion. Orange diamonds indicate the mealtime. Note that the estimated disturbance follows the expected profile after a meal, even in the second column where glucose does not increase after the meal.

rate of glucose appearance does not correspond to the derivative of glucose as one would expect since $R_A(t)$ appears in the equation of the glucose derivative (3.30). However, other terms affect the glucose derivative too. Since EGP is constant and $GEZI$ is negligible, the other relevant term dominating the glucose derivative is the glucose disappearance due to insulin effect, i.e., $I_{EFF}(t) \cdot G(t)$. As observed in Figure 4.3, the estimated glucose disappearance due to insulin has a similar magnitude, though slightly larger, as the estimated meal disturbance. Therefore, the observer estimated a meal-shaped disturbance to compensate for the effect of insulin so that the estimated glucose remained flat.

Another example that supports that the estimated disturbance is coherent with an expected meal rate of glucose appearance is that the area under the curve of the

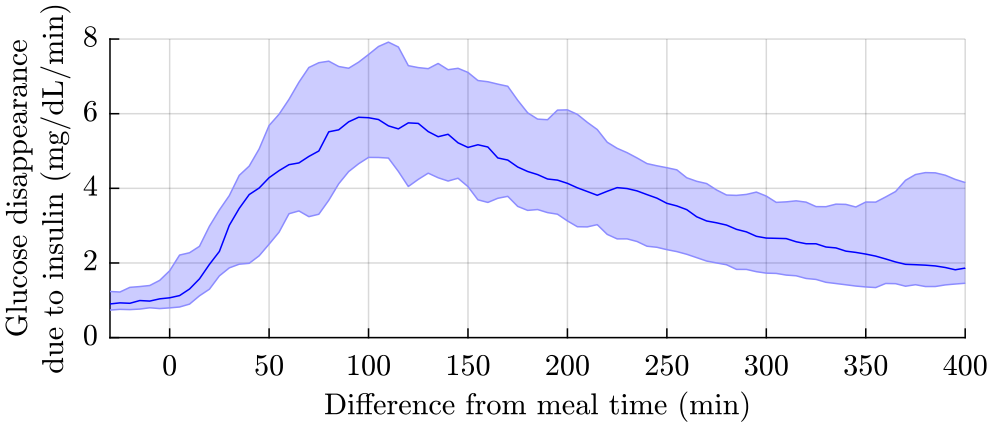

Figure 4.3: Estimated glucose disappearance due to insulin corresponding to 100-g meals. Representation of the estimation of the term $I_{EFF}(t) \cdot G(t)$ corresponding to (3.30) for the meals of 100 g. The thick line shows the median and the shaded areas, the interquartile range. Note that the estimated rate has a similar magnitude that the estimated meal rate of glucose appearance in Figure 4.1

estimated disturbances also increases for meals with higher carbohydrate content (Figure 4.4).

Although the estimated disturbance may seem acceptable in the median, the wide interquartile range (shaded areas in Figure 4.1) indicates a high variability. Indeed, in some individual cases, as shown in Figure 4.5, other disturbances besides meal (i.e., model mismatch errors, abrupt changes in the sensor, etc.) are coupled to the meal disturbance; consequently, the estimated disturbance no longer has a meal-like shape. The observer also estimates a negative glucose flux in Figure 4.5 even before any meal disturbance occurred. This negative flux may be indicative of a mismatch in the model used to design the observer.

4.5 Application of the observer to real exercise data

Dataset B was used for the analysis in this subsection. Out of 36 exercise sessions available, six aerobic and four anaerobic sessions were discarded because of sensors or insulin pump malfunctioning (Quirós et al. 2018). The clinical trial was conceived to evaluate a closed-loop system rather than estimating the exercise disturbance; thus, it has some particularities affecting the estimation. One of them is the presence of glucose and insulin intravenous infusions. The intravenous infusions are suitable for assessing the controller performance since they homogenize

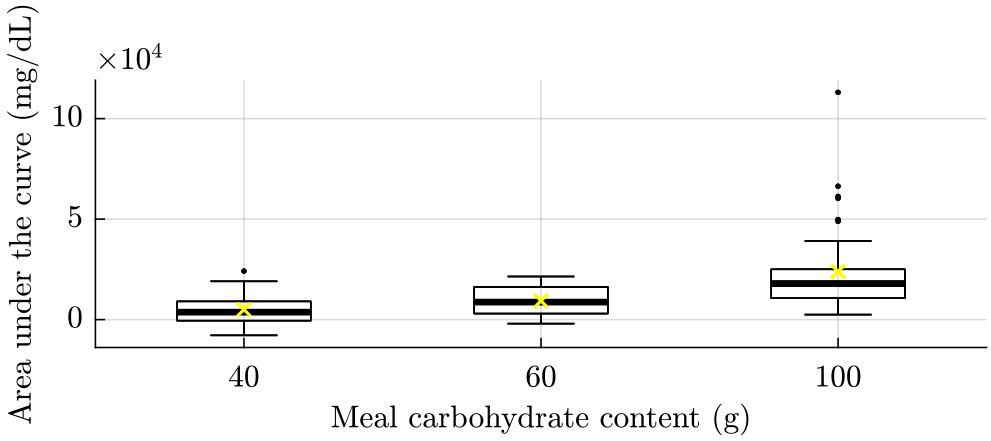

Figure 4.4: Area under the curve of estimated disturbances regarding the meal size. The horizontal black line inside the box represents the median and the yellow cross, the mean. The lower and upper hinges correspond to the 25th and 75th percentiles. The upper whisker extends from the hinge to the largest value no further than 1.5 times the interquartile range. The lower whisker extends from the hinge to the smallest value at most 1.5 times the interquartile range. Note that the area under the curve increases with the meal carbohydrate content.

the initial conditions. However, for the disturbance observation application, if the intravenous infusions are disregarded when designing the observer for the disturbance reconstruction, they will impact the estimation. Figure 4.6 shows an example: when the observer ignores the intravenous glucose infusion (i.e., it is not taken as an input), the estimated disturbance (orange line in the second panel) increases before the exercise starts (interval 550-650 min), a counterintuitive behavior in a basal situation. This increasing disturbance is because the observer cannot explain the rise observed in the glucose with only information from the subcutaneous infusion. Therefore, the observer must add an input glucose flux in the disturbance to replace the unknown (for the observer) intravenous glucose infusion.

The observer must consider the intravenous infusions to mitigate the effect of the intravenous infusions in the estimation. To this end, equations (3.73) and (3.75) are modified as follows:

$$\frac{\hat{I}_P[k] - \hat{I}_P[k-1]}{T_s} = -\frac{\hat{I}_P[k]}{\tau_2} + \frac{\hat{I}_{SC}[k]}{\tau_2} + \frac{1000\, intr_I[k]}{60\, BW\, V_I} \tag{4.1}$$

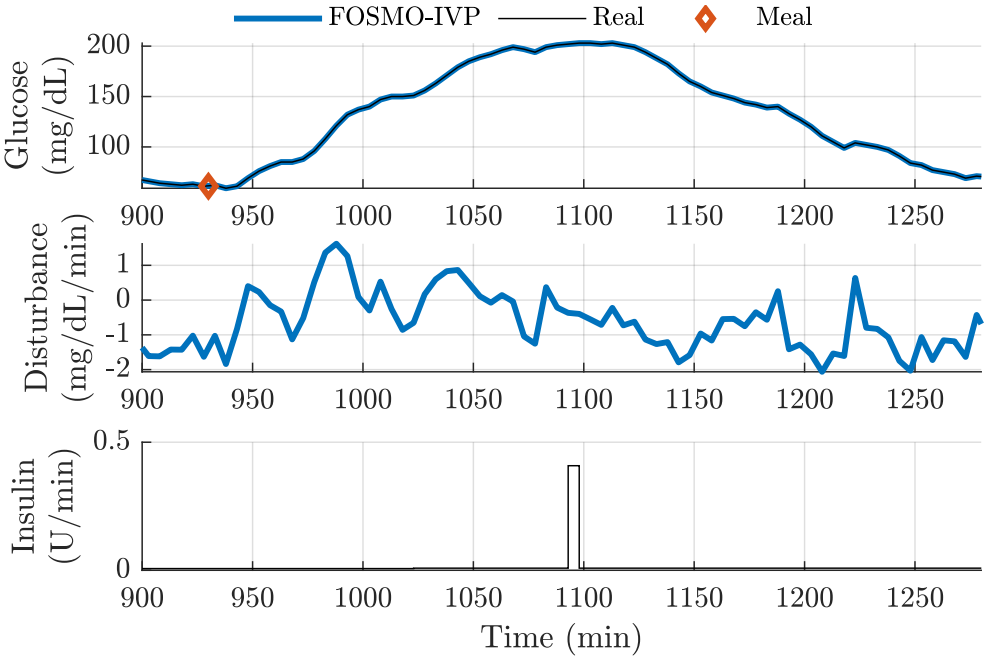

Figure 4.5: Example of the estimated meal disturbance where the variability distorts the expected meal profile. The top panel represents glucose values (black: actual CGM, blue: estimated), the middle panel depicts the estimated disturbance, and the bottom panel corresponds to the actual insulin infusion. The orange diamond indicates mealtime. Note that the estimated disturbance does not follow the expected profile after a meal due to the variability.

$$\frac{\hat{G}[k] - \hat{G}[k-1]}{T_s} = EGP + k\psi[k] - (GEZI + \hat{I}_{EFF}[k])\hat{G}[k] + \frac{intr_G[k]}{BW\, V_G} \tag{4.2}$$

where $intr_I[k]$ and $intr_G[k]$ are the intravenous infusions of insulin (U/h) and glucose (mg/min), respectively; BW (kg) is the individual body weight; and V_I and V_G are, respectively, the distribution volume of insulin (L/kg) and glucose (dL/kg), retrieved from the average adult in the academic version of the UVa/Padova simulator.

As shown in Figure 4.6, the estimated disturbance flattens once the observer considers the intravenous infusion (the green line in the second panel). However, note that the estimated perturbation in the pre-exercise period (around the interval

550-650 min) offsets from zero, likely denoting the effect of model parameters mismatch.

The exercise period of Figure 4.6 (the shaded areas in the first and second panels) also illustrated this model mismatch. Note that the green line within the exercise period does not experiment with any remarkable change regarding the disturbance evolution before the exercise begins. This evolution of the disturbance within physical activity is unrealistic given the high impact of exercise on glucose (upper panel). This behavior is because the observer is missing an input: the pre-exercise carbohydrate intake. When this meal intake is unknown to the observer, its effect leads to an increasing disturbance in the estimation that confounds, even counteracting, the decreasing disturbance caused by the exercise.

Since the pre-exercise carbohydrate intakes are available in the dataset, the observer can consider them as an input to mitigate their effect on the estimated perturbation. To this end, the carbohydrate absorption model in Hovorka et al. (2004), i.e.,

$$\begin{aligned} \frac{d_1[k] - d_1[k-1]}{T_S} &= A_g^{excho} \cdot u_{excho}[k] - \frac{d_1[k]}{\tau_{excho}} \\ \frac{d_2[k] - d_2[k-1]}{T_S} &= \frac{1}{\tau_{excho}} \left(d_1[k] - d_2[k]\right) \end{aligned} \quad , \tag{4.3}$$

was incorporated to the observer by modifying (3.75) as follows:

$$\begin{aligned} \frac{\hat{G}[k] - \hat{G}[k-1]}{T_s} = EGP + k\psi[k] - (GEZI + \hat{I}_{EFF}[k])\hat{G}[k] + \\ + \frac{intr_G[k]}{BW\, V_G} + \frac{d_2[k]}{V_g \tau_{excho}} \end{aligned} \tag{4.4}$$

where u_{excho} refers to the pre-exercise carbohydrate intake rate (mg/min) and d_1 and d_2 are the glucose masses (mg) in the two compartments of the absorption model. Regarding the parameters, A_g^{excho} is the carbohydrate bioavailability (unitless), and τ_{excho} is the time-to-maximum of carbohydrate absorption (min).

Once the pre-exercise carbohydrate intake has been considered in the observer as a new input (with $A_g^{excho} = 1$ and $\tau_{excho} = 30$ min), the estimated disturbance (dotted line in Figure 4.6) decreases within the exercise period. This decreasing trend in the disturbance is not exclusive to the aerobic exercise session in Figure 4.6. Indeed, the median estimated disturbance of all the analyzed anaerobic sessions

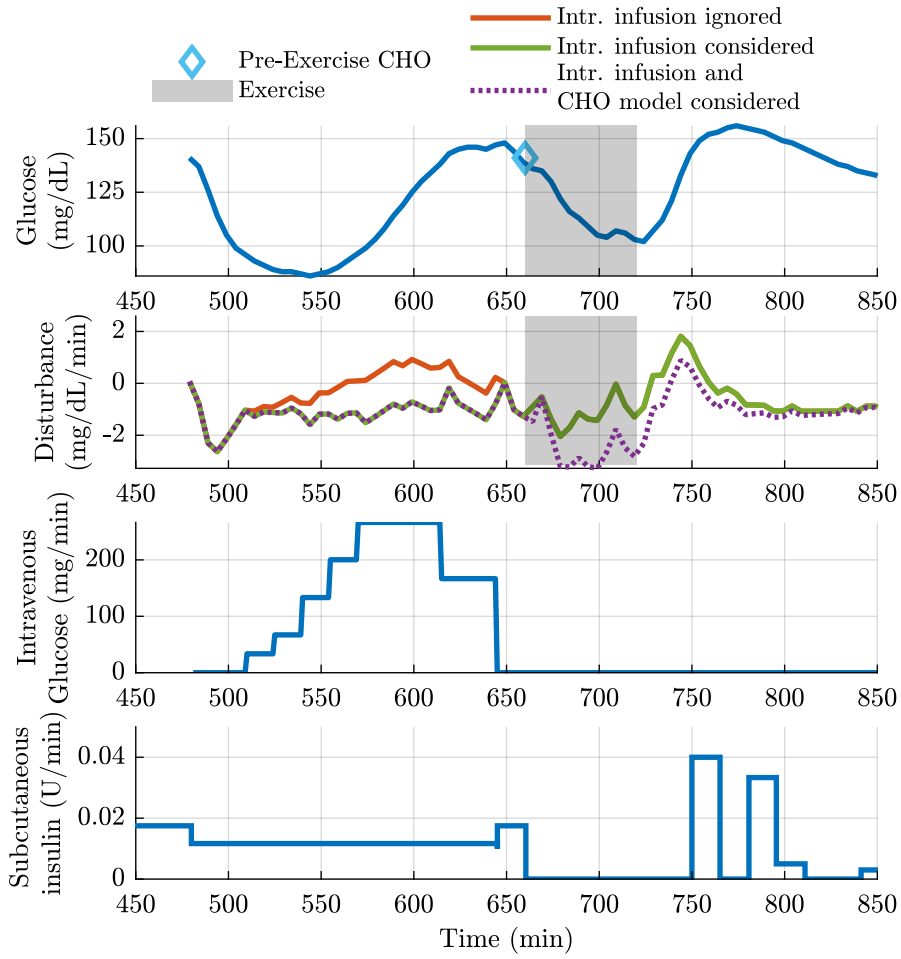

Figure 4.6: Need for considering intravenous infusions and the pre-exercise carbohydrate (CHO) intake as observer inputs. The first, third, and fourth panels show the preprocessed glucose signal, the intravenous glucose infusion, and the subcutaneous insulin infusion, respectively. The second panel includes the disturbance estimation under three cases: when the observer ignores the intravenous dose (orange line), when the observer accounted for it (green line), and when the observer considers the 23-g intake besides the intravenous infusion (dotted line). The blue diamond in the first panel denotes the 23-g carbohydrate consumed before exercise. The transparent gray areas in the first and the second panels represent the exercise period; this is an example of an aerobic session in the dataset.

also lowers within the exercise period regarding the pre-exercise period value (see the thick blue line in the second panel of Figure 4.7).

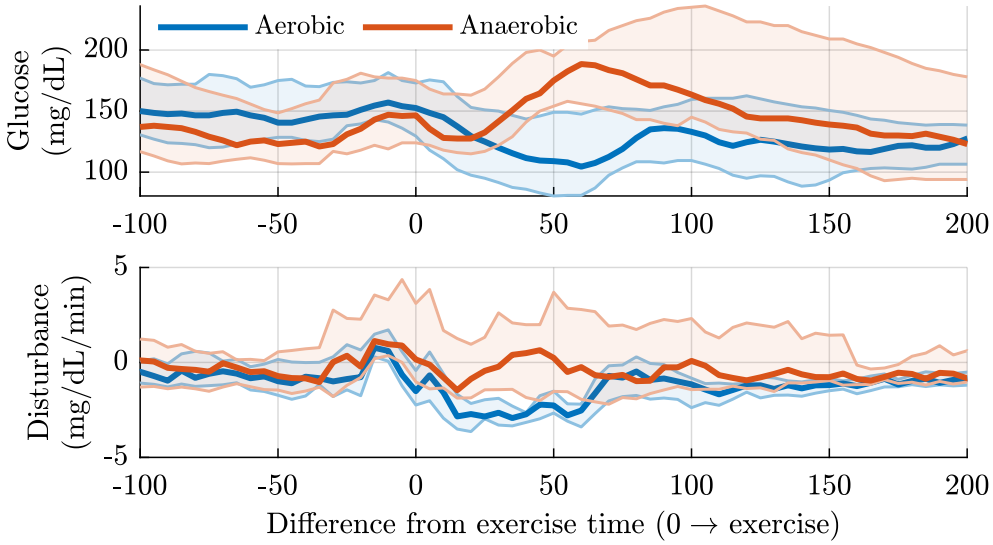

Figure 4.7: Exercise disturbance estimation from clinical data. The thick lines represent the median of the aerobic (blue) or anaerobic (orange) sessions and the shaded areas, the interquartile range. The 0 on the x-axis marks the exercise beginning.

Regarding the estimated disturbance of anaerobic exercise sessions, its median increases (see the thick orange line in the second panel of Figure 4.7). However, the estimated disturbance also decreases right after the exercise onset. This initial drop is highly dependent on the carbohydrate absorption model parameters, as illustrated in Figure 4.8 (top panel): the slower the carbohydrate absorption has been modeled, the lower will decrease the estimated disturbance. In fact, the initial drop is almost inexistent in the absence of a carbohydrate model. A similar effect of the carbohydrate absorption model parameters appears in the aerobic sessions: without the carbohydrate model, the estimated disturbance remains unaffected regarding the basal period, but the quicker the absorption is modeled, the sharper the disturbance drops within the exercise period.

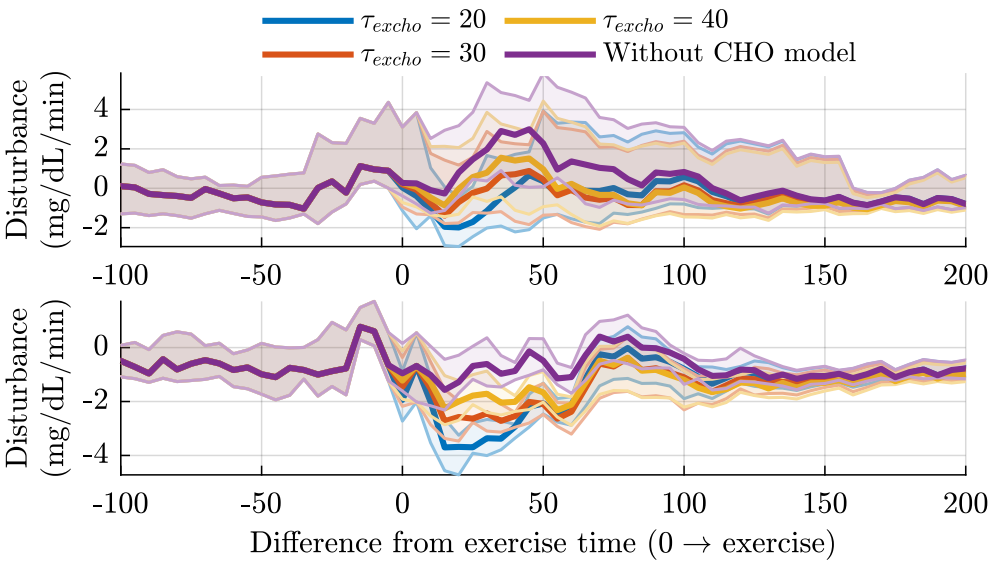

Figure 4.8: Effect of the carbohydrate absorption time of the model on the estimated disturbance. The thick lines represent the median of the aerobic (bottom panel) or anaerobic (top panel) sessions, and the shaded areas denote the interquartile range. The 0 on the x-axis marks the exercise beginning.

4.6 Conclusions

Real disturbances have been reconstructed retrospectively, feeding the observer (the FOSMO designed with the IVP model) with the CGM and pump infusions collected in clinical trials. Two datasets were used for this purpose: one for meal disturbances and another for exercise disturbances. On the one hand, the estimated meal disturbance follows the expected profile in the median. However, the variability was high, and, in some individual estimations, the variability hid the meal effect. On the other hand, the estimated exercise disturbances initially had a similar profile regardless of the exercise type (aerobic or anaerobic). Only after considering a carbohydrate rescue model and the intravenous infusions in the observer did the estimated disturbances related to the aerobic exercise slightly differ from those of the anaerobic sessions.

The examples of the estimated disturbances presented in this chapter evince that many unknown or unmodeled effects are lumped in the estimated disturbance, cofounding the estimation of the meal or exercise disturbance. Isolating the effect of the meal or the exercise from this lumped disturbance is challenging. Thus,

when designing a controller, disturbances must be treated holistically. In other words, the controller should not expect an ideal disturbance triggered by a single event (e.g., a meal or an exercise period); it should expect a disturbance signal where many perturbations are lumped on it.

Chapter 5

Super-twisting-based meal detector

Postprandial control requires increasing the insulin dosing at mealtime. To this end, hybrid artificial pancreas users must estimate the meal carbohydrate content and provide it to the system. An alternative to free users from this burdensome task is to detect the mealtime from the glucose measurements. In this chapter, a meal detector algorithm is designed. The proposed meal detector determines the meal occurrence from the glucose derivative and the discrepancy between the glucose reading and its estimation obtained from a super-twisting observer. The algorithm is also assessed using simulated and clinical datasets.

Authored publications related to this chapter:

- Sala-Mira, I.; Díez, J.-L.; Ricarte, B., et al. (2019). "Sliding-mode disturbance observers for an artificial pancreas without meal announcement". In: *Journal of Process Control (JCR 2019: Q2)* 78, pp. 68–77. ISSN: 09591524. DOI: 10.1016/j.jprocont.2019.03.008.

- Faccioli *, S.; Sala-Mira *, I.; Diez, J.-L., et al. (2021). "Super-Twisting Observer For Meal Detection Assessed In Realistic Scenarios using UVA/Padova T1D Simulator". In: *Diabetes Technology & Therapeutics. 14th International Conference on Advanced Technologies & Treatments for Diabetes*. Vol. 23. S2. Virtual, A–76. DOI: 10.1089/dia.2021.2525.abstracts.

- Faccioli *, S.; Sala-Mira *, I.; Díez, J., et al. (2022). "Super–twisting-based meal detector for type 1 diabetes management: Improvement and assessment in a real-life scenario". In: *Computer Methods and Programs in Biomedicine (JCR 2021: Q1)* 219, p. 106736. ISSN: 0169-2607. DOI: 10.1016/j.cmpb.2022.106736.

* *denotes equal contribution.*

5.1 Introduction

Hybrid AP systems adopt pre-meal insulin boluses from the open-loop therapy to advance the required insulin, reducing glucose fluctuation within the postprandial period. Nevertheless, to calculate these boluses, patients must estimate meal carbohydrates, which is a demanding, prone-to-error task.

Meal detection is appealing to free diabetic patients from carbohydrate counting. These algorithms can determine whether a meal occurred; with this information, the controller can temporaly increase the insulin delivery, infusing some insulin boluses (Fathi et al. 2019; Mahmoudi et al. 2019) or switching to a more aggressive controller (Fushimi et al. 2019; Bhattacharjee et al. 2019).

The design of a meal detector usually requires two steps: 1) to calculate signals and features that largely deviate when meals occur, and 2) to find rules determining whether a meal has occurred. Regarding the features selection, although some alternatives to the CGM signal exist (e.g., heart rate (Zheng et al. 2019), abdominal sound (Kolle et al. 2019), head movement (Rahman et al. 2015), etc.), most features usually root from CGM readings such as:

- CGM values (Dassau et al. 2008),
- approximations of the CGM derivative (Zheng et al. 2019)
- glucose predictions (Chen et al. 2019),
- innovation residuals (Fathi et al. 2019; Meneghetti et al. 2021),
- or meal rate of glucose appearance estimations (Ramkissoon et al. 2018)

Concerning the meal detector logic, the most extended method is to apply *ad-hoc* thresholds to the features (Harvey et al. 2014b). Other techniques rely on interval thresholds Meneghetti et al. 2021, hypothesis tests (Fathi et al. 2019; Mahmoudi et al. 2019), or binary classifiers (Kölle et al. 2020; Zheng et al. 2020). Moreover, other approaches have also addressed the estimation of the meal carbohydrate content, such as Samadi et al. (2018), Fathi et al. (2019), and Chen et al. (2019).

In this chapter, a meal detector is designed to be integrated next in the meal-announcement free system developed in Chapter 6. The meal detector uses the glucose derivative and the glucose residuals generated by a super-twisting observer as detection features. The detection logic is based on thresholds applied to these signals. Finally, the meal detector is evaluated with simulated and clinical data.

5.2 Super-twisting-based meal detector

The meal detection is addressed as a fault detection problem (Venkatasubramanian et al. 2003): the CGM reading signal is compared to an estimation to form a residual signal. The estimation must accurately follow the CGM reading in the absence of the meal disturbance but largely deviate from it when the disturbance appears (the fault). This sensitiveness to the disturbance will allow its detection with simple decision rules based on thresholds. This section details the estimator used to construct the residuals and the decision logic determining the detection occurrence.

5.2.1 Residual generator

Sliding mode observers can be tuned to estimate a predefined disturbance level signal accurately. If the actual disturbance is below this predefined level, the error will be attained to the sliding surface converging to zero. However, the estimation error will leave the sliding surface if the disturbance exceeds this level. This behavior appeals to construct residuals being sensitive to the disturbances: the residuals are close to zero when disturbances are low but deviate from zero when the disturbances exceed some level defined beforehand (Hermans et al. 1996; Hu et al. 2016). This section applies the super-twisting observer of Levant (1998) and Davila et al. (2005) to generate the residuals. The super-twisting observer is a second-order sliding mode observer that, like the first-order sliding mode observers, features robustness properties against matched disturbances. Despite FOSMO could have been used, we had to resource in Chapter 3 to an implicit discretization to alleviate chattering. In this chapter, super-twisting observers are investigated for such purpose. The advantage of the super-twisting observer is that the discontinuity of the output error injection term is hidden in the derivative, alleviating the chattering problem.

Levant (1998) proposed the super-twisting observer for the following dynamic system:

$$\begin{aligned} \dot{z}_1(t) &= z_2(t) \\ \dot{z}_2(t) &= f(z_1(t), z_2(t), u(t)) + \xi(t) \end{aligned} \tag{5.1}$$

where $z_1(t)$ is the measurable state variable and $z_2(t)$ its derivative; $f(z_1(t), z_2(t), u(t))$ is a know term of the system, and $\xi(t)$ is an unknown bounded disturbance.

The super-twisting observer is given by (Davila et al. 2005):

$$\begin{aligned}\dot{\hat{z}}_1(t) &= \hat{z}_2(t) + k_1 \left|\tilde{z}_1(t)\right|^{0.5} \operatorname{sign}\left(\tilde{z}_1(t)\right) \\ \dot{\hat{z}}_2(t) &= f(z_1(t), \hat{z}_2(t)) + k_2 \operatorname{sign}\left(\tilde{z}_1(t)\right)\end{aligned} \tag{5.2}$$

where $\hat{z}_1(t)$ and $\hat{z}_2(t)$ are the estimates of $z_1(t)$ and $z_2(t)$, respectively. $\tilde{z}_1$ denotes the estimation error (or residual), i.e., $\tilde{z}_1(t) = z_1(t) - \hat{z}_1(t)$. The parameters k_1 and k_2 are the gains to be designed.

The dynamics of the residuals are the following:

$$\begin{aligned}\dot{\tilde{z}}_1(t) &= \tilde{z}_2(t) - k_1 \left|\tilde{z}_1(t)\right|^{0.5} \operatorname{sign}\left(\tilde{z}_1(t)\right) \\ \dot{\tilde{z}}_2(t) &= F(t) - k_2 \operatorname{sign}\left(\tilde{z}_1(t)\right)\end{aligned} \tag{5.3}$$

where $F(t)$ is a disturbance term lumping the discrepancies between the nominal model and the actual system, i.e., $f(z_1(t), z_2(t)) - f(z_1(t), \hat{z}_2(t))$, and the disturbance $\xi(t)$. $F(t)$ is bounded as $|F(t)| < L$ for a positive scalar L.

By appropriately selecting k_1 and k_2, the variables $\tilde{z}_1(t)$ and $\dot{\tilde{z}}_1(t)$ converge to zero in finite time despite the disturbance $F(t)$. The convergence of the algorithm was proved with geometric methods (Levant 1998; Davila et al. 2005) and with Lyapunov-based techniques (Moreno et al. 2008). The tuning proposed by Levant (1998), i.e.,

$$k_1 = 1.5L^{0.5} \qquad k_2 = 1.1L \tag{5.4}$$

is utilized in this chapter since it is considered a trade-off between fast convergence and accuracy (Shtessel et al. 2014, Section 4.3.2).

Note that $F(t)$ can be regarded as the fault in the context of a fault detection problem (Hu et al. 2016). The parameter L controls the sensitivity of the detection: if L is too high, the algorithm will disregard most of the faults; if L is too low, any discrepancy on $f(z_1(t), z_2(t))$ or noise will be acknowledged as a fault.

Application to the meal detection problem

So far, it has been seen how the super-twisting observer can be applied as a residual generator for a system affected by the fault/disturbance $F(t)$. For the super-twisting to be applied in the meal detection problem, the disturbance $F(t)$ should be related to the meal disturbance. To illustrate this relation, consider the last two equations of the IVP model (see 3.3.1 for more details),

$$\dot{I}_{EFF}(t) = -p_2 \cdot I_{EFF}(t) + p_2 \cdot S_I \cdot I_P(t) \tag{5.5}$$

$$\begin{aligned} \dot{G}(t) = &-(GEZI + I_{EFF}(t)) \cdot G(t) + \\ &+ EPG + R_A(t) \end{aligned} \tag{5.6}$$

and apply the following change of variables:

$$\begin{aligned} z_1(t) &\coloneqq G(t) \\ z_2(t) &\coloneqq -(GEZI + I_{EFF}(t))G(t) + EPG \quad , \end{aligned} \tag{5.7}$$

which results in the dynamic system defined as follows:

$$\begin{aligned} \dot{z}_1(t) &= z_2(t) + R_A(t) \\ \dot{z}_2(t) &= f(z_1(t), z_2(t), I_P(t)) + p(z_1(t), z_2(t))R_A(t) \end{aligned} \tag{5.8}$$

with:

$$\begin{aligned} f(z_1(t), z_2(t), I_P(t)) &\coloneqq p_2(EGP - z_2(t) - GEZIz_1(t) - S_I I_P(t) z_1(t)) + \\ &\quad + \frac{z_2(t)^2}{z_1(t)} - EGP\frac{z_2(t)}{z_1(t)} \\ p(z_1(t), z_2(t)) &\coloneqq \frac{z_2(t) - EGP}{z_1(t)} \end{aligned} \tag{5.9}$$

The application of the observer (5.2) leads to the following residuals dynamic:

$$\begin{aligned} \dot{\tilde{z}}_1(t) &= \tilde{z}_2(t) - k_1 \left|\tilde{z}_1(t)\right|^{0.5} \operatorname{sign}\left(\tilde{z}_1(t)\right) + R_A(t) \\ \dot{\tilde{z}}_2(t) &= \left(f(z_1(t), z_2(t), I_P(t)) - f(z_1(t), \tilde{z}_2(t), I_P(t))\right) + \\ &\quad + p(z_1(t), z_2(t))R_A(t) - k_2 \operatorname{sign}\left(\tilde{z}_1(t)\right) \end{aligned} \tag{5.10}$$

where $I_P(t)$ can be calculated integrating the pharmacokinetic equations of the IVP model (3.27)–(3.28). Note that expression (5.10) does not resemble the super-twisting dynamics in (5.3) because $R_A(t)$ appears in the first equation. To remove the $R_A(t)$ from the first equation of (5.10), consider a new auxiliary variable defined as follows:

$$\phi(t) \coloneqq \tilde{z}_2(t) + R_A(t) \tag{5.11}$$

After applying the above transformation, the residuals becomes

$$\begin{aligned} \dot{\tilde{z}}_1(t) &= \phi(t) - k_1 \left|\tilde{z}_1(t)\right|^{0.5} \operatorname{sign}\left(\tilde{z}_1(t)\right) \\ \dot{\phi}(t) &= \Big(f(z_1(t), z_2(t), I_P(t)) - f(z_1(t), \tilde{z}_2(t), \hat{I}_P(t))\Big) + \quad , \\ &\quad + p(z_1(t), z_2(t))R_A(t) + \dot{R}_A(t) - k_2 \operatorname{sign}\left(\tilde{z}_1(t)\right) \end{aligned} \tag{5.12}$$

which has the form of (5.3) for

$$\begin{aligned} F(t) = &\left(f(z_1(t), z_2(t), u(t)) - f(z_1(t), \tilde{z}_2(t), u(t))\right) + \\ &+ p(z_1(t), z_2(t))R_A(t) + \dot{R}_A(t) \end{aligned} \tag{5.13}$$

Since $F(t)$ depends on the meal disturbance and its derivative, the residuals generated by the super-twisting are suitable for meal detection. The super-twisting can be designed to ensure that the residuals are close to zero in the absence of meal disturbances (see the first 200 min in Figure 5.1) while deviating from zero when meals are ingested (see Figure 5.1). Nevertheless, $F(t)$ also includes unmodeled dynamics; hence L must be selected large enough to avoid the observer losses the convergence due to these factors unrelated to the meal disturbance.

Another consideration before applying the super-twisting to the meal detection problem is its discretization. The super-twisting hides the discontinuities in the derivative, which reduces the chattering effect compared to first-order sliding mode observers, and allows the application of the explicit discretization. The Euler explicit discretization of the observer is given by:

$$\begin{aligned} \hat{z}_1[k] &= T_s \hat{z}_2[k-1] + T_s k_1 \left|\tilde{z}_1[k-1]\right|^{0.5} \operatorname{sign}\left(\tilde{z}_1[k-1]\right) + \hat{z}_1[k-1] \\ \hat{z}_2[k] &= T_s f(z_1[k-1], \hat{z}_2[k-1], u[k-1]) + \\ &\quad + T_s k_2 \operatorname{sign}\left(\tilde{z}_1[k-1]\right) + \hat{z}_2[k-1] \end{aligned} \tag{5.14}$$

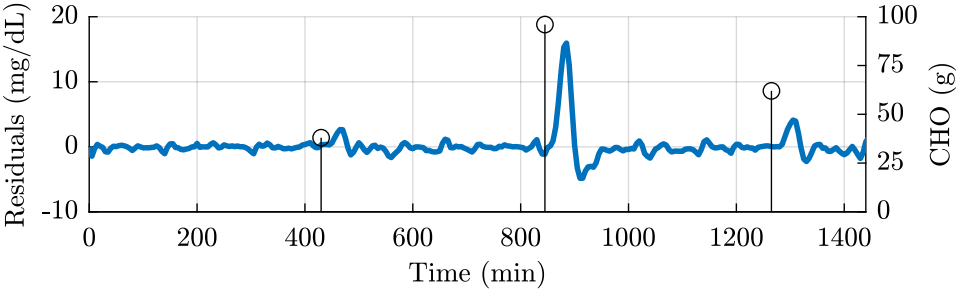

Figure 5.1: Example of the residual signal generated by the super-twisting. The simulation was performed with the modified version of the UVa/Padova simulator. The left axis refers to the residuals. The circles indicate the presence of a meal with a carbohydrate content given in the right axes.

where T_s is the sampling time, and k is the discrete iteration. However, despite the chattering reduction, its magnitude is still too high when $T_s = 5\,\text{min}$, the CGM sampling time (see blue line in 5.2). Although implicit discretization methods will be explored later (see Section 5.4.1), in a first implementation of the algorithm, it was decided to resort to subsampling: the discretized super-twisting observer (5.14) was executed N times within the measurement sampling period and the output of the last evaluation within the period was taken as the glucose estimation considered in the calculation of the residuals, i.e., $\tilde{z}_1 = z_1(t) - \hat{z}_1(t)$. Figure 5.2 compares the effect of the subsampling. Evaluating the algorithm only five times within the measurement sampling period ($N = 5$) considerably reduces the magnitude of the chattering.

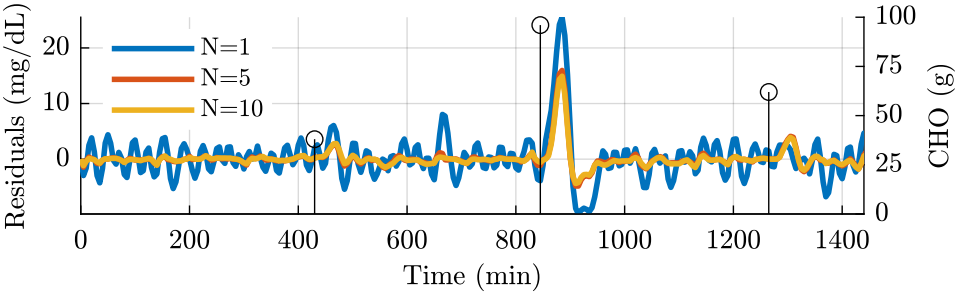

Figure 5.2: Use of subsampling to reduce the chattering in the super-twisting. The simulation was performed with the modified version of the UVa/Padova simulator. N defines the number of evaluations the super-twisting was executed within the 5 min of the measurement sampling time. The left axis refers to the residuals. The circles indicate the presence of a meal with a carbohydrate content given on the right axis.

5.2.2 Decision rules

Other disturbances besides meals (e.g., exercise) and uncertainties might also impact the residuals since, as shown in Chapter 4, $R_A(t)$ will be an aggregation of multiple disturbances on the glucose rate. Therefore, the algorithm also considers the glucose derivative to identify disturbances increasing the glucose. The glucose derivative is calculated with Euler's approximation:

$$\widehat{der}[k] = \frac{z_1[k] - z_1[k-1]}{T_s} \tag{5.15}$$

where T_s is the measurement sampling time, i.e., 5 min.

Figure 5.3 illustrates the detection process: the algorithm raises a detection flag when the residual signal overpasses a certain threshold ($\tilde{z}_1(k) > th_{res}$) and glucose increases at a specific rate ($\widehat{der}(k) > th_{der}$).

In addition, if a new detection occurred before 90 min (TW_{off}) from last detection, no flag would be raised to avoid multiple detections triggered by the same meal. Lastly, the algorithm inhibits any detection in the first 30 min (TW_{warmup}) after the initialization to prevent false detections caused by the transient of the super-twisting observer.

The parameters of the algorithm were tuned through exhaustive simulations under an scenario of 14 days with 3 daily meals generated by the modified version of the UVa/Padova simulator. The resulting parameters were the following:

$L = 0.09\,\mathrm{mg/(dL\,min^2)}$	$th_{res} = 1.75\,\mathrm{mg/dL}$	$th_{der} = 1.2\,\mathrm{mg/(dL\,min)}$
$N = 5$	$TW_{warmup} = 30\,\mathrm{min}$	$TW_{off} = 90\,\mathrm{min}$

Lastly, it was found that including the model information, i.e., the term $f(z_1[k-1], \hat{z}_2[k-1], u[k-1])$, has an unimportant impact on the residual generation; hence, it has eventually set to zero.

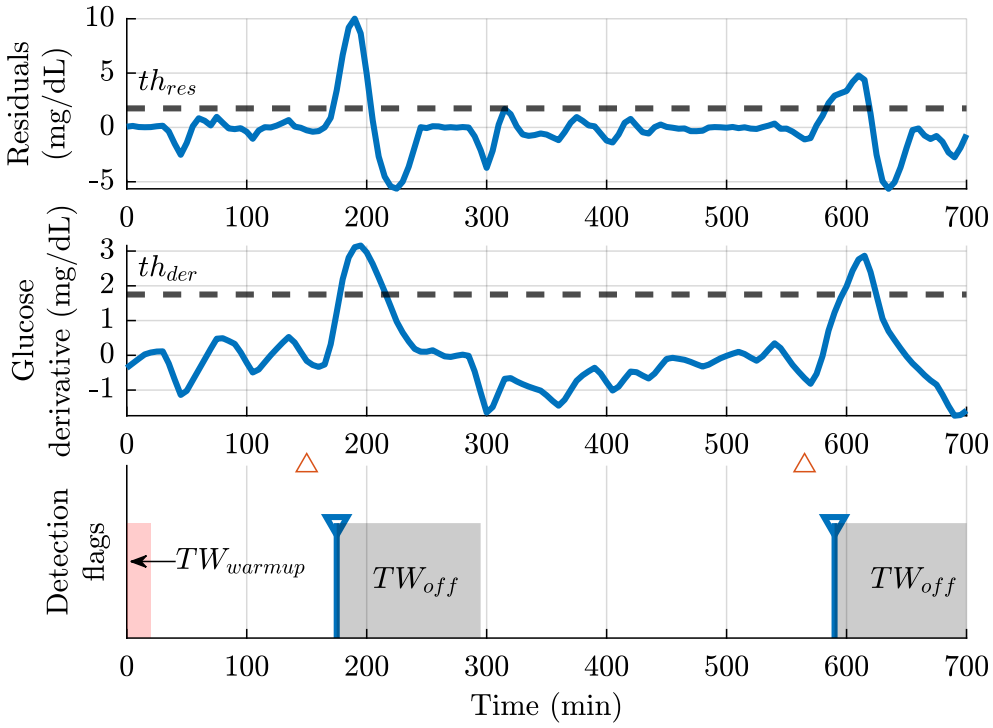

Figure 5.3: Meal detection process. The algorithm raises a flag (bottom panel, blue inverted triangles) when the residuals (upper panel) and the glucose derivative (middle panel) exceed, respectively, the thresholds th_{res} and th_{der}. Any detection within the warm-up window (TW_{warmup}) or the shut-off window (TW_{off}) is inhibited. Orange triangles in the bottom panel denote actual mealtimes.

5.3 In silico evaluation

The meal detector algorithm described in the above sections was evaluated with two versions of the UVa/Padova simulator: the modified academic version previously used in this dissertation and a more recent version of the simulator (Vettoretti et al. 2018), which was made accessible to the group in the context of a collaboration with University of Padova. This new version includes several features that allow more realistic simulations compared to the modified version: it has a more numerous adult cohort (100 virtual adults vs. 10 virtual adults); it extends the built-in physiological model with new phenomena real subjects experiment in the daily life, such as the "dawn effect"; it represents more realistically the variation of the

intra-day insulin-sensitivity and the subjects' therapy parameters; and, it upgrades the CGM model with the Dexcom G5 CGM noise model.

A scenario of 14-days with three daily meals was configured for both simulators. However, the new version of the simulator also included hypoglycemia treatments, that is, fast-absorption carbohydrates to recover from hypoglycemia. In addition, the new UVa/Padova simulates daily sensor calibrations, making the detection more challenging.

The following metrics were considered to assess the performance of the meal detector algorithm:

- **Number of True Positives (TPs)**: A TP occurs when the algorithm raises a detection flag within the first 120 min after a meal is consumed. This detection window was also considered in Ramkissoon et al. (2018).
- **Number of False Positives (FPs)**: A FP occurs when the algorithm raises a detection flag, but no meal has been ingested in the last 120 min. Also, the **number of FPs per day (FP/day)** is provided to simplify the comparison with datasets with different numbers of meals.
- **Number of False Negatives (FNs)**: A FN occurs when the algorithm does not raise any detection flag after 120 min of the meal consumption.
- **Recall**: Percentage of meals that are identified correctly, that is (Dalianis 2018):

$$\text{Recall} = \frac{TP}{TP + FN} \cdot 100$$

- **Precision**: Percentage of detections corresponding to actual meals, that is (Dalianis 2018):

$$\text{Precision} = \frac{TP}{TP + FP} \cdot 100$$

- **F1-score**: This metric merges in a single value the Recall and Precision, assuming them as equally important. The definition of the F1-score is the following (Dalianis 2018):

$$\text{F1-score} = 2 \cdot \frac{Precision \cdot Recall}{Precision + Recall}$$

- **Detection time**: The time (min) elapsing from the meal onset to the detection in the case of the TPs.
- **Carbohydrates related to FNs ($\mathbf{CH_{FN}}$)**: Meal carbohydrate content (g) of those meals undetected by the algorithm.

The hypoglycemia treatments were considered as meal intakes when computing the above metrics.

Table 5.1 summarizes the results of the validation. The results with the modified version of the simulator (first column of Table 5.1) are close to other works in the literature using a similar version of the simulator (but with different configurations of the scenarios, such as variability generation, and different evaluation criteria). For example, the proposed algorithm outperforms the 82 % mean recall of (Hyunjin et al. 2009), but it achieved a sligthly lower recall than Ramkissoon et al. (2018) (93 %) or Xie et al. (2017) (91 %). In addition, the proposed algorithm outperforms the detection time achieved by Ramkissoon et al. (2018) (37(83) min, mean (standard deviation)) and Xie et al. (2017) (45(83) min).

However, the algorithm performance declines under the scenario generated with the newest version of the simulator: the number of FP/day is 20 times greater than using the modified version, and the precision is reduced to 57[11] % (median, [interquartile range]). Meneghetti et al. (2021) also illustrate that the new UVa/-Padova simulator provides a more challenging scenario for meal detections. The detection time of the algorithm they proposed almost doubles the achieved by the super-twisting-based meal detector, although significantly enhancing the FP/day.

To understand why the newest version of the simulator led to more FPs, Figure 5.4 plots the signals involved in the detection (the residuals and the glucose derivative) for both simulators. Observe that the more challenging variability of the new simulator causes larger residuals and a noisier glucose derivative, hence being more likely to exceed the corresponding threshold. Therefore, a new tuning is needed.

5.4 Algorithm refinements

A straightforward method to reduce the FPs in the new version of the UVa/Padova simulator is increasing the thresholds of the derivative and the residuals (Figure 5.4). However, the price to pay is an increase in the detection time. In this section, three features are implemented that would allow reducing the number of FPs without a remarkable increase of the detection time: 1) an implicit discretization of the super-twisting to reduce the size of the residuals by increasing the L, ,

Table 5.1: Performance of the super-twisting-based meal detector with datasets generated in silico

Metrics	**Modified UVa/Padova**	**New UVa/Padova**	
	Original STMD	*Original*	*Enhanced*
Number of meals	42 [0]	50 [8]	50 [8]
TP	38 [5]	44 [8.5]	41 [13]
FN	4 [5]	6 [4]	9.5 [10]
FP	1 [1]	34 [9]	1 [1.5]
Recall (%)	90.5 [12]	88 [7]	82 [17]
Precision (%)	93.4 [6.5]	57 [11]	96 [5]
F1-score (%)	90.9 [8.1]	69 [9]	88 [10]
FP/day	0.1 [0]	2.4 [0.7]	0.1 [0.1]
CH_{FN} (g)	48.3 [6.4]	59 [42]	37 [34]
Detection time (min)	30 [5]	30 [20]	35 [15]

The results of two simulators are included: the modified academic UVa/Padova simulator (second column) and the newest version of the UVa/Padova simulator (third column), which includes more subjects and sources of variability (see Section 5.3 for more details). The second and third columns (*Original*) correspond to the results of the meal detector described in Section 5.2, while the fourth column (*Enhanced*) includes the refinements of Section 5.4. Metrics are expressed as median [interquartile range]. *Notation:* TP (true positive), FN (false negative), FP (false positive), CH_{FN} (meal size related to FN).

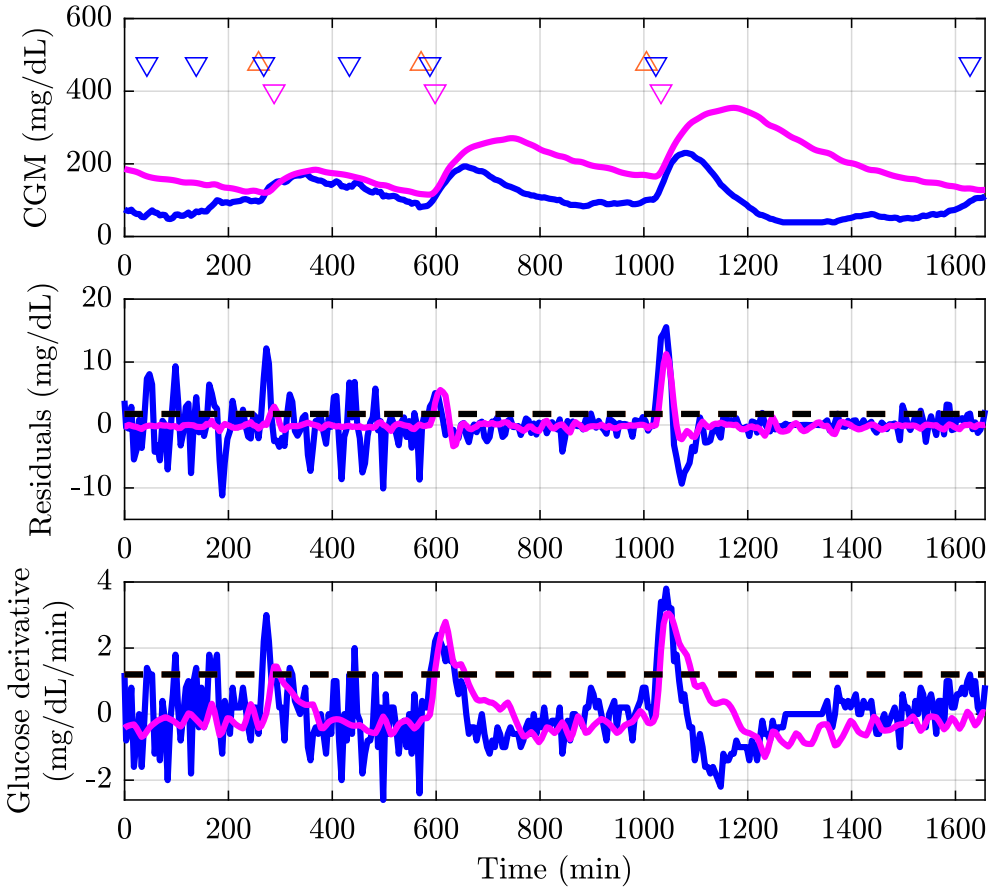

Figure 5.4: Comparison of the meal detector under the modified and the new UVa/Padova simulator version. The glucose (upper panel), the residuals (middle panel), and the glucose derivative (bottom panel) of the modified academic UVa/Padova simulator (magenta lines) and the new full version (blue lines) are represented. Orange upwards triangles denote actual mealtimes, while downwards triangles represent detection events under the modified version of the simulator (magenta) and the newest version (blue).

mitigating the increase of the chattering that this would provoke in an explicit discretization implementation; 2) a KF to smooth the glucose derivative; and 3) an alarm silencing logic to avoid calibration-related spurious detections, nonexistent in the own version of the simulator.

5.4.1 Implicit discretization of the super-twisting

Large residuals, especially in the absence of meals (see, for example, the first 200 min of Figure 5.4, reveals a convergence issue of the super-twisting observer caused because the uncertainty $F(t)$ in (5.10) is larger than the predefined upper bound L. Therefore, L must be increased to improve the convergence. However, the explicit discretization of the observer limits the maximum L since the larger the L, the larger the chattering will be (Brogliato et al. 2021).

Like for the FOSMO in Section 3.2.2, the implicit discretization of the super-twisting can effectively reduce the chattering even for large L (Xiong et al. 2020; Brogliato et al. 2020). The implicit discretized counterpart of (5.14) – considering, for simplicity, $f(z_1(t), \hat{z}_2(t)) = 0$ – is the following:

$$\begin{cases} \hat{z}_1[k] - \hat{z}_1[k-1] = T_s \hat{z}_2[k] + T_s k_1 \left|\tilde{z}_1[k]\right|^{0.5} \psi[k] & \text{(5.16a)} \\ \hat{z}_2[k] - \hat{z}_2[k-1] = T_s k_2 \psi[k] & \text{(5.16b)} \\ \psi[k] \in \operatorname{msign}\left(\tilde{z}_1[k]\right) & \text{(5.16c)} \end{cases}$$

where $\operatorname{msign}(\cdot)$ is the multi-valued signum function defined in (3.71). Like in Section 3.2.2, a causal expression for (5.16) can be obtained. First, plugging $\hat{z}_2[k]$ of (5.16b) into (5.16a) results in

$$\hat{z}_1[k] - g[k] = \left(T_s^2 k_2 + T_s k_1 \left|z_1[k] - \hat{z}_1[k]\right|^{0.5}\right) \psi[k] \quad , \tag{5.17}$$

with

$$g[k] \coloneqq \hat{z}_1[k-1] + T_s \hat{z}_2[k-1]$$

Then, expression (5.17) is solved for the three intervals $\operatorname{msign}(\cdot)$ defines (Xiong et al. 2020): $\tilde{z} = 0$, $\tilde{z} > 0$, and $\tilde{z} < 0$.

- **For $\tilde{\mathbf{z}}_\mathbf{1}[\mathbf{k}] = \mathbf{0}$**, it is immediate that $\hat{z}_1[k] = z[k]$ and, hence, (5.17) becomes:

$$\tilde{z}_1[k] \in z_1[k] - g[k] - T_s^2 k_2 \psi[k] \tag{5.18}$$

The above expression can be represented as (3.77), that is,

$$e_y[k] = e^*[k] - \beta[k]\psi[k]$$

with $e^*[k] = z_1[k] - g[k]$ and $\beta[k] = T_s^2 k_2$. Consequently, applying the same procedure in Section 3.4.2, the following solution for $\phi[k]$ is obtained:

$$\phi[k] = \text{proj}\left([-1,\, 1]\,;\, \frac{z_1[k] - g[k]}{T_s^2 k_2}\right) \tag{5.19}$$

where $\text{proj}\,(\cdot)$ can be expressed in terms of a saturation function as defined in (3.88).

- **For $\tilde{\mathbf{z}}_\mathbf{1}[\mathbf{k}] > \mathbf{0}$**, the definition of $\text{msign}\,(\cdot)$ implies that $\psi[k] = 1$, while (5.17) becomes:

$$\left(\frac{\hat{z}_1[k] - g[k] - T_s^2 k_2}{T_s k_1}\right) = |\tilde{z}_1|^{0.5} \tag{5.20}$$

Under the conditions $\tilde{z}_1[k] > 0$, $k_1 > 0$, $k_2 > 0$, and $T_s > 0$, set by definition, the following solution for $\hat{z}_1[k]$ exists from (5.20):

$$\begin{aligned}\hat{z}_1[k] = {} & g[k] + T_s^2 k_2 + \\ & + \frac{T_s^2 k_1^2}{2}\left(\sqrt{1 + \frac{4}{T_s^2 k_1^2}\left(z_1[k] - g[k] - k_2 T_s^2\right)} - 1\right)\end{aligned} \tag{5.21}$$

- **For $\tilde{\mathbf{z}}_\mathbf{1}[\mathbf{k}] < \mathbf{0}$**, $\psi[k] = -1$, and, proceeding like for $\tilde{z}_1[k] > 0$, $\hat{z}_1[k]$ is solved as:

$$\begin{aligned}\hat{z}_1[k] = {} & g[k] - T_s^2 k_2 - \\ & - \frac{T_s^2 k_1^2}{2}\left(\sqrt{1 - \frac{4}{T_s^2 k_1^2}\left(z_1[k] - g[k] - k_2 T_s^2\right)} - 1\right)\end{aligned} \tag{5.22}$$

Therefore, the implicit Euler discretization reads as (Xiong et al. 2020; Brogliato et al. 2020):

$$g[k] = \hat{z}_1[k-1] + T_s \hat{z}_2[k-1] \tag{5.23a}$$

$$\tilde{g}[k] = z_1[k] - g[k] \tag{5.23b}$$

$$\zeta[k] = \frac{4}{T_s^2 k_1^2} \left(\tilde{g}[k] - k_2 T_s^2 \right) \tag{5.23c}$$

$$\hat{z}_1[k] = \begin{cases} g[k] + T_s^2 k_2 + \dfrac{T_s^2 k_1^2}{2} \left(\sqrt{1 + \zeta[k]} - 1 \right) & \text{if } \tilde{g}[k] > T_s^2 k_2 \\ z_1[k] \text{ if } |\tilde{g}[k]| \leq T_s^2 k_2 \\ g[k] - T_s^2 k_2 - \dfrac{T_s^2 k_1^2}{2} \left(\sqrt{1 - \zeta[k]} - 1 \right) & \text{if } \tilde{g}[k] < -T_s^2 k_2 \end{cases} \tag{5.23d}$$

$$\psi[k] = \text{proj} \left([-1, 1]; \frac{\tilde{g}[k]}{T_s^2 k_2} \right) \tag{5.23e}$$

$$\hat{z}_2[k] = T_s k_2 \lambda[k] + \hat{z}_2[k-1] \tag{5.23f}$$

Figure 5.5 and Figure 5.6 illustrate the two benefits of implicit discretization regarding the explicit counterpart. On the one hand, the implicit discretization reduces the chattering amplitude, even removing it, when a sampling time of 5 min is used (Figure 5.5). On the other hand, the implicit discretization admits larger values for L without increasing the chattering (see bottom panel of Figure 5.6).

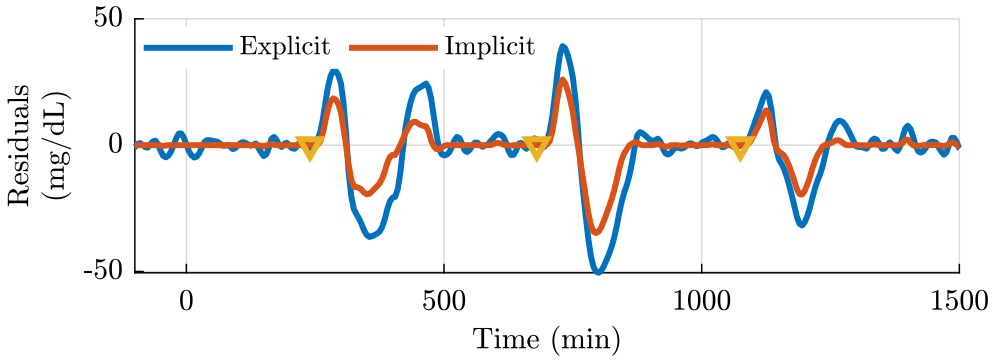

Figure 5.5: Chattering reduction at a 5-min sampling time. The implicit discretization reduces the chattering when no disturbances appear. Actual meal events are denoted with the orange triangles.

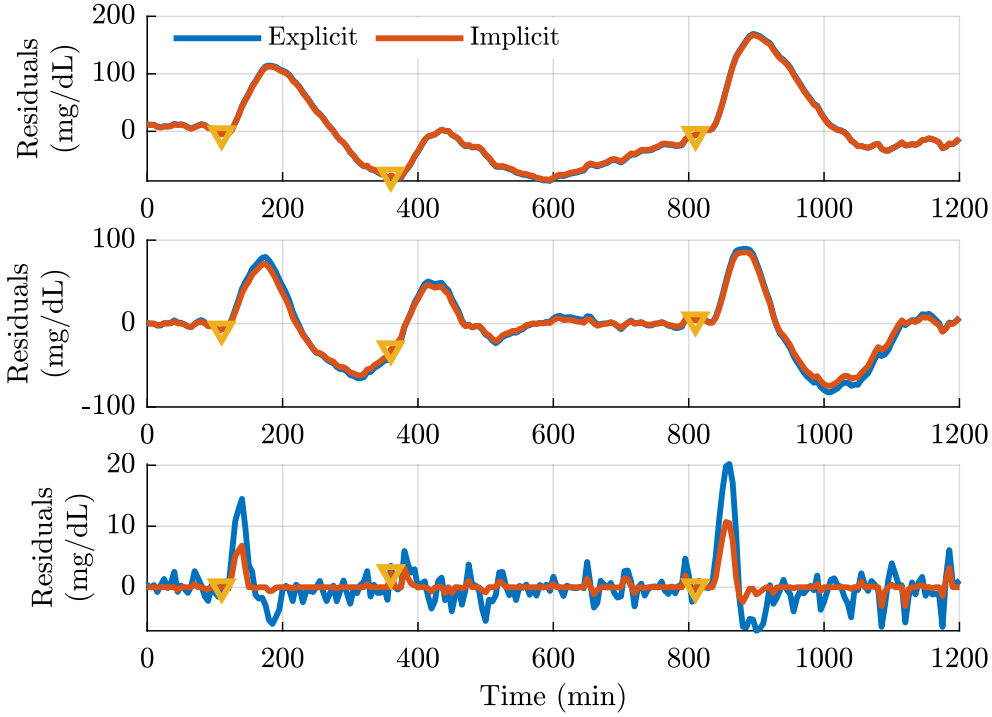

Figure 5.6: Comparison of discretization methods when increasing L. Three values for L were applied: $L = 0.001$ (upper panel), $L = 0.01$ (middle panel), and $L = 0.1$ (bottom panel). Actual meal events are denoted by the triangles.

5.4.2 Glucose derivative estimation with Kalman Filter

The noisy glucose derivative estimated by (5.15) was one of the reasons for the performance degradation when the meal detector was tested with the new version of the UVa/Padova simulator (see bottom panel of Figure 5.4). Here, a smoother glucose derivative estimation is provided using a KF.

The KF was built upon the following discrete-time third-order glucose description:

$$\begin{aligned} x[k+1] &= \underbrace{\begin{bmatrix} 1 & 1 & 0 \\ 0 & 1 & 1 \\ 0 & 0 & 1 \end{bmatrix}}_{A} \underbrace{\begin{bmatrix} cgm[k] \\ der[k] \\ f[k] \end{bmatrix}}_{x[k]} + \underbrace{\begin{bmatrix} 0 \\ 0 \\ 1 \end{bmatrix}}_{C} w[k] \\ y[k] &= \underbrace{\begin{bmatrix} 1 & 0 & 0 \end{bmatrix}}_{G} x[k] + v[k] \end{aligned} \tag{5.24}$$

where $cgm[k]$, $der[k]$, and $f[k]$ are, respectively, the glucose, its rate of change, and the rate of change of the rate of change (Dassau et al. 2008). The scalar noise signals, $w[k]$ and $v[k]$, are zero-mean with variance σ_v^2 and σ_w^2, respectively. These variances are selected as Bequette (2010): $\sigma_v^2 = 4$ and $\sigma_v^2 = 0.01$. It is assumed that $w[k]$ is uncorrelated from $v[\ell]$ for all k and ℓ.

The linear minimum variance estimate of the state vector can be obtained with the following linear recursive equations (Simon 2006, Section 5.3):

$$\begin{cases} K[k] = P^-[k]G^T[GP^-[k]G^T + \sigma_v^2]^{-1} \\ \hat{x}[k] = (I_3 - K[k]G)A\hat{x}[k-1] + K[k]y[k] \\ P[k] = (I_3 - K[k]G)(AP[k-1]A^T) + C\sigma_w^2 C^T \\ \hat{x}^-[k+1] = A\hat{x}^-[k] + K[k](y[k] - GA\hat{x}^-[k]) \\ P^-[k+1] = A(P^-[k] - K[k]G[k])A^T + C\sigma_w^2 C^T \end{cases} \tag{5.25}$$

where $\hat{x}^-[k]$ and $\hat{x}[k]$ are the a priori and a posteriori mean estimation of $x[k]$; and $P^-[k]$ and $P[k]$ are the corresponding covariance matrices. The above KF is the one-step formulation counterpart of the KF presented in Section 3.2.1 (Simon 2006).

5.4.3 Alarm silencing strategy

A CGM calibration could produce leaps in the CGM trace leading to spikes in the residuals and the glucose derivative. Therefore, the detection is disable for 30 min after calibration to avoid false detections.

5.4.4 Comparison with the initial proposal

The fourth column of Table 5.1 includes the results of the mean detector algorithm enhanced with the features described in the above subsections (i.e., implicit discretization of the super-twisting, KF for derivative estimation, and the alarm silencing strategy after calibrations). The enhanced meal detector considerably reduces the FP/day compared to the original version of the algorithm, with only an unimportant raise in the meal detection time, which still outperforms Meneghetti et al. (2021)'s proposal. However, the number of FNs increases from 6[4] to 9.5[10] regarding the initial version of the meal detector. Despite this increase of FNs, the carbohydrate content of the meals related to these FNs drops to 37[34] g. Therefore, while being more numerous, the FNs would likely have a lower impact on glucose; a feedback controller would handle these meals without requiring any feedforward action triggered by the meal detection (such as the proposed in Section 6). Indeed, 23 % of FNs will require no additional insulin injection since they correspond to carbohydrates supplementation ingested to avoid severe hypoglycemia.

5.5 Performance evaluation with clinical data

A retrospective evaluation with clinical data is presented in this section[1] to complement the above in silico comparisons.

[1]This work resulted from a collaboration with the Department of Information Engineering (DEI) of the University of Padova (Italy). Another PhD candidate (at the time of the work development), Simone Faccioli, participated in this evaluation and included it in his Phd dissertation. Therefore, this section only presents an overview of the contribution. More details can be found in his PhD dissertation and in the co-authored journal publication, Faccioli et al. (2022)

5.5.1 Dataset description

Data was collected in a multicenter clinical trial (Anderson et al. 2016, ClinicalTrials.gov Identifier: NCT02137512), originally conceived to evaluate the long-term feasibility of an AP system. The local IRB/ethical committee approved all experimental procedures.

The data employed for the retrospective analysis[2] correspond to a 14-day initial phase where 30 subjects underwent a sensor-augmented pump therapy in free-living conditions. Glucose data were measured every 5 min by a DexCom G4® sensor (DexCom, Inc., San Diego, CA, USA). Insulin was delivered with a Roche Accu-Check Spirit Combo® insulin pump (Roche Diabetes Care, Inc., Indianapolis, IN, USA). In addition, the participants were committed to entering the system all meals carbohydrate content to calculate the meal boluses. A total of 696 meals were registered.

5.5.2 Preprocessing

All the signals were synchronized to the same 5-min sample time grid. Regarding missing data in the CGM reading, on the one hand, entries with up to six consecutive missing values – a 30-min interval of missing data – were filled with the last available data. On the other hand, the meal detector algorithm was deactivated for entries with more than six consecutive missing values, being resumed when the CGM was recovered.

5.5.3 Parameters tuning

Data collected from free-living conditions are affected by a much larger incidence of unknown disturbances and confounding factors than in silico data; thus, retuning the parameters is necessary. The parameters th_{res} and th_{der} were selected to maximize the populational F1-score, a trade-off criterion between recall and precision. Although a subject-dependent tuning could also be considered by maximizing the individual F1-score, a populational tuning was preferred since some participants registered an insufficient number of meals (e.g., 11 out of 30 subjects have less than 20 registered meals for 14 days).

Regarding the parameter L, a new tuning is proposed to avoid using simulators as in Section 5.3. L roughly determines the maximum amplitude of $F[k]$ that

[2]The source of the data is the JDRF Artificial Pancreas Consortium coordinating center (JDRFAPPCC), but the analyses, content and conclusions presented herein are solely the responsibility of the authors and have not been reviewed or approved by the JDRFAPPCC. The public CTR3 dataset was financed by JDRF through the grants JDRF 22-2011-649 and JDRF 17-2013-509.

the super-twisting observer can handle without compromising the convergence. Since the observer should diverge after meal consumption for the meal detection problem, an ideal tuning for L would be to set this parameter as the upper bound of $F[k]$ within a starvation period, such as nighttime. However, the actual value of $F[k]$ is unknown. Alternatively, like for the estimation of the meal disturbance in Section 3.2.2, an estimation of $F[k]$, i.e., $\hat{F}[k]$, can be obtained by applying the equivalent control principle (Shtessel et al. 2014, Section 7.1.2): to maintain the sliding regime, the average value of $k_2 \operatorname{sign}(\tilde{z}_1)$, i.e., the equivalent injection term $k_2 \operatorname{sign}(\tilde{z}_1)_{eq}$, in (5.10) must be equal to $F[k]$. Since the equivalent injection term can be recovered by filtering the discontinuous term (Edwards et al. 2006), $\hat{F}[k]$ was calculated as follows:

$$\hat{F}[k] = \frac{T_s}{\tau_{ST}} \Big(k_2 \operatorname{sign}(\tilde{z}_1[k-1]) - \hat{F}[k-1] \Big) + \hat{F}[k-1] \tag{5.26}$$

where τ_{ST} is a positive constant set to 5 min.

Therefore, a personalized L was defined by selecting the maximum $\hat{F}[k]$ within the first night of each participant. Note that an a priori selection of L, i.e., L_0, is required to calculate $\hat{F}[k]$. If L_0 is too low, the estimation of the nocturnal $F[k]$ will be saturated; hence, L_0 must be chosen large enough to avoid this saturation. Selecting the super-twisting gains based on the estimated disturbance magnitude is frequently used for designing adaptive-gain super-twisting observers (e.g., Obeid et al. 2018).

5.5.4 Performance of the meal detector

The assessment metrics described in Section 5.3 were also applied to evaluate the meal detector algorithm in this section. However, the 120-min detection window used to consider a detection as a TP in Section 5.3 was extended to 180 min. This longer detection window, also utilized by Villeneuve et al. (2020), is required for a fair evaluation of the algorithm since several meals in the dataset remain flat, even decreasing, within the first 1-2 h after the participant registered the meal, as illustrated in Figure 5.7.

In addition, the dataset contains meals being registered very close to each other. If two meals elapsed less than 30 min, only the second one was accounted for computing the metrics. Lastly, hypoglycemia treatments were regarded as meals as in Section 5.3.

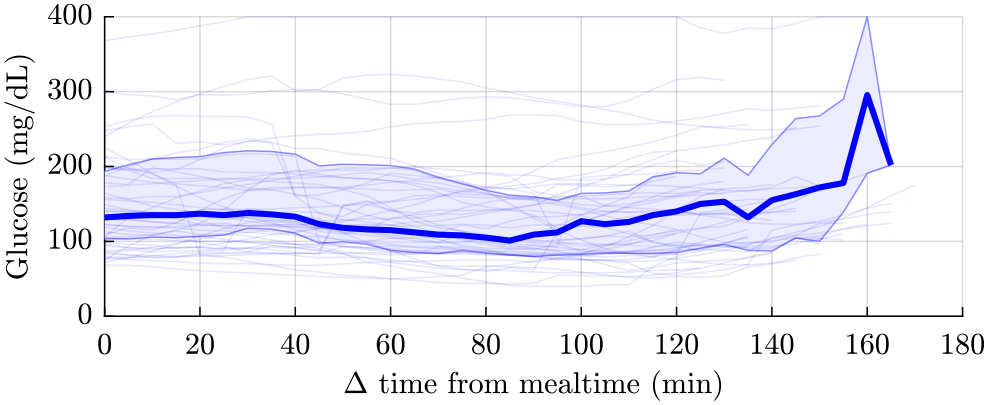

Figure 5.7: Postprandial response of slowly-absorbed meals. The 0 on the axis x corresponds to the mealtime. The thin lines are the individual postprandial responses, while the thicker blue line represents the median, and the shaded area is the interquartile range.

Table 5.2 compares the super-twisting-based meal detector with other algorithms assessed under real-life conditions in the literature. This comparison is only illustrative since it involved different datasets, preprocessing techniques, and evaluation criteria. The 70[13] % recall achieved by the proposed method is in line with most of the works found in the literature; only the PAIN (Weimer et al. 2016) and the LDA approaches (Koller 2016) outperform it. Conversely, the FP/day of the proposed algorithm tends to be lower, although the differences regarding "LDA CGM" and "Threshold Ra" are unimportant. Regarding the detection time, a median of 45 min may seem unsuitable for control purposes. Nevertheless, note that meals with a slow effect in increasing glucose distort this metric (see Figure 5.7). For instance, Figure 5.8 illustrates a case where the meal took more than 140 min to elevate glucose in 20 mg/dL. The algorithms in Kölle et al. (2020) outperform the proposed meal detector. However, the authors calculate the detection time as the difference between the detection and the time the glucose rate of change was more than 1 mg/(dL min); this criterion can lead to lower detection times than using the registered mealtime since it omits, for example, slow absorption periods like those shown in Figure 5.7.

The proposed algorithm has 7[3] FPs. In the context of a meal-free announcement AP system, an FP might trigger an unsuited insulin infusion leading to hypoglycemia. Most FPs occur when the glucose is high, about 160 mg/dL, and rising (see Figure 5.9). Indeed, 19 % of the FPs correspond to events where the glucose increases more than 50 mg/dL within 3 h, starting above 70 mg/dL. Such glucose profiles resemble unannounced meals; although not caused by meals, an

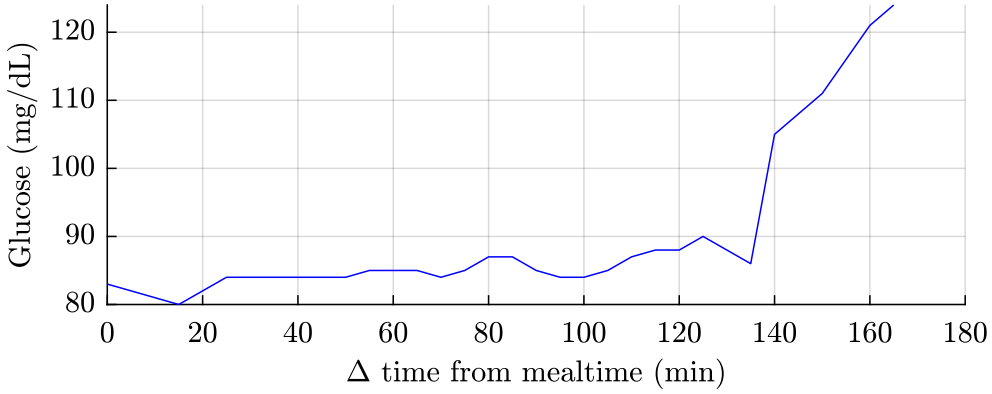

Figure 5.8: Example of slowly-absorbed meal. The 0 on the axis x corresponds to the mealtime.

extra insulin dosing triggered by the meal detection is not so risky, even, it would likely benefit blood glucose control quality.

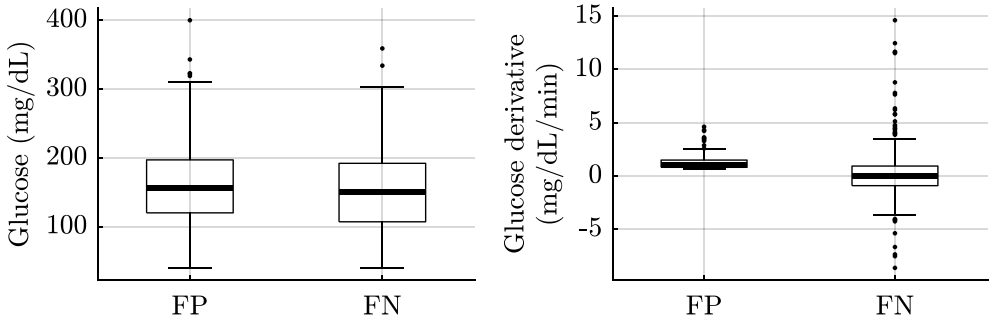

Figure 5.9: Boxplot of glucose (left) and glucose derivative (right) at False Negative (FN) events and False Positive (FP) events.

FNs are also dangerous since if meals remain undetected, no extra insulin complements the feedforward part of the controller, likely, leading to hyperglycemia. Although the proposed meal detector has 6[4] FNs, most of them relate to a postprandial period where the glucose concentration seldom increases, i.e., the derivative is close to zero (see right panel of Figure 5.9). Also, the carbohydrate content associated with FNs is 32[32] g, a low-to-medium meal size that could be handled with the feedforward part of the controller (Tornese et al. 2022). In fact, 14.3 % of FNs are hypoglycemia treatments that should not require an additional insulin dosing. Other sources of FNs are calibrations (9.7 % of FNs) and missing

Table 5.2: Performances' comparison between proposed meal detector and other literature works under free-living conditions

Algorithm	**Recall** (%)	**FP/day**	**DT** (min)
LDA Ra (in Kölle et al. 2020)	92.5 [2.0]	1.5 [0.4]	18.59 [1.84]
LDA CGM (in Kölle et al. 2020)	89.5 [4.0]	1.41 [0.42]	11.35 [2.05]
Threshold Ra (in Kölle et al. 2020)	74.5 [3.5]	1.47 [0.53]	30.94 [5.59]
GRID (in Kölle et al. 2020)	21.5 [7]	2.78 [0.41]	43.93 [4.7]
PAIN (in Kölle et al. 2020)	99 [11.26]	1.88 [0.72]	-
Dassau (in Weimer et al. 2016)	73.9[20.5]	1.62 [1.27]	-
Lee (in Weimer et al. 2016)	70.26 [20.07]	1.69 [1.21]	-
Harvey (in Weimer et al. 2016)	79.90 [15.10]	1.64 [1.34]	-
Enhanced STMD	70 [13]	1.4 [1.4]	45 [45]

Data are expressed as median [interquartile range]. *Notation:* DT (detection time), FP/day (false positives per day). Evaluation datasets and metric criteria differ among the works; hence, the results must be interpreted with caution.

data (19.9 % of FNs) since the algorithm resets after these events. These FNs could be avoided if current CGM had been available for the study; the new generation of CGMs, such as Dexcom G6 (Dexcom Inc., San Diego, CA, USA), is calibration-free and includes algorithms to reduce missing data (Didyuk et al. 2020).

5.6 Conclusions

A meal detector algorithm was designed as a crucial step forward in developing meal-announcement-free AP system (see Chapter 6). The algorithm implements a super-twisting observer to generate residuals and a threshold-based logic to determine the meal occurrence from the residuals and the glucose derivative.

The validation of the algorithm under the latest version of the UVa/Padova simulator (Vettoretti et al. 2018), which models more challenging scenarios than the academic modified version of the simulator, revealed limitations of the algorithm: the residuals and the glucose derivative were noisier than in previous evaluations with the modified version of the simulator, even in the absence of noise. These limitations were overcome by replacing the dirty derivative with a Kalman filter and discretizing the super-twisting observer with implicit methods.

The enhanced algorithm was further evaluated with a clinical dataset collected under free-living conditions, including 696 meals. The algorithm achieved competitive results among other works in the literature: a recall of 70[13]% (median [interquartile range]), a precision of 73[26]%, and 1.4[1.4] false positives per day. Remark, however, that a head-to-head comparison is unfeasible given the discrepancies between scenarios, data, and evaluation metrics, the different authors utilized.

Although false detections still existed, they were associated with low hypoglycemia and hyperglycemia risk situations. On the one hand, false positives mainly corresponded to rising glucose events that would likely benefit from an insulin injection triggered by the meal detector. On the other hand, false negatives occurred after small meals (including hypoglycemia treatments) or were caused by technological issues such as calibrations or missing samples.

Chapter 6

Unannounced meal compensation based on meal detection

This chapter designs a module for a hybrid system to release subjects from meal announcements. The module delivers a train of insulin boluses triggered by the meal detector of Chapter 5 and an estimation of the absorbed carbohydrates calculated through the disturbance estimator of Chapter 3. The module is implemented in a controller designed for a hybrid operation (i.e., with meal announcements). The controller is compared in silico with three cases of the hybrid controller: when the patient forgets bolusing, when the patient provides the exact carbohydrate meal content, and when the patient misestimates it.

Authored publications related to this chapter:

- Sala-Mira, I.; Ricarte, B.; Romero-Vivo, S., et al. (2018). "Unannounced Meal Control through Sliding Mode Techniques in an Artificial Pancreas". In: *18th Annual Diabetes Tecnology Meeting*. Vol. 50. 1, p. 78831.

- Sala-Mira, I.; Díez, J.-L.; Ricarte, B., et al. (2019). "Sliding-mode disturbance observers for an artificial pancreas without meal announcement". In: *Journal of Process Control (JCR 2019: Q2)* 78, pp. 68–77. ISSN: 09591524. DOI: 10.1016/j.jprocont.2019.03.008.

6.1 Introduction

This chapter addresses one of the dissertation's principal goals: designing an unannounced meal strategy to replace carbohydrate counting in hybrid AP systems.

Hybrid AP systems require carbohydrate counting to provide a pre-meal bolus, a feedforward action complementing the feedback control action to enhance the postprandial response (Weinzimer et al. 2008). Otherwise, the risk of hyperglycemia and late hypoglycemia would increase because the absorption delay, measurement lag, and insulin unidirectionality constrain the effectiveness of feedback control (Gingras et al. 2018b). However, patients usually struggle with carbohydrate counting; indeed, misestimation errors (Kawamura et al. 2015; Roversi et al. 2022), announcement omissions (Bishop et al. 2009), or delays (Boughton et al. 2019) are common and may compromise glucose control. Thus, releasing patients from this task is desirable.

Several techniques have been developed to replace carbohydrate counting. Some targets announcement simplification, requiring only the mealtime (Tsoukas et al. 2021a; Haidar et al. 2021) or a qualitative approximation of the carbohydrates (Gingras et al. 2016b). Others completely removed the meal announcement; most meal-announcement-free systems rely on meal detection (or, at least, some detection of persistent hyperglycemia, like in Colmegna et al. 2021a; Garcia-Tirado et al. 2021b; Majdpour et al. 2021) to trigger a set of feedforward actions playing the role of pre-meal boluses, that is, increasing the aggressiveness of the insulin delivery to reduce postprandial hyperglycemia. The three most frequent actions triggered at detection time are the following: 1) delivering a single insulin bolus (Mahmoudi et al. 2019; Samadi et al. 2017; Xie et al. 2017; Harvey et al. 2014b); 2) delivering a train of insulin boluses calculated through estimations of the glucose derivative or rate of glucose appearance (Garcia-Tirado et al. 2021b; Turksoy et al. 2015; Hyunjin et al. 2009); and 3) modifying the controller structure or tuning (Hajizadeh et al. 2020; Fushimi et al. 2019).

The module developed in this chapter employs the two latter actions mentioned above. On the one hand, a meal detector triggers a train of insulin boluses being delivered according to an estimation of the rate of glucose appearance (see Section 6.3). On the other hand, a parameter of the controller is modified to reduce the risk of late hypoglycemia.

The proposed module is added to the SAFE-AP, a controller designed by our group for a hybrid operation (see Appendix B). The resulting meal-announcement-free system (bolusing algorithm with the SAFE-AP) is validated in silico and

compared with the hybrid SAFE-AP in three cases: absence of pre-meal boluses, ideal pre-meal boluses, and misestimated pre-meal boluses.

6.2 Control architecture overview

The proposed module comprises the following three elements (see gray blocks in Figure 6.1):

- A *meal detector* triggering the bolusing algorithm. The meal detector developed in Chapter 5 is implemented here, but any other could have been employed too.
- A *meal rate of glucose appearance observer* to estimate the meal disturbance required, in turn, to approximate the absorbed carbohydrates (see Section 6.3). The FOSMO observer with the IVP model presented in Chapter 3 is used since it is the most straightforward combination in that chapter while achieving a similar performance than more complex options.
- A *bolusing algorithm* that calculates a train of boluses with the information of the meal detector and meal disturbance estimation. The details of this algorithm are provided in the subsequent sections.

The IVP model parameters were populational values except for insulin sensitivity. The identification of the parameters is similar to the one described in Section 3.3[1]. First, an average model was identified from a 2-day simulated dataset with three daily meals with the two-step approach of Section 3.3. Then, a new optimization problem was solved to individualize the insulin sensitivity, fixing the remaining parameters to the average model ones. The resulting parameters are included in Table 6.1

For the in silico validation of the proposed module, the module is integrated into the SAFE-AP (the main controller Figure 6.1). The details of the SAFE-AP are described in Appendix B. The SAFE-AP implements a PD controller extended by an IFB and a SMRC mechanism to upper-bound the insulin-on-board (Figure 6.2). To constrain the insulin-on-board, the SMRC increases the glucose reference, $G_r(t)$, through the discontinuous signal $\omega(t)$ defined by:

[1]This identification was proposed in (Sala-Mira et al. 2019), which was earlier than the material presented in Chapter 3. In that article, we looked for models identified only in gain as proposed by Van Heusden et al. (2012). For that reason, only the insulin sensitivity was identified

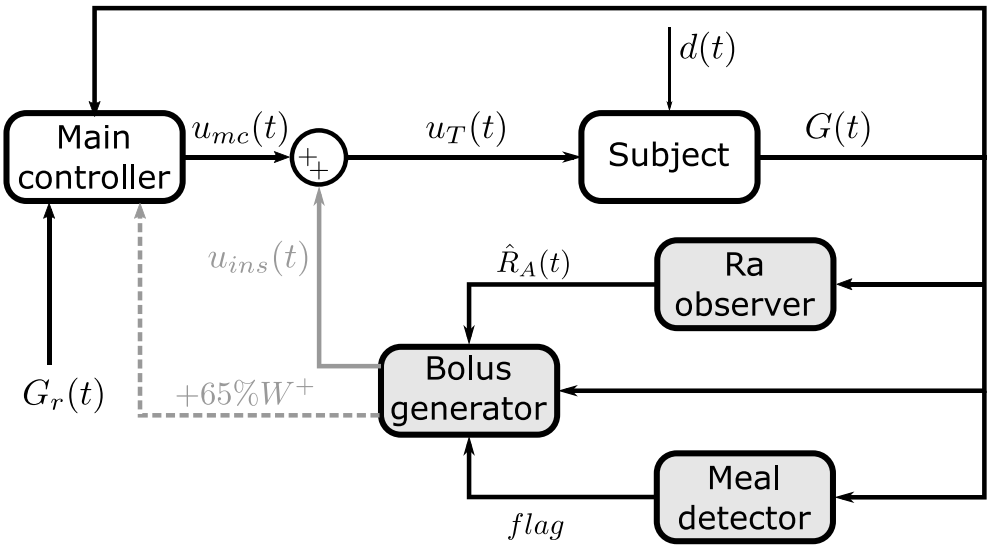

Figure 6.1: Proposed meal-announcement-free system. Gray-filled blocks indicate the elements of the proposed module: a meal rate of glucose appearance observer, a meal detector, and a bolusing algorithm. The bolus generator delivers boluses ($u_{ins}(t)$) to compensate for meals. Also, an internal parameter of the controller (W^+) is modified during the bolusing logic.

$$\omega(t) = \begin{cases} W^+ & \text{if } \sigma_{SM}(t) > 0 \\ 0 & \text{otherwise} \end{cases}$$

where W^+ is a large enough positive scalar with a nominal value set to 350 mg/dL, tuned in Sala-Mira et al. (2017) by extensive simulations. The condition $\sigma_{SM} > 0$ – σ_{SM} is given by (B.5) in Appendix B – indicates that the insulin-on-board has exceeded (or has a trend to do it shortly) its upper-limit. The modified setpoint $G_r(t) + \omega(t)$, once filtered by a first order filter, becomes the new setpoint ($G_{rf}(t)$) for the PD. Thus, whenever the insulin-on-board exceeds its upper-limit, the reference will increase by up to W^+, leading to an immediate pump shut-off preventing from insulin overdose, and, consequently, mitigating severe late post-prandial hypoglycemia. Note that, to mitigate hypoglycemia against unannounced meals, the proposed module has to increase the W^+ value to counteract the meal detection delay (see Section 6.4).

Table 6.1: Identified parameters of IVP model

Parameter	Average patient	Individual
S_I (mL/(µU min))	$6.92 \cdot 10^{-4}$	$2.52 \cdot 10^{-4}$ $4.18 \cdot 10^{-4}$ $4.42 \cdot 10^{-4}$ $7.03 \cdot 10^{-4}$ $7.36 \cdot 10^{-4}$ $7.65 \cdot 10^{-4}$ $8.34 \cdot 10^{-4}$ $8.86 \cdot 10^{-4}$ $9.12 \cdot 10^{-4}$ $9.75 \cdot 10^{-4}$
EGP (mg/(dL min))	1.49	-
C_I (mL/min)	$1.11 \cdot 10^{3}$	-
$GEZI$ (1/min)	$3.03 \cdot 10^{-8}$	-
τ_1 (min)	82.82	-
τ_2 (min)	21.43	-
p_2 (1/min)	$1.55 \cdot 10^{-2}$	-

6.3 Bolusing algorithm

The bolus generator targets compensating unannounced meals. For each detected meal, the following train of boluses is delivered:

$$u_{ins}(t) = \sum_{j=1}^{NB} B_j \delta(t - t_j) \tag{6.1}$$

where t_1 is the detection time, B_j and t_j are the jth-bolus size (U/min) and time, and $\delta(\cdot)$ represents the Dirac delta. The total number of boluses delivered after detecting a meal, NB, is unknown in advance. It depends on the logic described in Figure 6.3 determining B_j and t_j.

At detection time (t_1), a conservative bolus is delivered. Its size is calculated as follows:

$$B_1 = \frac{\alpha}{ICR} + \min\left(0, \frac{G(t_1) - G_r(t_1)}{CF}\right) \tag{6.2}$$

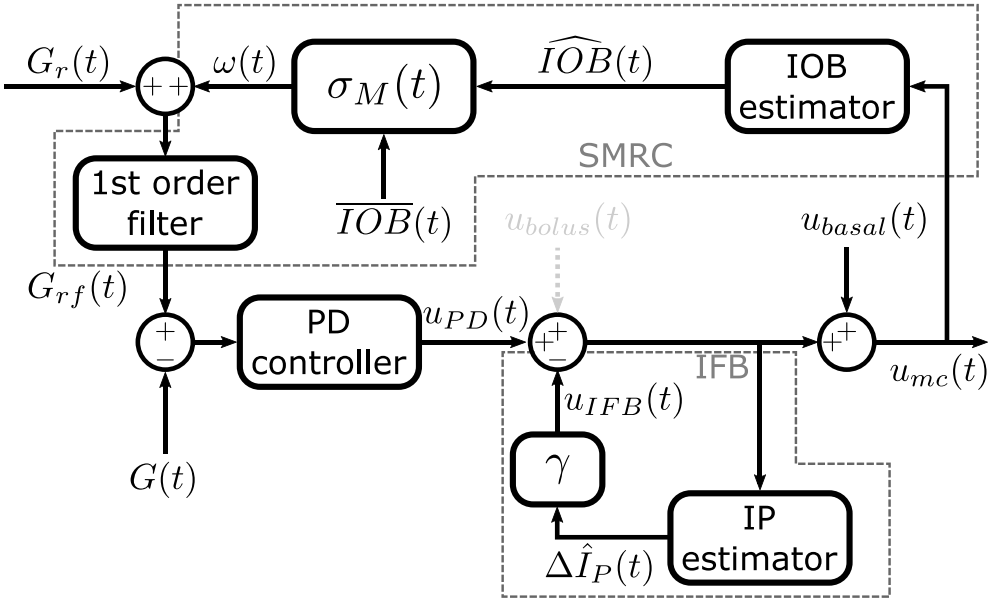

Figure 6.2: Description of the main controller. The main controller consists of a proportional-derivative controller (PD), an insulin feedback (IFB), and a sliding mode reference conditioning (SMRC). $G(t)$, $G_r(t)$, and $G_{rf}(t)$ denote the glucose reading, the glucose setpoint and the filtered setpoint; γ and $\Delta\hat{I}_P(t)$ are, respectively, the IFB gain and the estimated insulin plasma deviation regarding basal conditions. $\omega(t)$, $\widehat{IOB}(t)$, and $\overline{IOB}(t)$ correspond to the discontinuous signal, the estimated insulin-on-board, and the upper limit of the insulin-on-board. The total insulin provided by the main controller, u_{mc}, considers the PD-IFB output, the basal infusion ($u_{basal}(t)$), and, only if meals are announced, the pre-meal boluses ($u_{bolus}(t)$).

where $G(t_1)$ and $G_r(t_1)$ are the glucose value and the glucose set point at the detection time t_1, respectively. The parameters ICR (g/U) and CF (mg/(dL U)) denote, respectively, the insulin-to-carbohydrate ratio and the correction factor of the standard open-loop therapy (Reiterer et al. 2019). The parameter α refers to the equivalent meal bolus (Reiterer et al. 2019). In the standard open-loop therapy, α would equate to the estimated meal size. However, in this application, the meal size and time are unknown. In addition, the meal detector can raise a flag when no actual meal occurs (i.e., an FP). Therefore, α must be small enough to prevent hypoglycemia within an FP. The parameter α was selected as 8 g after exhaustive simulations. Other works in the literature, such as (Fathi et al. 2019), also have opted for conservative boluses to prevent FP-related hypoglycemias. The second term in (6.2) corresponds to the correction term of the standard

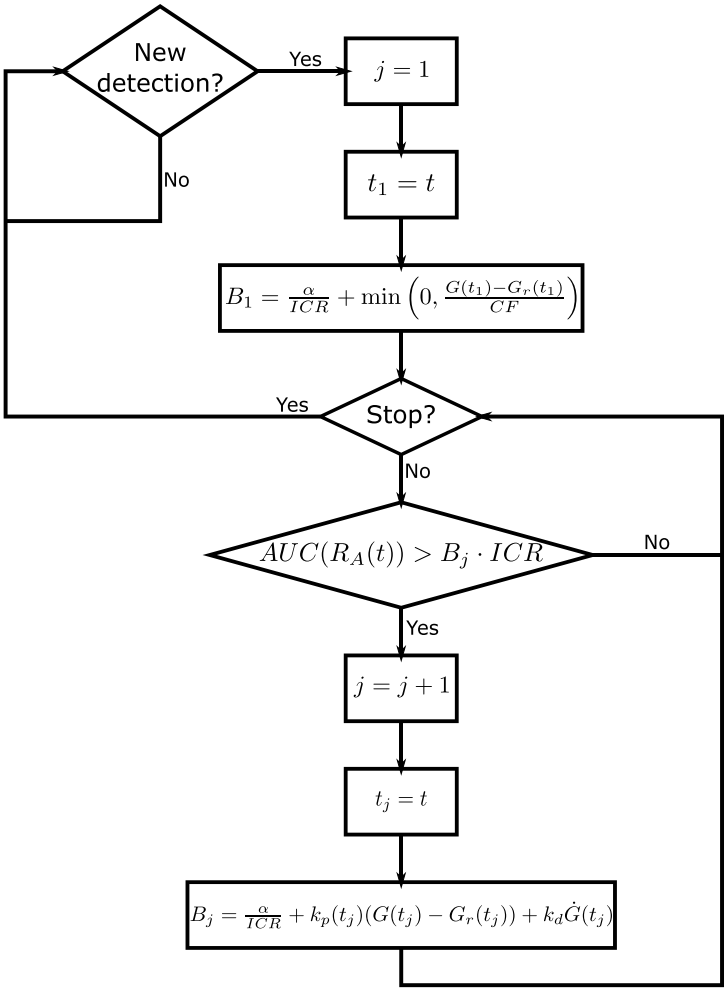

Figure 6.3: Bolus generator logic.

therapy but is upper bounded to zero. Corrections for $G(t_1) > G_r(t_1)$ were not considered to avoid insulin over-delivery when an FP occurred with an elevated glucose concentration. The coefficients k_d and β (set to $50\,\text{min}^{-1}$) were selected heuristically through simulations.

If the stop conditions (they will be described next) are not met, the module starts delivering a series of boluses. Their size follows a PD-like algorithm added to a constant α-g equivalent meal bolus:

$$B_j = \frac{\alpha}{ICR} + k_p(t_j)(G(t_j) - G_r(t_j)) + k_d\dot{G}(t_j) \tag{6.3}$$

with

$$k_p(t) = \frac{\exp\left(\frac{t-t_2}{\beta}\right)}{CF}, \quad k_d = \begin{cases} TDI/100 & \text{if } \dot{G}(t) \geq 0 \\ TDI/85 & \text{if } \dot{G}(t) < 0 \end{cases} \tag{6.4}$$

where t_2 is the time the second bolus was delivered (in min), and TDI is the total daily insulin (U/d). The gains $k_p(t)$ and k_d were time-dependent to reduce the bolus size. On the one hand, the $k_p(t)$ follows an exponential attenuation, where β is the time constant (1/min), to reduce the risk of hypoglycemia for meals with long absorption periods. On the other hand, the k_d favors glucose reductions more than glucose increases to avoid delivering a large bolus for a decreasing glucose trend.

The bolus generator module delivers a new bolus when the meal size of the last bolus has been absorbed. The meal size corresponding to a bolus is calculated as follows:

$$CHO_{j-1} = B_{j-1} \cdot ICR \tag{6.5}$$

where B_{j-1} is the last infused bolus. The absorbed carbohydrates are approximated through the area under the curve of the estimated meal disturbance, expressed in mass units: $\hat{R}_A \cdot V_G$ (mg/min). The area under the curve was calculated with the trapezoidal rule.

Before delivering a new bolus, some conditions are evaluated to determine if the bolus is required. These conditions prevent bolusing for two situations:

- *When most of the meal content has been absorbed.* A meal was considered to be absorbed if one of the following conditions is met:

  - The glucose value lowers from hyperglycemia ($G \geq 180\,\text{mg/dL}$) to normoglycemia ($G < 180\,\text{mg/dL}$).
  - The estimated meal disturbance reaches a small value. This value could be zero for a perfect estimation of the meal disturbance. However, as observed in Chapter 3, the meal disturbance estimation is coupled with noise and uncertainty. A threshold of $0.6\,\text{mg/(dL min)}$ is set after simulations.
  - The elapsed time from the detection time is longer than 150 min.

  The above conditions reduce the risk of delivering a bolus in the late postprandial phase when a bolus will likely cause hypoglycemia.

- *When an FP has occurred.* Although the algorithm cannot known if the detection is a TP or an FP, it is expected that the first bolus reduces the glucose more after an FP than after a TP. Consequently, the glucose concentration would recover its value at detection time earlier for an FP than for a TP (see Figure 6.4). Following this reasoning, the algorithm was deactivated when the slope of the line joining the glucose at detection time (t_1) and the actual time, that is,

$$slope = \frac{G(t) - G(t_1)}{t - t_1}$$

  goes below a threshold close to zero, set to $0.3\,\text{mg/(dL min)}$. This condition reduces the risk of delivering a second bolus after an FP.

6.4 Complementary feedforward action

In any hybrid controller provided with an insulin-on-board limitation mechanism, the meal bolus will immediately reduce the feedback control action at mealtime. Conversely, in the proposed meal-announcement-free system, the insulin-on-board limitation mechanism will be activated only after meal detection, when the train of boluses is delivered. Since the feedback controller has to cope with the meal disturbance until the meal is detected, the feedback control action will be larger in the meal-announcement-free system than in the hybrid system at the time

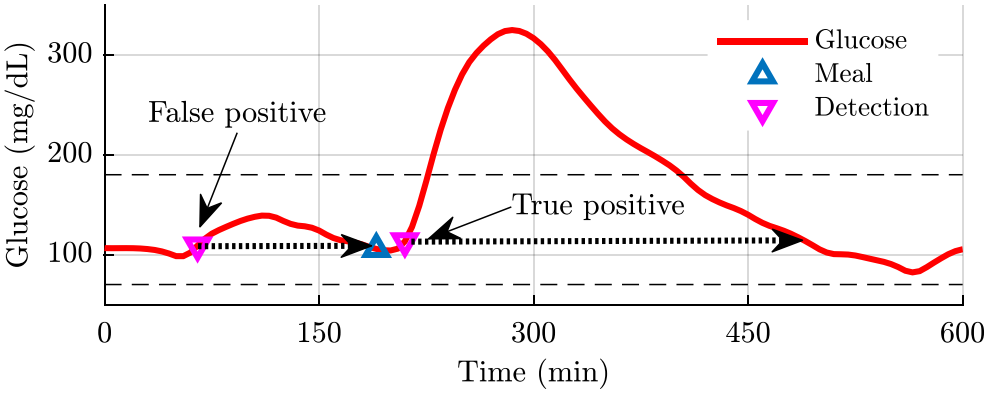

Figure 6.4: Recovery time from detection after a false positive and a true positive. The time for the glucose to return to the value at detection time (downward triangle) is shorter for false positives than for true positives. The upward triangle corresponds to the actual meal, and dotted line arrows represent the slope.

the insulin-on-board mechanism is activated. Thus, the bolus combined with a larger feedback control action, may lead to hypoglycemia despite the limitation of the insulin-on-board. To overcome this problem, the proposed system, besides delivering a train of boluses, modifies an internal parameter of the insulin-on-board mechanism to make more exigent in the limitation of the insulin-on-board given by the feedback controller.

In the particular case of the SAFE-AP, the proposed module modifies the parameter W^+. In the announced meal case, the pre-meal bolus makes the insulin-on-board exceed the constraint $\overline{IOB}$; hence the SMRC activates, increasing $G_r(t)$ by up to $W^+ = 350\,\text{mg/dL}$. The result is that the control action of the main controller zeroes ($u_{mc}(t) = 0$) just after the pre-meal bolus (see red line in Figure 6.5). However, in the unannounced meal case, the SMRC requires more time to set $u_{mc}(t) = 0$ (see blue line in the middle panel of Figure 6.5). Two reasons explain why the time to shut the continuous infusion off is longer than the announced case. On the one hand, the SMRC activates later than in the announced meal case because no pre-meal bolus is delivered. On the other hand, the main controller must face the postprandial glucose increase without any help of pre-meal boluses until the meal detector triggers the bolusing algorithm. As a result, the value of $u_{mc}(t)$ when the SMRC augments the reference $G_r(t)$ is greater for the unannounced case than the announced case. In the announced case, increasing the reference by up to $W^+ = 350\,\text{mg/dL}$ led to a shortly pump shut-off. However, this value might be insufficient for the unannounced case. For this reason, apart from the bolusing

algorithm, the proposed module increases W^+ (a 65 % to its nominal value was observed to be a compromise after extensive simulations) when the conditions for delivering a second bolus are met. This greater W^+ shortens the time until $u_{mc}(t)$ becomes zero, reducing the risk of hypoglycemia (see green line in Figure 6.5). W^+ recovers its nominal value when the stop conditions of the bolusing algorithm are held.

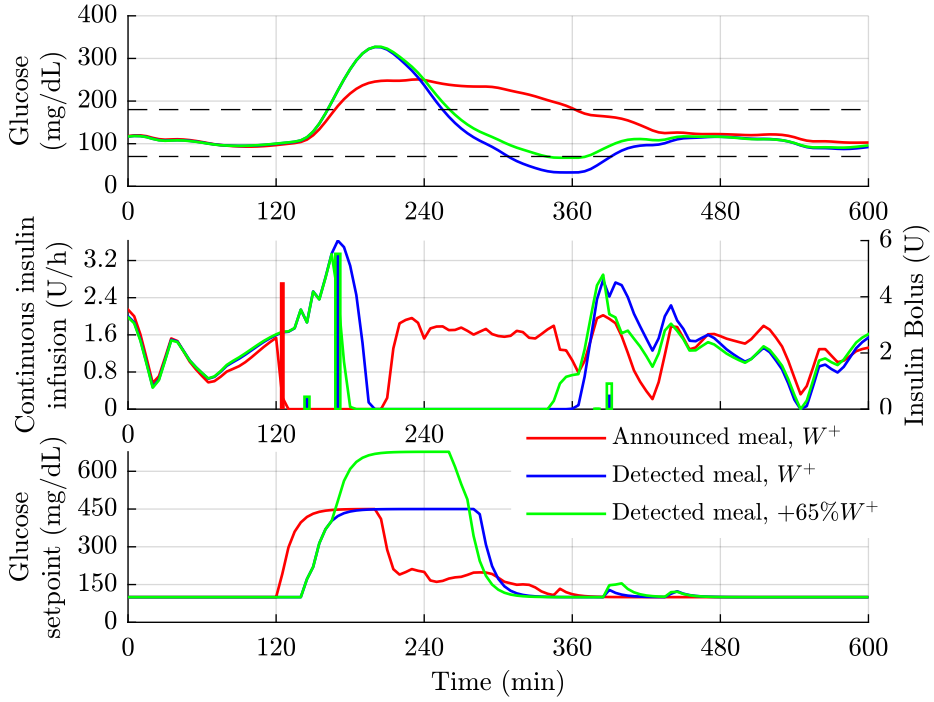

Figure 6.5: Need of a complementary feedforward action. In the announced meal case (red lines), the SMRC shuts the control action off (left, middle panel) right after the pre-meal bolus (right, central panel), only increasing glucose by W^+. In the unannounced case (blue lines), the control action takes longer to be zero with the same W^+. Increasing W^+ a 65 % (green lines) enhances the performance.

6.5 In silico comparison

The proposed meal-announcement-free system based on meal detection (henceforth denoted as MD) is compared with the main controller without meal compensation (NoComp), the main controller with ideal meal boluses (IB), and the main controller with miscalculated boluses (MB). The meal boluses of the hybrid controllers (IB and MB) were calculated as follows (Reiterer et al. 2019):

$$u_{bolus}(t) = \frac{d_{meal}}{ICR} \cdot \delta(t - t_{meal}) \tag{6.6}$$

where d_{meal} and t_{meal} are the announced meal dose (in g) and time (in min), respectively. The announced meal doses match the actual meal doses for the IB. In MB, meal announcements are subject to carbohydrate counting errors, as modeled in Kawamura et al. (2015)'s.

A 30-day scenario was configured with the modified version of the UVa/Padova simulator. It includes three daily meals with random variation in meal times (nominal daily values: 7 h, 14 h, and 21 h; standard deviation: ±10 min) and meal dose (nominal daily values: 45 g, 80 g, and 60 g; coefficient of variance: ±20 %). The meal absorption rate, carbohydrate bioavailability, and the subcutaneous insulin absorption rate changed at each meal following a uniform distribution of ±30 %, ±10 %, and ±30 %, respectively. In addition, the insulin sensitivity followed a circadian variation of 24 h with random amplitude (uniform distribution of ±30 %) and random phase. The simulations were performed for the ten virtual adults of the simulator, repeating the simulation three times per virtual subject with different instances of variability.

Standard metrics were evaluated, such as mean glucose, percent time in range, hypoglycemia or hyperglycemia (Battelino et al. 2019), and number of level 1 ($CGM < 70$ mg/dL) and level 2 ($CGM < 54$ mg/dL) hypoglycemia events. In addition, the effect of incorrect meal detections is assessed by the amount of carbohydrates leading to $CGM > 250$ mg/dL, the number of FP leading to $CGM < 70$ mg/dL or the number of FN leading to $CGM > 180$ mg/dL. All metrics were expressed as mean (SD) and median [25th percentile, 75th percentile]. The statistical significance level was 0.05. The difference significance between controllers was analyzed with the paired t-test or the Wilcoxon signed-rank test, depending on the normality.

6.5.1 Results

Table 6.2 summarizes the results of the in silico comparison. The proposed system beats the main controller without meal compensation (NoComp) since it reduces (with statistical significance) the mean and all levels of hyperglycemia without any statistically significant difference in hypoglycemia. In contrast, the hybrid systems (IB and MB) outperform the %time above 180 mg/dL and the %time above 250 mg/dL with statistical significance. This result was expected since delivering a bolus to compensate for a meal is the optimal therapy (Goodwin et al. 2015). The longer time in hyperglycemia achieved by the MD occurred because, besides the detection delay, the bolusing algorithm was tuned conservatively to avoid FP-related hypoglycemia events. Figure 6.6 illustrates this conservativeness: the postprandial glucose response achieved by the MD overlaps the NoComp response until the second bolus of the MD was delivered. Apart from the conservative tuning, FNs can lead to hyperglycemia. However, the existing FNs in this analysis are related to small-to-medium meals (46.3 ± 4.4 g) easily handled by the main controller without requiring an extra insulin infusion. Indeed, out of 6.6 ± 3.8 FNs, only 1.4 ± 1.2 FNs are associated with hyperglycemia. Although the time in hyperglycemia achieved by the MD is larger than the hybrid counterpart, it is below the 25 % recommended in the literature (Battelino et al. 2019).

The %time below 70 mg/dL and %time below 54 mg/dL are close to zero for all the controllers. The proposed system leads to a slight increase of level 1 and level 2 hypoglycemia events but without resulting in statistical significance. FP-related hypoglycemia events are sparse: only 0.033 ± 0.183 FPs lead to hypoglycemia; among them, only two level 2 hypoglycemia events were reported, both in subject 7 (49.14 mg/dL in the second instance and 45.32 mg/dL in the third). The low number of FPs causing hypoglycemia is because of the conservative tuning of the first bolus and the suitable selection of the stop conditions. For example, the slope stopping condition prevents a second bolus from being delivered in 75 % of FPs.

The hybrid systems achieve a statistically significant longer %time in 70–180 mg/dL; however, the median difference regarding (the more realistic) MB is less than 4 mg/dL. Finally, although IB outperforms (with statistical significance) the MD controller in terms of the mean glucose, no statistically significant difference was found between MB and MD.

Table 6.2: Performance metrics of meal compensation

	NoComp	MB	IB	MD
Mean CGM (mg/dL)	169.1 ± 22.41 * 160.1 [157.6, 193.2]	144.3 ± 11.01 141.5 [138.6, 154.3]	139.0 ± 9.074 * 137.0 [133.9, 146.5]	146.7 ± 12.20 143.4 [139.8, 148.1]
CGM time (%)				
>250 mg/dL	11.00 ± 8.906 * 8.328 [4.201, 18.32]	2.262 ± 3.200 * 0.793 [0.208, 3.056]	0.857 ± 1.936 * 0.029 [0.000, 0.856]	2.730 ± 2.452 2.297 [0.521, 4.560]
>180 mg/dL	37.74 ± 14.46 * 32.41 [30.94, 49.71]	18.65 ± 7.893 * 17.99 [13.74, 21.22]	14.10 ± 6.971 * 13.06 [9.063, 19.05]	22.51 ± 8.715 20.94 [18.96, 24.95]
[70 – 180] mg/dL	62.26 ± 14.46 * 67.59 [50.29, 69.06]	81.35 ± 7.894 * 82.01 [78.79, 86.26]	85.88 ± 6.975 * 86.94 [80.95, 90.94]	77.46 ± 8.706 78.96 [75.05, 81.04]
<70 mg/dL	0.003 ± 0.011 0.000 [0.000, 0.000]	0.004 ± 0.014 0.000 [0.000, 0.000]	0.013 ± 0.037 0.000 [0.000, 0.000]	0.029 ± 0.077 0.000 [0.000, 0.000]
<54 mg/dL	0.000 ± 0.000 0.000 [0.000, 0.000]	0.000 ± 0.000 0.000 [0.000, 0.000]	0.000 ± 0.000 0.000 [0.000, 0.000]	0.005 ± 0.018 0.000 [0.000, 0.000]
Hypoglycemia events				
Level 1	0.033 ± 0.183 0.000 [0.000, 0.000]	0.067 ± 0.254 0.000 [0.000, 0.000]	0.167 ± 0.461 0.000 [0.000, 0.000]	0.300 ± 0.702 0.000 [0.000, 0.000]
Level 2	0.000 ± 0.000 0.000 [0.000, 0.000]	0.000 ± 0.000 0.000 [0.000, 0.000]	0.000 ± 0.000 0.000 [0.000, 0.000]	0.067 ± 0.254 0.000 [0.000, 0.000]

Four meal compensation techniques, which share the main controller, were compared: 1) absence of meal compensation (NoComp), 2) announced meals with carbohydrate counting errors (MB), 3) announced meals with ideal boluses (IB), and 4) meal-detector-based compensation (MD). Metrics are expressed in mean ± standard deviation and median [25th percentile, 75th percentile] of the ten virtual adults. An asterisk represents statistically significant differences regarding MD.

6.6 Conclusions

A meal-announcement-free artificial pancreas is presented, combining the rate of glucose appearance and the meal detector developed in previous chapters with a novel bolusing algorithm.

The in silico analysis revealed that the proposed system achieved a mean glucose similar to that of a hybrid system with carbohydrate counting errors without increasing the risk of hypoglycemia.

Despite the promising results, the tuning of the algorithm, especially for the first bolus, is conservative, which, besides the meal detection delay, leads to an increase of hyperglycemia and decrease of %time in 70–180 mg/dL regarding the hybrid counterpart. This loss of performance was expected since the ideal hybrid controller

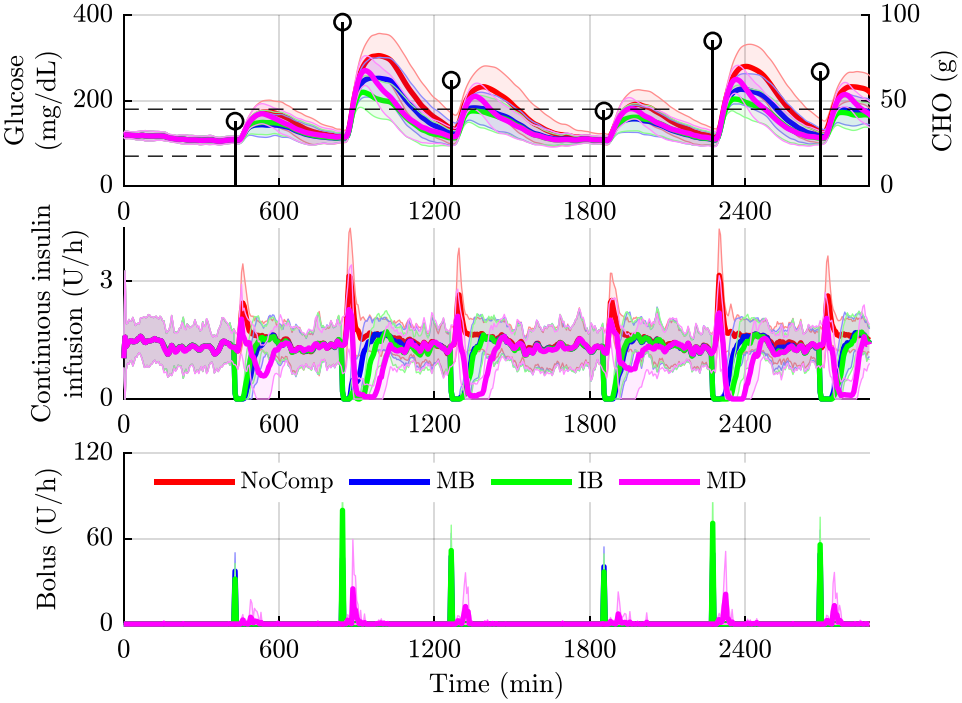

Figure 6.6: Populational glucose and insulin profiles of the comparison. Two of the 30 days are shown comparing the hybrid system without boluses (NoComp), the hybrid system with carbohydrate misestimation (MB), the hybrid system with ideal bolus (IB), and the proposed system (MD). Shaded areas correspond to standard deviation values, while solid lines are mean values.

(i.e., no misestimation errors) is the optimal therapy for postprandial control. Anyway, %time above 180 mg/dL hyperglycemia achieved by the proposed meal-announcement system is below the thresholds defined in the consensus statements (Battelino et al. 2019).

Another weakness of the analysis is related to the simulations. The meal-announcement-free system was evaluated for only ten virtual subjects. Also, the effect of proteins, fat, or alcohol on the algorithm could not be assessed since meals in the simulator only consider carbohydrates. Despite these limitations, the conditions under the proposed module have been evaluated and can be regarded as realistic since the scenario included multiple meals per day and sources of variability.

Finally, the proposed system is not flexible enough to handle exercise events, another disturbance that severely impacts glucose, usually leading to a sharp decrease. The next chapter presents an alternative strategy to deal with exercise.

Chapter 7

Unannounced meal and exercise compensation with a modified Internal Model Control

Likewise meal intake, exercise severely impacts glucose homeostasis. Low-to-moderate exercise usually lowers glucose; fear of hypoglycemia might discourage subjects from an active lifestyle, renouncing its benefits for managing diabetes. Hybrid artificial pancreas systems usually handle exercise by reducing the insulin dose before the exercise bout. Since planning exercise is not always possible in daily life, an automatic strategy to deal with unannounced exercise is desirable. This chapter includes the design, the tuning, and the in silico validation of an add-on module for a hybrid artificial pancreas to eliminate the need to announce meal intakes and exercise. As opposed to the previous chapter which was focused on meal control, here meal and exercise disturbances are considered in a holistic way. The module is built upon an internal model control and a switching logic that mitigate the impact of unannounced meals and exercise by modifying the insulin dose, reducing the insulin-on-board limits, and suggesting rescue carbohydrates.

Authored publications related to this chapter:

- Sala-Mira, I.; Garcia, P.; Díez, J.-L., et al. (2022a). "Internal model control based module for the elimination of meal and exercise announcements in hybrid artificial pancreas systems". In: *Computer Methods and Programs in Biomedicine (JCR 2021: Q1)*, p. 107061. ISSN: 0169-2607. DOI: `https://doi.org/10.1016/j.cmpb.2022.107061`.

- Sala-Mira, I.; García Gil, P. J.; Company Bondia, J., et al. (2022b). "Method for improving blood glucose control of a hybrid controller, add-on module for being incorporated to an artificial pancreas system for perfoming the method and artificial pancreas system incorporating the add-on module". Pat. req. P202230693. Universitat Politècnica de València (UPV).

7.1 Introduction

In type 1 diabetes, regular exercise improves fitness and well-being; it reduces insulin resistance and body fat; and it is related to a decreased the risk of cardiovascular complications and to more extended temporal beta-cell residual function, i.e., the "honeymoon" period (Chimen et al. 2012; Codella et al. 2017; Chetan et al. 2019). However, exercise perturbs the balance between muscle glucose uptake and hepatic glucose production or meal intake, lowering or raising the plasma glucose depending on its intensity, duration, or timing (Moser et al. 2020; Tagougui et al. 2019; Gomez et al. 2015). The counterregulatory mechanism – glucagon, epinephrine, norepinephrine, or cortisol – malfunctions or is lost in type 1 diabetes, increasing the risk of hypoglycemia during or after the exercise bout (Codella et al. 2017). Due to the fear of hypoglycemia, patients abandon an active lifestyle, renouncing all its benefits (Kime et al. 2018).

Traditional strategies to mitigate hypoglycemia rely on insulin dose reductions (basal or pre-meal boluses), but they are efficient only if applied with sufficient anticipation (e.g., 90 min; Zaharieva et al. 2020). Since planning exercise is not always possible, an additional control action is needed. Dual-hormone artificial pancreas systems complement the insulin infusion with exogenous glucagon infusion or boluses to reduce the risk of hypoglycemia without the patient intervention (Jones 2019; Infante et al. 2021). These systems under development reduce the %time below 70 mg/dL more than insulin-alone AP, but their advantages in severe hypoglycemia reduction are inconclusive (Haidar 2019). Moreover, glucagon infusion might have side effects (nausea, vomiting, headache) and require more complex and expensive hardware (Infante et al. 2021).

A more straightforward approach to manage exercise is carbohydrate supplements consumption (Patel et al. 2016), but subjects must decide the size and timing of these supplements (Moser et al. 2020). These decisions might become a burden (Scott et al. 2019); hence automating them is desirable.

The control algorithm described in Chapter 6 effectively compensates for unannounced meals. However, adding a carbohydrate suggestion feature would increase the already large number of tuning parameters. In addition, relating the estimation of the rate of glucose appearance with carbohydrate suggestions is not clear. For those reasons, a new add-on module based on an internal model controller , was designed in this chapter to manage either unannounced meal intakes or unannounced exercise events. As in Chapter 6, the module will be added to the SAFE-AP controller, and the complete system will be validated in silico.

7.2 Control architecture overview

Figure 7.1 shows the proposed module (see blocks in gray). It aims to substitute the disturbance-compensating actions following an announcement (meal intake or exercise) in an already designed hybrid artificial control algorithm (referred to as "main controller") with similar control actions that do not require announcements.

The module integrates an internal model control loop (IMC) (Chen et al. 2010) that estimates the output disturbance $\hat{d}(t)$ and calculates a virtual control signal $u_{IMC}(t)$ to compensate for it. Then, a switching logic converts this virtual control signal into a bolus-like insulin infusion ($u_{ins}(t)$) and rescue carbohydrates suggestions ($u_{resc}(t)$) to compensate for hyperglycemia and hypoglycemia, respectively. The switching logic also makes the tolerated insulin-on-board more restrictive after suggesting a rescue carbohydrate intake.

The modification of the tolerated insulin-on-board is the only change the proposed module applies to the internal parameters of the main controller. Most hybrid systems constrain the insulin-on-board through gains (Ruiz et al. 2012; Turksoy et al. 2014; Khodakaramzadeh et al. 2019; Villa-Tamayo et al. 2022) or thresholds (Ellingsen et al. 2009; Hu et al. 2015; Batmani et al. 2021); hence the modification of the main controller is immediate. As in Chapter 6, the main controller implements the SAFE-AP controller (Revert et al. 2013). This controller was extended with rescue carbohydrates (Beneyto et al. 2018; Viñals et al. 2021) and glucagon (Moscardó et al. 2019a) to compensate for unannounced exercise, but meal announcement was always required.

7.3 Internal model control loop

If the "Switching logic" is ignored from Figure 7.1, the loop constituted by the remaining blocks in gray frequently appears in the literature to improve the performance against disturbances of a given feedback controller (Peng et al. 2013; Vrančić et al. 2021): an internal model of the plant to estimate the output disturbance and a filter that ideally – without modeling errors, noise, saturation – would compensate the disturbance.

The IVP model is used in this chapter to estimate the disturbance since it is structurally simple and, at least in the context of observers, performed similarly to the Hovorka model (see Chapter 3). The model has already been described in Chapter 3. To consider the rescue carbohydrate suggested by the "Switching logic" or $u_{resc}(t)$ (Section 7.4.2) in the estimation of the disturbance, the following rapid carbohydrate absorption model is included in the IVP (Hovorka et al. 2004):

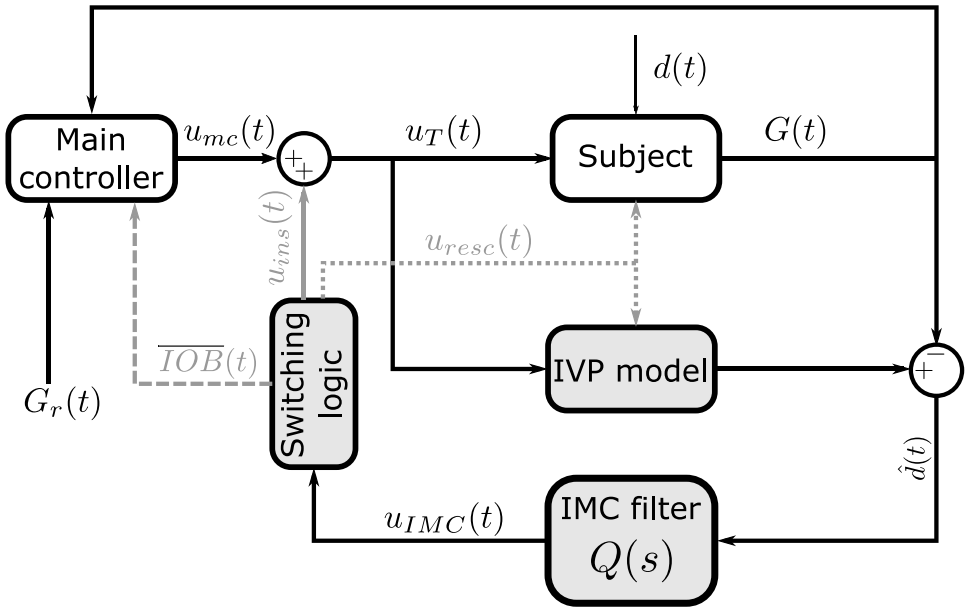

Figure 7.1: Diagram of the IMC-based add-on module. Blocks with gray background represent the proposed controller: an Internal Model Control (IMC) loop (IVP and IMC filter) with a non-linear logic (Switching logic). The controller provides three control actions: insulin (solid gray), rescue carbohydrates (dotted gray), and maximum insulin-on-board (IOB) limit command (dashed gray). *Notation*: G (glucose), G_r (glucose set point).

$$\dot{d_1}(t) = A_g^{resc} \cdot u_{resc}(t) - \frac{d_1(t)}{\tau_{resc}} \tag{7.1a}$$

$$\dot{d_2}(t) = \frac{1}{\tau_{resc}} \left(d_1(t) - d_2(t)\right) \tag{7.1b}$$

$$R_a^{resc}(t) = \frac{d_2(t)}{V_g \tau_{resc}} \tag{7.1c}$$

where d_1 and d_2 are the glucose masses (mg), τ_{resc} is the time to the peak absorption of the rescue carbohydrate and A_g^{resc} is the carbohydrate bioavailability Hovorka et al. 2004. The output R_a^{resc} is the rescue carbohydrate glucose rate of appearance; this output adds the glucose equation in the IVP.

The parameters of the model were identified from the ten virtual adults of the academic version of the UVa/Padova simulator (Dalla Man et al. 2014) because this is the cohort used in the in-slico validation (Section 7.6.1). The scenario for

identification corresponds to a two-week-length basal-bolus therapy with three daily meals and multiple sources of variability (CGM noise, variability in the insulin sensitivity, variability in the insulin pharmacokinetics, and variability in meal absorption). The parameters of the rescue model were a priori selected to represent a fast-acting meal (see the corresponding values in Table 7.1); hence, these parameters were excluded from the identification. The identification of the remaining parameters used information available in practical settings such as CGM reading or insulin infusion. Unlike in Chapter 3, the identification did not consider the meal rate of glucose appearance as an input signal, since this signal is not available in a practical setting. Alternatively, the information about mealtime and meal dose, more easily accessible in real-life conditions, is fed into a meal model to estimate the meal rate of glucose appearance. The meal model has the same structure than the rescue model described by (7.1), though with different parameters. Remark that the meal model was only used for identification purposes; it was not used by the internal model-based module since meals, except for carbohydrate rescues, are assumed to be unknown. The parameters of the IVP were selected according to the structural identifiability (Chis et al. 2011), the global sensitivity (Brun et al. 2001), and the collinearity index (Brun et al. 2001) to reduce identifiability issues (see Garcia-Tirado et al. (2018) for a similar approach). Table 7.1 includes the identified parameters.

The IMC filter $Q(s)$ generates a virtual action (in insulin units) that attenuates the effect of the disturbance. The filter $Q(s)$ was selected as in the two-degree-of-freedom IMC (Chen et al. 2010; Vrančić et al. 2021):

$$Q(s) = F(s) \cdot H^{-1}(s) \tag{7.2}$$

where s is the Laplace variable. $H(s)$ is the linearization of the IVP model (for $u_{resc}(t) = 0$, i.e., the linearized effect of insulin infusion on glucose) given by

$$\begin{aligned} H(s) := \frac{G(s)}{u_T(s)} = \\ = \frac{S_I G_0^2}{C_I EGP \left(\frac{1}{p_2}s + 1\right)(\tau_1 s + 1)(\tau_2 s + 1)\left(\frac{G_0}{EGP}s + 1\right)} \end{aligned} \tag{7.3}$$

where G_0 is the steady-state glucose value reached for the patient's basal insulin infusion.

Finally, the filter $F(s)$ reads as:

Table 7.1: Control model parameters corresponding to the virtual adults in UVa/Padova simulator

Subject	EGP (mg/(dL min))	SI (mL/(μU min))	Vg (dL)	p_2 (1/min)
1	1.32	$5.17 \cdot 10^{-4}$	$2.35 \cdot 10^{2}$	$2.53 \cdot 10^{-3}$
2	1.20	$4.24 \cdot 10^{-4}$	$2.48 \cdot 10^{2}$	$4.08 \cdot 10^{-2}$
3	1.05	$3.35 \cdot 10^{-4}$	$1.85 \cdot 10^{2}$	$2.03 \cdot 10^{-3}$
4	1.49	$7.23 \cdot 10^{-4}$	$2.90 \cdot 10^{2}$	$3.39 \cdot 10^{-3}$
5	$7.62 \cdot 10^{-1}$	$2.52 \cdot 10^{-4}$	$5.81 \cdot 10^{2}$	$1.12 \cdot 10^{-2}$
6	$9.25 \cdot 10^{-1}$	$2.43 \cdot 10^{-4}$	$1.83 \cdot 10^{2}$	$4.08 \cdot 10^{-2}$
7	$9.16 \cdot 10^{-1}$	$2.84 \cdot 10^{-4}$	$2.54 \cdot 10^{2}$	$2.03 \cdot 10^{-3}$
8	$9.25 \cdot 10^{-1}$	$2.39 \cdot 10^{-4}$	$4.57 \cdot 10^{2}$	$6.90 \cdot 10^{-3}$
9	$6.99 \cdot 10^{-1}$	$3.26 \cdot 10^{-4}$	$2.77 \cdot 10^{2}$	$4.08 \cdot 10^{-2}$
10	1.53	$6.03 \cdot 10^{-4}$	$2.99 \cdot 10^{2}$	$6.01 \cdot 10^{-3}$
Populational Values				
A_g^{resc} (unitless)			$9.00 \cdot 10^{-1}$	
CI (mL/min)			$1.22 \cdot 10^{3}$	
$GEZI$ (1/min)			$2.35 \cdot 10^{-3}$	
τ_1 (min)			$7.43 \cdot 10^{1}$	
τ_2 (min)			$4.54 \cdot 10^{1}$	
τ_{resc} (min)			$2.00 \cdot 10^{1}$	

The first column represents the subject identifier in the simulator. Parameters EGP, SI, Vg, and p_2 resulted from optimization. Parameters CI, $GEZI$, τ_1, and τ_2 are populational values and correspond to the average of the values in Kanderian et al. (2009). Parameters A_g^{resc} and τ_{resc} were a priori chosen to represent a fast-acting carbohydrate rescue; they are populational values too and were excluded from the identification.

$$F(s) = \frac{k}{(\tau s + 1)^5} \tag{7.4}$$

where k is the gain of the filter (see Section 7.5 for its tuning). The order of the filter is set to 5 for $Q(s)$ to be a strictly proper transfer function when inverting the fourth-order transfer function $H(s)$. The time constant τ determines the aggressiveness of $Q(s)$. Meal intakes and exercise severely perturb plasma glucose in the short term, but they eventually fade; hence an impulse-like $u_{IMC}(t)$ is required. Also, because of measurement lags, the effect of the disturbance will appear in $\hat{d}(t)$ with a delay. Therefore, for a high value of τ, the peak of $u_{IMC}(t)$ will occur much after the disturbance peak; the effect of the filter will be negligible and even counterproductive (e.g., in postprandial control, delayed insulin may lead to hypoglycemia). Instead, the filter must quickly react against any deviation in $\hat{d}(t)$ to reduce the effect of disturbances on glucose. For this reason, τ is set to $\tau = 10$ min, a low value close to the CGM reading rate (usually, 5 min).

7.4 Switching logic

A low value of τ is required for $u_{IMC}(t)$ to timely react against the disturbances (see Section 7.3). However, this tuning also amplifies the CGM noise, and $u_{IMC}(t)$ becomes oscillatory. In the absence of disturbances, these oscillations would be around zero (Figure 7.2). Hence, the slow dynamics of the insulin absorption would filter $u_{IMC}(t)$; its negative areas would counteract the positive ones ($\int_0^T u_{IMC}(t) \approx 0$), mitigating the influence of these oscillations in the CGM (Figure 7.2 blue lines). Nevertheless, the actual insulin infused to the patient, i.e., $u_T(t)$, cannot be lower than zero since it cannot be removed exogenously. This means that in the absence of the "Switching logic" in Figure 7.1, the integral of $u_T(t)$ is always positive, causing an undesirable glucose drop and, eventually, hypoglycemia (Figure 7.2 orange lines). The first goal of the switching logic is to ensure that the add-on module computes an insulin infusion only if a disturbance has occurred; that is, it eliminates from $u_{IMC}(t)$ the oscillations caused by measurement noise.

The switching logic also adequates the type of control action to the effect of disturbance on the glucose. Insulin can compensate for the glucose rise following a meal. However, insulin reductions inefficiently handle hypoglycemia-leading disturbances, such as low-to-moderate aerobic exercise (Moser et al. 2020; Zaharieva et al. 2020). To compensate for glucose drop – usually related to exercise and insulin overdoses within the postprandial period – the switching logic reduces the tolerated insulin-on-board and suggests rescue carbohydrates to the subject. Therefore, the second goal of the switching logic is to convert the virtual control signal $u_{IMC}(t)$ into three feedforward actions: insulin infusion, rescue suggestion, and insulin-on-board limit modification. The details of this logic are provided in the following subsections.

7.4.1 Hyperglycemia mitigation

The proposed loop mitigates a glucose rise with the insulin infusion $u_{ins}(t)$ (Figure 7.1). This insulin infusion is calculated according to the following three-phase logic (Figure 7.3):

1. *Dead-zone.* The insulin $u_{ins}(t)$ is set to 0 if $u_{IMC}(t)$ is lower than a threshold $th_{ins} > 0$ to avoid an insulin overdose due to oscillations in $u_{IMC}(t)$.

2. *Glucose rise mitigation.* A rising-glucose disturbance, such as meal intake, will likely require an $u_{IMC}(t)$ that exceeds th_{ins}. To compensate for the glucose rise, $u_{ins}(t)$ matches $u_{IMC}(t)$ until it reaches an upper saturation threshold $th_{sat} > 0$, set to avoid overdosing.

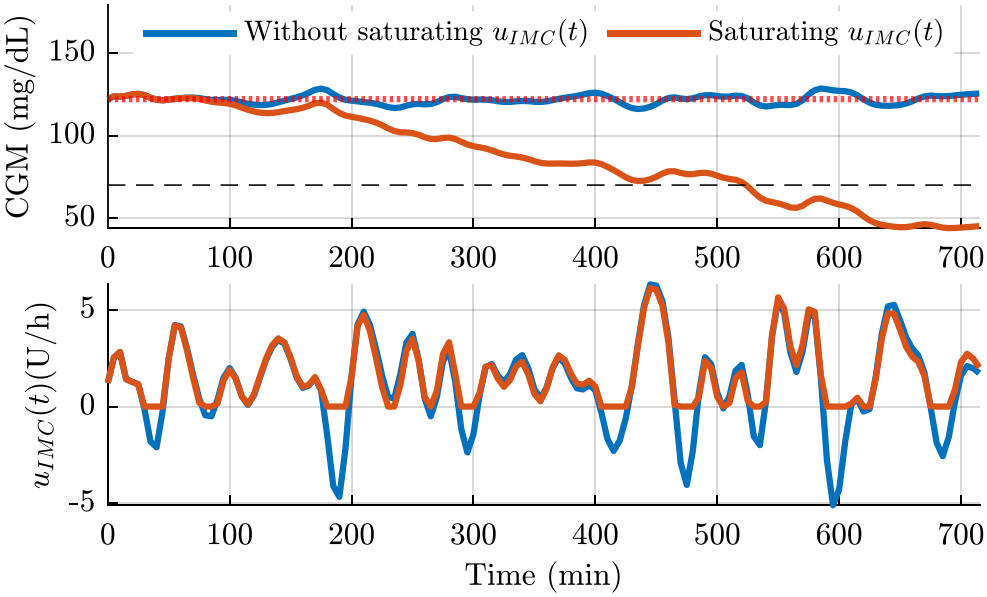

Figure 7.2: Example of hypoglycemia after $\mathbf{u_{IMC}(t)}$ saturation. Saturating $u_{IMC}(t)$ (orange line) lowers the glucose (upper panel), even leading to hypoglycemia. Without saturation, the negative peaks of $u_{IMC}(t)$ counteract the positive ones; hence, the glucose remains at the basal level. In this simulation, $u_{mc}(t) = 1.22\,\text{U/h}$ (basal insulin), $u_{ins}(t) = u_{IMC}(t)$.

3. *Later hypoglycemia prevention.* Against a glucose rise, the IMC filter reacts first with a positive peak (above phase), but then, it will have a negative insulin peak (see the green areas in Figure 7.3). If $u_{IMC}(t)$ is higher than $th_{resc} < 0$, $u_{ins}(t)$ will equal $u_{IMC}(t)$ to subtract insulin from the main controller hence avoiding overdosing and the likely related hypoglycemia. If $u_{IMC}(t)$ overpasses th_{res} from above, reducing the insulin from the main controller may be insufficient. Therefore, the negative-valued insulin is converted into rescue carbohydrates suggestions ($u_{resc}(t)$, see Section 7.4.2) and $u_{ins}(t)$ zeroed to avoid both types of control actions coupling each other.

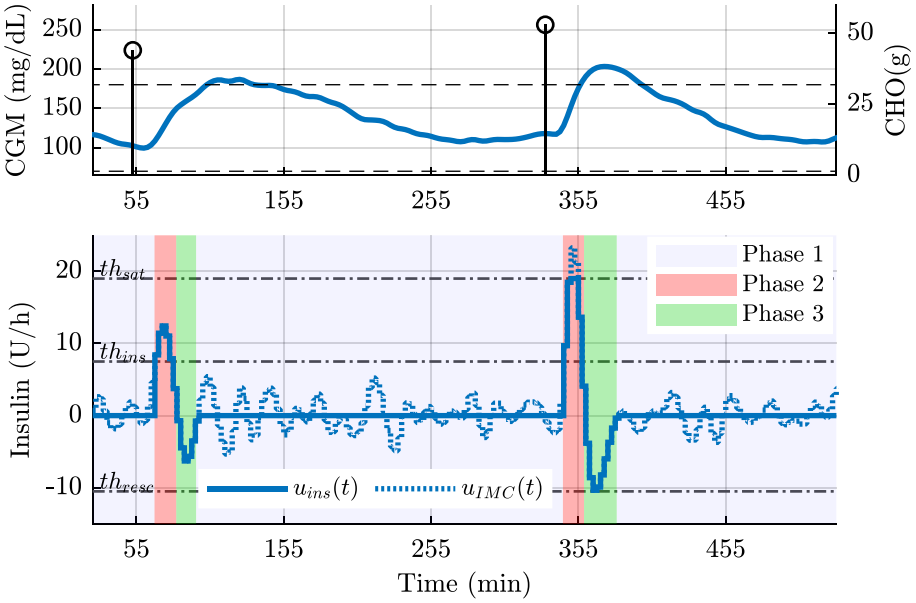

Figure 7.3: Control logic to compensate meals. The switching logic processes the virtual action $u_{IMC}(t)$ in three phases: dead-zone (Phase 1), glucose rise mitigation (Phase 2), and later hypoglycemia prevention (Phase 3). The insulin infusion $u_{ins}(t)$ added to the main controller. Parameters $th_{ins} > 0$, $th_{sat} > 0$, and $th_{resc} < 0$ are the thresholds to inhibit $u_{IMC}(t)$, saturate it, or convert it into rescue carbohydrate suggestions, respectively.

7.4.2 Hypoglycemia mitigation

The $u_{IMC}(t)$ signal might be lower than zero if a sustained glucose reduction occurs. The switching logic module converts this "negative insulin" into rescue carbohydrate suggestions (see around 200 min at Figure 7.4) to avoid or mitigate hypoglycemia. To this end, first, a virtual unquantized carbohydrate signal, $u_{int}(t)$, is calculated by integrating $u_{IMC}(t)$ in a sliding window of length t_w ($t_w = 60$min) as follows:

$$u^*_{IMC}(t) = \begin{cases} u_{IMC}(t) & \text{if} \quad u_{IMC}(t) \leq th_{resc} \\ 0 & \text{otherwise} \end{cases} \tag{7.5}$$

$$u_{int}(t) = -k_{resc} \int_{t-t_w}^{t} u^*_{IMC}(\tau) W(\tau) d\tau - \\ - \int_{t-t_w-T_s}^{t-T_s} u_{resc}(\tau) W(\tau) d\tau \tag{7.6}$$

The first integral in (7.6) accumulates the "negative insulin" and converts it into carbohydrates units (g) through the gain k_{resc}, similarly to Ramkissoon et al. (2019). Minor fluctuations of $u_{IMC}(t)$ below zero ($th_{resc} \leq u_{IMC}(t) \leq 0$) might correspond to noise or unrelevant glucose reduction that can be handled with just reducing insulin (as in Phase 3 of Section 7.4.1). To avoid suggesting rescue carbohydrates in those cases, the expression (7.6) stops considering the "negative insulin" by setting the auxiliary variable $u^*_{IMC}(t)$ in (7.5) to zero. In addition, the forgetting factor $W(t)$ attenuates the earlier values of $u^*_{IMC}(t)$ in the sliding window $[t - t_w, t]$. $W(t)$ reads as:

$$W(t^*) = e^{-2} \cdot e^{(t^* - t + t_w)/30} \tag{7.7}$$

for $t^* \in [t - t_w, t]$ where t refers to the current time and $t - t_w$ the beginning of the sliding window (when the earliest value of $u^*_{IMC}(t)$ is considered).

The second integral in (7.6) subtracts the carbohydrates suggested within the sliding window to avoid increasing $u_{int}(t)$.

The virtual carbohydrate signal, $u_{int}(t)$, must be quantized for user convenience. The quantized rescue signal, $u_{resc}(t)$, follows the next logic:

$$u_{resc}(t) = \begin{cases} \left\lfloor \frac{u_{int}(t)}{\widetilde{cho}} \right\rceil \cdot \widetilde{cho} & \text{if } u_{int}(t) \geq \widetilde{cho}/2 \text{ and} \\ & \quad G^*(t) \leq 70 \text{ and} \\ & \quad \Delta t_{resc} > 15 \\ \widetilde{cho} & \text{if } CGM(t) \leq 70 \text{ and} \\ & \quad G^*(t) \leq 54 \text{ and} \\ & \quad \Delta t_{resc} > 15 \\ 0 & \text{otherwise} \end{cases} \tag{7.8}$$

where $\lfloor \cdot \rceil$ denotes the nearest integer operator, Δt_{resc} is the elapsed time between two consecutive rescue suggestions (in min), and $\widetilde{cho}$ is the minimum carbohydrate rescue dose (quantization level). The parameter $\widetilde{cho}$ was set to 15 g since it is the most available size of commercial glucose supplements, e.g., Dex4 (Can-Am

Care, Alpharetta, GA, USA), Glutose15 (Paddock Laboratories, Minneapolis, MN, USA), TruePlus (Trividia Health, Fort Lauderdale, FL, USA), etc.

$G^*(t)$ is the 30-min ahead glucose prediction (in mg/dL) computed with the following linear extrapolation:

$$G^*(t) = CGM(t) + 30 \cdot C\dot{G}M(t) \tag{7.9}$$

According to (7.8), the controller suggests carbohydrates in two situations:

- *When the system predicts risk of moderate hypoglycemia and the accumulated rescue carbohydrates is large enough.* If $u_{int}(t)$ halves the minimum rescue dose – as implemented in Moscardó et al. (2019a) and Beneyto et al. (2018) – the algorithm calculates a rescue carbohydrate suggestion by approximating $u_{int}(t)$ to the nearest multiple of $\widetilde{cho}$. If the predicted glucose is outside hypoglycemia risk, the system will not suggest a rescue carbohydrate even though $u_{int}(t) \geq \widetilde{cho}/2$ (see the orange squares in Figure 7.4).
- *When the subject is in moderate hypoglycemia and the glucose tends to severe hypoglycemia.* Here, the system suggests a $\widetilde{cho}$-g rescue carbohydrate regardless of the value of $u_{int}(t)$.

The algorithm considers a minimum elapsed time of 15 min between rescue carbohydrates suggestions to avoid frequent recommendations.

Since the exercise impacts the insulin sensitivity even after the exercise event (Schiavon et al. 2013), the switching logic also reduces the insulin-on-board limitation of the main controller to 70% of its nominal value and zeroes $u_{ins}(t)$ within the 3h following the last rescue suggestion (see the red area in Figure 7.4). Reducing the insulin-on-board is a common practice in the literature to control exercise (Moser et al. 2020; Beneyto et al. 2018; Zaharieva et al. 2020). The system restores the nominal values of insulin-on-board limitation and $u_{ins}(t)$ whenever a risk of hyperglycemia exists: when $CGM(t) \geq 140$ mg/dL and $G^*(t) \geq 180$ mg/dL.

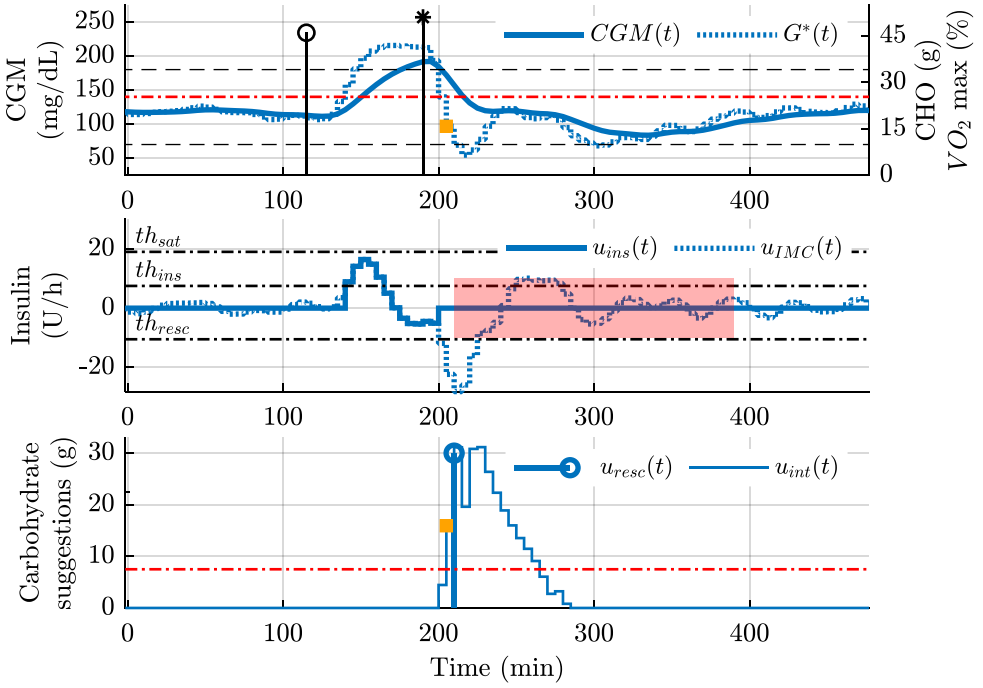

Figure 7.4: Example of hypoglycemia mitigation. The switching logic converts the negative insulin of the IMC ($u_{IMC}(t)$, middle panel) into a continuous carbohydrate signal ($u_{int}(t)$, bottom panel). If the predicted glucose ($G^*(t)$, upper panel) is in hypoglycemia and $u_{int}(t) \geq 7.5$ (dashed red line in bottom panel), the algorithm suggests a rescue $u_{resc}(t)$ (bottom panel) by quantizing $u_{int}(t)$. Orange squares illustrate that rescue carbohydrates are inhibited if no hypoglycemia risk exists. Insulin $u_{ins}(t)$ is inhibited after the rescue carbohydrate suggestion (red area in bottom panel).

7.5 Tuning

The proposed controller requires an individual tuning of the following five parameters: the gain of $F(s)$ (k_{ins}), the gain factor converting insulin into carbohydrates (k_{resc}), and the three thresholds of the switching logic (th_{ins}, th_{sat}, and th_{resc}).

Relating these parameters with parameters of the open-loop therapy (weight, total daily insulin, etc.) would simplify the application of the add-on module in a clinical setting. To this end, first, the five parameters were individualized for the ten virtual adults of the UVa/Padova simulator according to optimal performance criteria (areas in risks, Section 7.5.1). Then, multi-linear regression models were

fit between the optimal tuning and open-loop parameters to find their relation (Section 7.5.2).

7.5.1 Optimization-based tuning

An overview of the optimization procedure is illustrated in Figure 7.5: for each subject, twelve iterations with different instances of variability were simulated, and the highest cost within them is optimized. Each simulation consisted of a 7-day ($T_{sim} = 10\,080$ min) scenario with three daily meals and one daily exercise session.

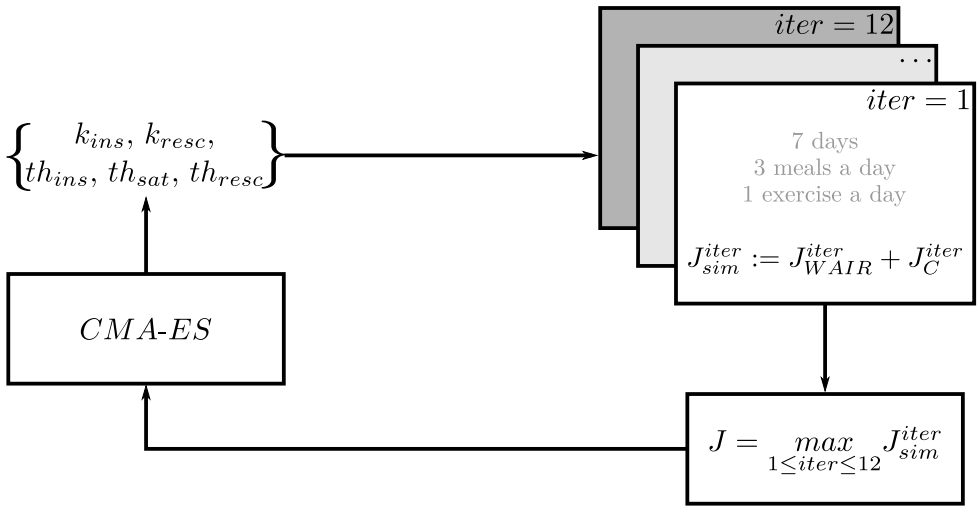

Figure 7.5: Min-max optimization overview for a virtual subject. The parameters to individualize are the gain of $F(s)$ (k_{ins}), the gain factor converting insulin into carbohydrates (k_{resc}), and the three thresholds of the switching logic (th_{ins}, th_{sat}, and th_{resc}). The worst-case among the 12 iterations with different variability is optimized with the CMA-ES algorithm to individualize the parameters.

The cost related to each simulation instance reads as:

$$J_{sim} := J_{WAIR} + J_C \tag{7.10}$$

This cost penalizes the weighted areas in risk (J_{WAIR}) and constrains the magnitude or shape of the control actions (J_C). The weighted areas in risk consider the areas of the CGM exceeding the thresholds 54, 70, 180, and 250 mg/dL as defined as:

$$
\begin{aligned}
J_{WAIR} = a_{uu} \cdot \int_0^{Tsim} (G_{uu}(\tau) - 250)\, d\tau + \\
+ a_u \cdot \int_0^{Tsim} (G_u(\tau) - 180)\, d\tau + \\
+ a_l \cdot \left| \int_0^{Tsim} (70 - G_l(\tau)) \right| d\tau + \\
+ a_{ll} \cdot \left| \int_0^{Tsim} (54 - G_{ll}(\tau)) \right| d\tau + \\
+ a_{resc} \cdot \int_0^{Tsim} (G_{resc}(\tau) - 140)\, d\tau
\end{aligned}
\tag{7.11}
$$

where the scalars $a_{uu} = 175$, $a_u = 1$, $a_l = 5000$, $a_{ll} = 10000$, $a_{resc} = 50$ are the weights. Those weights were tuned so that the areas in hypoglycemia cost more than those in hyperglycemia. Although this definition of the cost is more complex than other optimization-based tuning proposals in the literature (Olcomendy et al. 2020), it provides more flexibility in configuring the optimal performance. All the integrals were calculated using the trapezoidal rule. Signals $G_{uu}(t)$, $G_u(t)$, $G_l(t)$, $G_{ll}(t)$ in (7.11) correspond to the CGM after being saturated to the enclosing thresholds as follows:

$$
G_{uu}(t) := \begin{cases} 250 & \text{if } CGM(t) \leq 250 \\ CGM(t) & \text{otherwise} \end{cases} \tag{7.12}
$$

$$
G_u(t) := \begin{cases} 180 & \text{if } CGM(t) \leq 180 \\ 250 & \text{if } CGM(t) > 250 \\ CGM(t) & \text{otherwise} \end{cases} \tag{7.13}
$$

$$
G_l(t) := \begin{cases} 54 & \text{if } CGM(t) < 54 \\ 70 & \text{if } CGM(t) \geq 70 \\ CGM(t) & \text{otherwise} \end{cases} \tag{7.14}
$$

$$
G_{ll}(t) := \begin{cases} 54 & \text{if } CGM(t) \geq 54 \\ CGM(t) & \text{otherwise} \end{cases} \tag{7.15}
$$

The add-on module might suggest rescue carbohydrates for a glucose drop caused by an excessive insulin delivery. If the recommended carbohydrate size is large, the add-on module might even provide an additional insulin infusion after the

glucose rise, which, at the same time, triggers more rescue suggestions. The last addend of (7.11) penalizes the glucose rebound after carbohydrate suggestions to avoid this undesirable oscillatory behavior. Signal $G_{resc}(t)$ represents the value of the CGM that overpasses 140 mg/dL in the first 3 h after rescue carbohydrate suggestions or up to mealtime if a meal occurs before then, as defined in:

$$G_{resc}(t) = \begin{cases} CGM(t) & \text{if} \quad (CGM(t) \geq 140) \\ & \quad \text{and } t \in [t_{resc}, \min(t_{resc} + 3\text{h}, t_{meal})] \\ 140 & \text{otherwise} \end{cases} \tag{7.16}$$

where t_{resc} and t_{meal} denote the rescue carbohydrates and meals times, respectively. Mealtimes were available to define the cost function but were unknown to the controller.

The cost J_C penalizes the number of times the IMC activates the insulin mode (Phase 2 of Figure 7.3) for $u_{ins}(t)$ to behave like a bolus: being active a short time with large insulin doses rather than being continuously activated with reduced amounts. The cost J_C also constrains the size of rescue carbohydrates. To reduce the risk of compensating insulin overdosing with rescue carbohydrate suggestions, the ones followed by meals (meal rescue carbohydrate) were weighted more than those followed by exercise sessions (exercise rescue carbohydrate). For the exercise-related rescue carbohydrates, the average rescue size per exercise event was limited to 45g. The expression of J_C is the following:

$$\begin{aligned} J_C = b_{act} \cdot \max\left(\frac{n_{imc\_act}}{n_{meal}} - 1, 0\right) + \\ + \quad b_{meal\_resc} \cdot \sum_{i=1}^{n_{meal\_resc}} meal\_resc_i + \\ + \quad b_{ex\_resc} \cdot \left(\frac{\sum_{i=1}^{n_{ex\_resc}} ex\_resc_i}{45 n_{ex\_sessions}} - 1, 0\right) \end{aligned} \tag{7.17}$$

where $b_{act} = 1400$, $b_{meal\_resc} = 15000$, and $b_{ex\_resc} = 4500$ are weights. Terms n_{imc_act}, n_{meal_resc}, n_{ex_resc}, $n_{ex\_session}$ denote the number of times the IMC enters Phase 2, the number of meal-related rescue carbohydrate, the number of exercise-related rescue carbohydrate, and the number of exercise sessions, respectively. $meal\_resc_i$ represents the meal rescue sizes (from $i = 1$ to $i = n_{meal\_resc}$) and $meal\_ex_i$ the exercise carbohydrate suggestion sizes (from $i = 1$ to $i = n_{ex\_resc}$).

The min-max problem was solved with the Covariance Matrix - Adaptation Evolution Strategy (CMA-ES) algorithm, a black-box search optimizer suitable for non-linear or non-convex problems (Hansen 2016). Table 7.2 includes the starting values and the bounds of the parameters. To reduce the computational time, the optimization was executed in the computing cluster of the Politechnical University of Valencia (Universitat Politècnica de València, València, Spain) using 12 cores of 3 GB (Mullor Casero et al. 2020).

Table 7.2: Initial values and bounds of the parameters in the optimization

	Initial value	**Lower limit**	**Upper limit**
k_{ins} (-)	$5 \cdot 10^{-1}$	$1 \cdot 10^{-2}$	1
th_{min}(U/h)	5	1	$3.0 \cdot 10^{1}$
th_{max}(U/h)	$1.0 \cdot 10^{1}$	1	$3.0 \cdot 10^{1}$
th_{resc}(U/h)	-1	-5	$-5 \cdot 10^{-2}$
k_{resc}(g/(U h))	$-1 \cdot 10^{-1}$	$-5 \cdot 10^{-1}$	$-5 \cdot 10^{-4}$

Table 7.3 contains the resulted optimal tuning for the add-on module parameters.

Table 7.3: Control parameters that resulted from optimization

Subject	$\boldsymbol{k_{ins}}$ **(-)**	$\boldsymbol{th_{min}}$ **(U/h)**	$\boldsymbol{th_{max}}$ **(U/h)**	$\boldsymbol{k_{resc}}$ **(g/(U h))**	$\boldsymbol{th_{resc}}$ **(U/h)**
1	$4 \cdot 10^{-2}$	4.43	9.38	$-9 \cdot 10^{-2}$	$-4.8 \cdot 10^{-1}$
2	$1.7 \cdot 10^{-1}$	1.46	$1.434 \cdot 10^{1}$	$-3.1 \cdot 10^{-1}$	$-1.5 \cdot 10^{-1}$
3	$3 \cdot 10^{-2}$	1.08	$1.320 \cdot 10^{1}$	$-6 \cdot 10^{-2}$	$-5.3 \cdot 10^{-1}$
4	$8 \cdot 10^{-2}$	5.50	$1.219 \cdot 10^{1}$	$-1.2 \cdot 10^{-1}$	$-7 \cdot 10^{-2}$
5	$1.1 \cdot 10^{-1}$	3.72	$2.595 \cdot 10^{1}$	$-9 \cdot 10^{-2}$	$-7 \cdot 10^{-2}$
6	$2.5 \cdot 10^{-1}$	7.57	$1.962 \cdot 10^{1}$	$-1.2 \cdot 10^{-1}$	-2.08
7	$2 \cdot 10^{-2}$	5.42	$1.025 \cdot 10^{1}$	$-9 \cdot 10^{-2}$	$-1.2 \cdot 10^{-1}$
8	$1.4 \cdot 10^{-1}$	6.83	$1.522 \cdot 10^{1}$	$-5 \cdot 10^{-2}$	-2.45
9	$3.4 \cdot 10^{-1}$	2.34	8.08	$-1.6 \cdot 10^{-1}$	$-7.2 \cdot 10^{-1}$
10	$1.4 \cdot 10^{-1}$	9.69	$1.569 \cdot 10^{1}$	$-9 \cdot 10^{-2}$	$-3.5 \cdot 10^{-1}$

The first column represents the virtual adult identifier in the UVa/Padova Simulator. The second, third, and fourth columns include the parameters used for meal compensation, while the remaining columns correspond to the exercise compensation (see Section 7.5).

7.5.2 Regression-based tuning

The optimization-based tuning of Section 7.5.1 is only feasible for in silico studies. To provide an initial tuning for a clinical trial, the optimal parameters were related to the following standard parameters of the open-loop therapy (Reiterer et al. 2019): the weight (BW, in kg), the total daily insulin (TDI, in U), the basal insulin (u_b, in U/h), the carbohydrate-to-insulin ratio (CR, in g/U), and the correction factor (CF, in mg/(dL U)). The values of these parameters were available in the UVa/Padova simulator.

For each optimal parameter (k_{ins}, k_{resc}, th_{ins}, th_{sat}, and th_{resc}), a relation to open-loop parameters was found as follows:

1. The 80 linear models that fit the corresponding optimal parameter with the lowest root sum of squares error were selected. Models had up to 8 coefficients, including pairwise interactions of the open-loop parameters. The selection was performed with the function `regsubset` (Fortran code by Alan Miller 2020) of the R software (R Core Team 2021).

2. To mitigate the risk of overfitting, the selected models were fitted using leave-one-out cross-validation (Kuhn 2021).

3. The final model was the model with the lowest number of coefficients that had an accurate root-mean-squared error of the cross-validation ($RMSE_{loocv}$) and satisfied the diagnosis assumptions (normality and homoscedasticity of the residuals).

The resulted multilinear models relating the optimal tuning with the open-loop parameters are shown in Table 7.4. The adjusted R^2 ($adjR^2$) and $RMSE_{loocv}$ values indicate a proper fitting.

7.6 In silico validations

The proposed add-on module was validated in the UVa/Padova simulator. Since the simulator models the 5-min sampling of the CGM readings, the module must be discretized. The IVP model was discretized with Euler, whereas the filter $Q(s)$ (7.2) and the integral of the switching logic (7.6) were discretized with the trapezoidal approximation. All discretization used a sample time of $T_s = 5$ min.

Table 7.4: Regression equations of the controller's parameters and related goodness of fit metrics

	$adjR^2$	$RMSE_{loocv}$
$\hat{k}_{ins} = 14.2 + 6.17 \cdot 10^{-2} \cdot TDI - 2.59 \cdot u_b - 1.61 \cdot 10^{-3} \cdot BW \cdot CF + + 3.93 \cdot 10^{-3} \cdot BW \cdot CR - 4.67 \cdot 10^{-3} \cdot CF \cdot TDI - - 6.57 \cdot 10^{-3} \cdot CR \cdot TDI$	$9.72 \cdot 10^{-1}$	$4.71 \cdot 10^{-2}$
$\hat{th}_{ins} = -51.6 + 28.9 \cdot CR + 0.872 \cdot BW \cdot u_b - 2.53 \cdot 10^{-2} \cdot BW \cdot CF - - 12.9 \cdot CR \cdot u_b - 0.226 \cdot CF \cdot CR$	$7.52 \cdot 10^{-1}$	1.95
$\hat{th}_{sat} = 4.01 \cdot 10^2 - 1.05 \cdot 10^2 \cdot u_b - 20.8 \cdot CR - 8.82 \cdot 10^{-2} \cdot BW \cdot CF + + 0.209 \cdot BW \cdot CR + 0.150 \cdot CF \cdot CR$	$8.90 \cdot 10^{-1}$	3.16
$\hat{k}_{resc} = 3.02 + 7.6 \cdot 10^{-2} \cdot CR - 3.11 \cdot 10^{-4} \cdot BW \cdot TDI + + 1.74 \cdot 10^{-2} \cdot BW \cdot u_b - 1.76 \cdot 10^{-4} \cdot BW \cdot CF - - 8.18 \cdot 10^{-2} \cdot CF \cdot u_b$	$7.76 \cdot 10^{-1}$	$6.76 \cdot 10^{-2}$
$\hat{th}_{resc} = 12.3 + 0.133 \cdot BW + 0.295 \cdot TDI - 0.103 \cdot BW \cdot u_b - - 1.48 \cdot 10^{-2} \cdot CF \cdot TDI + 2.55 \cdot 10^{-3} \cdot CF \cdot CR$	$9.55 \cdot 10^{-1}$	$2.09 \cdot 10^{-1}$

Evaluated metrics are the adjusted coefficient of determination ($adjR^2$) for multivariable regression models and root-mean-squared error of the leave-one-out cross-validation ($RMSE_{loocv}$). The five models have a low $RMSE_{loocv}$ and acceptable coefficients of determination.

7.6.1 Validation setting

The following three validations were performed to study the effectiveness of the proposed add-on module:

- *Validation 1* analyzes whether the regression-based tuning (henceforth denoted with mIMC) preserves the performance of the optimal tuning (mIMC-Opt).
- *Validation 2* studies the effectiveness of the proposed module (mIMC) to handle unannounced meals in the main controller (denoted as NoComp). Also, this validation compares the mIMC to two controllers with meal compensation: the main controller with announced meals (referred as Hybrid) but with carbohydrate counting errors, following the model of Kawamura et al. (2015); and the main controller extended with the meal-detector-based bolusing algorithm presented in Chapter 6 (referred here as MD).

- *Validation 3* assesses the benefits of the rescue carbohydrate feature of the mIMC to deal with unannounced hypoglycemia-inducing exercise events. To this end, the mIMC is compared to two controllers that only can mitigate glucose drops by inhibiting insulin: the mIMC controller with the rescue carbohydrate suggestions deactivated (referred to as NoExComp) and the MD controller.

All the validations were performed with a modified version of the UVa/Padova simulator. Two scenarios were configured:

- *Scenario 1*: The scenario considers 30 days with 3 daily meals. The meals have random size and timing: 49.5 [33.0,55.0] g for breakfast at 6.92 [6.75, 7.08] h , 81.0 [72.0, 93.0] g at 13.75 [13.58, 14.17] h for lunch, and 64.0 [54.0, 79.0] g at 20.9 [20.8, 21.1] h for dinner, median [interquartile range] (Figure 7.6). This scenario was used in *Validation 2* (Section 7.6.3).
- *Scenario 2*: This scenario shares the duration and the meal distribution of *Scenario 1* and includes one daily exercise. The exercise effect on glucose is modeled as a variation on insulin sensitivity, following the pattern described by Schiavon et al. (2013). The insulin sensitivity pattern in Schiavon et al. (2013) approximately corresponds to an aerobic exercise of 60 min with an intensity of 50 $\%VO_2$max (maximum percentage of oxygen volume). In the simulation, a uniform distribution was added to this duration and intensity (Figure 7.7). Exercise time was uniformly assigned to occur from 45 min to 240 min after a randomly selected meal of the day (i.e., breakfast, lunch, or dinner), as illustrated in Figure 7.7 (see the top panel and left bottom panel). Exercise beyond midnight was avoided. With this setting, the exercise occurred 282.5 [230.0, 360.0] min before the immediate later meal and 157.5 [115.0, 195.0] min after the immediate earlier meal. This scenario was used for *Validation 1* (Section 7.6.2) and *Validation 3* (Section 7.6.4).

The scenarios described above share the following sources of variability: CGM noise, one-day period sinusoidal-type insulin sensitivity variation with random amplitude and phase, variation of subcutaneous insulin absorption rate at each meal following a uniform distribution of $\pm 30\%$, and variability of the meal absorption parameters.

The corresponding scenario is repeated in all the validations for each of the ten virtual subjects included in the simulator. Meal features (time and size of Figure 7.6) and exercise features (time, duration, intensity of Figure 7.7) are shared between subjects. Other sources of variability (CGM noise, parameters variability, etc.) were subject-dependent. Moreover, all the subjects ingested

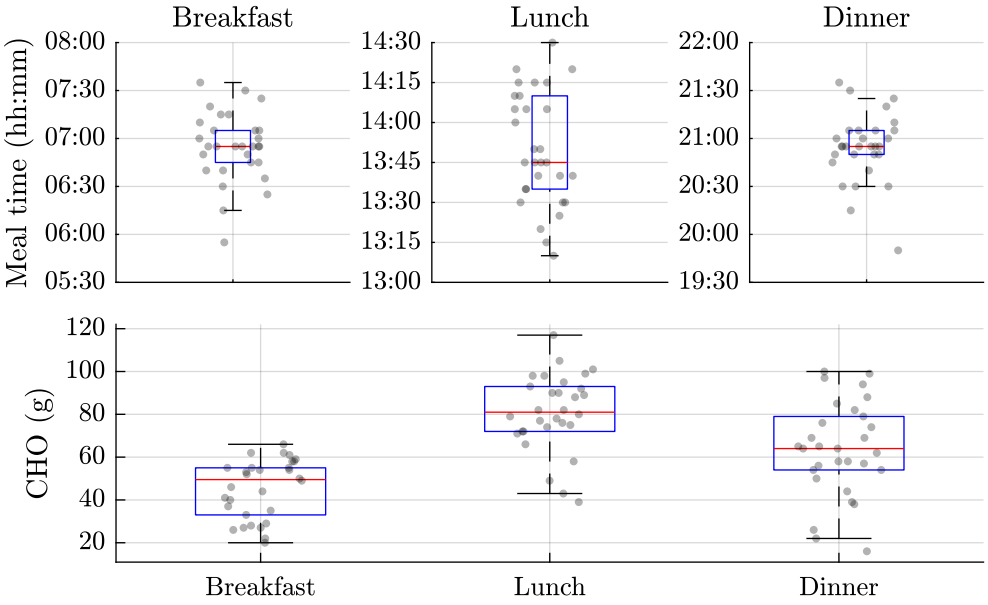

Figure 7.6: Timing and size distributions of the meal intakes in the Validation 2 scenario. In the boxplots, the red line indicates the median, the blue box width encloses the interquartile range, the whisker encloses the extreme data (1.5 times the interquartile range), and the dots represent the actual meal intake size.

the suggested rescue carbohydrate in the precise time and amount as commonly assumed in the literature (Moscardó et al. 2019a; Beneyto et al. 2018; Ramkissoon et al. 2019).

The performance within tunings (*Validation 1*) or controllers (*Validation 2* and *Validation 3*) was assessed through the following standard metrics (Battelino et al. 2019): CGM mean, CGM coefficient of variance (CV), %time above 250 mg/dL, %time above 180 mg/dL, %time in 70–180 mg/dL, %time below 70 mg/dL, %time below 54 mg/dL, and total daily insulin. In *Validation 2*, percentage-time-related metrics within the postprandial period (from the mealtime until 3 h after each meal) was calculated too. In addition, since the mIMC might suggest rescue carbohydrates after insulin overdose, the percentage of meal intakes requiring at least one rescue carbohydrate suggestion and the size of these suggestions were reported. In *Validation 3*, the following exercise-related metrics were also computed: the %time in hypoglycemia within the exercise period (from the exercise time to 3 h after it), the %time above 140 mg/dL up to 3 h after each rescue, the

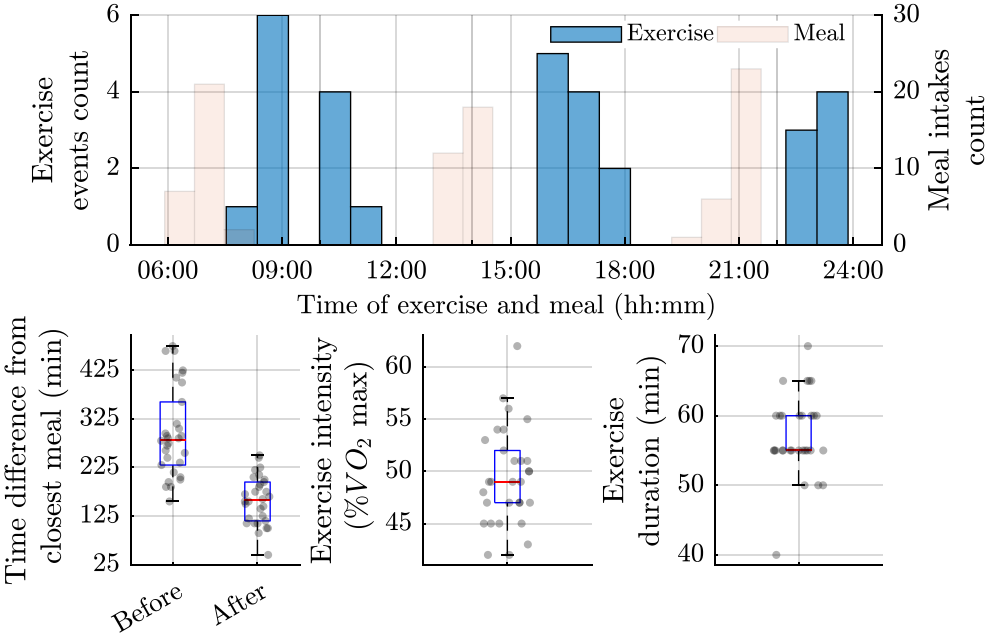

Figure 7.7: Timing, duration and intensity distributions of the exercise events in the in the Validation 1 and Validation 3 scenario. *Panel description*: (top) exercise time and mealtime expressed as hh:mm; (bottom, left) represents the time difference between the exercise and the closest meal "Before" or "After" the exercise; (bottom, middle) shows the exercise intensity given in maximum percentage of oxygen volume; and (bottom, right) shows the exercise duration in minutes. In the boxplots, the red line indicates the median, the blue box width encloses the interquartile range, the whisker encloses the extreme data (1.5 times the interquartile range), and dots represent the actual exercise event.

percentage of exercise events needing at least one rescue carbohydrate, and the mean rescue size suggested for those events.

To compare the above metrics within tunings or controllers, linear random-intercept (Barr et al. 2013) models with 95% Wald confidence intervals (Luke 2017) were applied. Linear random-intercept models are similar to linear regression models, but intercepts are individualized to one independent variable (random factor). In this case, the random intercept is the virtual subject identifier in the simulator (*sub*). Varying the intercept within subjects overcomes the data independence condition assumed by linear models (Barr et al. 2013), which fails in the current analysis since all simulations share the virtual subjects. The structure of the random-intercept model is the following:

$$y_{sub} = \beta_0 + S_{sub} + \sum_{i=1}^{n_C-1} \beta_i x_i + e_{sub} \tag{7.18}$$

where y_{sub} is the corresponding metric value for a given subject identifier, *sub*, and n_C is the number of controllers to be compared (or tuning in the case of *Validation 1*). S_{sub} is the random intercept and e_{sub} are the residuals, following a zero-mean normal distribution (Barr et al. 2013). Fixed effects x_is are dichotomous-coded variables representing the controller (or tuning): for a specific controller $i = k$ only x_k is 1, while other variables are 0. Fixed coefficient β_0 is the intercept, i.e., the estimated mean of the metric for the controller taken as the reference for comparison. The coefficients β_i can be interpreted as the difference in means regarding the intercept given the dichotomous nature of x_i. Since the data presented some outliers, the linear random-intercept models were fitted with the robust method presented in Koller (2016) using the statistics software R (R Core Team 2021).

No statistic inference analysis was performed for the %time below 70 mg/dL and %time below 54 mg/dL in *Validation 2* since the normal assumption of the residuals fails because these metrics contains many zeros. As a result, no linear model can be applied directly. Several methods exist to handle data with an excess of zeros (Min et al. 2002). However, they led to such wide confidence intervals that they were uninformative. Therefore, these methods were discarded as well.

Results in the text are presented as median [25th percentile, 75th percentile] or estimated difference in means (confidence interval).

7.6.2 Validation 1: Comparison of the regression-based tuning with the optimal tuning

Figure 7.8 shows the glucose traces of 2 of the 30 days of *Scenario 2*, comparing the optimization tuning (mIMC-Opt) with the regression-based tuning (mIMC). Most of the time, the glucose profile of the regression-based tuning matches the glucose of the optimal tuning. As a result, the mIMC achieved metrics that are very similar to the mIMC-Opt (Table 7.7): the difference in means (regarding mIMC-Opt) in %time in 70–180 mg/dL (0.0303 (−1.30, 1.91) %), %time above 180 mg/dL (−0.470 (−2.29, 1.35) %), and %time below 70 mg/dL (0.0576 (−0.199, 0.315) %) are negligible in magnitude and no significant difference is concluded from the confidence intervals. These results indicate that the regression-based tuning preserves the performance achieved by the optimal tuning.

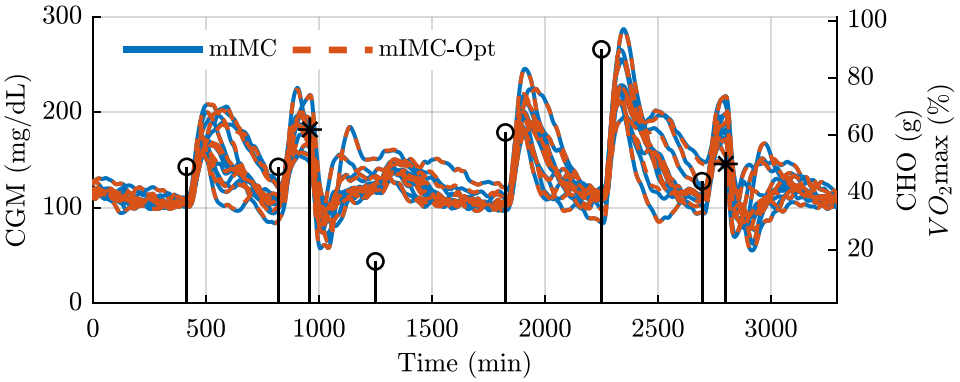

Figure 7.8: Comparison of the regression-based tuning with the optimal tuning. The black circles in the upper panel represent meal intake events whose carbohydrate contents are shown on the right axis. The black asterisks indicate exercise events whose maximum oxygen volume is shown on the right axis.

7.6.3 Validation 2: Results of postprandial control

Calculated metrics are summarized in Table 7.5, and the mixed-effect model estimations are in Table 7.6. Also, Figure 7.9 includes the glucose and insulin traces of 2 of the 30 days of the simulation (*Scenario 1*).

Table 7.5: Performance metrics of meal compensation (Validation 2)

	NoComp	Hybrid	MD	mIMC
Overall				
Mean CGM (mg/dL)	170.8 ± 22.1 161.6 [158.9, 189.5]	144.7 ± 9.8 140.6 [139.0, 154.2]	145.5 ± 11.9 141.8 [139.0, 145.6]	140.9 ± 9.0 140.0 [132.9, 144.8]
CV (%)	31.4 ± 3.9 30.5 [28.7, 33.7]	25.9 ± 3.4 25.2 [23.4, 26.5]	27.2 ± 3.8 25.8 [24.4, 29.2]	26.5 ± 3.3 25.2 [24.4, 28.6]
CGM time (%)				
>250 mg/dL	11.5 ± 8.4 8.2 [4.8, 19.5]	1.9 ± 2.3 1.2 [0.3, 2.3]	2.2 ± 1.7 1.9 [0.7, 4.0]	1.5 ± 1.3 1.4 [0.3, 2.3]
>180 mg/dL	37.2 ± 14.5 31.8 [29.9, 45.2]	18.1 ± 6.7 16.0 [13.6, 24.1]	19.9 ± 8.4 17.3 [16.2, 20.4]	16.6 ± 6.0 14.7 [11.8, 22.1]
[70 – 180] mg/dL	62.8 ± 14.5 68.2 [54.8, 70.1]	81.9 ± 6.7 84.0 [75.9, 86.4]	79.8 ± 8.3 81.9 [79.3, 83.8]	83.4 ± 5.9 85.1 [77.9, 88.1]
<70 mg/dL	0.0 ± 0.0 0.0 [0.0, 0.0]	0.0 ± 0.0 0.0 [0.0, 0.0]	0.3 ± 0.8 0.0 [0.0, 0.1]	0.1 ± 0.1 0.0 [0.0, 0.1]
<54 mg/dL	0.0 ± 0.0 0.0 [0.0, 0.0]	0.0 ± 0.0 0.0 [0.0, 0.0]	0.2 ± 0.5 0.0 [0.0, 0.0]	0.0 ± 0.0 0.0 [0.0, 0.0]
Daily insulin (U)	35.8 ± 7.9 34.7 [29.8, 37.4]	39.4 ± 8.8 38.6 [34.0, 41.3]	38.9 ± 9.1 38.3 [32.9, 39.9]	39.6 ± 8.5 38.5 [34.1, 41.4]
Postprandial control				
CGM time (%)				
>250 mg/dL	19.7 ± 10.9 17.5 [9.4, 28.3]	3.9 ± 4.4 2.6 [0.9, 4.2]	5.5 ± 4.3 5.1 [1.7, 9.4]	3.8 ± 3.4 3.5 [0.7, 5.9]
>180 mg/dL	56.0 ± 9.9 57.2 [49.1, 62.3]	32.6 ± 8.4 34.0 [25.7, 35.5]	42.0 ± 9.7 41.4 [37.6, 47.5]	36.3 ± 9.7 34.9 [29.4, 45.5]
<70 mg/dL	0.0 ± 0.0 0.0 [0.0, 0.0]	0.0 ± 0.0 0.0 [0.0, 0.0]	0.1 ± 0.2 0.0 [0.0, 0.0]	0.0 ± 0.0 0.0 [0.0, 0.0]
<54 mg/dL	0.0 ± 0.0 0.0 [0.0, 0.0]	0.0 ± 0.0 0.0 [0.0, 0.0]	0.0 ± 0.0 0.0 [0.0, 0.0]	0.0 ± 0.0 0.0 [0.0, 0.0]
Meals needing rescues (%)	0.0 ± 0.0 0.0 [0.0, 0.0]	0.0 ± 0.0 0.0 [0.0, 0.0]	0.0 ± 0.0 0.0 [0.0, 0.0]	2.7 ± 5.1 0.0 [0.0, 1.1]
Mean rescues (g)	- -	- -	- -	15.0 ± 0.0 15.0 [15.0, 15.0]

Four meal compensation techniques, which share the main controller, were compared: 1) absence of meal compensation (NoComp), 2) announced-based compensation (Hybrid), 3) meal-detector-based compensation (MD), and 4) proposed approach (mIMC). Metrics are expressed in mean ± standard deviation and median [25th percentile, 75th percentile] of the ten virtual adults. "Overall metrics" consider the entire simulation period (30 days), while "Postprandial" control metrics refer to a specific period of the postprandial: percent of time-related metrics aggregate the 3-h period after the meal, and rescue-related metrics aggregate meal-to-meal period.

The proposed module (mIMC), once added to the main controller, reduces in 19.29 (15.07, 23.52) mg/dL (Table 7.6) the %time above 180 mg/dL achieved by the main controller without meal announcement (NoComp). The %time below 70 mg/dL slightly increases compared to NoComp (mIMC: 0.0 [0.0, 0.1] mg/dL vs NoComp: 0.0 [0.0, 0.0] mg/dL) but it never reaches the safety upper limit of 4% (Battelino et al. 2019). Although the rescue carbohydrates suggestions are crucial to avoid severe hypoglycemia, the controller recommended them only for four subjects within the 30 days of the simulation: two subjects received a single rescue carbohydrate, one subject received ten rescue carbohydrates, and another received twelve rescue carbohydrates. All the rescue carbohydrate suggestions contained 15 g.

Most of the confidence intervals of the original main controller with carbohydrate counting errors (Hybrid) overlap with those of the mIMC. Therefore, the mIMC improves the NoComp in a similar, not statistically significant, degree, with the advantage of avoiding meal announcements (see columns "Hybrid" and "mIMC" of Table 7.6). The most considerable difference between both controllers occurred in the early postprandial period. Since the Hybrid timely delivers an insulin bolus, its achieved glucose peak tends to be lower than the one achieved by the mIMC (see Figure 7.9). The Hybrid also tends to reduce the %time above 180 mg/dL within the postprandial period more than the mIMC, which reacts later to the meal. However, the confidence intervals are too wide to conclude a statistically significant difference. In contrast, when considering the entire simulation period to compute the %time in 70–180 mg/dL and %time above 180 mg/dL, the confidence intervals of Hybrid and mIMC are much closer to each other even with a slight trend in favor of mIMC. The reason is that Hybrid takes longer to compensate for large meals than the mIMC (see the fifth meal in Figure 7.9) because the carbohydrate counting error model, which represents the most frequent practice of real subjects, underestimates those meals (Kawamura et al. 2015).

Lastly, as expected from the results of Chapter 6, the MD improves, with statistical significance, the %time in 70–180 mg/dL of the NoComp. The confidence intervals of the MD overlaps with those of the mIMC, meaning that the mIMC might be an alternative to the MD for unannounced meal compensation. The most relevant difference between both controllers is the rescue carbohydrate suggestion feature. Counteracting glucose drops is more challenging for the MD than for the mIMC. Indeed, one virtual subject had severe hypoglycemia with the MD, while the mIMC avoided them. Furthermore, the MD tends to be less aggressive than the mIMC: it delivered less insulin and achieved greater hyperglycemia, especially for the early postprandial period (Table 7.5).

Table 7.6: Estimated intercept and coefficients of mixed-effect models for meal compensation scenario (Validation 2)

			Difference in mean regarding NoComp					
	NoComp		Hybrid		MD		mIMC	
	Est.	*CI*	*Est.*	*CI*	*Est.*	*CI*	*Est.*	*CI*
Overall								
Mean CGM (mg/dL)	167.5	(159.3,175.7)	-23.3	(-28.6,-18.0)	-22.0	(-27.4,-16.7)	-27.0	(-32.3,-21.7)
CV (%)	31.1	(28.8,33.5)	-5.5	(-6.4,-4.6)	-4.2	(-5.1,-3.3)	-4.7	(-5.6,-3.8)
CGM time (%)								
>250 mg/dL	9.2	(7.5,10.9)	-7.3	(-8.6,-6.1)	-7.0	(-8.2,-5.8)	-7.7	(-8.9,-6.5)
>180 mg/dL	35.8	(29.9,41.7)	-17.8	(-22.1,-13.6)	-16.0	(-20.2,-11.7)	-19.3	(-23.5,-15.1)
[70 – 180] mg/dL	64.1	(58.2,70.1)	17.8	(13.7,22.0)	15.8	(11.6,19.9)	19.3	(15.1,23.4)
Daily insulin (U)	35.0	(30.4,39.7)	3.2	(2.4,4.1)	2.8	(1.9,3.7)	3.4	(2.6,4.3)
Postprandial								
>250 mg/dL	18.9	(15.3,22.5)	-15.1	(-17.3,-12.9)	-13.4	(-15.6,-11.2)	-15.1	(-17.3,-12.9)
>180 mg/dL	56.0	(49.0,63.0)	-23.3	(-28.4,-18.3)	-13.9	(-19.0,-8.9)	-19.7	(-24.7,-14.6)

The column "NoComp" includes the estimation (Est) and the Wald 95% confidence interval (CI) of the intercept, i.e, the estimated mean of the corresponding metric for the main controller without any meal compensation. The columns "Hybrid", "MD", and "mIMC" correspond to the estimated coefficients of the mixed-effect model for the hybrid main controller with carbohydrates counting error, the main controller extended with the meal detector and the main controller extended with the proposed add-on module, respectively. These coefficients are interpreted as the difference in mean of the corresponding metric regarding the main controller without any meal compensation.

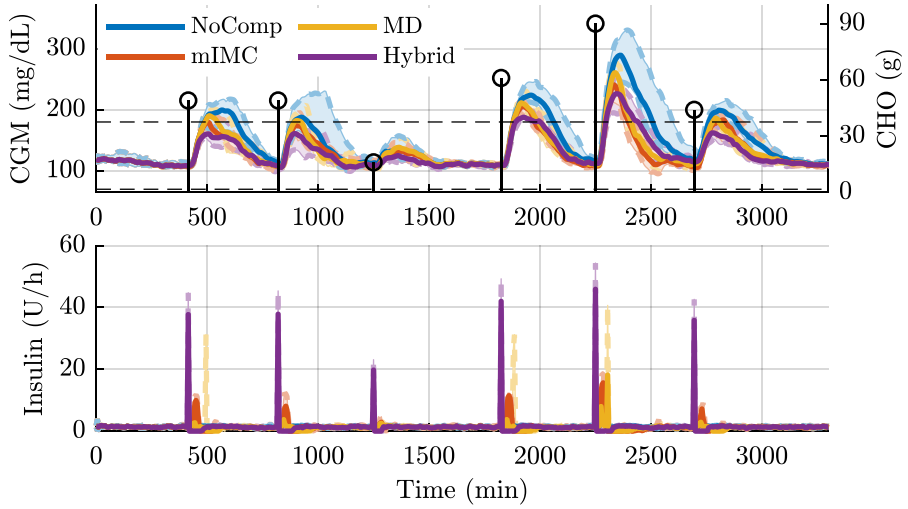

Figure 7.9: Population glucose and insulin profiles of meal scenario. It shows 2 of the 30 days of the simulation comparing four meal compensation techniques: absence of meal compensation (NoComp), announced-based compensation with carbohydrate error counting (Hybrid), meal-detector-based compensation (MD), and proposed approach (mIMC). The solid lines represent the median of the ten virtual adults, the shaded area is the interquartile range, and the dashed lines are the 25th and 75th percentiles. The black circles in the upper panel represent meal events whose carbohydrate contents are shown on the right axis.

7.6.4 Validation 3: Results of exercise control

Table 7.7 and Table 7.8 summarize the calculated metrics and the statistic analysis, respectively. Figure 7.10 illustrates 3 of the 30 days of the simulation comparing the proposed module (mIMC) with two controllers without rescue carbohydrates: the meal-detector-based controller (MD) and the mIMC controller with rescue carbohydrate feature unable (NoExComp).

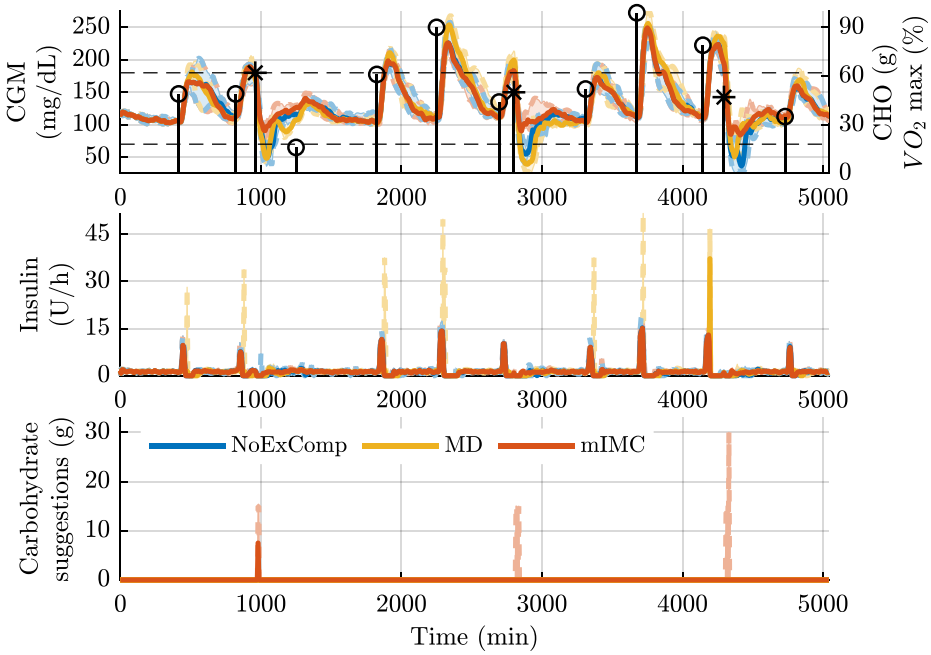

Figure 7.10: Population glucose, insulin profiles, and rescue carbohydrate suggestions of exercise scenario. It shows 3 of the 30 days of the simulation comparing two controllers without rescue carbohydrate suggestions (NoExComp and MD) with the proposed controller (mIMC). MD is the meal-detector-based controller, and NoExComp implements the disturbance compensation strategy of mIMC, but without rescue carbohydrate suggestions. The solid lines represent the median of the ten virtual adults, the shaded area is the interquartile range, and the dashed lines are the 25th and 75th percentiles. The black circles in the upper panel represent meal intake events whose carbohydrate contents are shown on the right axis. The black asterisks indicate exercise events whose maximum oxygen volume is shown on the right axis.

The rescue carbohydrate suggestion capability of the mIMC lowered more than 3% the %time below 70 mg/dL and the %time below 54 mg/dL achieved without carbohydrate suggestions in the NoExComp (Table 7.8). With this reduction, the mIMC hypoglycemia-related metrics are within clinically acceptable ranges – %time below 54 mg/dL and %time below 70 mg/dL is more down than 1% and 4%, respectively (Battelino et al. 2019)– while NoExComp exceeds them (Table 7.8).

For reducing %time in hypoglycemia, the mIMC suggested 27.2 [23.7, 31.0] g of carbohydrate per exercise session, which is comparable with other results of unannounced exercise events in the literature (Beneyto et al. 2018; Ramkissoon

et al. 2019; Moscardó et al. 2019a). Although more than 95% of exercise events required at least one rescue carbohydrate, the mIMC preserves the %time above 180 mg/dL and the %time above 250 mg/dL achieved by the NoExComp. The glucose mean increases 4.3 (1.2, 7.3) mg/dL regarding NoExComp; this increase is admissible considering the relevant reduction in hypoglycemia.

The MD also enhances the %time below 70 mg/dL and %time below 54 mg/dL of NoExComp (Table 7.7), but only at the price of increasing %time above 180 mg/dL. In addition, the reduction of %time in hypoglycemia by the MD is inconsistent within the simulation. For example, Figure 7.10 shows how the MD can either behave like the NoExpComp (first exercise event), underperform it (second exercise event), or overperform it (third exercise event). Also, the average reduction of %time in hypoglycemia is negligible compared to the mIMC (e.g., the mIMC lowers %time in hypoglycemia seven times more than MD within the 3 h after the exercise, as observed in Table 7.8), which manifests the limitations of handling exercise-induced hypoglycemia with only insulin reduction.

Table 7.7: Performance metrics in the exercise case (Validation 3)

	NoExComp	MD	mIMC	mIMC-Opt
Overall				
Mean CGM (mg/dL)	136.9 ± 6.0 138.2 [132.1, 141.7]	138.3 ± 8.2 136.9 [135.6, 138.5]	141.1 ± 6.3 141.9 [136.5, 146.2]	141.7 ± 5.9 140.5 [138.4, 145.4]
CV (%)	33.5 ± 3.7 33.3 [31.4, 34.4]	34.5 ± 4.1 34.1 [33.1, 35.1]	29.7 ± 3.0 29.6 [27.4, 32.0]	29.7 ± 3.0 29.5 [27.5, 32.3]
CGM time (%)				
>250 mg/dL	2.1 ± 1.7 1.6 [0.8, 2.9]	2.5 ± 1.6 2.2 [1.5, 3.6]	2.2 ± 1.6 1.6 [1.0, 2.9]	2.2 ± 1.7 1.7 [1.0, 2.7]
>180 mg/dL	17.7 ± 4.1 19.2 [13.5, 21.1]	19.6 ± 5.6 19.2 [18.1, 20.6]	18.0 ± 4.0 19.8 [13.6, 20.8]	18.5 ± 3.8 18.9 [16.0, 21.0]
[70 – 180] mg/dL	76.9 ± 5.0 75.5 [72.7, 81.5]	75.6 ± 5.9 76.5 [71.6, 77.0]	81.1 ± 4.3 79.6 [77.5, 85.5]	80.7 ± 4.2 80.2 [77.6, 83.6]
<70 mg/dL	5.4 ± 1.8 5.3 [4.5, 6.6]	4.8 ± 1.7 4.6 [4.0, 5.1]	0.8 ± 0.6 0.9 [0.4, 1.1]	0.8 ± 0.6 0.8 [0.2, 1.2]
<54 mg/dL	3.4 ± 1.8 3.7 [2.2, 4.1]	3.0 ± 1.6 2.8 [2.0, 3.4]	0.1 ± 0.1 0.0 [0.0, 0.0]	0.1 ± 0.1 0.0 [0.0, 0.0]
Daily insulin (U)	38.6 ± 8.4 37.9 [33.0, 40.7]	38.3 ± 9.1 37.6 [31.8, 39.6]	38.7 ± 8.4 37.7 [33.2, 40.6]	38.7 ± 8.6 37.6 [32.9, 40.6]
Daily CHO (g)	- -	- -	28.1 ± 8.4 27.5 [23.9, 31.0]	27.4 ± 7.0 27.2 [21.9, 29.8]
Exercise control				
CGM time (%)				
<70 mg/dL	37.4 ± 10.1 38.3 [34.6, 44.1]	34.0 ± 8.8 34.7 [30.7, 39.2]	6.4 ± 4.4 6.5 [3.0, 8.7]	5.9 ± 4.5 6.0 [1.9, 9.4]
<54 mg/dL	24.1 ± 11.3 27.0 [17.0, 30.4]	21.8 ± 8.9 21.6 [16.1, 26.4]	0.5 ± 1.0 0.1 [0.0, 0.3]	0.4 ± 0.9 0.0 [0.0, 0.3]
>140 mg/dL (rescues)	- -	- -	12.2 ± 11.6 9.6 [5.6, 12.8]	13.0 ± 12.0 8.0 [5.8, 17.2]
Events needing rescues (%)	- -	- -	96.3 ± 1.1 96.7 [96.7, 96.7]	96.7 ± 0.0 96.7 [96.7, 96.7]
Mean rescues (g)	- -	- -	27.9 ± 8.0 27.2 [23.7, 31.0]	27.3 ± 7.2 26.9 [22.0, 29.7]

Metrics summary of the controllers assessed in *Validation 3*: the meal-detector based controller (MD), the proposed controller (mIMC), and the proposed controller with the rescue suggestion module unable. The column "mIMC-Opt" includes the results of the mIMC tuned with the optimal parameters (*Validation 1*). Metrics are expressed in mean ± standard deviation and median [25th percentile, 75th percentile] of the ten virtual adults. "Overall" metrics aggregate the entire simulation period (30 days), while "Exercise control" metrics refer to a specific period after the exercise time: percent of time-related metrics aggregate the 3-h period after the exercise, and rescue-related metrics aggregate exercise-to-exercise period.

Table 7.8: Estimated intercept and coefficients of mixed-effect models for exercise compensation scenario (Validation 3)

			Difference in mean regarding NoExComp			
	NoExComp		MD		mIMC	
	Est.	*CI*	*Est.*	*CI*	*Est.*	*CI*
Overall						
Mean CGM (mg/dL)	136.8	(132.3,141.3)	1.2	(-1.9,4.3)	4.3	(1.2,7.3)
CV (%)	33.2	(31.1,35.3)	1.0	(-0.2,2.3)	-3.7	(-5.0,-2.4)
CGM time (%)						
>250 mg/dL	2.0	(0.9,3.0)	0.4	(0.1,0.7)	0.1	(-0.2,0.4)
>180 mg/dL	17.7	(14.5,20.9)	2.0	(0.0,4.0)	0.3	(-1.7,2.3)
[70 – 180] mg/dL	76.8	(73.2,80.4)	-1.5	(-3.2,0.2)	4.2	(2.5,5.9)
<70 mg/dL	5.5	(4.7,6.2)	-0.9	(-2.0,0.1)	-4.6	(-5.6,-3.6)
<54 mg/dL	3.3	(2.7,4.0)	-0.6	(-1.5,0.3)	-3.3	(-4.2,-2.4)
Daily insulin (U)	37.6	(32.8,42.3)	-0.3	(-1.0,0.4)	0.1	(-0.6,0.8)
Exercise						
CGM time (%)						
<70 mg/dL	38.9	(34.7,43.2)	-4.4	(-10.4,1.6)	-32.5	(-38.5,-26.6)
<54 mg/dL	24.8	(20.0,29.5)	-3.4	(-9.6,2.8)	-24.2	(-30.4,-18.0)

The column "NoExComp" includes the estimation (Est) and the Wald 95% confidence interval (CI) of the intercept, i.e, the estimated mean of the corresponding metric for the mIMC with unable rescue suggestion feature. The columns "MD" and "mIMC" correspond to the estimated coefficients of the mixed-effect model for the main controller extended with the meal detector, and the main controller extended with the proposed add-on module, respectively. These coefficients are interpreted as the difference in mean of the corresponding metric regarding NoExComp.

7.7 Conclusions

The proposed module satisfactorily managed unannounced meals in the SAFE-AP controller: the reduction in %time above 180 mg/dL is comparable to the original hybrid SAFE-AP (considering carbohydrate counting error), and the %time below 70 mg/dL remains under 4%.

In a scenario with hypoglycemia-inducing exercise, the rescue carbohydrate suggestion feature of the proposed module compensates hypoglycemia more effectively than other controllers that only inhibit insulin, without increasing the %time in hyperglycemia.

Although the proposed module covers the chapter goals (eliminating meal and exercise announcements with adequate %time in 70–180 mg/dL and %time in hypoglycemia), some room for improvement still exists. In the tuning of the add-on module, only ten subjects were used – the adult cohort in the simulator–, which increases the risk of overfitting. The subject cohort must be extended in future work, ideally with information from earlier clinical studies (Ahmad et al. 2021).

Furthermore, the add-on module was assessed only against hypoglycemia-inducing exercise corresponding to a low-to-moderate aerobic exercise. Nevertheless, depending on the type of exercise, intensity, duration, or timing, exercise can even cause a glucose rise (Ruegemer et al. 1990; Moser et al. 2020), which might require a different strategy to compensate for it. The simulator neither accounted for the high intrapatient variability in the exercise (Notkin et al. 2021). Similarly, the simulator considers that meals are composed of carbohydrates only. However, meals also contain proteins, fats, or alcohol, modifying the absorption profiles expected by the simulator. Due to the limitations of the in silico validations, complete validation of the proposed module is only possible in clinical trials.

Chapter 8

Conclusions and future work

This chapter closes the dissertation by outlining the main contributions. Furthermore, it will overview the limitations of the developed methods and the opportunities for future work to overcome them.

Food eating or exercise workout for people with type diabetes may be constant reminders of their disease. Even with the most advanced insulin therapies commercially available, i.e., hybrid artificial pancreas systems, patients must intervene to compensate for these disturbances through meal announcements (carbohydrate counting) or exercise announcements (announce the exercise event hours in advance). This dissertation aimed to develop methods that release patients from these burdensome and life-restricting announcements without compromising the glycemic outcomes.

8.1 Conclusions

The thesis resulted in the following two contributions (see "List of publications" for the related publications):

1. A bolusing algorithm module that removes the need for meal announcement in artificial pancreas systems.
2. An internal-model-based module calculating bolus-like insulin infusions and suggesting carbohydrate rescues to release patients from meal and exercise announcements.

The bolusing algorithm module builds upon a meal disturbance estimator (Chapter 3), a meal detector (Chapter 5), and a PD-like logic that computes corrective boluses based on the meal disturbance estimation and the detection event (Chapter 6). To design the meal disturbance estimator, an observer-based approach was utilized. Factors like model complexity, observation algorithm, and intra-patient variability are known to affect the estimation accuracy; the contribution of each factor in the estimation of the meal disturbance was evaluated in an in silico analysis in this dissertation (Chapter 3). The results revealed that the intra-patient variability has the most considerable contribution in explaining the variations of the estimation error; hence, more individualized models would result in a reduced error. In addition, the estimated disturbance appears coupled with other disturbances. This limitation was underscored in Chapter 4. This chapter illustrated the estimation of disturbances when signals (i.e., glucose and insulin infusions) from real datasets are fed into the observer. Two clinical datasets were used, one for meals and the other to reconstruct the disturbance caused by exercise. On the one hand, the estimated meal disturbance resembled the expected meal-like shape in the median. However, some examples were presented wherein other disturbances or model mismatches hid the expected meal disturbance profile in the estimated disturbance (e.g., oscillation, disturbance below zero). On the other hand, the exercise disturbance was reconstructed assuming that the exercise effect on glucose can be represented as an additive disturbance. It was shown that the impact of carbohydrate intake before exercise mostly absorbed the effect of aerobic exercise in the estimated disturbance.

The bolusing algorithm is triggered by a meal detection event. The meal detector consists of a super-twisting-based residual generation and a decision logic that determines the meal occurrence based on the residuals and glucose first derivative. It has been exhaustively evaluated with synthetic and clinical datasets, achieving acceptable results in the line of other meal detectors presented in the literature.

At detection time, the bolusing algorithm infuses a reduced-size bolus. If glucose keeps increasing after that (indicative of a positive detection), corrective boluses are delivered based on the estimated disturbance and a PD-like logic. As an application example, the module was integrated into a hybrid artificial pancreas system (the SAFE-AP, designed by the research group hosting this thesis project). The complete system was also validated in silico under unannounced meal conditions. It achieved similar glucose mean to the hybrid counterpart (when carbohydrate misestimation errors were considered) without significantly increasing time spent on hypoglycemia. However, the conservative tuning of the first bolus and the detection delay led to a slightly longer time in hyperglycemia.

This first contribution led to three journal articles (Sala-Mira et al. 2019; Sala-Mira et al. 2021; Faccioli et al. 2022), two conference articles (Sala et al. 2018; Sala-Mira et al. 2020), and two conference abstracts (Sala-Mira et al. 2018; Faccioli et al. 2021). Sala et al. (2018) presented a preliminary implementation of an observer to estimate meal disturbances. Sala-Mira et al. (2019) first showed the superiority of the First Order Sliding Mode Observer described in Chapter 3 over the first proposal in Sala et al. (2018). The articles Sala-Mira et al. (2020) and Sala-Mira et al. (2021) included the comparison of the First Order Sliding Mode Observer and the Kalman Filter described in Chapter 3. Sala-Mira et al. (2019) also presented and validated a preliminary implementation of the meal detector and the bolusing algorithm. Finally, the improvements of the meal detector algorithm described in Chapter 5 (e.g., implicit discretization or noise reduction) were presented in Faccioli et al. (2021) and Faccioli et al. (2022), including more comprehensive validations than the one included in Chapter 3.

The module developed in the first contribution yielded acceptable results against unannounced meals; however, exercise-induced hypoglycemia would unlikely be compensated with this module due to the long offset action of insulin. Thus, a new module was designed to overcome this limitation by suggesting carbohydrate intake (Chapter 7).

The module consisted of a filter, designed based on the internal model control principle. The filter mitigates the discrepancy between the glucose measurement and the glucose estimated with a glucose-insulin model. The output of this filter is fed to a switching logic that, depending on the value of the filter output, the glucose, and a glucose prediction, routes the filter output to the insulin pump or converts it to carbohydrate suggestions. For convenience, the module was integrated into the SAFE-AP to assess the module performance. However, any other hybrid controller with some insulin-on-board limitation mechanism could have been applied. Once integrated into the SAFE-AP, the complete system without meal announcements yielded comparable results in %time in range and %time in hyperglycemia than the hybrid counterpart with carbohydrate mismatch. In a challenging scenario with daily unannounced exercises, the system markedly reduced the time in hypoglycemia with an acceptable amount of suggested carbohydrates.

The second contribution gave rise to a journal article (Sala-Mira et al. 2022a) describing the internal model-based module presented in Chapter 7. A patent application related to this module was also submitted.

8.2 Future work

The main limitation of the methods developed in this dissertation is that they have been adjusted and validated in a small cohort of virtual patients. Although the simulations performed in this dissertation included challenging conditions (e.g., parameter variability, sensor noise, and meals with different carbohydrate content, timing, and absorption profile), complete validation is possible only in clinical settings. A pilot clinical trial evaluating the bolusing algorithm with unannounced meals has been projected for the near future under the scope of the National project TAILOR (ref: PID2019-107722RB-C21)

Even if future clinical trials supported the feasibility of the proposed methods, more effort should be made to apply these methods in real-life conditions. The aggressiveness of the proposed modules should be adapted to overcome glycemic changes due to circadian rhythms, hormonal changes, stress, or illness. Addressing technical issues (e.g., pump occlusion, signal loss) is also required for long-term use. In addition, the proposed methods were conceived to remove the meal and exercise announcements entirely. However, patients with an active implication in their disease management may initially untrust the system and feel uncomfortable rendering complete control to the system. Thus, the proposed modules should be more flexible and allow announcements if patients consider them. These requirements will be addressed in the project Prometeo FLEX-AP (ref: CIPROM/2021/012)

List of publications

Listed below are the publications resulted from this thesis. The asterisk * indicates authors that equally contributed to the work.

Journal articles

Sala-Mira, **I.**; Garcia, P.; Díez, J.-L., and Bondia, J. (2022a). "Internal model control based module for the elimination of meal and exercise announcements in hybrid artificial pancreas systems". In: *Computer Methods and Programs in Biomedicine (JCR 2021: Q1)*, p. 107061. ISSN: 0169-2607. DOI: https://doi.org/10.1016/j.cmpb.2022.107061 (cit. on pp. 146, 181).

Faccioli *, S.; **Sala-Mira** *, **I.**; Díez, J.; Facchinetti, A.; Sparacino, G.; Del Favero, S., and Bondia, J. (2022). "Super–twisting-based meal detector for type 1 diabetes management: Improvement and assessment in a real-life scenario". In: *Computer Methods and Programs in Biomedicine (JCR 2021: Q1)* 219, p. 106736. ISSN: 0169-2607. DOI: 10.1016/j.cmpb.2022.106736 (cit. on pp. 103, 121, 181).

Sala-Mira *, **I.**; Siket *, M.; Kovacs, L.; Eigner, G., and Bondia, J. (2021). "Effect of Model, Observer and their Interaction on State and Disturbance Estimation in Artificial Pancreas: an In-Silico Study". In: *IEEE Access (JCR 2021: Q2)*, pp. 1–15. ISSN: 2169-3536. DOI: 10.1109/ACCESS.2021.3120880 (cit. on pp. 39, 71, 181).

Sala-Mira, **I.**; Díez, J.-L.; Ricarte, B., and Bondia, J. (2019). "Sliding-mode disturbance observers for an artificial pancreas without meal announcement". In: *Journal of Process Control (JCR 2019: Q2)* 78, pp. 68–77. ISSN: 09591524. DOI: 10.1016/j.jprocont.2019.03.008 (cit. on pp. 39, 103, 129, 131, 181).

Conference articles

Sala-Mira *, **I.**; Siket *, M.; Eigner, G.; Bondia, J., and Kovacs, L. (2020). "Kalman filter and sliding mode observer in artificial pancreas: an in-silico comparison". In: *21th IFAC World Congress. IFAC-PapersOnLine*. Vol. 53. 2. Berlin (Germany): Elsevier Ltd, pp. 16227–16232. DOI: 10.1016/j.ifacol.2020.12.617 (cit. on pp. 39, 181).

Sala, **I.**; Diez, J., and Bondia, J. (2018). "Generalized extended state observer design for the estimation of the rate of glucose appearance in artificial pancreas". In: *2018 European Control Conference (ECC)*. Limassol (Cyprus): IEEE, pp. 2393–2398. ISBN: 978-3-9524-2698-2. DOI: 10.23919/ECC.2018.8550123 (cit. on pp. 51, 181).

Sala-Mira, **I.**; Díez, J., and Bondia, J. (2017). "Insulin limitation in the Artificial Pancreas by Sliding Mode Reference Conditioning and Insulin Feedback: an in silico comparison". In: *20th IFAC World Congress. IFAC-PapersOnLine*. Vol. 50. 1. Toulouse (France), pp. 7743–7748. DOI: 10.1016/j.ifacol.2017.08.1153 (cit. on pp. 132, 197).

Abstracts and posters

Faccioli *, S.; **Sala-Mira** *, **I.**; Diez, J.-L.; Facchinetti, A.; Sparacino, G.; Del Favero, S., and Bondia, J. (2021). "Super-Twisting Observer For Meal Detection Assessed In Realistic Scenarios using UVA/Padova T1D Simulator". In: *Diabetes Technology & Therapeutics. 14th International Conference on Advanced Technologies & Treatments for Diabetes*. Vol. 23. S2. Virtual, A–76. DOI: 10.1089/dia.2021.2525.abstracts (cit. on pp. 103, 181).

Sala-Mira, **I.**; Ricarte, B.; Romero-Vivo, S.; Diez, J.-L., and Bondia, J. (2018). "Unannounced Meal Control through Sliding Mode Techniques in an Artificial Pancreas". In: *18th Annual Diabetes Tecnology Meeting*. Vol. 50. 1, p. 78831 (cit. on pp. 129, 181).

Patent applications

Sala-Mira, **I.**; García Gil, P. J.; Company Bondia, J., and Diez Ruano, J. L. (2022b). "Method for improving blood glucose control of a hybrid controller, add-on module for being incorporated to an artificial pancreas system for perfoming the method and artificial pancreas system incorporating the add-on module". Pat. req. P202230693. Universitat Politècnica de València (UPV) (cit. on p. 146).

Appendices

Appendix A

Implicit discretization of sliding mode observers

According to the methodology described in Section 3.4.2, the implicit discretization of the FOSMO applied to the Hovorka model follows the steps below:

- Calculate the output injection term and the output error

$$\psi[k] = \begin{cases} \frac{e^*[k]}{\beta[k]}, & \text{if } \frac{e^*[k]}{\beta[k]} \in [-1,\, 1] \\ 1, & \text{if } \frac{e^*[k]}{\beta[k]} > 1 \\ -1, & \text{if } \frac{e^*[k]}{\beta[k]} < 1 \end{cases} \tag{A.1}$$

$$e_y[k] = e^*[k] - \beta[k]\psi[k] \tag{A.2}$$

- Update the state estimation

$$Q_1[k] = V_G\left(y[k] - e_y[k]\right) \tag{A.3}$$

$$S_1[k] = \frac{T_s u[k-1] + S_1[k-1]}{1 + \frac{T_s}{\tau_S}} \tag{A.4}$$

$$S_2[k] = \frac{\frac{T_s}{\tau_S} S_1[k] + S_2[k-1]}{1 + \frac{T_s}{\tau_S}} \tag{A.5}$$

$$I[k] = \frac{\frac{T_s}{\tau_S V_I} S_2[k] + I[k-1]}{1 + T_s k_e} \tag{A.6}$$

$$x_1[k] = \frac{T_s k_{b_1} I[k] + x_1[k-1]}{1 + T_s k_{a_1}} \tag{A.7}$$

$$x_2[k] = \frac{T_s k_{b_2} I[k] + x_2[k-1]}{1 + T_s k_{a_2}} \tag{A.8}$$

$$x_3[k] = \frac{T_s k_{b_3} I[k] + x_3[k-1]}{1 + T_s k_{a_3}} \tag{A.9}$$

$$Q_2[k] = \frac{T_s x_1[k] Q_1[k] + Q_2[k-1]}{1 + T_s k_{12} + T_s x_2[k]} \tag{A.10}$$

The terms $e^*[k]$ and $\beta[k]$ are calculated with the following MATLAB script:

```
%%%%%%%%%%%%%%%%%%%%%%%%%%%%%%%%%%%%%%%%%%%%%%%%%%%
%% IMPLICIT DISCRETIZATION FOSMO WITH HOVORKA MODEL
% This script generates the function to calculate
% the discontinuous term v(k)
%%%%%%%%%%%%%%%%%%%%%%%%%%%%%%%%%%%%%%%%%%%%%%%%%%
syms S1k S2k Ik x1k x2k x3k ...
Q2k Q1k positive %states at current iteration
syms S1km1 S2km1 Ikm1 x1km1 x2km1 ...
x3km1 Q2km1 Q1km1 positive %states at k-1
syms uk positive %insulin input
syms F01ck Frk positive%
syms tmaxI Vi ke ka1 ka2 ka3 kb1 kb2 kb3 k12...
EGP0 Vg invC2 positive %parameters
syms K k real % FOSMO gains
syms Ts positive %sample time
syms eyk psik yk real %output error, discontinuous
                  %term, actual output

%% Unmeasurable states
```

```
% Equations of the unmeasurable states
% after implicit discretization
eqs={(S1k-S1km1)/Ts==uk-S1k/tmaxI
        (S2k-S2km1)/Ts==S1k/tmaxI-S2k/tmaxI
        (Ik-Ikm1)/Ts==S2k/(tmaxI*Vi)-ke*Ik
        (x1k-x1km1)/Ts==-ka1*x1k+kb1*Ik
        (x2k-x2km1)/Ts==-ka2*x2k+kb2*Ik
        (x3k-x3km1)/Ts==-ka3*x3k+kb3*Ik
        (Q2k-Q2km1)/Ts==x1k*Q1k-k12*Q2k-x2k*Q2k};

sol=solve(eqs,[S1k S2k Ik x1k x2k x3k Q2k]);


S1_k=sol.S1k;
S2_k=sol.S2k;
I_k=sol.Ik;
x1_k=sol.x1k;
x2_k=sol.x2k;
x3_k=sol.x3k;
Q2_k_1=sol.Q2k;

%% Measurable states
% Equation of the measurable state
% after implicit discretization
Q2_k_2=simplify(solve((Q1k-Q1km1)/Ts==-F01ck-...
x1_k*Q1k+k12*Q2k-Frk+EGP0*(1-x3_k)-K*eyk...
+k*invC2*psik,Q2k));

%% Calculate ey
% Consider that eyk=yk-hat(yk)
Q1_k=invC2*(yk-eyk);

% Solve the system of equations
Q2_k_1_subs=subs(Q2_k_1,Q1k,Q1_k);
Q2_k_2_subs=subs(Q2_k_2,Q1k,Q1_k);
ey_k=solve(Q2_k_1_subs==Q2_k_2_subs,eyk);

% Get e*(k) and B(k)
co=coeffs(ey_k,psik);
B_k=-simplify(co(2));
east_k=simplify(co(1));
```

```
61
62
63 %% Matlab function
64 % Write a function to create the terms B(k)
65 % and e*(k)
66 matlabFunction(B_k,east_k,'File',...
67 'getAuxiliarTerms','Optimize',false,...
68 'Vars',{[S1km1,S2km1,Ikm1,x1km1,...
69         x2km1,x3km1,Q2km1,Q1km1],yk,uk,K,k,Ts,F01ck,...
70         Frk,invC2,EGP0,k12,ka1,ka2,ka3,kb1,kb2,...
71         kb3,ke,tmaxI,Vi})
```

The script first defines the symbolic variables for the states, the parameters, and the gains (lines 6–16). In lines 22–30, the Hovorka counterpart of the system equations (3.31)–(3.38) are solved to obtain the unmeasurable state variables. Then, the condition $e_y[k] = y_k - \hat{y}_k$ is considered to obtain an expression for $e_y[k]$, or `eyk` in above snippet (lines 44–55). In lines 58–60, the function `coeffs()` is used to obtain $e^*[k]$ (or `east_k`) and $\beta[k]$ (or `B_k`). Finally, the function `matlabFunction()` converts the symbolic expression to a MATLAB function.

Appendix B

Description of the main controller

B.1 Context

The SAFE-AP controller is the main controller the control algorithms developed in this dissertation build upon. This controller has been developed by the research group this thesis project belongs to: the Spanish Consortium on Artificial Pancreas and Diabetes Technology. This is a multidisciplinary consortium integrated by two engineering groups (The Lab on Artificial Pancreas and Diabetes Technology from the Universitat Politècnica de València and the Modeling, Identification & Control Engineering Laboratory from the Universitat of Girona) and three clinical groups (Hospital Clínic de Barcelona, Hospital Clínico Universitario de Valencia y Hospital Francesc de Borja de Gandia).

A first version of the controller was presented in Revert et al. (2013), where the principal feature of the controller is described: an Sliding Mode Reference Conditioning (SMRC) approach to constraint the insulin-on-board. In an 8-h inpatient clinical trial, the controller yielded promising results under an announced mixed meal test, outperforming the %time in 70–180 mg/dL achieved by pump therapy without increasing the %time spent in hypoglycemia (Rossetti et al. 2017).

Furthermore, Quirós et al. (2018) evaluated the SAFE-AP under aerobic and anaerobic exercise sessions. Although the results were satisfactory, the user had to announce the exercise 45 min in advance, something impractical in an ambulatory use. The contributions of Beneyto et al. (2018), Ramkissoon et al. (2019), and Bertachi et al. (2019) overcame this limitation with new rules to adapt the upper bound limit of the insulin-on board, a carbohydrate suggester module, and an exercise detection algorithm. The upgraded version of the SAFE-AP underwent a clinical trial with a heavy aerobic session in both announced and unannounced conditions. The SAFE-AP halved the number of hypoglycemic events achieved by the open-loop therapy, decreased the %time below 70 mg/dL, and increased the %time in 70–180 mg/dL (Viñals et al. 2021).

B.2 Basic controller architecture

This sections details the basic architecture of the SAFE controller. For simplicity, the carbohydrate suggester module (Beneyto et al. 2018; Ramkissoon et al. 2019) was not considered in this dissertation.

Figure B.1 overviews the SAFE controller. On the one hand, an Insulin Feedback (IFB) limits the output of a PD controller when the estimated plasma insulin exceeds its equilibrium value. On the other hand, an Sliding Mode Reference Conditioning (SMRC) safety layer upper-bounds the insulin-on-board (insulin stacked in the subcutaneous tissues) by modifying the PD controller set-point. The insulin calculated by the SAFE controller, u_{mc}, considers, besides the contribution of the PD-IFB, the insulin basal infusion ($u_{basal}(t)$), required by the patient to maintain normal (usually around 100 mg/dL) plasma glucose during starvation periods. In addition, the control action considers a pre-meal bolus since the original controller is hybrid. In Chapter 6 and Chapter 7, two strategies have been addressed to remove this pre-meal bolus with minor additional modifications to the SAFE controller.

The three elements integrating the system (the PD controller, the IFB structure, and the SMRC layer) are described in the following subsections:

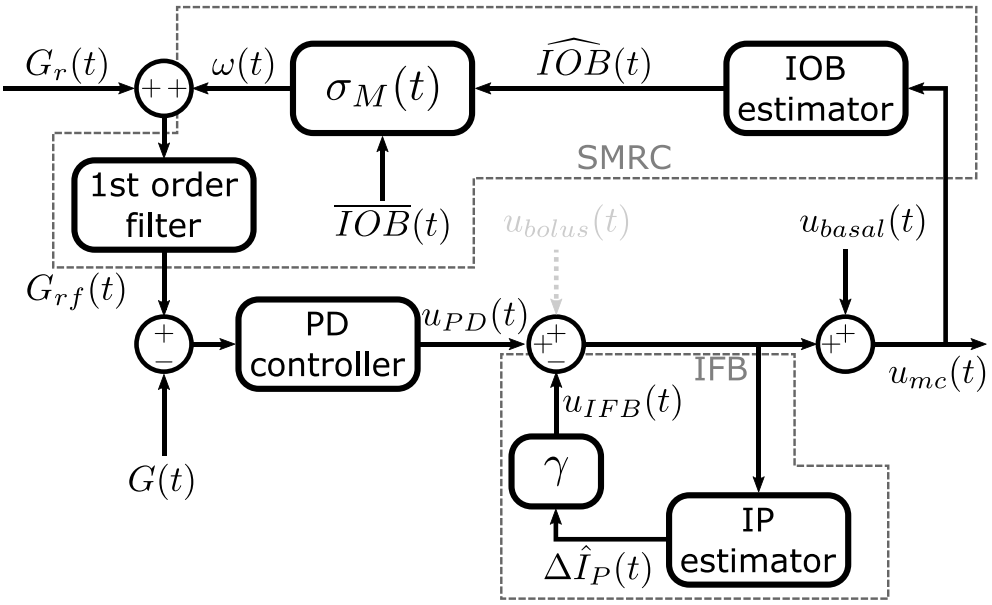

Figure B.1: Description of the main controller. The main controller consists of a proportional-derivative controller (PD), an insulin feedback (IFB), and a sliding mode reference conditioning (SMRC). $G(t)$, $G_r(t)$, and $G_{rf}(t)$ denote the glucose reading, the glucose setpoint and the filtered setpoint; γ and $\Delta\hat{I}_P(t)$ are, respectively, the IFB gain and the estimated insulin plasma deviation regarding basal conditions. $\omega(t)$, $\widehat{IOB}(t)$, and $\overline{IOB}(t)$ correspond to the discontinuous signal, the estimated insulin-on-board and the upper limit of the insulin-on-board. The total insulin provided by the main controller, u_{mc}, considers the PD-IFB output, the basal infusion ($u_{basal}(t)$), and, only if meal are announced, the pre-meal boluses ($u_{bolus}(t)$)

B.2.1 PD controller

The form of the PD controller including the derivative term in the forward path has been adopted to avoid the "derivative kick" issue of the standard PD (Johnson et al. 2005, Section 1.3), that is,

$$u_{PD}(t) = K_p \left(G(t) - G_{rf}(t)\right) + K_p T_d \dot{G}(t) \tag{B.1}$$

where $G(t)$ is the CGM reading and $G_{rf}(t)$ is the filtered glucose reference required for the SMRC layer (see Section B.2.3). The derivative time, T_d, is set to 60 min and the proportional gain, K_p (in U dL/(h mg)), is selected as (Palerm 2011):

$$K_p = \frac{60}{T_d}\frac{TDI}{1500} \tag{B.2}$$

where TDI is the subject's total daily insulin (U).

B.2.2 Insulin Feedback

The IFB imitates the auto-suppression of endogenous insulin production found in in vivo experiments (Palerm 2011), inhibiting the output of the PD controller as follows:

$$u_{IFB}(t) = u_{PD}(t) + u_{bolus}(t) - \gamma\Delta\hat{I}_P(t) \tag{B.3}$$

where γ is a gain (set to 0.42 L/min) and $\Delta\hat{I}_P(t) = \hat{I}_P(t) - \hat{I}_P^*$ is the deviation of the estimated plasma insulin ($\hat{I}_P(t)$) regarding its equilibrium value ($\hat{I}_P^*$). Limiting the controller output depending on $\Delta\hat{I}_P(t)$ rather than $\hat{I}_P(t)$ (as Palerm (2011) initially proposed) avoids retuning the controller to retain the steady state conditions of the PD controller without IFB.

The methods to measure plasma insulin in clinical trials are too invasive to be applied for control purposes; hence the plasma insulin must be estimated from the infused insulin. In this dissertation, the Identifiable Virtual Patient (IVP) model (Kanderian et al. 2009), described in 3.3.1, is used.

B.2.3 Sliding Mode Reference Conditioning

The SMRC targets preventing severe hypoglycemia by constraining the insulin-on-board through reference modulation (Revert et al. 2013). This technique roots in invariance concepts: to constraint the insulin-on-board to an upper limit $\overline{IOB}$, a discontinuous law ($\omega(t)$) modulating the reference forces the surface $\Sigma \coloneqq \left\{x(t)|\widehat{IOB}(t) - \overline{IOB}\right\}$ – with $x(t)$ being the extended state including the insulin-on-board dynamics, controller, and set point filter states – to be invariant, that is, for any $x(0)$ verifying $IOB(0) \leq IOB(t)$ the constraint will hold for all t. The discontinuous law achieving this purpose is given by:

$$\omega(t) = \begin{cases} W^+ & \text{if } \sigma_{SM}(t) > 0 \\ 0 & \text{otherwise} \end{cases} \tag{B.4}$$

where $W^+ > 0$ is a large enough constant with a nominal value set to 350 mg/dL (Sala-Mira et al. 2017) and $\sigma_{SM}(t)$ is defined as:

$$\sigma_{SM}(t) = \widehat{IOB}(t) - \overline{IOB}(t) + \sum_{i=1}^{l-1} \tau_{SM_i} \left(\widehat{IOB}(t)^{(i)} - \overline{IOB}(t)^{(i)} \right) \tag{B.5}$$

where l is the relative degree between $\widehat{IOB}(t)$ and $\omega(t)$, τ_{SM_i} are gains, and the superscript (i) refers to the ith-derivatives. In addition, a first order filter smooths the modulated glucose set point:

$$\dot{G}_{rf}(t) = -\tau_{rf} G_{rf}(t) + \tau_{rf} \left(G_r(t) + \omega(t) \right) \tag{B.6}$$

with τ_{rf} being the filter rate constant set as 0.1/min (Sala-Mira et al. 2017).

Like for the IFB, the insulin-on-board is estimated with the IVP models specifically, selecting the first-order dynamics of the subcutaneous insulin, i.e., $\widehat{IOB}(t) = I_{SC}(t)$. Given this insulin-on-board dynamics, and the filter and controller described above, the relative degree $l = 2$; thus only the first derivative of $\widehat{IOB}(t)$ must be considered in (B.5). Finally, τ_{SM_1} is tuned as $\tau_{SM} = 10$ min.

Bibliography

Acary, V.; Brogliato, B., and Orlov, Y. V. (2012). "Chattering-Free Digital Sliding-Mode Control With State Observer and Disturbance Rejection". In: *IEEE Transactions on Automatic Control* 57.5, pp. 1087–1101. ISSN: 0018-9286. DOI: 10.1109/TAC.2011.2174676 (cit. on pp. 77, 78).

Acharya, D. and Das, D. K. (2022). "Extended Kalman filter state estimation–based nonlinear explicit model predictive control design for blood glucose regulation of type 1 diabetic patient". In: *Medical and Biological Engineering and Computing* 60 (5), pp. 1347–1361. ISSN: 17410444. DOI: 10.1007/S11517-022-02511-5/FIGURES/12 (cit. on p. 71).

Ahmad, S.; Ramkissoon, C. M.; Beneyto, A.; Conget, I.; Giménez, M., and Vehi, J. (2021). "Generation of Virtual Patient Populations That Represent Real Type 1 Diabetes Cohorts". In: *Mathematics* 9.11, p. 1200. ISSN: 2227-7390. DOI: 10.3390/math9111200 (cit. on p. 177).

Alsahli, M.; Shrayyef, M. Z., and Gerich, J. E. (2017). "Normal Glucose Homeostasis". In: *Principles of Diabetes Mellitus*. Cham: Springer International Publishing, pp. 23–42. DOI: 10.1007/978-3-319-18741-9_2 (cit. on p. 2).

Alzate, C. M.; Villa-Tamayo, M. F., and Rivadeneira, P. S. (2022). "On-line meal detection module coupled with a zone MPC for closed-loop blood glucose control". In: *2022 IEEE Conference on Control Technology and Applications (CCTA)*, pp. 1390–1395. DOI: 10.1109/CCTA49430.2022.9966047 (cit. on pp. 19, 21).

American Diabetes Association (2001). "Postprandial Blood Glucose". In: *Diabetes Care* 24.4, pp. 775–778. ISSN: 0149-5992. DOI: 10.2337/diacare.24.4.775 (cit. on p. 11).

Andersen, G.; Meiffren, G.; Famulla, S.; Heise, T.; Ranson, A.; Seroussi, C.; Eloy, R.; Gaudier, M.; Charvet, R.; Chan, Y. P.; Soula, O., and DeVries, J. H. (2021). "ADO09, a co-formulation of the amylin analogue pramlintide and the insulin analogue A21G, lowers postprandial blood glucose versus insulin lispro in type 1 diabetes". In: *Diabetes, obesity & metabolism* 23.4, pp. 961–970. ISSN: 1463-1326. DOI: 10.1111/DOM.14302 (cit. on p. 28).

Anderson, S. M.; Raghinaru, D.; Pinsker, J. E.; Boscari, F.; Renard, E.; Buckingham, B. A.; Nimri, R.; Doyle Francis J., I.; Brown, S. A.; Keith-Hynes, P.; Breton, M. D.; Chernavvsky, D.; Bevier, W. C.; Bradley, P. K.; Bruttomesso, D.; Del Favero, S.; Calore, R.; Cobelli, C.; Avogaro, A.; Farret, A.; Place, J.; Ly, T. T.; Shanmugham, S.; Phillip, M.; Dassau, E.; Dasanayake, I. S.; Kollman, C.; Lum, J. W.; Beck, R. W.; Kovatchev, B., and Control to Range Study Group, for the (2016). "Multinational Home Use of Closed-Loop Control Is Safe and Effective". In: *Diabetes Care* 39.7, pp. 1143–1150. ISSN: 0149-5992. DOI: 10.2337/dc15-2468 (cit. on p. 122).

Aronoff, S. L.; Berkowitz, K.; Shreiner, B., and Want, L. (2004). "Glucose Metabolism and Regulation: Beyond Insulin and Glucagon". In: *Diabetes Spectrum* 17.3, pp. 183–190. ISSN: 1040-9165. DOI: 10.2337/DIASPECT.17.3.183 (cit. on p. 2).

Askari, M. R.; Rashid, M.; Sun, X.; Sevil, M.; Shahidehpour, A.; Kawaji, K., and Cinar, A. (2022). "Meal and Physical Activity Detection from Free-Living Data for Discovering Disturbance Patterns of Glucose Levels in People with Diabetes". In: *BioMedInformatics 2022, Vol. 2, Pages 297-317* 2 (2), pp. 297–317. ISSN: 2673-7426. DOI: 10.3390/BIOMEDINFORMATICS2020019 (cit. on pp. 20, 21, 23).

Atlas, E.; Nimri, R.; Miller, S.; Grunberg, E. A., and Phillip, M. (2010). "MD-Logic Artificial Pancreas SystemA pilot study in adults with type 1 diabetes". In: *Diabetes Care* 33.5, pp. 1072–1076. ISSN: 0149-5992. DOI: 10.2337/DC09-1830 (cit. on p. 25).

Balsa-Canto, E.; Alonso, A. A., and Banga, J. R. (2010). "An iterative identification procedure for dynamic modeling of biochemical networks". In: *BMC Systems Biology* 4.1, p. 11. ISSN: 1752-0509. DOI: 10.1186/1752-0509-4-11 (cit. on pp. 56, 57, 59–61).

Balsa-Canto, E.; Henriques, D.; Gábor, A., and Banga, J. R. (2016). "AMIGO2, a toolbox for dynamic modeling, optimization and control in systems biology". In: *Bioinformatics* 32.21, pp. 3357–3359. ISSN: 1367-4803. DOI: 10.1093/bioinformatics/btw411 (cit. on p. 61).

Barr, D. J.; Levy, R.; Scheepers, C., and Tily, H. J. (2013). "Random effects structure for confirmatory hypothesis testing: Keep it maximal". In: *Journal of Memory and Language* 68.3, pp. 255–278. ISSN: 0749596X. DOI: 10.1016/j.jml.2012.11.001 (cit. on pp. 166, 167).

Basu, A.; Dube, S.; Veettil, S.; Slama, M.; Kudva, Y. C.; Peyser, T.; Carter, R. E.; Cobelli, C., and Basu, R. (2015). "Time Lag of Glucose From Intravascular to Interstitial Compartment in Type 1 Diabetes". In: *Journal of Diabetes Science and Technology* 9.1, p. 63. ISSN: 19322968. DOI: 10.1177/1932296814554797 (cit. on p. 12).

Basu, R.; Di Camillo, B.; Toffolo, G.; Basu, A.; Shah, P.; Vella, A.; Rizza, R., and Cobelli, C. (2003). "Use of a novel triple-tracer approach to assess postprandial glucose metabolism". In: *American Journal of Physiology-Endocrinology and Metabolism* 284.1, E55–E69. ISSN: 0193-1849. DOI: 10.1152/ajpendo.00190.2001 (cit. on p. 40).

Batmani, Y.; Khodakaramzadeh, S., and Moradi, P. (2021). "Automatic Artificial Pancreas Systems Using an Intelligent Multiple-Model PID Strategy". In: *IEEE Journal of Biomedical and Health Informatics* 2194.c. ISSN: 21682208. DOI: 10.1109/JBHI.2021.3116376 (cit. on p. 148).

Battelino, T.; Danne, T.; Bergenstal, R. M.; Amiel, S. A.; Beck, R.; Biester, T.; Bosi, E.; Buckingham, B. A.; Cefalu, W. T.; Close, K. L.; Cobelli, C.; Dassau, E.; DeVries, J. H.; Donaghue, K. C.; Dovc, K.; Doyle, F. J.; Garg, S.; Grunberger, G.; Heller, S.; Heinemann, L.; Hirsch, I. B.; Hovorka, R.; Jia, W.; Kordonouri, O.; Kovatchev, B.; Kowalski, A.; Laffel, L.; Levine, B.; Mayorov, A.; Mathieu, C.; Murphy, H. R.; Nimri, R.; Nørgaard, K.; Parkin, C. G.; Renard, E.; Rodbard, D.; Saboo, B.; Schatz, D.; Stoner, K.; Urakami, T.; Weinzimer, S. A., and Phillip, M. (2019). "Clinical Targets for Continuous Glucose Monitoring Data Interpretation: Recommendations From the International Consensus on Time in Range". In: *Diabetes Care* 42.8, pp. 1593–1603. ISSN: 0149-5992. DOI: 10.2337/dci19-0028 (cit. on pp. 4, 25, 140, 141, 143, 165, 170, 173).

Beato-Víbora, P. I.; Gallego-Gamero, F.; Ambrojo-López, A.; Gil-Poch, E.; Martín-Romo, I., and Arroyo-Díez, F. J. (2021). "Amelioration of user experiences and glycaemic outcomes with an Advanced Hybrid Closed Loop System in a real-world clinical setting". In: *Diabetes Research and Clinical Practice* 178, p. 108986. ISSN: 01688227. DOI: 10.1016/j.diabres.2021.108986 (cit. on p. 5).

Bekiari, E.; Kitsios, K.; Thabit, H.; Tauschmann, M.; Athanasiadou, E.; Karagiannis, T.; Haidich, A.-B.; Hovorka, R., and Tsapas, A. (2018). "Artificial pancreas treatment for outpatients with type 1 diabetes: systematic review and meta-analysis". In: *BMJ* 361, p. 1310. ISSN: 0959-8138. DOI: 10.1136/BMJ.K1310 (cit. on pp. 5, 6).

Bell, K. J.; Toschi, E.; Steil, G. M., and Wolpert, H. A. (2016). "Optimized Mealtime Insulin Dosing for Fat and Protein in Type 1 Diabetes: Application of a Model-Based Approach to Derive Insulin Doses for Open-Loop Diabetes Management". In: *Diabetes Care* 39.9, pp. 1631–1634. ISSN: 0149-5992. DOI: 10.2337/dc15-2855 (cit. on p. 10).

Beneyto, A.; Bertachi, A.; Bondia, J., and Vehi, J. (2018). "A New Blood Glucose Control Scheme for Unannounced Exercise in Type 1 Diabetic Subjects". In: *IEEE Transactions*

on Control Systems Technology PP, pp. 1–8. ISSN: 1063-6536. DOI: 10.1109/TCST.2018.2878205 (cit. on pp. 7, 37, 148, 156, 165, 173, 194).

Bequette, B. W. (2010). "Continuous glucose monitoring: Real-time algorithms for calibration, filtering, and alarms". In: *Journal of Diabetes Science and Technology* 4.2, pp. 404–418. ISSN: 19322968. DOI: 10.1177/193229681000400222 (cit. on p. 120).

Bergman, R. N.; Finegood, D. T., and Ader, M. (1985). "Assessment of insulin sensitivity in vivo". In: *Endocrine Reviews* 6.1, pp. 45–86. ISSN: 0163769X. DOI: 10.1210/edrv-6-1-45 (cit. on p. 51).

Bertachi, A.; Ramkissoon, C. M.; Beneyto, A., and Vehí, J. (2019). "Exercise-induced hypoglycemia in type 1 diabetes: in-silico comparison between announced and unannounced strategies in closed-loop control". In: *IFAC-PapersOnLine* 52.1, pp. 1000–1005. ISSN: 2405-8963. DOI: 10.1016/J.IFACOL.2019.06.193 (cit. on p. 194).

Bhattacharjee, A.; Easwaran, A.; Leow, M. K.-s., and Cho, N. (2019). "Design of an online-tuned model based compound controller for a fully automated artificial pancreas". In: *Medical & Biological Engineering & Computing* 57.7, pp. 1437–1449. ISSN: 0140-0118. DOI: 10.1007/s11517-019-01972-5 (cit. on pp. 21, 104).

Biester, T.; Muller, I.; Berge, T. von dem; Atlas, E.; Nimri, R.; Phillip, M.; Battelino, T.; Bratina, N.; Dovc, K.; Scheerer, M. F.; Kordonouri, O., and Danne, T. (2021). "Add-on therapy with dapagliflozin under full closed loop control improves time in range in adolescents and young adults with type 1 diabetes: The DAPADream study". In: *Diabetes, Obesity and Metabolism* 23.2, pp. 599–608. ISSN: 1463-1326. DOI: 10.1111/DOM.14258 (cit. on p. 30).

Bishop, F. K.; Maahs, D. M.; Spiegel, G.; Owen, D.; Klingensmith, G. J.; Bortsov, A.; Thomas, J., and Mayer-Davis, E. J. (2009). "The Carbohydrate Counting in Adolescents With Type 1 Diabetes (CCAT) Study". In: *Diabetes Spectrum* 22.1, pp. 56–62. ISSN: 1040-9165. DOI: 10.2337/diaspect.22.1.56 (cit. on pp. 4, 11, 130).

Blauw, H.; Bon, A. C. van; Koops, R., and DeVries, J. H. (2016). "Performance and safety of an integrated bihormonal artificial pancreas for fully automated glucose control at home". In: *Diabetes, Obesity and Metabolism* 18.7, pp. 671–677. ISSN: 1463-1326. DOI: 10.1111/DOM.12663 (cit. on pp. 33, 36).

Blauw, H.; Onvlee, A. J.; Klaassen, M.; Bon, A. C. van, and DeVries, J. H. (2021). "Fully Closed Loop Glucose Control With a Bihormonal Artificial Pancreas in Adults With Type 1 Diabetes: An Outpatient, Randomized, Crossover Trial". In: *Diabetes care* 44.3, pp. 836–838. ISSN: 19355548. DOI: 10.2337/dc20-2106 (cit. on p. 21).

Boiroux, D.; Aradóttir, T. B.; Nørgaard, K.; Poulsen, N. K.; Madsen, H., and Jørgensen, J. B. (2017). "An Adaptive Nonlinear Basal-Bolus Calculator for Patients with Type 1 Diabetes". In: *Journal of Diabetes Science and Technology* 11.1, pp. 29–36. ISSN: 19322968. DOI: 10.1177/1932296816666295 (cit. on p. 51).

Boiroux, D.; Bátora, V.; Hagdrup, M.; Wendt, S. L.; Poulsen, N. K.; Madsen, H., and Jørgensen, J. B. (2018). "Adaptive model predictive control for a dual-hormone artificial pancreas". In: *Journal of Process Control* 68, pp. 105–117. ISSN: 0959-1524. DOI: 10.1016/J.JPROCONT.2018.05.003 (cit. on p. 35).

Bon, A. C. van; Hermanides, J.; Koops, R.; Hoekstra, J. B., and DeVries, J. H. (2010). "Postprandial glycemic excursions with the use of a closed-loop platform in subjects with type 1 diabetes: a pilot study". In: *Journal of diabetes science and technology* 4.4, pp. 923–928. ISSN: 1932-2968. DOI: 10.1177/193229681000400423 (cit. on pp. 20, 21, 30).

Boscari, F.; Ferretto, S.; Cavallin, F., and Bruttomesso, D. (2022). "Switching from predictive low glucose suspend to advanced hybrid closed loop control: Effects on glucose control and patient reported outcomes". In: *Diabetes Research and Clinical Practice* 185.February, p. 109784. ISSN: 18728227. DOI: 10.1016/j.diabres.2022.109784 (cit. on p. 5).

Boughton, C. K.; Hartnell, S.; Allen, J. M., and Hovorka, R. (2019). "The importance of prandial insulin bolus timing with hybrid closed-loop systems". In: *Diabetic Medicine*, dme.14116. ISSN: 0742-3071. DOI: 10.1111/dme.14116 (cit. on pp. 6, 11, 130).

Breton, M. D.; Brown, S. A.; Karvetski, C. H.; Kollar, L.; Topchyan, K. A.; Anderson, S. M., and Kovatchev, B. P. (2014). "Adding Heart Rate Signal to a Control-to-Range Artificial Pancreas System Improves the Protection Against Hypoglycemia During Exercise in Type 1 Diabetes". In: *Diabetes Technology & Therapeutics* 16.8, pp. 506–511. ISSN: 1520-9156. DOI: 10.1089/dia.2013.0333 (cit. on p. 33).

Breton, M. D.; Cherñavvsky, D. R.; Forlenza, G. P.; DeBoer, M. D.; Robic, J.; Wadwa, R. P.; Messer, L. H.; Kovatchev, B. P., and Maahs, D. M. (2017). "Closed-Loop Control During Intense Prolonged Outdoor Exercise in Adolescents With Type 1 Diabetes: The Artificial Pancreas Ski Study". In: *Diabetes Care* 40.12, pp. 1644–1650. ISSN: 0149-5992. DOI: 10.2337/DC17-0883 (cit. on p. 33).

Breton, M. D. and Kovatchev, B. P. (2021). "One Year Real-World Use of the Control-IQ Advanced Hybrid Closed-Loop Technology". In: *Diabetes Technology & Therapeutics* 23.9, pp. 601–608. ISSN: 1520-9156. DOI: 10.1089/dia.2021.0097 (cit. on p. 5).

Brogliato, B. and Polyakov, A. (2021). "Digital implementation of sliding-mode control via the implicit method: A tutorial". In: *International Journal of Robust and Nonlinear*

Control 31.9, pp. 3528–3586. ISSN: 1049-8923. DOI: 10.1002/rnc.5121 (cit. on pp. 81, 82, 116).

Brogliato, B.; Polyakov, A., and Efimov, D. (2020). "The Implicit Discretization of the Supertwisting Sliding-Mode Control Algorithm". In: *IEEE Transactions on Automatic Control* 65.8, pp. 3707–3713. ISSN: 15582523. DOI: 10.1109/TAC.2019.2953091 (cit. on pp. 116, 118).

Brun, R.; Reichert, P., and Künsch, H. R. (2001). "Practical identifiability analysis of large environmental simulation models". In: *Water Resources Research* 37.4, pp. 1015–1030. ISSN: 00431397. DOI: 10.1029/2000WR900350 (cit. on pp. 60, 61, 150).

Cai, D.; Liu, W.; Dassau, E.; Doyle Iii, F. J.; Cai, X.; Wang, J.; Ji, L., and Shi, D. (2020). "An Adaptive Disturbance Rejection Controller for Artificial Pancreas". In: *IFAC-PapersOnLine* 53.2, pp. 16372–16379. ISSN: 24058963. DOI: 10.1016/j.ifacol.2020.12.674 (cit. on pp. 22, 24).

Cameron, F. M.; Ly, T. T.; Buckingham, B. A.; Maahs, D. M.; Forlenza, G. P.; Levy, C. J.; Lam, D.; Clinton, P.; Messer, L. H.; Westfall, E.; Levister, C.; Xie, Y. Y.; Baysal, N.; Howsmon, D.; Patek, S. D., and Bequette, B. W. (2017). "Closed-Loop Control Without Meal Announcement in Type 1 Diabetes". In: *Diabetes Technology & Therapeutics* 19.9, pp. 527–532. ISSN: 1520-9156. DOI: 10.1089/dia.2017.0078 (cit. on p. 23).

Cameron, F.; Niemeyer, G., and Bequette, B. W. (2012). "Extended multiple model prediction with application to blood glucose regulation". In: *Journal of Process Control* 22.8, pp. 1422–1432. ISSN: 09591524. DOI: 10.1016/j.jprocont.2012.05.014 (cit. on pp. 20, 23).

Cameron, F.; Niemeyer, G.; Wilson, D. M.; Bequette, B. W.; Benassi, K. S.; Clinton, P., and Buckingham, B. A. (2014). "Inpatient Trial of an Artificial Pancreas Based on Multiple Model Probabilistic Predictive Control with Repeated Large Unannounced Meals". In: *Diabetes Technology & Therapeutics* 16 (11), pp. 728–734. ISSN: 1520-9156. DOI: 10.1089/dia.2014.0093 (cit. on p. 23).

Castellanos, L. E.; Balliro, C. A.; Sherwood, J. S.; Jafri, R.; Hillard, M. A.; Greaux, E.; Selagamsetty, R.; Zheng, H.; El-Khatib, F. H.; Damiano, E. R., and Russell, S. J. (2021). "Performance of the Insulin-Only iLet Bionic Pancreas and the Bihormonal iLet Using Dasiglucagon in Adults With Type 1 Diabetes in a Home-Use Setting". In: *Diabetes Care* 44.6, e118–e120. ISSN: 0149-5992. DOI: 10.2337/DC20-1086 (cit. on p. 18).

Cescon, M.; Choudhary, D.; Pinsker, J. E.; Dadlani, V.; Church, M. M.; Kudva, Y. C.; Doyle III, F. J.; Dassau, E.; Doyle, F. J., and Dassau, E. (2021). "Activity detection and classification from wristband accelerometer data collected on people with type 1 diabetes

in free-living conditions". In: *Computers in Biology and Medicine* 135, p. 104633. ISSN: 0010-4825. DOI: 10.1016/J.COMPBIOMED.2021.104633 (cit. on p. 33).

Chakrabarty, A.; Gregory, J. M.; Moore, L. M.; Williams, P. E.; Farmer, B.; Cherrington, A. D.; Lord, P.; Shelton, B.; Cohen, D.; Zisser, H. C.; Doyle, F. J., and Dassau, E. (2019). "A new animal model of insulin-glucose dynamics in the intraperitoneal space enhances closed-loop control performance". In: *Journal of Process Control* 76, pp. 62–73. ISSN: 09591524. DOI: 10.1016/j.jprocont.2019.01.002 (cit. on pp. 26, 27).

Chen, G.; Zhang, J., and Zhao, Z. (2010). "A Two-Degree-of-Freedom IMC Parameters Online Intelligent Tuning Method". In: *2010 International Conference on Computational Aspects of Social Networks*. IEEE, pp. 483–486. ISBN: 978-1-4244-8785-1. DOI: 10.1109/CASoN.2010.114 (cit. on pp. 148, 150).

Chen, H.; Paoletti, N.; Smolka, S. A., and Lin, S. (2019). "Committed Moving Horizon Estimation for Meal Detection and Estimation in Type 1 Diabetes". In: *2019 American Control Conference (ACC)*. IEEE, pp. 4765–4772. ISBN: 978-1-5386-7926-5. DOI: 10.23919/ACC.2019.8814868 (cit. on pp. 40, 104).

Cherñavvsky, D. R.; DeBoer, M. D.; Keith-Hynes, P.; Mize, B.; McElwee, M.; Demartini, S.; Dunsmore, S. F.; Wakeman, C.; Kovatchev, B. P., and Breton, M. D. (2016). "Use of an artificial pancreas among adolescents for a missed snack bolus and an underestimated meal bolus". In: *Pediatric Diabetes* 17.1, pp. 28–35. ISSN: 1399543X. DOI: 10.1111/pedi.12230 (cit. on p. 11).

Chetan, M. R.; Charlton, M. H.; Thompson, C.; Dias, R. P.; Andrews, R. C., and Narendran, P. (2019). "The Type 1 diabetes 'honeymoon' period is five times longer in men who exercise: a case-control study". In: *Diabetic Medicine* 36.1, pp. 127–128. ISSN: 07423071. DOI: 10.1111/dme.13802 (cit. on p. 147).

Chimen, M.; Kennedy, A.; Nirantharakumar, K.; Pang, T. T.; Andrews, R., and Narendran, P. (2012). "What are the health benefits of physical activity in type 1 diabetes mellitus? A literature review". In: *Diabetologia* 55.3, pp. 542–551. ISSN: 0012186X. DOI: 10.1007/s00125-011-2403-2 (cit. on p. 147).

Chis, O.-T.; Banga, J. R., and Balsa-Canto, E. (2011). "Structural Identifiability of Systems Biology Models: A Critical Comparison of Methods". In: *PLoS ONE* 6.11. Ed. by J. Jaeger, e27755. ISSN: 1932-6203. DOI: 10.1371/journal.pone.0027755 (cit. on pp. 56, 57, 150).

Codella, R.; Terruzzi, I., and Luzi, L. (2017). "Why should people with type 1 diabetes exercise regularly?" In: *Acta Diabetologica* 54.7, pp. 615–630. ISSN: 0940-5429. DOI: 10.1007/s00592-017-0978-x (cit. on pp. 13, 15, 90, 147).

Colmegna, P. H.; Bianchi, F. D., and Sanchez-Pena, R. S. (2021a). "Automatic glucose control during meals and exercise in type 1 diabetes: Proof-of-concept in silico tests using a switched LPV approach". In: *2021 American Control Conference (ACC)*. Vol. 2021-May. 5. IEEE, pp. 4952–4957. ISBN: 978-1-6654-4197-1. DOI: 10.23919/ACC50511.2021.9483386 (cit. on p. 130).

Colmegna, P.; Cengiz, E.; Garcia-Tirado, J.; Kraemer, K., and Breton, M. D. (2021b). "Impact of Accelerating Insulin on an Artificial Pancreas System Without Meal Announcement: An In Silico Examination". In: *Journal of Diabetes Science and Technology* 15 (4), pp. 833–841. ISSN: 1932-2968. DOI: 10.1177/1932296820928067 (cit. on p. 25).

Colmegna, P.; Garelli, F.; De Battista, H., and Sánchez-Peña, R. (2018). "Automatic regulatory control in type 1 diabetes without carbohydrate counting". In: *Control Engineering Practice* 74.February, pp. 22–32. ISSN: 09670661. DOI: 10.1016/j.conengprac.2018.02.003 (cit. on pp. 19, 21, 25).

Colmegna, P. H.; Sánchez Peña, R. S.; Gondhalekar, R.; Dassau, E.; Doyle III, F. J.; Sánchez-Peña, R. S.; Gondhalekar, R.; Dassau, E., and Doyle, F. J. (2016). "Reducing Glucose Variability Due to Meals and Postprandial Exercise in T1DM Using Switched LPV Control: In Silico Studies". In: *Journal of Diabetes Science and Technology* 10.3, pp. 744–753. ISSN: 19322968. DOI: 10.1177/1932296816638857 (cit. on p. 20).

Corbett, J. P.; Colmegna, P.; Garcia-Tirado, J., and Breton, M. D. (2020). "Anticipating Meals with Behavioral Profiles in an Artificial Pancreas System - An Informed Multistage Model Predictive Control Approach". In: *IFAC-PapersOnLine* 53.2, pp. 16305–16310. ISSN: 2405-8963. DOI: 10.1016/J.IFACOL.2020.12.652 (cit. on pp. 23, 34).

Corbett, J. P.; Garcia-Tirado, J.; Colmegna, P.; Diaz Castaneda, J. L., and Breton, M. D. (2022). "Using an Online Disturbance Rejection and Anticipation System to Reduce Hyperglycemia in a Fully Closed-Loop Artificial Pancreas System". In: *Journal of Diabetes Science and Technology* 16.1, pp. 52–60. ISSN: 19322968. DOI: 10.1177/19322968211059159 (cit. on pp. 20, 23).

Da Silva, J.; Bosi, E.; Jendle, J.; Arrieta, A.; Castaneda, J.; Grossman, B.; Cordero, T. L.; Shin, J., and Cohen, O. (2021). "Real-world performance of the MiniMed™ 670G system in Europe". In: *Diabetes, Obesity and Metabolism* 23.8, pp. 1942–1949. ISSN: 14631326. DOI: 10.1111/dom.14424 (cit. on p. 5).

Dalianis, H. (2018). "Evaluation Metrics and Evaluation". In: *Clinical Text Mining*. Cham: Springer International Publishing, pp. 45–53. DOI: 10.1007/978-3-319-78503-5_6 (cit. on p. 112).

Dalla Man, C.; Camilleri, M., and Cobelli, C. (2006). "A system model of oral glucose absorption: Validation on gold standard data". In: *IEEE Transactions on Biomedical*

Engineering 53.12, pp. 2472–2478. ISSN: 00189294. DOI: 10.1109/TBME.2006.883792 (cit. on p. 40).

Dalla Man, C.; Micheletto, F.; Lv, D.; Breton, M.; Kovatchev, B., and Cobelli, C. (2014). "The UVA/PADOVA type 1 diabetes simulator: New features". In: *Journal of Diabetes Science and Technology* 8.1, pp. 26–34. ISSN: 19322968. DOI: 10.1177/1932296813514502 (cit. on pp. 50, 52, 65, 71, 149).

Dassau, E.; Bequette, B. W.; Buckingham, B. A., and Doyle III, F. J. (2008). "Detection of a Meal Using Continuous Glucose Monitoring". In: *Diabetes Care* 31.2, pp. 295–300. ISSN: 19355548. DOI: 10.2337/dc07-1293.B.W.B. (cit. on pp. 19, 20, 104, 120).

Dassau, E.; Renard, E.; Place, J.; Farret, A.; Pelletier, M.-J. J.; Lee, J.; Huyett, L. M.; Chakrabarty, A.; Doyle, F. J., and Zisser, H. C. (2017). "Intraperitoneal insulin delivery provides superior glycaemic regulation to subcutaneous insulin delivery in model predictive control-based fully-automated artificial pancreas in patients with type 1 diabetes: a pilot study". In: *Diabetes, Obesity and Metabolism* 19.12, pp. 1698–1705 (cit. on p. 26).

Davila, J.; Fridman, L., and Levant, A. (2005). "Second-order sliding-mode observer for mechanical systems". In: *IEEE Transactions on Automatic Control* 50.11, pp. 1785–1789. ISSN: 0018-9286. DOI: 10.1109/TAC.2005.858636 (cit. on pp. 105, 106).

De Bock, M.; Dart, J.; Roy, A.; Davey, R.; Soon, W.; Berthold, C.; Retterath, A.; Grosman, B.; Kurtz, N.; Davis, E., and Jones, T. (2017). "Exploration of the Performance of a Hybrid Closed Loop Insulin Delivery Algorithm That Includes Insulin Delivery Limits Designed to Protect Against Hypoglycemia". In: *Journal of Diabetes Science and Technology* 11.1, pp. 68–73. ISSN: 19322968. DOI: 10.1177/1932296816668876 (cit. on pp. 6, 11).

Díaz-Flores, M. and Baiza-Gutman, L. A. (2019). "Biochemical Mechanisms of Vascular Complications in Diabetes". In: *The Diabetes Textbook*. Cham: Springer International Publishing, pp. 695–707. DOI: 10.1007/978-3-030-11815-0_45 (cit. on p. 3).

Didyuk, O.; Econom, N.; Guardia, A.; Livingston, K., and Klueh, U. (2020). "Continuous Glucose Monitoring Devices: Past, Present, and Future Focus on the History and Evolution of Technological Innovation". In: *Journal of Diabetes Science and Technology*. ISSN: 19322968. DOI: 10.1177/1932296819899394 (cit. on p. 126).

DiMeglio, L. A.; Evans-Molina, C., and Oram, R. A. (2018). "Type 1 diabetes". In: *The Lancet* 391.10138, pp. 2449–2462. ISSN: 01406736. DOI: 10.1016/S0140-6736(18)31320-5 (cit. on pp. 2, 3).

Dingena, C. F.; Marsh, A.; Ajjan, R., and Campbell, M. (2020). "Postprandial Glucose Variability in People with Type 1 Diabetes Is Individual and Impacted by Physiological

and Clinical Parameters". In: *Diabetes* 69.Supplement_1. ISSN: 0012-1797. DOI: 10.2337/db20-733-P (cit. on p. 13).

Domingo-Lopez, D. A.; Lattanzi, G.; H. J. Schreiber, L.; Wallace, E. J.; Wylie, R.; O'Sullivan, J.; Dolan, E. B., and Duffy, G. P. (2022). "Medical Devices, Smart Drug Delivery, Wearables and Technology for the treatment of Diabetes Mellitus". In: *Advanced Drug Delivery Reviews*, p. 114280. ISSN: 0169409X. DOI: 10.1016/j.addr.2022.114280 (cit. on pp. 3, 9).

Dovc, K.; Piona, C.; Mutlu, G. Y.; Bratina, N.; Bizjan, B. J.; Lepej, D.; Nimri, R.; Atlas, E.; Muller, I.; Kordonouri, O.; Biester, T.; Danne, T.; Phillip, M., and Battelino, T. (2020). "Faster Compared with Standard Insulin Aspart during Day-And-Night Fully Closed-Loop Insulin Therapy in Type 1 Diabetes: A Double-Blind Randomized Crossover Trial". In: *Diabetes Care* 43.1, pp. 29–36. ISSN: 19355548. DOI: 10.2337/dc19-0895 (cit. on pp. 6, 24, 25).

Edgerton, D. S.; Moore, M. C.; Gregory, J. M.; Kraft, G., and Cherrington, A. D. (2021). "Importance of the route of insulin delivery to its control of glucose metabolism". In: *American Journal of Physiology - Regulatory Integrative and Comparative Physiology* 320.5, E891–E897. ISSN: 15221490. DOI: 10.1152/AJPENDO.00628.2020 (cit. on p. 12).

Edwards, C.; Spurgeon, S. K., and Patton, R. J. (2000). "Sliding mode observers for fault detection and isolation". In: *Automatica* 36.4, pp. 541–553. ISSN: 00051098. DOI: 10.1016/S0005-1098(99)00177-6 (cit. on pp. 49, 50).

Edwards, C. and Spurgeon, S. K. (1994). "On the development of discontinuous observers". In: *International Journal of Control* 59.5, pp. 1211–1229. ISSN: 13665820. DOI: 10.1080/00207179408923128 (cit. on p. 46).

Edwards, C. and Tan, C. P. (2006). "A Comparison of Sliding Mode and Unknown Input Observers for Fault Reconstruction". In: *European Journal of Control* 12.3, pp. 245–260. ISSN: 09473580. DOI: 10.3166/ejc.12.245-260 (cit. on pp. 50, 123).

El Maalouf, I. R.; Capoccia, K., and Priefer, R. (2022). "Non-invasive ways of administering insulin". In: *Diabetes & Metabolic Syndrome: Clinical Research & Reviews* 16.4, p. 102478. ISSN: 18714021. DOI: 10.1016/j.dsx.2022.102478 (cit. on p. 3).

El Malahi, A.; Van Elsen, M.; Charleer, S.; Dirinck, E.; Ledeganck, K.; Keymeulen, B.; Crenier, L.; Radermecker, R. D.; Taes, Y.; Vercammen, C.; Nobels, F.; Mathieu, C.; Gillard, P., and De Block, C. (2022). "Relationship Between Time in Range, Glycemic Variability, HbA1c, and Complications in Adults With Type 1 Diabetes Mellitus". In: *The Journal of Clinical Endocrinology & Metabolism* 107.2, e570–e581. ISSN: 0021-972X. DOI: 10.1210/CLINEM/DGAB688 (cit. on p. 5).

Ellingsen, C.; Dassau, E.; Zisser, H.; Grosman, B.; Percival, M. W.; Jovanovič, L., and Doyle, F. J. (2009). "Safety constraints in an artificial pancreatic β cell: An implementation of model predictive control with insulin on board". In: *Journal of Diabetes Science and Technology* 3.3, pp. 536–544. ISSN: 19322968. DOI: 10.1177/193229680900300319 (cit. on p. 148).

Enright, P. J. (2021). *Frequency-Domain Analysis and Design of Insulin-Glucose Controllers*. DOI: 10.13140/RG.2.2.16987.85282 (cit. on p. 51).

Fabra, E. M.; Díez, J.-L.; Bondia, J., and Sanz, A. J. L. (2021). "A Comprehensive Review of Continuous Glucose Monitoring Accuracy during Exercise Periods". In: *Sensors 2021, Vol. 21, Page 479* 21.2, p. 479. DOI: 10.3390/S21020479 (cit. on p. 13).

Fan, S.; Nagamune, R.; Altintas, Y.; Fan, D., and Zhang, Z. (2010). "Comparison study on disturbance estimation techniques in precise slow motion control". In: vol. 7544. SPIE, p. 754433. ISBN: 9780819479402. DOI: 10.1117/12.885262 (cit. on p. 46).

Fang, Z.; Liu, M.; Tao, J.; Li, C.; Zou, F., and Zhang, W. (2022). "Efficacy and safety of closed-loop insulin delivery versus sensor-augmented pump in the treatment of adults with type 1 diabetes: a systematic review and meta-analysis of randomized-controlled trials". In: *Journal of Endocrinological Investigation* 45.3, pp. 471–481. ISSN: 1720-8386. DOI: 10.1007/s40618-021-01674-6 (cit. on p. 5).

Faradji, R. N.; Barriga-Menchaca, A. P. D., and Sainz de la Maza Viadero, M. E. (2019a). "Use of Insulin in Outpatient Diabetes Management". In: *The Diabetes Textbook*. Cham: Springer International Publishing, pp. 541–554. DOI: 10.1007/978-3-030-11815-0_35 (cit. on p. 3).

Faradji, R. N.; Uribe-Wiechers, A. C., and Sainz de la Maza Viadero, M. E. (2019b). "Hypoglycemia: Diagnosis, Management, and Prevention". In: *The Diabetes Textbook*. Cham: Springer International Publishing, pp. 629–653. DOI: 10.1007/978-3-030-11815-0_42 (cit. on p. 4).

Farrington, C. (2018). "Psychosocial impacts of hybrid closed-loop systems in the management of diabetes: a review". In: *Diabetic Medicine* 35.4, pp. 436–449. ISSN: 07423071. DOI: 10.1111/dme.13567 (cit. on p. 5).

Fathi, A. E.; Gingras, V.; Boulet, B.; El Fathi, A.; Raef Smaoui, M.; Gingras, V.; Boulet, B., and Haidar, A. (2018). "The Artificial Pancreas and Meal Control: An overview of postprandial glucose regulation in type 1 diabetes". In: *IEEE Control Systems* 38.February, pp. 67–85. ISSN: 1066033X. DOI: 10.1109/MCS.2017.2766323 (cit. on pp. 12, 68).

Fathi, A. E.; Palisaitis, E.; Boulet, B.; Legault, L., and Haidar, A. (2019). "An Unannounced Meal Detection Module for Artificial Pancreas Control Systems". In: *2019 American Control Conference (ACC)*. Vol. 2019-July. IEEE, pp. 4130–4135. ISBN: 978-1-5386-7926-5. DOI: 10.23919/ACC.2019.8814932 (cit. on pp. 19–21, 28, 104, 134).

FORGETDIABETES (2020). *FORGETDIABETES - The revolution in diabetes treatment*. URL: https://forgetdiabetes.eu/ (visited on 06/07/2022) (cit. on p. 27).

Forlenza, G. P.; Cameron, F. M.; Ly, T. T.; Lam, D.; Howsmon, D. P.; Baysal, N.; Kulina, G.; Messer, L.; Clinton, P.; Levister, C.; Patek, S. D.; Levy, C. J.; Wadwa, R. P.; Maahs, D. M.; Bequette, B. W., and Buckingham, B. A. (2018). "Fully Closed-Loop Multiple Model Probabilistic Predictive Controller Artificial Pancreas Performance in Adolescents and Adults in a Supervised Hotel Setting". In: *Diabetes Technology & Therapeutics* 20.5, pp. 335–343. ISSN: 1520-9156. DOI: 10.1089/dia.2017.0424 (cit. on p. 23).

Forlenza, G. P. and Ekhlaspour, L. (2020). "Predictive low glucose suspend systems". In: *Glucose Monitoring Devices*. Elsevier, pp. 275–292. DOI: 10.1016/B978-0-12-816714-4.00014-4 (cit. on p. 4).

Fortin, A.; Rabasa-Lhoret, R.; Roy-Fleming, A.; Desjardins, K.; Brazeau, A. S.; Ladouceur, M., and Gingras, V. (2017). "Practices, perceptions and expectations for carbohydrate counting in patients with type 1 diabetes – Results from an online survey". In: *Diabetes Research and Clinical Practice* 126, pp. 214–221. ISSN: 18728227. DOI: 10.1016/j.diabres.2017.02.022 (cit. on p. 10).

Fortran code by Alan Miller, T. L. based on (2020). *leaps: Regression Subset Selection*. R package version 3.1 (cit. on p. 162).

Friedland, B. (1969). "Treatment of bias in recursive filtering". In: *IEEE Transactions on Automatic Control* 14.4, pp. 359–367. ISSN: 0018-9286. DOI: 10.1109/TAC.1969.1099223 (cit. on p. 44).

Fritz, C. O.; Morris, P. E., and Richler, J. J. (2012). "Effect size estimates: Current use, calculations, and interpretation". In: *Journal of Experimental Psychology: General* 141.1. Place: US Publisher: American Psychological Association, pp. 2–18. ISSN: 1939-2222(Electronic),0096-3445(Print). DOI: 10.1037/a0024338 (cit. on p. 84).

Fuchs, J. and Hovorka, R. (2020). "Closed-loop control in insulin pumps for type-1 diabetes mellitus: safety and efficacy". In: *Expert Review of Medical Devices* 17.7, pp. 707–720. ISSN: 1743-4440. DOI: 10.1080/17434440.2020.1784724 (cit. on p. 6).

Furió-Novejarque, C.; Sanz, R.; Reenberg, A. T.; Ritschel, T. K.; Ranjan, A. G.; Nørgaard, K.; Díez, J.-L.; Jørgensen, J. B., and Bondia, J. (2022). "Assessment of a new model of

glucagon action with glucagon receptor dynamics". In: *IFAC-PapersOnLine* 55 (20), pp. 647–652. ISSN: 2405-8963. DOI: 10.1016/J.IFACOL.2022.09.169 (cit. on p. 52).

Fushimi, E.; Battista, H. A. D., and Garelli, F. (2022). "A Dual-Hormone Multicontroller for Artificial Pancreas Systems". In: *IEEE Journal of Biomedical and Health Informatics*. ISSN: 21682208. DOI: 10.1109/JBHI.2022.3182581 (cit. on p. 30).

Fushimi, E.; Colmegna, P.; De Battista, H.; Garelli, F., and Sánchez-Peña, R. (2019). "Unannounced meal analysis of the ARG algorithm". In: *Proceedings of the American Control Conference* 2019-July, pp. 4740–4745. ISSN: 07431619. DOI: 10.23919/acc.2019.8814719 (cit. on pp. 20, 21, 30, 104, 130).

Fushimi, E.; Serafini, M. C.; De Battista, H., and Garelli, F. (2020). "Automatic glycemic regulation for the pediatric population based on switched control and time-varying IOB constraints: an in silico study". In: *Medical and Biological Engineering and Computing* 58.10, pp. 2325–2337. ISSN: 17410444. DOI: 10.1007/S11517-020-02213-W/TABLES/8 (cit. on pp. 21, 22).

Galias, Z. and Yu, X. (2007). "Euler's Discretization of Single Input Sliding-Mode Control Systems". In: *IEEE Transactions on Automatic Control* 52.9, pp. 1726–1730. ISSN: 0018-9286. DOI: 10.1109/TAC.2007.904289 (cit. on p. 75).

García, A.; Moscardó, V.; Ramos-Prol, A.; Díaz, J.; Boronat, M.; Bondia, J., and Rossetti, P. (2021). "Effect of meal composition and alcohol consumption on postprandial glucose concentration in subjects with type 1 diabetes: a randomized crossover trial". In: *BMJ Open Diabetes Research & Care* 9.1, e002399. DOI: 10.1136/bmjdrc-2021-002399 (cit. on pp. 10, 13).

Garcia-Tirado, J.; Brown, S. A.; Laichuthai, N.; Colmegna, P.; Koravi, C. L.; Ozaslan, B.; Corbett, J. P.; Barnett, C. L.; Pajewski, M.; Oliveri, M. C.; Myers, H., and Breton, M. D. (2021a). "Anticipation of Historical Exercise Patterns by a Novel Artificial Pancreas System Reduces Hypoglycemia during and after Moderate-Intensity Physical Activity in People with Type 1 Diabetes". In: *Diabetes Technology & Therapeutics* 23.4, pp. 277–285. ISSN: 15578593. DOI: 10.1089/dia.2020.0516 (cit. on pp. 21, 34, 35).

Garcia-Tirado, J.; Colmegna, P.; Corbett, J. P.; Ozaslan, B., and Breton, M. D. (2019). "In Silico Analysis of an Exercise-Safe Artificial Pancreas With Multistage Model Predictive Control and Insulin Safety System". In: *Journal of Diabetes Science and Technology* 13.6, pp. 1054–1064. ISSN: 1932-2968. DOI: 10.1177/1932296819879084 (cit. on pp. 33, 34).

Garcia-Tirado, J.; Diaz, J. L.; Esquivel-Zuniga, R.; Koravi, C. L.; Corbett, J. P.; Dawson, M.; Wakeman, C.; Barnett, C. L.; Oliveri, M. C.; Myers, H.; Krauthause, K.; Breton, M. D., and DeBoer, M. D. (2021b). "Advanced Closed-Loop Control System Improves

Postprandial Glycemic Control Compared With a Hybrid Closed-Loop System Following Unannounced Meal". In: *Diabetes Care* 44.10, pp. 2379–2387. ISSN: 0149-5992. DOI: 10.2337/DC21-0932 (cit. on pp. 20, 130).

Garcia-Tirado, J.; Lv, D.; Corbett, J. P.; Colmegna, P., and Breton, M. D. (2021c). "Advanced hybrid artificial pancreas system improves on unannounced meal response - In silico comparison to currently available system". In: *Computer Methods and Programs in Biomedicine* 211, p. 106401. ISSN: 18727565. DOI: 10.1016/j.cmpb.2021.106401 (cit. on pp. 20, 22, 24).

Garcia-Tirado, J.; Zuluaga-Bedoya, C., and Breton, M. D. (2018). "Identifiability Analysis of Three Control-Oriented Models for Use in Artificial Pancreas Systems". In: *Journal of Diabetes Science and Technology* 12.5, pp. 937–952. ISSN: 19322968. DOI: 10.1177/1932296818788873 (cit. on pp. 55, 59, 61–63, 150).

Garelli, F.; Fushimi, E.; Rosales, N.; Arambarri, D.; Mendoza, L.; Serafini, M. C.; Moscoso-Vásquez, M.; Stasi, M.; Duette, P.; García-Arabehety, J.; Giunta, J. N.; De Battista, H.; Sánchez-Peña, R., and Grosembacher, L. (2022). "First Outpatient Clinical Trial of a Full Closed-Loop Artificial Pancreas System in South America". In: *Journal of Diabetes Science and Technology*, p. 193229682210961. ISSN: 1932-2968. DOI: 10.1177/19322968221096162 (cit. on pp. 19, 31).

Ghosh, T. and Sazonov, E. (2021). "Systematic Review of Passive Sensors for Detection of Food Intake". In: *Reference Module in Biomedical Sciences*. DOI: 10.1016/B978-0-12-822548-6.00086-8 (cit. on p. 20).

Gingras, V.; Rabasa-Lhoret, R.; Messier, V.; Ladouceur, M.; Legault, L., and Haidar, A. (2016a). "Efficacy of dual-hormone artificial pancreas to alleviate the carbohydrate-counting burden of type 1 diabetes: A randomized crossover trial". In: *Diabetes and Metabolism* 42.1, pp. 47–54. ISSN: 18781780. DOI: 10.1016/j.diabet.2015.05.001 (cit. on pp. 18, 30).

Gingras, V.; Bonato, L.; Messier, V.; Roy-Fleming, A.; Smaoui, M. R.; Ladouceur, M., and Rabasa-Lhoret, R. (2018a). "Impact of macronutrient content of meals on postprandial glucose control in the context of closed-loop insulin delivery: A randomized cross-over study". In: *Diabetes, Obesity and Metabolism* 20.11, pp. 2695–2699. ISSN: 1462-8902. DOI: 10.1111/dom.13445 (cit. on pp. 10, 13).

Gingras, V.; Haidar, A.; Messier, V.; Legault, L.; Ladouceur, M., and Rabasa-Lhoret, R. (2016b). "A Simplified Semiquantitative Meal Bolus Strategy Combined with Single- and Dual-Hormone Closed-Loop Delivery in Patients with Type 1 Diabetes: A Pilot Study". In: *Diabetes Technology & Therapeutics* 18.8, pp. 464–471. ISSN: 1520-9156. DOI: 10.1089/dia.2016.0043 (cit. on pp. 18, 130).

Gingras, V.; Taleb, N.; Roy-Fleming, A.; Legault, L., and Rabasa-Lhoret, R. (2018b). "The challenges of achieving postprandial glucose control using closed-loop systems in patients with type 1 diabetes". In: *Diabetes, Obesity and Metabolism* 20.2, pp. 245–256. ISSN: 14628902. DOI: 10.1111/dom.13052 (cit. on pp. 11, 12, 130).

Gomez, A. M.; Gomez, C.; Aschner, P.; Veloza, A.; Muñoz, O.; Rubio, C., and Vallejo, S. (2015). "Effects of Performing Morning Versus Afternoon Exercise on Glycemic Control and Hypoglycemia Frequency in Type 1 Diabetes Patients on Sensor-Augmented Insulin Pump Therapy". In: *Journal of Diabetes Science and Technology* 9.3, pp. 619–624. ISSN: 1932-2968. DOI: 10.1177/1932296814566233 (cit. on p. 147).

Gómez-Díaz, R. A. (2019). "Pathophysiology of Type 1 Diabetes". In: *The Diabetes Textbook*. Cham: Springer International Publishing, pp. 89–99. DOI: 10.1007/978-3-030-11815-0_7 (cit. on p. 2).

Goodwin, G. C.; Medioli, A. M.; Carrasco, D. S.; King, B. R., and Fu, Y. (2015). "A fundamental control limitation for linear positive systems with application to Type 1 diabetes treatment". In: *Automatica*. Vol. 55. Elsevier Ltd, pp. 73–77. DOI: 10.1016/j.automatica.2015.02.041 (cit. on pp. 12, 16, 141).

Gregory, G. A.; Robinson, T. I. G.; Linklater, S. E.; Wang, F.; Colagiuri, S.; Beaufort, C. de; Donaghue, K. C.; Magliano, D. J.; Maniam, J.; Orchard, T. J.; Rai, P., and Ogle, G. D. (2022). "Global incidence, prevalence, and mortality of type 1 diabetes in 2021 with projection to 2040: a modelling study". In: *The Lancet Diabetes & Endocrinology* 10.10, pp. 741–760. ISSN: 22138587. DOI: 10.1016/S2213-8587(22)00218-2 (cit. on p. 1).

Grosman, B.; Ilany, J.; Roy, A.; Kurtz, N.; Wu, D.; Parikh, N.; Voskanyan, G.; Konvalina, N.; Mylonas, C.; Gottlieb, R.; Kaufman, F., and Cohen, O. (2016). "Hybrid Closed-Loop Insulin Delivery in Type 1 Diabetes during Supervised Outpatient Conditions". In: *Journal of Diabetes Science and Technology* 10.3, pp. 708–713. ISSN: 19322968. DOI: 10.1177/1932296816631568 (cit. on p. 11).

Haidar, A. (2019). "Insulin-and-Glucagon Artificial Pancreas Versus Insulin-Alone Artificial Pancreas: A Short Review". In: *Diabetes Spectrum* 32.3, pp. 215–221. DOI: 10.2337/ds18-0097 (cit. on pp. 36, 147).

Haidar, A.; Yale, J. F.; Lovblom, L. E.; Cardinez, N.; Orszag, A.; Falappa, C. M.; Gouchie-Provencher, N.; Tsoukas, M. A.; El Fathi, A.; Rene, J.; Eldelekli, D.; Lanctôt, S. O.; Scarr, D., and Perkins, B. A. (2021). "Reducing the need for carbohydrate counting in type 1 diabetes using closed-loop automated insulin delivery (artificial pancreas) and empagliflozin: A randomized, controlled, non-inferiority, crossover pilot trial". In: *Diabetes, Obesity and Metabolism* 23.6, pp. 1272–1281. DOI: 10.1111/DOM.14335 (cit. on pp. 29, 30, 130).

Hajizadeh, I.; Hobbs, N.; Sevil, M.; Rashid, M.; Askari, M. R.; Brandt, R., and Cinar, A. (2020). "Performance Monitoring , Assessment and Modification of an Adaptive MPC : Automated Insulin Delivery in Diabetes". In: *2020 European Control Conference (ECC)*. Saint Petersburg, Russia, pp. 283–288. ISBN: 9783907144022 (cit. on p. 130).

Hajizadeh, I.; Rashid, M.; Samadi, S.; Feng, J.; Sevil, M.; Hobbs, N.; Lazaro, C.; Maloney, Z.; Brandt, R.; Yu, X.; Turksoy, K.; Littlejohn, E.; Cengiz, E., and Cinar, A. (2018). "Adaptive and Personalized Plasma Insulin Concentration Estimation for Artificial Pancreas Systems". In: *Journal of Diabetes Science and Technology* 12.3, pp. 639–649. ISSN: 19322968. DOI: 10.1177/1932296818763959 (cit. on p. 53).

Hajizadeh, I.; Rashid, M.; Samadi, S.; Sevil, M.; Hobbs, N.; Brandt, R., and Cinar, A. (2019a). "Adaptive personalized multivariable artificial pancreas using plasma insulin estimates". In: *Journal of Process Control* 80, pp. 26–40. ISSN: 09591524. DOI: 10.1016/j.jprocont.2019.05.003 (cit. on pp. 19, 22, 24, 33).

Hajizadeh, I.; Samadi, S.; Sevil, M.; Rashid, M., and Cinar, A. (2019b). "Performance Assessment and Modication of An Adaptive MPC for Automated Insulin Delivery by A Multivariable Articial Pancreas". In: *Industrial & Engineering Chemistry Research*, pp. 11506–11520. ISSN: 0888-5885. DOI: 10.1021/acs.iecr.8b06202 (cit. on pp. 23, 33, 34).

Hanaire, H.; Franc, S.; Borot, S.; Penfornis, A.; Benhamou, P. Y.; Schaepelynck, P.; Renard, E.; Guerci, B.; Jeandidier, N.; Simon, C.; Hannaert, P.; Xhaard, I.; Doron, M.; Huneker, E.; Charpentier, G., and Reznik, Y. (2020). "Efficacy of the Diabeloop closed-loop system to improve glycaemic control in patients with type 1 diabetes exposed to gastronomic dinners or to sustained physical exercise". In: *Diabetes, Obesity and Metabolism* 22.3, pp. 324–334. ISSN: 14631326. DOI: 10.1111/dom.13898 (cit. on p. 53).

Hand, D. J. (2012). *Understanding The New Statistics: Effect Sizes, Confidence Intervals, and Meta-Analysis*. Vol. 80. 2, pp. 344–345. ISBN: 9780415879675. DOI: 10.1111/j.1751-5823.2012.00187_26.x (cit. on p. 84).

Hansen, N. (2016). *The CMA Evolution Strategy: A Tutorial* (cit. on p. 161).

Harkless, L. B.; Shapiro, J., and Breshars, L. D. (2019). "Foot Complications". In: *The Diabetes Textbook*. Cham: Springer International Publishing, pp. 899–918. DOI: 10.1007/978-3-030-11815-0_58 (cit. on p. 3).

Harvey, R. A.; Dassau, E.; Bevier, W. C.; Seborg, D. E.; Jovanovič, L.; Doyle, F. J., and Zisser, H. C. (2014a). "Clinical Evaluation of an Automated Artificial Pancreas Using Zone-Model Predictive Control and Health Monitoring System". In: *Diabetes Technology & Therapeutics* 16.6, pp. 348–357 (cit. on p. 36).

Harvey, R. A.; Dassau, E.; Zisser, H.; Seborg, D. E., and Doyle, F. J. (2014b). "Design of the Glucose Rate Increase Detector". In: *Journal of Diabetes Science and Technology* 8.2, pp. 307–320. ISSN: 1932-2968. DOI: 10.1177/1932296814523881 (cit. on pp. 19–21, 104, 130).

Harvey, R. A.; Dassau, E.; Zisser, H.; Seborg, D. E.; Jovanovič, L., and Doyle, F. J. (2012). "Design of the health monitoring system for the artificial pancreas: Low glucose prediction module". In: *Journal of Diabetes Science and Technology* 6.6, pp. 1345–1354. ISSN: 19322968. DOI: 10.1177/193229681200600613 (cit. on p. 36).

He, J.; Renard, E.; Lord, P.; Cohen, D.; Cem-Duranty, E.; Place, J.; Gu, B.; Wang, X.; Yenduri, G., and Burgess, D. J. (2021). "Root cause determination of intraperitoneal catheter obstructions: Insulin amyloid aggregates vs foreign body reaction". In: *Journal of Controlled Release* 336, pp. 1–15. ISSN: 0168-3659. DOI: 10.1016/J.JCONREL.2021.06.005 (cit. on p. 27).

Heinemann, L. (2002). "Variability of Insulin Absorption and Insulin Action". In: *Diabetes Technology & Therapeutics* 4.5, pp. 673–682. ISSN: 1520-9156. DOI: 10.1089/152091502320798312 (cit. on p. 13).

Hermans, F. and Zarrop, M. (1996). "Sliding Mode Observers for Robust Sensor Monitoring". In: *IFAC Proceedings Volumes* 29.1, pp. 6530–6535. ISSN: 1474-6670. DOI: 10.1016/S1474-6670(17)58730-3 (cit. on p. 105).

Herrero, P.; Bondia, J.; Oliver, N., and Georgiou, P. (2017). "A coordinated control strategy for insulin and glucagon delivery in type 1 diabetes". In: *Computer Methods in Biomechanics and Biomedical Engineering* 20.13, pp. 1474–1482. ISSN: 14768259. DOI: 10.1080/10255842.2017.1378352 (cit. on pp. 31, 35).

Herrero, P.; Georgiou, P.; Oliver, N.; Reddy, M.; Johnston, D., and Toumazou, C. (2013). "A Composite Model of Glucagon-Glucose Dynamics for In Silico Testing of Bihormonal Glucose Controllers". In: *Journal of Diabetes Science and Technology* 7.4, pp. 941–951. ISSN: 1932-2968. DOI: 10.1177/193229681300700416 (cit. on p. 35).

Hinshaw, L.; Man, C. D.; Nandy, D. K.; Saad, A.; Bharucha, A. E.; Levine, J. A.; Rizza, R. A.; Basu, R.; Carter, R. E.; Cobelli, C.; Kudva, Y. C., and Basu, A. (2013). "Diurnal Pattern of Insulin Action in Type 1 Diabetes: Implications for a Closed-Loop System". In: *Diabetes* 62.7, pp. 2223–2229. ISSN: 0012-1797. DOI: 10.2337/DB12-1759 (cit. on p. 13).

Hirsh, M. L.; Shalit, R.; Shalem, S.; Cohen, O.; Kurtz, N.; Roy, A.; Grosman, B.; Cukierman-Yaffe, T., and Tirosh, A. (2022). "554-P: Complex Meal Handling with Advanced Hybrid Closed-Loop (AHCL) System". In: *Diabetes* 71.Supplement_1. ISSN: 0012-1797. DOI: 10.2337/DB22-554-P (cit. on p. 19).

Hovorka, R.; Allen, J. M.; Elleri, D.; Chassin, L. J.; Harris, J.; Xing, D.; Kollman, C.; Hovorka, T.; Larsen, A. M. F.; Nodale, M.; De Palma, A.; Wilinska, M. E.; Acerini, C. L., and Dunger, D. B. (2010). "Manual closed-loop insulin delivery in children and adolescents with type 1 diabetes: a phase 2 randomised crossover trial". In: *The Lancet* 375.9716, pp. 743–751. ISSN: 01406736. DOI: 10.1016/S0140-6736(09)61998-X (cit. on p. 53).

Hovorka, R.; Canonico, V.; Chassin, L. J.; Haueter, U.; Massi-Benedetti, M.; Federici, M. O.; Pieber, T. R.; Schaller, H. C.; Schaupp, L.; Vering, T., and Wilinska, M. E. (2004). "Nonlinear model predictive control of glucose concentration in subjects with type 1 diabetes". In: *Physiological Measurement* 25.4, pp. 905–920. ISSN: 09673334. DOI: 10.1088/0967-3334/25/4/010 (cit. on pp. 40, 50–54, 58, 97, 148, 149).

Hovorka, R.; Shojaee-Moradie, F.; Carroll, P. V.; Chassin, L. J.; Gowrie, I. J.; Jackson, N. C.; Tudor, R. S.; Margot Umpleby, A., and Jones, R. H. (2002). "Partitioning glucose distribution/transport, disposal, and endogenous production during IVGTT". In: *American Journal of Physiology - Endocrinology and Metabolism* 282.5 45-5, pp. 992–1007. ISSN: 01931849 (cit. on pp. 55, 61).

Hu, R. and Li, C. (2015). "An Improved PID Algorithm Based on Insulin-on-Board Estimate for Blood Glucose Control with Type 1 Diabetes". In: *Computational and Mathematical Methods in Medicine* 2015. ISSN: 17486718. DOI: 10.1155/2015/281589 (cit. on p. 148).

Hu, Z.; Zhao, G.; Zhang, L., and Zhou, D. (2016). "Fault Estimation for Nonlinear Dynamic System Based on the Second-Order Sliding Mode Observer". In: *Circuits, Systems, and Signal Processing* 35.1, pp. 101–115. ISSN: 0278-081X. DOI: 10.1007/s00034-015-0060-2 (cit. on pp. 105, 106).

Huangfu, Y.; Xu, J.; Zhuo, S.; Xie, M., and Liu, Y. (2017). "A novel adaptive sliding mode observer for SOC estimation of lithium batteries in electric vehicles". In: *2017 7th International Conference on Power Electronics Systems and Applications - Smart Mobility, Power Transfer & Security (PESA)*. IEEE, pp. 1–6. ISBN: 978-1-5386-1387-0. DOI: 10.1109/PESA.2017.8277750 (cit. on p. 75).

Hughes, C. S.; Patek, S. D.; Breton, M. D., and Kovatchev, B. P. (2010). "Hypoglycemia Prevention via Pump Attenuation and Red-Yellow-Green "Traffic" Lights Using Continuous Glucose Monitoring and Insulin Pump Data". In: *Journal of Diabetes Science and Technology* 4.5, p. 1146. ISSN: 19322968. DOI: 10.1177/193229681000400513 (cit. on p. 33).

Huyett, L. M.; Dassau, E.; Zisser, H. C., and Doyle, F. J. (2015). "Design and Evaluation of a Robust PID Controller for a Fully Implantable Artificial Pancreas". In: *Industrial & Engineering Chemistry Research* 54 (42), pp. 10311–10321. ISSN: 0888-5885. DOI: 10.1021/acs.iecr.5b01237 (cit. on pp. 24, 27).

Huyett, L. M.; Ly, T. T.; Forlenza, G. P.; Reuschel-DIvirgilio, S.; Messer, L. H.; Wadwa, R. P.; Gondhalekar, R.; Doyle, F. J.; Pinsker, J. E.; Maahs, D. M.; Buckingham, B. A., and Dassau, E. (2017). "Outpatient Closed-Loop Control with Unannounced Moderate Exercise in Adolescents Using Zone Model Predictive Control". In: *Diabetes Technology & Therapeutics* 19.6, pp. 331–339. ISSN: 1520-9156. DOI: 10.1089/dia.2016.0399 (cit. on p. 36).

Hyunjin, L.; Buckingham, B. A.; Wilson, D. M., and Bequette, B. W. (2009). "A closed-loop artificial pancreas using model predictive control and a sliding meal size estimator." In: *J Diabetes Sci Technol* 3.5, pp. 1082–1090 (cit. on pp. 20, 21, 24, 113, 130).

Ilkowitz, J. T.; Katikaneni, R.; Cantwell, M.; Ramchandani, N., and Heptulla, R. A. (2016). "Adjuvant liraglutide and insulin versus insulin monotherapy in the closed-loop system in type 1 diabetes: A randomized open-labeled crossover design trial". In: *Journal of Diabetes Science and Technology* 10.5, pp. 1108–1114. ISSN: 19322968. DOI: 10.1177/1932296816647976 (cit. on p. 29).

Iman, R. L.; Helton, J. C., and Campbell, J. E. (1981). "An Approach to Sensitivity Analysis of Computer Models: Part I—Introduction, Input Variable Selection and Preliminary Variable Assessment". In: *Journal of Quality Technology* 13.3, pp. 174–183. ISSN: 0022-4065. DOI: 10.1080/00224065.1981.11978748 (cit. on p. 60).

Infante, M.; Baidal, D. A.; Rickels, M. R.; Fabbri, A.; Skyler, J. S.; Alejandro, R., and Ricordi, C. (2021). "Dual-hormone artificial pancreas for management of type 1 diabetes: Recent progress and future directions". In: *Artificial Organs* 45.9, pp. 968–986. ISSN: 0160-564X. DOI: 10.1111/aor.14023 (cit. on pp. 12, 30, 36, 147).

International Diabetes Federation (2021). *IDF Diabetes Atlas. 10th edition.* URL: https://diabetesatlas.org/atlas/tenth-edition/.pdf (cit. on p. 1).

Iversen, G. R. (2011). "Analysis of Variance". en. In: *International Encyclopedia of Statistical Science*. Ed. by M. Lovric. Berlin, Heidelberg: Springer Berlin Heidelberg, pp. 44–46. ISBN: 978-3-642-04897-5 978-3-642-04898-2. DOI: 10.1007/978-3-642-04898-2_117 (cit. on p. 84).

Jacobs, P. G.; Resalat, N.; Youssef, J. E.; Reddy, R.; Branigan, D.; Preiser, N.; Condon, J., and Castle, J. (2015). "Incorporating an exercise detection, grading, and hormone dosing algorithm into the artificial pancreas using accelerometry and heart rate". In: *Journal of Diabetes Science and Technology* 9.6, pp. 1175–1184. ISSN: 19322968. DOI: 10.1177/1932296815609371 (cit. on pp. 33, 35).

Jacobsen, S. S.; Hommel, E.; Ranjan, A. G., and Nørgaard, K. (2022). "Glycemic Effects and Predictors of Increased Time-in-Range After Initiating MiniMed 670G: A 12-Month

Observational Study". In: *Diabetes Technology & Therapeutics*. ISSN: 1520-9156. DOI: 10.1089/dia.2021.0532 (cit. on p. 5).

JDRF (2020). *JDRF-Gore Invest in Development of Implantable Insulin Delivery System*. URL: https://www.jdrf.org/blog/2020/01/22/jdrf-gore-invest-development-o-implantable-insulin-delivery-system/ (visited on 05/29/2022) (cit. on p. 27).

Jennings, P. and Hussain, S. (2020). "Do-It-Yourself Artificial Pancreas Systems: A Review of the Emerging Evidence and Insights for Healthcare Professionals". In: *Journal of Diabetes Science and Technology* 14.5, pp. 868–877. ISSN: 1932-2968. DOI: 10.1177/1932296819894296 (cit. on p. 5).

Jiao, X.; Shen, Y., and Chen, Y. (2022). "Better TIR, HbA1c, and less hypoglycemia in closed-loop insulin system in patients with type 1 diabetes: a meta-analysis". In: *BMJ Open Diabetes Research & Care* 10 (2), e002633. ISSN: 2052-4897. DOI: 10.1136/bmjdrc-2021-002633 (cit. on pp. 5, 6).

Johnson, M. A. and Moradi, M. H., eds. (2005). *PID Control*. London: Springer-Verlag. ISBN: 1-85233-702-8. DOI: 10.1007/1-84628-148-2 (cit. on p. 195).

Jones, R. W. (2019). "Glucagon Control Strategies for the Bi-hormonal Artificial Pancreas". In: *2019 14th IEEE Conference on Industrial Electronics and Applications (ICIEA)*. IEEE, pp. 1051–1056. ISBN: 978-1-5386-9490-9. DOI: 10.1109/ICIEA.2019.8833900 (cit. on pp. 35, 147).

Jones, R. W.; Gianni, F.; Despotou, G., and Katzis, K. (2017). "The artificial pancreas: Reducing safety risk via intra-peritoneal insulin delivery". In: *Studies in Health Technology and Informatics*. Vol. 238. IOS Press, pp. 56–59. ISBN: 9781614997801. DOI: 10.3233/978-1-61499-781-8-56 (cit. on p. 26).

Kanderian, S.; Steil, and Steil, G. (2009). "Identification of Intraday Metabolic Profiles during Closed-Loop Glucose Control in Individuals with Type 1 Diabetes". In: *Journal of Diabetes Science and Technology* 3.5, pp. 1047–1057. DOI: 10.1177/193229680900300508 (cit. on pp. 40, 50, 52, 58, 61, 64, 151, 196).

Karageorgiou, V.; Papaioannou, T. G.; Bellos, I.; Alexandraki, K.; Tentolouris, N.; Stefanadis, C.; Chrousos, G. P., and Tousoulis, D. (2019). "Effectiveness of artificial pancreas in the non-adult population: A systematic review and network meta-analysis". In: *Metabolism: Clinical and Experimental* 90, pp. 20–30. ISSN: 15328600. DOI: 10.1016/j.metabol.2018.10.002 (cit. on p. 5).

Kawamura, T.; Takamura, C.; Hirose, M.; Hashimoto, T.; Higashide, T.; Kashihara, Y.; Hashimura, K., and Shintaku, H. (2015). "The factors affecting on estimation of carbohydrate content of meals in carbohydrate counting". In: *Clinical Pediatric Endocrinology*

24.4, pp. 153–165. ISSN: 0918-5739. DOI: 10.1297/cpe.24.153 (cit. on pp. 10, 130, 140, 163, 170).

Keating, B.; Smart, C. E. M.; Harray, A. J.; Paramalingam, N.; Smith, G.; Jones, T. W.; King, B. R., and Davis, E. A. (2021). "Additional Insulin Is Required in Both the Early and Late Postprandial Periods for Meals High in Protein and Fat: A Randomized Trial". In: *The Journal of Clinical Endocrinology & Metabolism* 106.9, e3611–e3618. ISSN: 0021-972X. DOI: 10.1210/clinem/dgab318 (cit. on p. 10).

El-Khatib, F. H.; Balliro, C.; Hillard, M. A.; Magyar, K. L.; Ekhlaspour, L.; Sinha, M.; Mondesir, D.; Esmaeili, A.; Hartigan, C.; Thompson, M. J.; Malkani, S.; Lock, J. P.; Harlan, D. M.; Clinton, P.; Frank, E.; Wilson, D. M.; DeSalvo, D.; Norlander, L.; Ly, T.; Buckingham, B. A.; Diner, J.; Dezube, M.; Young, L. A.; Goley, A.; Kirkman, M. S.; Buse, J. B.; Zheng, H.; Selagamsetty, R. R.; Damiano, E. R., and Russell, S. J. (2017). "Home use of a bihormonal bionic pancreas versus insulin pump therapy in adults with type 1 diabetes: a multicentre randomised crossover trial". In: *The Lancet* 389.10067, pp. 369–380. ISSN: 0140-6736. DOI: 10.1016/S0140-6736(16)32567-3 (cit. on p. 18).

El-Khatib, F. H.; Russell, S. J.; Magyar, K. L.; Sinha, M.; McKeon, K.; Nathan, D. M., and Damiano, E. R. (2014). "Autonomous and Continuous Adaptation of a Bihormonal Bionic Pancreas in Adults and Adolescents With Type 1 Diabetes". In: *The Journal of Clinical Endocrinology and Metabolism* 99.5, p. 1701. ISSN: 19457197. DOI: 10.1210/JC.2013-4151 (cit. on p. 18).

El-khatib, F. H.; Russell, S. J.; Nathan, D. M.; Sutherlin, R. G., and Damiano, E. R. (2010). "Bi-hormonal Closed-Loop Blood Glucose Control for Type 1 Diabetes". In: *Science translational medicine* 2.27, 27ra27. ISSN: 19466242. DOI: 10.1126/SCITRANSLMED.3000619 (cit. on pp. 18, 24, 30).

Khodakaramzadeh, S.; Batmani, Y., and Meskin, N. (2019). "Automatic blood glucose control for type 1 diabetes: A trade-off between postprandial hyperglycemia and hypoglycemia". In: *Biomedical Signal Processing and Control* 54, p. 101603. ISSN: 1746-8094. DOI: 10.1016/J.BSPC.2019.101603 (cit. on p. 148).

Kikuuwe, R.; Pasaribu, R., and Byun, G. (2019). "A first-order differentiator with first-order sliding mode filtering". In: *IFAC-PapersOnLine* 52.16, pp. 771–776. ISSN: 24058963. DOI: 10.1016/j.ifacol.2019.12.056 (cit. on pp. 75, 77, 78, 82).

Kim, D.-W. and Park, C.-S. (2017). "Application of Kalman Filter for Estimating a Process Disturbance in a Building Space". In: *Sustainability* 9 (10), p. 1868. ISSN: 2071-1050. DOI: 10.3390/su9101868 (cit. on p. 46).

Kime, N. H.; Pringle, A.; Rivett, M. J., and Robinson, P. M. (2018). "Physical activity and exercise in adults with type 1 diabetes: Understanding their needs using a person-

centered approach". In: *Health Education Research* 33.5, pp. 375–388. ISSN: 14653648. DOI: 10.1093/her/cyy028 (cit. on p. 147).

Kolle, K.; Fougner, A. L.; Ellingsen, R.; Carlsen, S. M., and Stavdahl, O. (2019). "Feasibility of Early Meal Detection Based on Abdominal Sound". In: *IEEE Journal of Translational Engineering in Health and Medicine* 7, pp. 1–12. ISSN: 2168-2372. DOI: 10.1109/JTEHM.2019.2940218 (cit. on p. 104).

Kölle, K.; Biester, T.; Christiansen, S.; Fougner, A. L., and Stavdahl, Ø. (2020). "Pattern Recognition Reveals Characteristic Postprandial Glucose Changes: Non-Individualized Meal Detection in Diabetes Mellitus Type 1". In: *IEEE Journal of Biomedical and Health Informatics* 24.2, pp. 594–602. ISSN: 21682208. DOI: 10.1109/JBHI.2019.2908897 (cit. on pp. 21, 104, 124, 126).

Kölle, K.; Fougner, A. L., and Stavdahl, O. (2017). "Meal detection based on non-individualized moving horizon estimation and classification". In: *1st Annual IEEE Conference on Control Technology and Applications, CCTA 2017*, pp. 529–535. ISBN: 9781509021826. DOI: 10.1109/CCTA.2017.8062516 (cit. on pp. 20, 21, 40, 52).

Koller, M. (2016). "Robustlmm: An R package for Robust estimation of linear Mixed-Effects models". In: *Journal of Statistical Software* 75.1. ISSN: 15487660. DOI: 10.18637/jss.v075.i06 (cit. on pp. 124, 167).

Kotta, Ü. and Kaldmäe, A. (2020). "A brief tutorial overview of disturbance observers for nonlinear systems: application to flatness-based control". In: *Proceedings of the Estonian Academy of Sciences* 69 (1), p. 57. ISSN: 1736-6046. DOI: 10.3176/proc.2020.1.07 (cit. on p. 46).

Kovacs, L.; Eigner, G.; Siket, M., and Barkai, L. (2019). "Control of Diabetes Mellitus by Advanced Robust Control Solution". In: *IEEE Access* 4, pp. 1–1. ISSN: 2169-3536. DOI: 10.1109/ACCESS.2019.2938267 (cit. on pp. 40, 53, 71).

Kovács, L. (2017). "Linear parameter varying (LPV) based robust control of type-I diabetes driven for real patient data". In: *Knowledge-Based Systems* 122, pp. 199–213. ISSN: 09507051. DOI: 10.1016/j.knosys.2017.02.008 (cit. on p. 68).

Kuhn, M. (2021). *caret: Classification and Regression Training* (cit. on p. 162).

Kurtz, M. J. and Henson, M. A. (1998). "State and disturbance estimation for nonlinear systems affine in the unmeasured variables". In: *Computers Chem. Engng* 22 (10), pp. 1441–1459 (cit. on p. 46).

Laguna, A. J.; Rossetti, P.; Ampudia-Blasco, F. J.; Vehí, J., and Bondia, J. (2010). "Optimal design for individual model identification based on ambulatory continuous glucose

monitoring in patients with type 1 diabetes". In: *IET Seminar Digest*. Vol. 2010. 4, pp. 595–600. ISBN: 9781846000386. DOI: 10.1049/ic.2010.0349 (cit. on pp. 90, 92).

Lal, R. A.; Ekhlaspour, L.; Hood, K., and Buckingham, B. (2019). "Realizing a Closed-Loop (Artificial Pancreas) System for the Treatment of Type 1 Diabetes". In: *Endocrine Reviews* 40.6, pp. 1521–1546. ISSN: 0163-769X. DOI: 10.1210/er.2018-00174 (cit. on p. 26).

Lane, W.; Lambert, E.; George, J.; Rathor, N., and Thalange, N. (2021). "Exploring the burden of mealtime insulin dosing in adults and children with type 1 diabetes". In: *Clinical Diabetes* 39.4, pp. 347–357. ISSN: 08918929. DOI: 10.2337/CD20-0117 (cit. on pp. 10, 11).

Lawton, J.; Blackburn, M.; Rankin, D.; Allen, J.; Campbell, F.; Leelarathna, L.; Tauschmann, M.; Thabit, H.; Wilinska, M. E., and Hovorka, R. (2019). "The impact of using a closed-loop system on food choices and eating practices among people with Type 1 diabetes: a qualitative study involving adults, teenagers and parents". In: *Diabetic Medicine* 36.6, pp. 753–760. ISSN: 0742-3071. DOI: 10.1111/dme.13887 (cit. on pp. 1, 4).

Lee, J.; Dassau, E.; Zisser, H.; Jovanovič, L., and Doyle III, F. (2012). "Evaluation of Zone-MPC for Intraperitoneal Insulin Delivery". In: *American Diabetes Association 72nd Scientific Sessions*. Vol. 61 (8). Philadelphia, USA, A253 (cit. on p. 26).

Lee, J. J.; Dassau, E.; Zisser, H., and Doyle, F. J. (2014). "Design and in silico evaluation of an intraperitoneal-subcutaneous (IP-SC) artificial pancreas". In: *Computers and Chemical Engineering* 70, pp. 180–188. ISSN: 00981354. DOI: 10.1016/j.compchemeng.2014.02.024 (cit. on p. 26).

Lee, J. J.; Dassau, E.; Zisser, H.; Tamborlane, W.; Weinzimer, S., and Doyle, F. J. (2013). "The impact of insulin pharmacokinetics and pharmacodynamics on the closed-loop artificial pancreas". In: *Proceedings of the IEEE Conference on Decision and Control*. Institute of Electrical and Electronics Engineers Inc., pp. 127–132. ISBN: 9781467357173. DOI: 10.1109/CDC.2013.6759870 (cit. on p. 25).

Lee, S. H. and Yoon, K. H. (2021). "A century of progress in diabetes care with insulin: A history of innovations and foundation for the future". In: *Diabetes and Metabolism Journal* 45.5, pp. 629–640. ISSN: 22336087. DOI: 10.4093/DMJ.2021.0163 (cit. on p. 25).

León-Vargas, F.; Oviedo, J. A. A., and Wandurraga, H. J. L. (2022). "Two Decades of Research in Artificial Pancreas: Insights from a Bibliometric Analysis". In: *Journal of Diabetes Science and Technology* 16 (2), pp. 434–445. ISSN: 1932-2968. DOI: 10.1177/19322968211005500 (cit. on p. 4).

Levant, A. (1998). "Robust exact differentiation via sliding mode technique". In: *Automatica* 34.3, pp. 379–384. ISSN: 00051098. DOI: 10.1016/S0005-1098(97)00209-4 (cit. on pp. 105, 106).

Li, R. and Zhao, G. (2010). "An Improved Adaptive Sliding Mode Observer for Sensorless Control of PMSM". In: *Life System Modeling and Intelligent Computing. ICSEE 2010, LSMS 2010. Lecture Notes in Computer Science*, pp. 199–206. DOI: 10.1007/978-3-642-15597-0_22 (cit. on p. 75).

Li, S.; Yang, J.; Chen, W.-H. H., and Chen, X. (2012). "Generalized Extended State Observer Based Control for Systems With Mismatched Uncertainties". In: *IEEE Transactions on Industrial Electronics* 59.12, pp. 4792–4802. ISSN: 0278-0046. DOI: 10.1109/TIE.2011.2182011 (cit. on pp. 44, 46).

Lieber, B. A.; Taylor, B.; Appelboom, G.; Prasad, K.; Bruce, S.; Yang, A.; Bruce, E.; Christophe, B., and Connolly, E. S. (2015). "Meta-analysis of telemonitoring to improve HbA1c levels: Promise for stroke survivors". In: *Journal of Clinical Neuroscience* 22.5, pp. 807–811. ISSN: 09675868. DOI: 10.1016/j.jocn.2014.11.009 (cit. on p. 3).

Ligon, T. S.; Fröhlich, F.; Chi?, O. T.; Banga, J. R.; Balsa-Canto, E., and Hasenauer, J. (2018). "GenSSI 2.0: multi-experiment structural identifiability analysis of SBML models". In: *Bioinformatics* 34.8. Ed. by J. Wren, pp. 1421–1423. ISSN: 1367-4803. DOI: 10.1093/bioinformatics/btx735 (cit. on p. 56).

Lin, C. F. and Ulsoy, A. G. (1995). "Vehicle dynamics and external disturbance estimation for future vehicle path prediction". In: *Proceedings of the American Control Conference* 1, pp. 155–159. ISSN: 07431619. DOI: 10.1109/ACC.1995.529227 (cit. on p. 46).

Linder, S. and Shafai, B. (1997). "Rejecting disturbances to flexible structures using PI Kalman filters". In: *Proceedings of the 1997 IEEE International Conference on Control Applications*. IEEE, pp. 475–477. ISBN: 0-7803-3876-6. DOI: 10.1109/CCA.1997.627699 (cit. on p. 44).

Ling, W.; Huang, Y.-M.; Qiao, Y.-C.; Zhang, X.-X., and Zhao, H.-L. (2019). "Human Amylin: From Pathology to Physiology and Pharmacology". In: *Current Protein & Peptide Science* 20.9, pp. 944–957. ISSN: 13892037. DOI: 10.2174/1389203720666190328111833 (cit. on p. 12).

Livingstone, S. J.; Levin, D.; Looker, H. C.; Lindsay, R. S.; Wild, S. H.; Joss, N.; Leese, G.; Leslie, P.; McCrimmon, R. J.; Metcalfe, W.; McKnight, J. A.; Morris, A. D.; Pearson, D. W. M.; Petrie, J. R.; Philip, S.; Sattar, N. A.; Traynor, J. P., and Colhoun, H. M. (2015). "Estimated Life Expectancy in a Scottish Cohort With Type 1 Diabetes, 2008-2010". In: *JAMA* 313.1, p. 37. ISSN: 0098-7484. DOI: 10.1001/jama.2014.16425 (cit. on p. 3).

Luke, S. G. (2017). "Evaluating significance in linear mixed-effects models in R". In: *Behavior Research Methods* 49.4, pp. 1494–1502. ISSN: 15543528. DOI: 10.3758/s13428-016-0809-y (cit. on p. 166).

Lum, J. W.; Bailey, R. J.; Barnes-Lomen, V.; Naranjo, D.; Hood, K. K.; Lal, R. A.; Arbiter, B.; Brown, A. S.; Desalvo, D. J.; Pettus, J.; Calhoun, P., and Beck, R. W. (2021). "A Real-World Prospective Study of the Safety and Effectiveness of the Loop Open Source Automated Insulin Delivery System". In: *Diabetes Technology & Therapeutics* 23.5, p. 367. ISSN: 15578593. DOI: 10.1089/DIA.2020.0535 (cit. on p. 5).

Ly, T. T.; Buckingham, B. A.; De Salvo, D. J.; Shanmugham, S.; Satin-Smith, M.; De Boer, M. D.; Oliveri, M. C.; Schertz, E.; Breton, M. D., and Cherñavvsky, D. R. (2016). "Day-and-Night Closed-Loop Control Using the Unified Safety System in Adolescents With Type 1 Diabetes at Camp". In: *Diabetes care* 39.8, e106–e107. ISSN: 1935-5548. DOI: 10.2337/DC16-0817 (cit. on p. 33).

Mahmoudi, Z.; Boiroux, D., and Jbrgensen, J. B. (2018). "Meal Detection for Type 1 Diabetes Using Moving Horizon Estimation". In: *2018 IEEE Conference on Control Technology and Applications, CCTA 2018*, pp. 1674–1679. DOI: 10.1109/CCTA.2018.8511537 (cit. on p. 20).

Mahmoudi, Z.; Cameron, F.; Poulsen, N. K.; Madsen, H.; Bequette, B. W., and Jørgensen, J. B. (2019). "Sensor-based detection and estimation of meal carbohydrates for people with diabetes". In: *Biomedical Signal Processing and Control* 48, pp. 12–25. ISSN: 1746-8094. DOI: 10.1016/J.BSPC.2018.09.012 (cit. on pp. 19–21, 51, 104, 130).

Mahmoudi, Z.; Nørgaard, K.; Poulsen, N. K.; Madsen, H., and Jørgensen, J. B. (2017). "Fault and meal detection by redundant continuous glucose monitors and the unscented Kalman filter". In: *Biomedical Signal Processing and Control* 38, pp. 86–99. ISSN: 17468108. DOI: 10.1016/j.bspc.2017.05.004 (cit. on pp. 19, 20).

Majdpour, D.; Tsoukas, M. A.; Yale, J.-F.; Fathi, A. E.; Rutkowski, J.; Rene, J.; Garfield, N.; Legault, L., and Haidar, A. (2021). "Fully Automated Artificial Pancreas for Adults With Type 1 Diabetes Using Multiple Hormones: Exploratory Experiments". In: *Canadian Journal of Diabetes* 45 (8), pp. 734–742. ISSN: 14992671. DOI: 10.1016/j.jcjd.2021.02.002 (cit. on pp. 21, 28, 30, 130).

MathWorks (2022). *Find minimum of function using genetic algorithm - MATLAB ga*. URL: https://www.mathworks.com/help/gads/ga.html (visited on 02/06/2022) (cit. on pp. 64, 71).

Meneghetti, L.; Facchinetti, A., and Favero, S. D. (2021). "Model-Based Detection and Classification of Insulin Pump Faults and Missed Meal Announcements in Artificial Pancreas Systems for Type 1 Diabetes Therapy". In: *IEEE Transactions on Biomedical*

Engineering 68.1, pp. 170–180. ISSN: 0018-9294. DOI: 10.1109/TBME.2020.3004270 (cit. on pp. 51, 104, 113, 121).

Min, Y. and Agresti, A. (2002). "Modeling Nonnegative Data with Clumping at Zero : A Survey Models for Semicontinuous Data". In: *Journal of The Iranian Statistical Society* 1, pp. 7–33 (cit. on p. 167).

MohammadRidha, T.; Ait-Ahmed, M.; Chaillous, L.; Krempf, M.; Guilhem, I.; Poirier, J.-Y., and Moog, C. H. (2018). "Model Free iPID Control for Glycemia Regulation of Type-1 Diabetes". In: *IEEE Transactions on Biomedical Engineering* 65.1, pp. 199–206. ISSN: 0018-9294. DOI: 10.1109/TBME.2017.2698036 (cit. on p. 22).

Moore, J. B. and Anderson, B. D. (1980). "Coping with singular transition matrices in estimation and control stability theory". In: *International Journal of Control* 31.3, pp. 571–586. ISSN: 13665820. DOI: 10.1080/00207178008961063 (cit. on p. 46).

Moreno, J. A. and Osorio, M. (2008). "A Lyapunov approach to second order sliding mode controller and observers". In: *47th Conference on Decision and Control*, pp. 2856–2861. DOI: 10.1109/CDC.2008.4739356 (cit. on p. 106).

Moscardó, V.; Díez, J. L., and Bondia, J. (2019a). "Parallel Control of an Artificial Pancreas with Coordinated Insulin, Glucagon, and Rescue Carbohydrate Control Actions". In: *Journal of Diabetes Science and Technology* 13.6, pp. 1026–1034. ISSN: 1932-2968. DOI: 10.1177/1932296819879093 (cit. on pp. 7, 37, 148, 156, 165, 174).

Moscardó, V.; Herrero, P.; Díez, J.-L.; Giménez, M.; Rossetti, P.; Georgiou, P., and Bondia, J. (2019b). "Coordinated dual-hormone artificial pancreas with parallel control structure". In: *Computers & Chemical Engineering* 128, pp. 322–328. DOI: 10.1016/j.compchemeng.2019.06.012 (cit. on pp. 7, 35, 37).

Moser, O.; Riddell, M. C.; Eckstein, M. L.; Adolfsson, P.; Rabasa-Lhoret, R.; Boom, L. van den; Gillard, P.; Nørgaard, K.; Oliver, N. S.; Zaharieva, D. P.; Battelino, T.; Beaufort, C. de; Bergenstal, R. M.; Buckingham, B.; Cengiz, E.; Deeb, A.; Heise, T.; Heller, S.; Kowalski, A. J.; Leelarathna, L.; Mathieu, C.; Stettler, C.; Tauschmann, M.; Thabit, H.; Wilmot, E. G.; Sourij, H.; Smart, C. E.; Jacobs, P. G.; Bracken, R. M., and Mader, J. K. (2020). "Glucose management for exercise using continuous glucose monitoring (CGM) and intermittently scanned CGM (isCGM) systems in type 1 diabetes: position statement of the European Association for the Study of Diabetes (EASD) and of the International Society for Pediatric and Adolescent Diabetes (ISPAD) endorsed by JDRF and supported by the American Diabetes Association (ADA)". In: *Diabetologia* 63 (12), pp. 2501–2520. ISSN: 0012-186X. DOI: 10.1007/s00125-020-05263-9 (cit. on pp. 13, 14, 147, 152, 156, 177).

Mullor Casero, R. and Izquierdo Sebastián, F. J. (2020). *Clúster de Cálculo: Rigel [Computing cluster: Rigel]*. URL: https://wiki.upv.es/confluence/pages/viewpage.action?pageId=264044546 (cit. on p. 161).

Nath, A. and Dey, R. (2020). "Robust guaranteed-cost output feedback control of blood glucose in type 1 diabetes patient with intrapatient variability". In: *Optimal Control Applications and Methods* June 2018, pp. 1–17. ISSN: 10991514. DOI: 10.1002/oca.2607 (cit. on p. 22).

Nguyen, N. P. and Hong, S. K. (2018). "Sliding Mode Thau Observer for Actuator Fault Diagnosis of Quadcopter UAVs". In: *Applied Sciences* 8.10, p. 1893. ISSN: 2076-3417. DOI: 10.3390/app8101893 (cit. on p. 75).

Notkin, G. T.; Kristensen, P. L.; Pedersen-Bjergaard, U.; Jensen, A. K., and Molsted, S. (2021). "Reproducibility of glucose fluctuations induced by moderate intensity cycling exercise in persons with type 1 diabetes". In: *Journal of Diabetes Research* 2021. ISSN: 23146753. DOI: 10.1155/2021/6640600 (cit. on p. 177).

Obeid, H.; Fridman, L.; Laghrouche, S.; Harmouche, M., and Golkani, M. A. (2018). "Adaptation of Levant's differentiator based on barrier function". In: *International Journal of Control* 91.9, pp. 2019–2027. ISSN: 0020-7179. DOI: 10.1080/00207179.2017.1406149 (cit. on p. 123).

Olcomendy, L.; Pirog, A.; Bornat, Y.; Cieslak, J.; Gucik-Derigny, D.; Henry, D.; Catargi, B., and Renaud, S. (2020). "Tuning of an Artificial Pancreas Controller: An in silico methodology based on clinically-relevant criteria". In: *Proceedings of the Annual International Conference of the IEEE Engineering in Medicine and Biology Society, EMBS* 2020-July, pp. 2544–2547. ISSN: 1557170X. DOI: 10.1109/EMBC44109.2020.9175292 (cit. on p. 159).

Orban, J.-C.; Van Obberghen, E., and Ichai, C. (2018). "Acute Complications of Diabetes". In: *Metabolic Disorders and Critically Ill Patients*. Cham: Springer International Publishing. Chap. 15, pp. 341–363. DOI: 10.1007/978-3-319-64010-5_15 (cit. on pp. 3, 4).

Orchard, T. J.; Nathan, D. M.; Zinman, B.; Cleary, P.; Brillon, D.; Backlund, J.-Y. C., and Lachin, J. M. (2015). "Association Between 7 Years of Intensive Treatment of Type 1 Diabetes and Long-term Mortality". In: *JAMA* 313.1, p. 45. ISSN: 0098-7484. DOI: 10.1001/jama.2014.16107 (cit. on p. 4).

Orozco-Lopez, J. O.; Castaneda, C. E.; Rodriguez-Herrero, A.; Garcia-Saez, G., and Hernando, E. (2018). "Linear Time-Varying Luenberger Observer Applied to Diabetes". In: *IEEE Access* 6, pp. 23612–23625. ISSN: 21693536. DOI: 10.1109/ACCESS.2018.2825989 (cit. on p. 52).

Palerm, C. C. (2011). "Physiologic insulin delivery with insulin feedback: A control systems perspective". In: *Computer Methods and Programs in Biomedicine* 102.2, pp. 130–137. ISSN: 01692607. DOI: 10.1016/j.cmpb.2010.06.007 (cit. on pp. 24, 195, 196).

Palisaitis, E.; El Fathi, A.; Oettingen, J. E. von; Haidar, A., and Legault, L. (2021). "A Meal Detection Algorithm for the Artificial Pancreas: A Randomized Controlled Clinical Trial in Adolescents With Type 1 Diabetes". In: *Diabetes Care* 44.2, pp. 604–606. ISSN: 0149-5992. DOI: 10.2337/dc20-1232 (cit. on pp. 20, 21).

Paoletti, N.; Liu, K. S.; Chen, H.; Smolka, S. A., and Lin, S. (2020). "Data-Driven Robust Control for a Closed-Loop Artificial Pancreas". In: *IEEE/ACM Transactions on Computational Biology and Bioinformatics* 17.6, pp. 1981–1993. ISSN: 15579964. DOI: 10.1109/TCBB.2019.2912609 (cit. on pp. 23, 24, 34).

Patek, S. D.; Breton, M. D.; Chen, Y.; Solomon, C., and Kovatchev, B. (2007). "Linear quadratic gaussian-based closed-loop control of type 1 diabetes". In: *Journal of Diabetes Science and Technology* 1 (6), pp. 834–841. ISSN: 19322968. DOI: 10.1177/193229680700100606 (cit. on p. 71).

Patel, N. S.; Name, M. A. V.; Cengiz, E.; Carria, L. R.; Tichy, E. M.; Weyman, K.; Weinzimer, S. A.; Tamborlane, W. V., and Sherr, J. L. (2016). "Mitigating Reductions in Glucose During Exercise on Closed-Loop Insulin Delivery: The Ex-Snacks Study". In: *Diabetes Technology & Therapeutics* 18.12, pp. 794–799. DOI: 10.1089/dia.2016.0311 (cit. on pp. 36, 147).

Pease, A.; Lo, C.; Earnest, A.; Kiriakova, V.; Liew, D., and Zoungas, S. (2020). "Time in range for multiple technologies in type 1 diabetes: A systematic review and network meta-analysis". In: *Diabetes Care* 43.8, pp. 1967–1975. ISSN: 19355548. DOI: 10.2337/dc19-1785 (cit. on p. 5).

Peng, C.; Zhang, Z.; Zou, J.; Li, K., and Zhang, J. (2013). "Internal model based robust inversion feedforward and feedback 2DOF control for LPV system with disturbance". In: *Journal of Process Control* 23.10, pp. 1415–1425. ISSN: 09591524. DOI: 10.1016/j.jprocont.2013.09.004 (cit. on p. 148).

Pereda, D. de; Romero-Vivo, S.; Ricarte, B.; Rossetti, P.; Ampudia-Blasco, F. J., and Bondia, J. (2016). "Real-time estimation of plasma insulin concentration from continuous glucose monitor measurements". In: *Computer Methods in Biomechanics and Biomedical Engineering* 19 (9), pp. 934–942. ISSN: 1025-5842. DOI: 10.1080/10255842.2015.1077234 (cit. on p. 71).

Peters, T. M. and Haidar, A. (2018). "Dual-hormone artificial pancreas: benefits and limitations compared with single-hormone systems". In: *Diabetic Medicine* 35.4, pp. 450–459. ISSN: 1464-5491. DOI: 10.1111/DME.13581 (cit. on p. 30).

Phillip, M.; Nimri, R.; Bergenstal, R. M.; Barnard-Kelly, K.; Danne, T.; Hovorka, R.; Kovatchev, B. P.; Messer, L. H.; Parkin, C. G.; Ambler-Osborn, L.; Amiel, S. A.; Bally, L.; Beck, R. W.; Biester, S.; Biester, T.; Blanchette, J. E.; Bosi, E.; Boughton, C. K.; Breton, M. D.; Brown, S. A.; Buckingham, B. A.; Cai, A.; Carlson, A. L.; Castle, J. R.; Choudhary, P.; Close, K. L.; Cobelli, C.; Criego, A. B.; Davis, E.; Beaufort, C. de; Bock, M. I. de; DeSalvo, D. J.; DeVries, J. H.; Dovc, K.; Doyle, F. J.; Ekhlaspour, L.; Shvalb, N. F.; Forlenza, G. P.; Gallen, G.; Garg, S. K.; Gershenoff, D. C.; Gonder-Frederick, L. A.; Haidar, A.; Hartnell, S.; Heinemann, L.; Heller, S.; Hirsch, I. B.; Hood, K. K.; Isaacs, D.; Klonoff, D. C.; Kordonouri, O.; Kowalski, A.; Laffel, L.; Lawton, J.; Lal, R. A.; Leelarathna, L.; Maahs, D. M.; Murphy, H. R.; Nørgaard, K.; O'Neal, D.; Oser, S.; Oser, T.; Renard, E.; Riddell, M. C.; Rodbard, D.; Russell, S. J.; Schatz, D. A.; Shah, V. N.; Sherr, J. L.; Simonson, G. D.; Wadwa, R. P.; Ward, C.; Weinzimer, S. A.; Wilmot, E. G., and Battelino, T. (2022). "Consensus Recommendations for the Use of Automated Insulin Delivery (AID) Technologies in Clinical Practice". In: *Endocrine Reviews*. ISSN: 0163-769X. DOI: 10.1210/ENDREV/BNAC022 (cit. on pp. 6, 9, 10).

Pintaudi, B.; Gironi, I.; Riccardo, N.; Meneghini, E.; Disoteo, O.; Mion, E., and Bertuzzi, F. (2022). "Minimed Medtronic 780G optimizes glucose control in patients with type 1 diabetes mellitus". In: *Nutrition, Metabolism and Cardiovascular Diseases*. ISSN: 09394753. DOI: 10.1016/j.numecd.2022.03.031 (cit. on p. 5).

Polonsky, W. H.; Hood, K. K.; Levy, C. J.; MacLeish, S. A.; Hirsch, I. B.; Brown, S. A.; Bode, B. W.; Carlson, A. L.; Shah, V. N.; Weinstock, R. S.; Bhargava, A.; Jones, T. C.; Aleppo, G.; Mehta, S. N.; Laffel, L. M.; Forlenza, G. P.; Sherr, J. L.; Huyett, L. M.; Vienneau, T. E., and Ly, T. T. (2022). "How introduction of automated insulin delivery systems may influence psychosocial outcomes in adults with type 1 diabetes: Findings from the first investigation with the Omnipod® 5 System". In: *Diabetes Research and Clinical Practice* 190, p. 109998. ISSN: 0168-8227. DOI: 10.1016/J.DIABRES.2022.109998 (cit. on p. 5).

Qu, S.; Xia, X., and Zhang, J. (2014). "Dynamical behaviors of an euler discretized sliding mode control systems". In: *IEEE Transactions on Automatic Control* 59.9, pp. 2525–2529. ISSN: 00189286. DOI: 10.1109/TAC.2014.2308620 (cit. on p. 75).

Quirk, H.; Blake, H.; Dee, B., and Glazebrook, C. (2014). ""you can't just jump on a bike and go": A qualitative study exploring parents' perceptions of physical activity in children with type 1 diabetes". In: *BMC Pediatrics* 14.1, pp. 1–12. ISSN: 14712431. DOI: 10.1186/S12887-014-0313-4/PEER-REVIEW (cit. on p. 11).

Quirós, C.; Bertachi, A.; Giménez, M.; Biagi, L.; Viaplana, J.; Viñals, C.; Vehí, J.; Conget, I., and Bondia, J. (2018). "Control de la glucemia durante el ejercicio físico aeróbico y anaeróbico mediante un nuevo sistema de páncreas artificial [Blood Glucose Monitoring during Aerobic and Anaerobic Physical Exercise Using a New Artificial Pancreas System]". In: *Endocrinología, Diabetes y Nutrición* 65.6, pp. 342–347. ISSN: 25300164. DOI: 10.1016/j.endinu.2017.12.012 (cit. on pp. 90, 91, 94, 194).

R Core Team (2021). *R: A Language and Environment for Statistical Computing*. R Foundation for Statistical Computing. Vienna, Austria (cit. on pp. 84, 162, 167).

Rahman, S. A.; Merck, C.; Huang, Y., and Kleinberg, S. (2015). "Unintrusive Eating Recognition using Google Glass". In: ICST, pp. 108–111. ISBN: 978-1-63190-045-7. DOI: 10.4108/icst.pervasivehealth.2015.259044 (cit. on p. 104).

Ramkissoon, C.; Herrero, P.; Bondia, J., and Vehi, J. (2018). "Unannounced Meals in the Artificial Pancreas: Detection Using Continuous Glucose Monitoring". In: *Sensors* 18.3, p. 884. ISSN: 1424-8220. DOI: 10.3390/s18030884 (cit. on pp. 20, 40, 104, 112, 113).

Ramkissoon, C. M.; Bertachi, A.; Beneyto, A.; Bondia, J., and Vehi, J. (2019). "Detection and Control of Unannounced Exercise in the Artificial Pancreas without Additional Physiological Signals". In: *IEEE Journal of Biomedical and Health Informatics* 2194.c, pp. 1–1. ISSN: 2168-2194. DOI: 10.1109/JBHI.2019.2898558 (cit. on pp. 7, 31, 52, 155, 165, 173, 194).

Ranjan, A. G.; Schmidt, S., and Nørgaard, K. (2021). "Glucagon for hypoglycaemia treatment in type 1 diabetes". In: *Diabetes/Metabolism Research and Reviews* 37.5, e3409. ISSN: 1520-7552. DOI: 10.1002/dmrr.3409 (cit. on pp. 30, 36).

Rasmussen, O. (1993). "Day-to-day variation of the glycemic response in subjects with insulin-dependent diabetes with standardized premeal blood glucose and prandial insulin concentrations". In: *The American Journal of Clinical Nutrition* 57.6, pp. 908–911. ISSN: 0002-9165. DOI: 10.1093/ajcn/57.6.908 (cit. on p. 13).

Reiterer, F. and Freckmann, G. (2019). "Advanced carbohydrate counting: An engineering perspective". In: *Annual Reviews in Control* 48, pp. 401–422. ISSN: 13675788. DOI: 10.1016/j.arcontrol.2019.06.003 (cit. on pp. 3, 134, 140, 162).

Renard, E.; Costalat, G.; Chevassus, H., and Bringer, J. (2006). "Artificial beta-cell: clinical experience toward an implantable closed-loop insulin delivery system". In: *Diabetes & metabolism* 32.5 Pt 2, pp. 497–502. ISSN: 1262-3636. DOI: 10.1016/S1262-3636(06)72802-6 (cit. on p. 26).

Renard, E. (2008). "Insulin Delivery Route for the Artificial Pancreas: Subcutaneous, Intraperitoneal, or Intravenous? Pros and Cons". In: *Journal of Diabetes Science and Technology* 2 (4), pp. 735–738. ISSN: 1932-2968. DOI: 10.1177/193229680800200429 (cit. on p. 3).

Renard, E.; Farret, A., and Place, J. (2019). "Use of intraperitoneal insulin delivery for artificial pancreas". In: *The Artificial Pancreas*. Elsevier, pp. 105–121. ISBN: 9780128156551. DOI: 10.1016/B978-0-12-815655-1.00014-4 (cit. on p. 26).

Renukuntla, V. S.; Ramchandani, N.; Trast, J.; Cantwell, M., and Heptulla, R. A. (2014). "Role of glucagon-like peptide-1 analogue versus amylin as an adjuvant therapy in type 1 diabetes in a closed loop setting with ePID algorithm". In: *Journal of diabetes science and technology* 8.5, pp. 1011–1017. ISSN: 1932-2968. DOI: 10.1177/1932296814542153 (cit. on pp. 27–29).

Resalat, N.; El Youssef, J.; Reddy, R., and Jacobs, P. G. (2016). "Design of a dual-hormone model predictive control for artificial pancreas with exercise model". In: *2016 38th Annual International Conference of the IEEE Engineering in Medicine and Biology Society (EMBC)*. IEEE, pp. 2270–2273. ISBN: 978-1-4577-0220-4. DOI: 10.1109/EMBC.2016.7591182 (cit. on pp. 33, 35, 52).

Revert, A.; Garelli, F.; Pico, J.; De Battista, H.; Rossetti, P.; Vehi, J., and Bondia, J. (2013). "Safety Auxiliary Feedback Element for the Artificial Pancreas in Type 1 Diabetes". In: *IEEE Transactions on Biomedical Engineering* 60.8, pp. 2113–2122. ISSN: 0018-9294. DOI: 10.1109/TBME.2013.2247602 (cit. on pp. 24, 90, 148, 193, 196).

Riddell, M. C.; Gallen, I. W.; Smart, C. E.; Taplin, C. E.; Adolfsson, P.; Lumb, A. N.; Kowalski, A.; Rabasa-Lhoret, R.; McCrimmon, R. J.; Hume, C.; Annan, F.; Fournier, P. A.; Graham, C.; Bode, B.; Galassetti, P.; Jones, T. W.; Millán, I. S.; Heise, T.; Peters, A. L.; Petz, A., and Laffel, L. M. (2017). "Exercise management in type 1 diabetes: a consensus statement". In: *The Lancet Diabetes & Endocrinology* 5.5, pp. 377–390. ISSN: 22138587. DOI: 10.1016/S2213-8587(17)30014-1 (cit. on pp. 6, 13, 31).

Rodríguez-Sarmiento, D. L.; León-Vargas, F., and García-Jaramillo, M. (2022). "Artificial pancreas systems: experiences from concept to commercialisation". In: *Expert Review of Medical Devices* 19 (11), pp. 877–894. ISSN: 1743-4440. DOI: 10.1080/17434440.2022.2150546 (cit. on pp. 9, 22).

Rose, A. J. and Richter, E. A. (2005). "Skeletal muscle glucose uptake during exercise: How is it regulated?" In: *Physiology* 4, pp. 260–270. ISSN: 15489213. DOI: 10.1152/physiol.00012.2005 (cit. on p. 13).

Rossetti, P.; Ampudia-Blasco, F. J.; Laguna, A.; Revert, A.; Vehì, J.; Ascaso, J. F., and Bondia, J. (2012). "Evaluation of a novel continuous glucose monitoring-based method for mealtime insulin dosing-The iBolus-In subjects with type 1 diabetes using continuous subcutaneous insulin infusion therapy: A randomized controlled trial". In: *Diabetes Technology and Therapeutics* 14.11, pp. 1043–1052. ISSN: 15209156. DOI: 10.1089/dia.2012.0145 (cit. on pp. 89, 90).

Rossetti, P.; Quirós, C.; Moscardó, V.; Comas, A.; Giménez, M.; Ampudia-Blasco, F. J.; León, F.; Montaser, E.; Conget, I.; Bondia, J., and Vehí, J. (2017). "Closed-Loop Control of Postprandial Glycemia Using an Insulin-on-Board Limitation Through Continuous Action on Glucose Target". In: *Diabetes Technology & Therapeutics* 19.6, pp. 355–362. ISSN: 1520-9156. DOI: 10.1089/dia.2016.0443 (cit. on p. 193).

Roversi, C.; Vettoretti, M.; Del Favero, S.; Facchinetti, A., and Sparacino, G. (2020). "Modeling Carbohydrate Counting Error in Type 1 Diabetes Management". In: *Diabetes Technology & Therapeutics* 22.10, pp. 749–759. ISSN: 1520-9156. DOI: 10.1089/dia.2019.0502 (cit. on p. 10).

Roversi, C.; Vettoretti, M.; Favero, S. D.; Facchinetti, A.; Choudhary, P., and Sparacino, G. (2022). "Impact of Carbohydrate Counting Error on Glycemic Control in Open-Loop Management of Type 1 Diabetes: Quantitative Assessment Through an In Silico Trial". In: *Journal of Diabetes Science and Technology* 16 (6), pp. 1541–1549. ISSN: 1932-2968. DOI: 10.1177/19322968211012392 (cit. on p. 130).

Roy, A.; Grosman, B.; Miller, D.; Engel, T.; Cohen, O.; Shalit, R.; Shalem, S.; Hirsh, M. L.; Cohen, Y., and Tirosh, A. (2022). "287-OR: Eliminating Manual Meal Bolusing: A Feasibility Trial Using MiniMed 780G and Hand Gesture Algorithms". In: *Diabetes* 71.Supplement_1. ISSN: 0012-1797. DOI: 10.2337/DB22-287-OR (cit. on p. 20).

Ruegemer, J. J.; Squires, R. W.; Marsh, H. M.; Haymond, M. W.; Cryer, P. E.; Rizza, R. A., and Miles, J. M. (1990). "Differences Between Prebreakfast and Late Afternoon Glycemic Responses to Exercise in IDDM Patients". In: *Diabetes Care* 13.2, pp. 104–110. ISSN: 0149-5992. DOI: 10.2337/DIACARE.13.2.104 (cit. on p. 177).

Ruiz, J. L.; Sherr, J. L.; Cengiz, E.; Carria, L.; Roy, A.; Voskanyan, G.; Tamborlane, W. V., and Weinzimer, S. A. (2012). "Effect of insulin feedback on closed-loop glucose control: A crossover study". In: *Journal of Diabetes Science and Technology* 6.5, pp. 1123–1130. ISSN: 19322968. DOI: 10.1177/193229681200600517 (cit. on p. 148).

Russell, S. J.; Beck, R. W.; Damiano, E. R.; El-Khatib, F. H.; Ruedy, K. J.; Balliro, C. A.; Li, Z.; Calhoun, P.; Wadwa, R. P.; Buckingham, B.; Zhou, K.; Daniels, M.; Raskin, P.; White, P. C.; Lynch, J.; Pettus, J.; Hirsch, I. B.; Goland, R.; Buse, J. B.; Kruger, D.; Mauras, N.; Muir, A.; McGill, J. B.; Cogen, F.; Weissberg-Benchell, J.; Sherwood, J. S.; Castellanos, L. E.; Hillard, M. A.; Tuffaha, M.; Putman, M. S.; Sands, M. Y.; Forlenza, G.; Slover, R.; Messer, L. H.; Cobry, E.; Shah, V. N.; Polsky, S.; Lal, R.; Ekhlaspour, L.; Hughes, M. S.; Basina, M.; Hatipoglu, B.; Olansky, L.; Bhangoo, A.; Forghani, N.; Kashmiri, H.; Sutton, F.; Choudhary, A.; Penn, J.; Jafri, R.; Rayas, M.; Escaname, E.; Kerr, C.; Favela-Prezas, R.; Boeder, S.; Trikudanathan, S.; Williams, K. M.; Leibel, N.; Kirkman, M. S.; Bergamo, K.; Klein, K. R.; Dostou, J. M.; Machineni, S.; Young, L. A.; Diner, J. C.; Bhan, A.; Jones, J. K.; Benson, M.; Bird, K.; Englert, K.; Permuy, J.; Cossen, K.; Felner, E.; Salam, M.; Silverstein, J. M.; Adamson, S.; Cedeno, A.; Meighan, S., and Dauber, A. (2022). "Multicenter, Randomized Trial of a Bionic Pancreas in Type 1 Diabetes". In: *New England Journal of Medicine* 387.13, pp. 1161–1172. ISSN: 0028-4793. DOI: 10.1056/NEJMoa2205225 (cit. on p. 18).

Russell, S. J.; Jafri, R.; Sherwood, J. S.; Balliro, C. A.; Hillard, M. A.; Ekhlaspour, L.; Hsu, L.; Buckingham, B.; El-Khatib, F. H., and Damiano, E. R. (2020). "302 / Abstract ID 890. Use of the ultra-rapid insulin fiasp in the iLet bionic pancreas". In: *Diabetes Technology*

& Therapeutics. The Official Journal of ATTD Advanced Technologies & Treatments for Diabetes Conference Madrid, Spain—February 19–22, 2020. Vol. 22. S1, A–1–A–250. DOI: 10.1089/dia.2020.2525.abstracts (cit. on pp. 18, 25).

Russell, S. J.; El-Khatib, F. H.; Nathan, D. M.; Magyar, K. L.; Jiang, J., and Damiano, E. R. (2012). "Blood Glucose Control in Type 1 Diabetes With a Bihormonal Bionic Endocrine Pancreas". In: *Diabetes Care* 35.11, pp. 2148–2155. ISSN: 0149-5992. DOI: 10.2337/DC12-0071 (cit. on pp. 18, 35).

Russell, S. J.; El-Khatib, F. H.; Sinha, M.; Magyar, K. L.; McKeon, K.; Goergen, L. G.; Balliro, C.; Hillard, M. A.; Nathan, D. M., and Damiano, E. R. (2014). "Outpatient Glycemic Control with a Bionic Pancreas in Type 1 Diabetes". In: *New England Journal of Medicine* 371.4, pp. 313–325. ISSN: 0028-4793. DOI: 10.1056/NEJMOA1314474/SUPPL_FILE/NEJMOA1314474_DISCLOSURES.PDF (cit. on p. 18).

Samadi, S.; Rashid, M.; Turksoy, K.; Feng, J.; Hajizadeh, I.; Hobbs, N.; Lazaro, C.; Sevil, M.; Littlejohn, E., and Cinar, A. (2018). "Automatic Detection and Estimation of Unannounced Meals for Multivariable Artificial Pancreas System". In: *Diabetes Technology & Therapeutics* 20.3, pp. 235–246. ISSN: 1520-9156. DOI: 10.1089/dia.2017.0364 (cit. on p. 104).

Samadi, S.; Turksoy, K.; Hajizadeh, I.; Feng, J.; Sevil, M., and Cinar, A. (2017). "Meal Detection and Carbohydrate Estimation Using Continuous Glucose Sensor Data". In: *IEEE Journal of Biomedical and Health Informatics* 21.3, pp. 619–627. ISSN: 21682194. DOI: 10.1109/JBHI.2017.2677953 (cit. on pp. 19–21, 130).

Sánchez-Peña, R.; Colmegna, P.; Garelli, F.; De Battista, H.; García-Violini, D.; Moscoso-Vásquez, M.; Rosales, N.; Fushimi, E.; Campos-Náñez, E.; Breton, M.; Beruto, V.; Scibona, P.; Rodriguez, C.; Giunta, J.; Simonovich, V.; Belloso, W. H.; Cherñavvsky, D., and Grosembacher, L. (2018). "Artificial Pancreas: Clinical Study in Latin America Without Premeal Insulin Boluses". In: *Journal of Diabetes Science and Technology* 12.5, p. 914. ISSN: 19322968. DOI: 10.1177/1932296818786488 (cit. on p. 19).

Sanz, R.; Garcia, P.; Fridman, E., and Albertos, P. (2018). "Rejection of mismatched disturbances for systems with input delay via a predictive extended state observer". In: *International Journal of Robust and Nonlinear Control* 28.6, pp. 2457–2467. ISSN: 10991239. DOI: 10.1002/rnc.4027 (cit. on p. 46).

Sanz, R.; Garcia, P.; Díez, J. L., and Bondia, J. (2020). "Artificial Pancreas System With Unannounced Meals Based on a Disturbance Observer and Feedforward Compensation". In: *IEEE Transactions on Control Systems Technology*, pp. 1–7. ISSN: 1063-6536. DOI: 10.1109/TCST.2020.2975147 (cit. on pp. 22, 24, 40).

Sawaryn, B.; Klaassen, M.; Beijnum, B. J. van; Zwart, H., and Veltink, P. H. (2021). "Identification of Movements and Postures Using Wearable Sensors for Implementation in a Bi-Hormonal Artificial Pancreas System". In: *Sensors* 21.17, p. 5954. ISSN: 1424-8220. DOI: 10.3390/S21175954 (cit. on p. 33).

Schiavon, M.; Man, C. D.; Kudva, Y. C.; Basu, A., and Cobelli, C. (2013). "In Silico Optimization of Basal Insulin Infusion Rate during Exercise: Implication for Artificial Pancreas". In: *Journal of Diabetes Science and Technology* 7.6, pp. 1461–1469. ISSN: 1932-2968. DOI: 10.1177/193229681300700606 (cit. on pp. 156, 164).

Scott, S.; Kempf, P.; Bally, L., and Stettler, C. (2019). "Carbohydrate intake in the context of exercise in people with type 1 diabetes". In: *Nutrients* 11.12, pp. 1–21. ISSN: 20726643. DOI: 10.3390/nu11123017 (cit. on p. 147).

Seetharaman, R.; Pawar, S., and Advani, M. (2022). "One hundred years since insulin discovery: An update on current and future perspectives for pharmacotherapy of diabetes mellitus". In: *British Journal of Clinical Pharmacology* 88.4, pp. 1598–1612. ISSN: 0306-5251. DOI: 10.1111/bcp.15100 (cit. on pp. 3, 29).

Sevil, M.; Rashid, M.; Askari, M. R.; Maloney, Z.; Hajizadeh, I., and Cinar, A. (2020). "Detection and Characterization of Physical Activity and Psychological Stress from Wristband Data". In: *Signals* 1.2, pp. 188–208. ISSN: 2624-6120. DOI: 10.3390/signals1020011 (cit. on p. 33).

Sharma, A. K.; Taneja, G.; Kumar, A.; Sahu, M.; Sharma, G.; Kumar, A.; Sardana, S., and Deep, A. (2019). "Insulin analogs: Glimpse on contemporary facts and future prospective". In: *Life Sciences* 219, pp. 90–99. ISSN: 0024-3205. DOI: 10.1016/J.LFS.2019.01.011 (cit. on p. 12).

Sherr, J. L.; Patel, N. S.; Michaud, C. I.; Palau-Collazo, M. M.; Van Name, M. A.; Tamborlane, W. V.; Cengiz, E.; Carria, L. R.; Tichy, E. M., and Weinzimer, S. A. (2016). "Mitigating Meal-Related Glycemic Excursions in an Insulin-Sparing Manner During Closed-Loop Insulin Delivery: The Beneficial Effects of Adjunctive Pramlintide and Liraglutide". In: *Diabetes Care* 39.7, p. 1127. ISSN: 19355548. DOI: 10.2337/DC16-0089 (cit. on p. 27).

Shi, D.; Dassau, E., and Doyle, F. J. (2019). "Adaptive Zone Model Predictive Control of Artificial Pancreas Based on Glucose- and Velocity-Dependent Control Penalties". In: *IEEE Transactions on Biomedical Engineering* 66.4, pp. 1045–1054. ISSN: 0018-9294. DOI: 10.1109/TBME.2018.2866392 (cit. on pp. 22, 24, 33).

Shtessel, Y.; Edwards, C.; Fridman, L., and Levant, A. (2014). *Sliding Mode Control and Observation*. Control Engineering. New York, NY: Springer New York, pp. 1–356. ISBN: 978-0-8176-4892-3. DOI: 10.1007/978-0-8176-4893-0 (cit. on pp. 46, 47, 49, 75, 106, 123).

Silva, J. D.; Lepore, G.; Battelino, T.; Arrieta, A.; Castañeda, J.; Grossman, B.; Shin, J., and Cohen, O. (2022). "Real-World Performance of the MiniMed™ 780G System: First Report of Outcomes from 4120 Users". In: *Diabetes Technology & Therapeutics* 24.2, pp. 113–119. ISSN: 1520-9156. DOI: 10.1089/dia.2021.0203 (cit. on p. 5).

Simon, D. (2006). *Optimal state estimation: Kalman, H_∞, and nonlinear approaches*, pp. 1–526. ISBN: 9780470045343. DOI: 10.1002/0470045345 (cit. on pp. 44, 45, 120).

Sira-Ramírez, H. and Spurgeon, S. K. (1994). "On the robust design of sliding observers for linear systems". In: *Systems & Control Letters* 23.1, pp. 9–14. ISSN: 01676911. DOI: 10.1016/0167-6911(94)90076-0 (cit. on p. 46).

Slotine, J. J. and Sastry, S. S. (1983). "Tracking control of non-linear systems using sliding surfaces, with application to robot manipulators". In: *International Journal of Control* 38.2, pp. 465–492. ISSN: 0020-7179. DOI: 10.1080/00207178308933088 (cit. on p. 76).

Soylu, S. and Danisman, K. (2018). "In silico testing of optimized Fuzzy P+D controller for artificial pancreas". In: *Biocybernetics and Biomedical Engineering* 38.2, pp. 399–408. ISSN: 0208-5216. DOI: 10.1016/J.BBE.2018.02.009 (cit. on p. 22).

Staal, O. M.; Salid, S.; Fougner, A. L., and Stavdahl, O. (2019). "Meal estimation from Continuous Glucose Monitor data using Kalman filtering and hypothesis testing". In: *2019 IEEE 58th Conference on Decision and Control (CDC)*. Vol. 2019-Decem. Cdc. IEEE, pp. 5654–5661. ISBN: 978-1-7281-1398-2. DOI: 10.1109/CDC40024.2019.9028912 (cit. on p. 19).

Steil, G. M.; Panteleon, A. E., and Rebrin, K. (2004). "Closed-loop insulin delivery—the path to physiological glucose control". In: *Advanced Drug Delivery Reviews* 56.2, pp. 125–144. ISSN: 0169-409X. DOI: 10.1016/J.ADDR.2003.08.011 (cit. on p. 26).

Steil, G. M.; Palerm, C. C.; Kurtz, N.; Voskanyan, G.; Roy, A.; Paz, S., and Kandeel, F. R. (2011). "The effect of insulin feedback on closed loop glucose control". In: *Journal of Clinical Endocrinology and Metabolism* 96.5, pp. 1402–1408. ISSN: 0021972X. DOI: 10.1210/jc.2010-2578 (cit. on p. 24).

Stocker, D.; Kanderian, S.; Cortina, G.; Nitzan, T.; Plummer, J.; Steil, G. M., and Mastrototaro, J. (2006). *Virtual patient software system for educating and treating individuals with diabetes* (cit. on p. 51).

Szablewski, L. (2017). "Glucose Homeostasis". In: *Gluconeogenesis*. InTech. ISBN: 978-953-51-3324-7. DOI: 10.5772/67222 (cit. on p. 2).

Szalay, P.; Molnar, A.; Muller, M.; Eigner, G.; Rudas, I.; Benyó, Z., and Kovács, L. (2014). "Comparison of Sigma-Point Filters for State Estimation of Diabetes Models". In: vol. 2014. DOI: 10.1109/smc.2014.6974298 (cit. on p. 68).

Tagougui, S.; Taleb, N.; Molvau, J.; Nguyen, É.; Raffray, M., and Rabasa-Lhoret, R. (2019). "Artificial Pancreas Systems and Physical Activity in Patients with Type 1 Diabetes: Challenges, Adopted Approaches, and Future Perspectives". In: *Journal of Diabetes Science and Technology* August, p. 193229681986931. ISSN: 1932-2968. DOI: 10.1177/1932296819869310 (cit. on pp. 6, 15, 31, 35, 36, 90, 147).

Tašić, J.; Takács, M., and Kovács, L. (2022). "Control Engineering Methods for Blood Glucose Levels Regulation". In: *Acta Polytechnica Hungarica* 19.7, pp. 127–152. ISSN: 17858860 (cit. on p. 5).

Teff, K. L. (2011). "How neural mediation of anticipatory and compensatory insulin release helps us tolerate food". In: *Physiology and Behavior* 103.1, pp. 44–50. ISSN: 00319384. DOI: 10.1016/j.physbeh.2011.01.012 (cit. on p. 11).

Thabit, H.; Lal, R., and Leelarathna, L. (2021). "Automated insulin dosing systems: Advances after a century of insulin". In: *Diabetic Medicine* July, pp. 1–10. ISSN: 14645491. DOI: 10.1111/dme.14695 (cit. on pp. 6, 11).

The Diabetes Control and Complications Trial Research Group (1993). "The Effect of Intensive Treatment of Diabetes on the Development and Progression of Long-Term Complications in Insulin-Dependent Diabetes Mellitus". In: *New England Journal of Medicine* 329.14, pp. 977–986. ISSN: 0028-4793. DOI: 10.1056/NEJM199309303291401 (cit. on p. 4).

Thomas, A. and Heinemann, L. (2021). "Algorithms for Automated Insulin Delivery: An Overview". In: *Journal of Diabetes Science and Technology*, p. 193229682110084. ISSN: 1932-2968. DOI: 10.1177/19322968211008442 (cit. on pp. 5, 12).

Toffanin, C.; Messori, M.; Palma, F. D.; Nicolao, G. D.; Cobelli, C., and Magni, L. (2013). "Artificial pancreas: Model predictive control design from clinical experience". In: *Journal of Diabetes Science and Technology* 7 (6), pp. 1470–1483. ISSN: 19322968. DOI: 10.1177/193229681300700607 (cit. on p. 71).

Tornese, G.; Carletti, C.; Giangreco, M.; Nisticò, D.; Faleschini, E., and Barbi, E. (2022). "Carbohydrate Tolerance Threshold for Unannounced Snacks in Children and Adolescents With Type 1 Diabetes Using an Advanced Hybrid Closed-Loop System". In: *Diabetes Care* 45 (6), pp. 1486–1488. ISSN: 0149-5992. DOI: 10.2337/DC21-2643 (cit. on p. 125).

Tsoukas, M. A.; Cohen, E.; Legault, L.; Oettingen, J. E. von; Yale, J. F.; Vallis, M.; Odabassian, M.; El Fathi, A.; Rutkowski, J.; Jafar, A.; Ghanbari, M.; Gouchie-Provencher, N.; René,

J.; Palisaitis, E., and Haidar, A. (2021a). "Alleviating carbohydrate counting with a FiASP-plus-pramlintide closed-loop delivery system (artificial pancreas): Feasibility and pilot studies". In: *Diabetes, Obesity and Metabolism* 23.9, pp. 2090–2098. ISSN: 1463-1326. DOI: 10.1111/DOM.14447 (cit. on pp. 28, 130).

Tsoukas, M. A.; Majdpour, D.; Yale, J.-F.; Fathi, A. E.; Garfield, N.; Rutkowski, J.; Rene, J.; Legault, L., and Haidar, A. (2021b). "A fully artificial pancreas versus a hybrid artificial pancreas for type 1 diabetes: a single-centre, open-label, randomised controlled, crossover, non-inferiority trial". In: *The Lancet Digital Health* 3.11, e723–e732. ISSN: 25897500. DOI: 10.1016/S2589-7500(21)00139-4 (cit. on pp. 25, 28).

Tukey, J. W. (1949). "Comparing Individual Means in the Analysis of Variance". In: *Biometrics* 5.2, p. 99. ISSN: 0006341X. DOI: 10.2307/3001913 (cit. on p. 84).

Turksoy, K.; Bayrak, E. S.; Quinn, L.; Littlejohn, E., and Cinar, A. (2013). "Multivariable Adaptive Closed-Loop Control of an Artificial Pancreas Without Meal and Activity Announcement". In: *Diabetes Technology & Therapeutics* 15 (5), pp. 386–400. ISSN: 1520-9156. DOI: 10.1089/dia.2012.0283 (cit. on p. 33).

Turksoy, K. and Cinar, A. (2015). "Real-Time Insulin Bolusing for Unannounced Meals Using CGM Measurements". In: *IFAC-PapersOnLine*. Vol. 48. 20. Elsevier, pp. 219–224. DOI: 10.1016/J.IFACOL.2015.10.142 (cit. on pp. 20, 130).

Turksoy, K.; Hajizadeh, I.; Hobbs, N.; Kilkus, J.; Littlejohn, E.; Samadi, S.; Feng, J.; Sevil, M.; Lazaro, C.; Ritthaler, J.; Hibner, B.; Devine, N.; Quinn, L., and Cinar, A. (2018). "Multivariable Artificial Pancreas for Various Exercise Types and Intensities". In: *Diabetes Technology & Therapeutics* 20 (10), pp. 662–671. ISSN: 1520-9156. DOI: 10.1089/dia.2018.0072 (cit. on p. 37).

Turksoy, K.; Hajizadeh, I.; Samadi, S.; Feng, J.; Sevil, M.; Park, M.; Quinn, L.; Littlejohn, E., and Cinar, A. (2017). "Real-time insulin bolusing for unannounced meals with artificial pancreas". In: *Control Engineering Practice* 59, pp. 159–164. ISSN: 0967-0661. DOI: 10.1016/J.CONENGPRAC.2016.08.001 (cit. on p. 21).

Turksoy, K.; Kilkus, J.; Hajizadeh, I.; Samadi, S.; Feng, J.; Sevil, M.; Lazaro, C.; Frantz, N.; Littlejohn, E., and Cinar, A. (2016a). "Hypoglycemia Detection and Carbohydrate Suggestion in an Artificial Pancreas". In: *Journal of Diabetes Science and Technology* 10.6, pp. 1236–1244. ISSN: 19322968. DOI: 10.1177/1932296816658666 (cit. on p. 36).

Turksoy, K.; Quinn, L.; Littlejohn, E., and Cinar, A. (2014). "Multivariable adaptive identification and control for artificial pancreas systems". In: *IEEE Transactions on Biomedical Engineering* 61.3, pp. 883–891. ISSN: 00189294. DOI: 10.1109/TBME.2013.2291777 (cit. on p. 148).

Turksoy, K.; Samadi, S.; Feng, J.; Littlejohn, E.; Quinn, L., and Cinar, A. (2016b). "Meal Detection in Patients With Type 1 Diabetes: A New Module for the Multivariable Adaptive Artificial Pancreas Control System". In: *IEEE Journal of Biomedical and Health Informatics* 20.1, pp. 47–54. ISSN: 2168-2194. DOI: 10.1109/JBHI.2015.2446413 (cit. on p. 20).

Ullah, N. and Muhammad, A. S. (2020). "Novel algebraic meal disturbance estimation based adaptive robust control design for blood glucose regulation in type 1 diabetes patients". In: *IET Systems Biology* 14.4, pp. 200–210. ISSN: 17518849. DOI: 10.1049/iet-syb.2020.0002 (cit. on p. 40).

Utkin, V. and Lee, H. (2006). "Chattering Problem in Sliding Mode Control Systems". In: *IFAC Proceedings Volumes* 39.5, p. 1. ISSN: 14746670. DOI: 10.3182/20060607-3-IT-3902.00003 (cit. on p. 75).

Van Bon, A. C.; Jonker, L. D.; Koebrugge, R.; Koops, R.; Hoekstra, J. B., and DeVries, J. H. (2012). "Feasibility of a bihormonal closed-loop system to control postexercise and postprandial glucose excursions". In: *Journal of Diabetes Science and Technology* 6.5, pp. 1114–1122. ISSN: 19322968. DOI: 10.1177/193229681200600516 (cit. on p. 31).

Van Bon, A. C.; Luijf, Y. M.; Koebrugge, R.; Koops, R.; Hoekstra, J. B., and Devries, J. H. (2014). "Feasibility of a Portable Bihormonal Closed-Loop System to Control Glucose Excursions at Home Under Free-Living Conditions for 48 Hours". In: *Diabetes Technology & Therapeutics* 16.3, p. 131. ISSN: 15209156. DOI: 10.1089/DIA.2013.0166 (cit. on p. 35).

Van Heusden, K.; Dassau, E.; Zisser, H. C.; Seborg, D. E., and Doyle, F. J. (2012). "Control-relevant models for glucose control using a priori patient characteristics". In: *IEEE Transactions on Biomedical Engineering* 59.7, pp. 1839–1849. ISSN: 00189294. DOI: 10.1109/TBME.2011.2176939 (cit. on p. 131).

Varimo, T.; Pulkkinen, M.-A.; Hakonen, E.; Hero, M.; Miettinen, P. J., and Tuomaala, A.-K. (2021). "First year on commercial hybrid closed-loop system—experience on 111 children and adolescents with type 1 diabetes". In: *Pediatric Diabetes* 22.6, pp. 909–915. ISSN: 1399-543X. DOI: 10.1111/pedi.13235 (cit. on p. 5).

Veluvolu, K. C. and Chai, S. Y. (2009). "High gain observers with multiple sliding mode for state and unknown input estimations". In: *2009 4th IEEE Conference on Industrial Electronics and Applications, ICIEA 2009* 56.9, pp. 1179–1186. ISSN: 02780046. DOI: 10.1109/ICIEA.2009.5138381 (cit. on p. 50).

Venkatasubramanian, V.; Rengaswamy, R.; Yin, K., and Kavuri, S. N. (2003). "A review of process fault detection and diagnosis". In: *Computers & Chemical Engineering* 27 (3), pp. 293–311. ISSN: 00981354. DOI: 10.1016/S0098-1354(02)00160-6 (cit. on p. 105).

Vetrani, C.; Calabrese, I.; Cavagnuolo, L.; Pacella, D.; Napolano, E.; Di Rienzo, S.; Riccardi, G.; Rivellese, A. A.; Annuzzi, G., and Bozzetto, L. (2022). "Dietary determinants of postprandial blood glucose control in adults with type 1 diabetes on a hybrid closed-loop system". In: *Diabetologia* 65.1, pp. 79–87. ISSN: 14320428. DOI: 10.1007/s00125-021-05587-0 (cit. on p. 10).

Vettoretti, M.; Facchinetti, A.; Sparacino, G., and Cobelli, C. (2018). "Type-1 diabetes patient decision simulator for in silico testing safety and effectiveness of insulin treatments". In: *IEEE Transactions on Biomedical Engineering* 65.6, pp. 1281–1290. ISSN: 15582531. DOI: 10.1109/TBME.2017.2746340 (cit. on pp. 111, 126).

Villa-Tamayo, M. F.; García-Jaramillo, M.; León-Vargas, F., and Rivadeneira, P. S. (2022). "Interval Safety Layer Coupled With an Impulsive MPC for Artificial Pancreas to Handle Intrapatient Variability". In: *Frontiers in Endocrinology* 13.February, pp. 1–13. DOI: 10.3389/fendo.2022.796521 (cit. on p. 148).

Villaverde, A. F.; Barreiro, A., and Papachristodoulou, A. (2016). "Structural Identifiability Analysis via Extended Observability and Decomposition". In: *IFAC-PapersOnLine* 49.26, pp. 171–177. ISSN: 24058963. DOI: 10.1016/j.ifacol.2016.12.121 (cit. on p. 57).

Villeneuve, E.; Lachal, S.; Desir, C.; Benhamou, P.-Y.; Franc, S.; Charpentier, G.; Huneker, E., and Doron, M. (2020). "Increasing the safety of unannounced meal detection for artificial pancreas closed-loop with patient's hourly meal schedule". In: *2020 42nd Annual International Conference of the IEEE Engineering in Medicine & Biology Society (EMBC)*. IEEE, pp. 5093–5096. ISBN: 978-1-7281-1990-8. DOI: 10.1109/EMBC44109.2020.9176470 (cit. on pp. 19, 20, 123).

Viñals, C.; Beneyto, A.; Martín-SanJosé, J.-F.; Furió-Novejarque, C.; Bertachi, A.; Bondia, J.; Vehi, J.; Conget, I., and Giménez, M. (2021). "Artificial Pancreas With Carbohydrate Suggestion Performance for Unannounced and Announced Exercise in Type 1 Diabetes". In: *The Journal of Clinical Endocrinology & Metabolism* 106.1, pp. 55–63. ISSN: 0021-972X. DOI: 10.1210/clinem/dgaa562 (cit. on pp. 7, 37, 148, 194).

Virk, S. A.; Donaghue, K. C.; Cho, Y. H.; Benitez-Aguirre, P.; Hing, S.; Pryke, A.; Chan, A., and Craig, M. E. (2016). "Association Between HbA 1c Variability and Risk of Microvascular Complications in Adolescents With Type 1 Diabetes". In: *The Journal of Clinical Endocrinology & Metabolism* 101.9, pp. 3257–3263. ISSN: 0021-972X. DOI: 10.1210/jc.2015-3604 (cit. on p. 4).

Vrančić, D. and Huba, M. (2021). "Improving Disturbance-Rejection by Using Disturbance Estimator". In: *Control Based on PID Framework - The Mutual Promotion of Control and Identification for Complex Systems*. IntechOpen, p. 13. DOI: 10.5772/intechopen.95615 (cit. on pp. 148, 150).

Walcott, B. L. and Zak, S. H. (1988). "Combined Observer-Controller Synthesis for Uncertain Dynamical Systems with Applications". In: *IEEE Transactions on Systems, Man and Cybernetics* 18.1, pp. 88–104. ISSN: 21682909. DOI: 10.1109/21.87057 (cit. on p. 47).

Walter, E. and Lecourtier, Y. (1982). "Global approaches to identifiability testing for linear and nonlinear state space models". In: *Mathematics and Computers in Simulation* 24.6, pp. 472–482. ISSN: 03784754. DOI: 10.1016/0378-4754(82)90645-0 (cit. on p. 56).

Wang, B.; Brogliato, B.; Acary, V.; Boubakir, A., and Plestan, F. (2015). "Experimental Comparisons Between Implicit and Explicit Implementations of Discrete-Time Sliding Mode Controllers: Toward Input and Output Chattering Suppression". In: *IEEE Transactions on Control Systems Technology* 23.5, pp. 2071–2075. ISSN: 1063-6536. DOI: 10.1109/TCST.2015.2396473 (cit. on p. 75).

Wang, B.; Yu, X.; Wang, L., and Zhang, Z. (2011). "Periodic behaviors in sampled-data sliding mode based observers". In: *Proceedings of the 30th Chinese Control Conference, CCC 2011*, pp. 2544–2548 (cit. on p. 75).

Wang, Y.; Dassau, E.; Zisser, H.; Jovanovič, L., and Doyle, F. J. (2010). "Automatic Bolus and Adaptive Basal Algorithm for the Artificial Pancreatic β-Cell". In: *https://home.liebertpub.com/dia* 12.11, pp. 879–887. ISSN: 15209156. DOI: 10.1089/DIA.2010.0029 (cit. on p. 20).

Weimer, J.; Chen, S.; Peleckis, A.; Rickels, M. R., and Lee, I. (2016). "Physiology-Invariant Meal Detection for Type 1 Diabetes". In: *Diabetes Technology & Therapeutics* 18.10, pp. 616–624. ISSN: 15578593. DOI: 10.1089/dia.2015.0266 (cit. on pp. 19, 20, 124, 126).

Weinzimer, S. A.; Sherr, J. L.; Cengiz, E.; Kim, G.; Ruiz, J. L.; Carria, L.; Voskanyan, G.; Roy, A., and Tamborlane, W. V. (2012). "Effect of pramlintide on prandial glycemic excursions during closed-loop control in adolescents and young adults with type 1 diabetes". In: *Diabetes care* 35.10, pp. 1994–1999. ISSN: 1935-5548. DOI: 10.2337/DC12-0330 (cit. on p. 27).

Weinzimer, S. A.; Steil, G. M.; Swan, K. L.; Dziura, J.; Kurtz, N., and Tamborlane, W. V. (2008). "Fully Automated Closed-Loop Insulin Delivery Versus Semiautomated Hybrid Control in Pediatric Patients With Type 1 Diabetes Using an Artificial Pancreas". In: *Diabetes Care* 31.5, pp. 934–939. ISSN: 0149-5992 (cit. on pp. 3, 6, 10, 130).

Wendt, S. L.; Møller, J. K.; Knudsen, C. B.; Madsen, H.; Haidar, A., and Jørgensen, J. B. (2016). *PK / PD modelling of glucose-insulin-glucagon dynamics in healthy dogs after a subcutaneous bolus administration of native glucagon or a novel glucagon analogue*. Tech. rep. 2. Technical University of Denmark (cit. on p. 52).

Wilinska, M. E.; Chassin, L. J.; Acerini, C. L.; Allen, J. M.; Dunger, D. B., and Hovorka, R. (2010). "Simulation Environment to Evaluate Closed-Loop Insulin Delivery Systems

in Type 1 Diabetes". In: *Journal of Diabetes Science and Technology* 4.1, pp. 132–144. ISSN: 1932-2968. DOI: 10.1177/193229681000400117 (cit. on p. 52).

Wilson, L. M.; Jacobs, P. G.; Ramsey, K. L.; Resalat, N.; Reddy, R.; Branigan, D.; Leitschuh, J.; Gabo, V.; Guillot, F.; Senf, B.; El Youssef, J.; Steineck, I. I. K.; Tyler, N. S., and Castle, J. R. (2020). "Dual-Hormone Closed-Loop System Using a Liquid Stable Glucagon Formulation Versus Insulin-Only Closed-Loop System Compared With a Predictive Low Glucose Suspend System: An Open-Label, Outpatient, Single-Center, Crossover, Randomized Controlled Trial". In: *Diabetes Care* 43.11, pp. 2721–2729. ISSN: 0149-5992. DOI: 10.2337/DC19-2267 (cit. on p. 35).

Wilson, M. L.; Davies, I. G.; Waraksa, W.; Khayyatzadeh, S. S.; Al-Asmakh, M., and Mazidi, M. (2021). "The Impact of Microbial Composition on Postprandial Glycaemia and Lipidaemia: A Systematic Review of Current Evidence". In: *Nutrients* 13.11, p. 3887. ISSN: 2072-6643. DOI: 10.3390/nu13113887 (cit. on p. 13).

Witczak, M.; Puig, V.; Rotondo, D., and Witczak, P. (2017). "A necessary and sufficient condition for total observability of discrete-time linear time-varying systems". In: *IFAC-PapersOnLine* 50 (1), pp. 729–734. ISSN: 24058963. DOI: 10.1016/j.ifacol.2017.08.232 (cit. on p. 70).

Xie, J. and Wang, Q. (2016). "Meal Detection and Meal Size Estimation for Type 1 Diabetes Treatment: A Variable State Dimension Approach". In: *ASME 2015 Dynamic Systems and Control Conference, DSCC 2015* 1. DOI: 10.1115/DSCC2015-9905 (cit. on p. 20).

— (2017). "A variable state dimension approach to meal detection and meal size estimation: In silico evaluation through basal-bolus insulin therapy for type 1 diabetes". In: *IEEE Transactions on Biomedical Engineering* 64.6, pp. 1249–1260. ISSN: 15582531. DOI: 10.1109/TBME.2016.2599073 (cit. on pp. 20, 113, 130).

Xiong, X.; Kikuuwe, R.; Kamal, S., and Jin, S. (2020). "Implicit-Euler Implementation of Super-Twisting Observer and Twisting Controller for Second-Order Systems". In: *IEEE Transactions on Circuits and Systems II: Express Briefs* 67 (11), pp. 2607–2611. ISSN: 1549-7747. DOI: 10.1109/TCSII.2019.2957271 (cit. on pp. 116, 118).

Xu, J. and Song, R. (2021). "Meal estimation based on UKF and postprandial glucose control for patients with type I diabetes". In: IEEE, pp. 6827–6832. ISBN: 978-1-6654-2647-3. DOI: 10.1109/CAC53003.2021.9727766 (cit. on pp. 19, 71).

Yan, X. G. and Edwards, C. (2007). "Nonlinear robust fault reconstruction and estimation using a sliding mode observer". In: *Automatica* 43.9, pp. 1605–1614. ISSN: 00051098. DOI: 10.1016/j.automatica.2007.02.008 (cit. on pp. 46, 47, 49, 75).

Yapanis, M.; James, S.; Craig, M. E.; O'Neal, D., and Ekinci, E. I. (2022). "Complications of Diabetes and Metrics of Glycemic Management Derived From Continuous Glucose Monitoring". In: *The Journal of Clinical Endocrinology & Metabolism* XX, pp. 1–16. ISSN: 0021-972X. DOI: 10.1210/CLINEM/DGAC034 (cit. on p. 5).

Yu, X. (2006). "Complex Discretization Behaviors of a Simple Sliding-Mode Control System". In: *IEEE Transactions on Circuits and Systems II: Express Briefs* 53.8, pp. 652–656. ISSN: 15583791. DOI: 10.1109/TCSII.2006.875377 (cit. on p. 75).

Zaharieva, D. P.; McGaugh, S.; Pooni, R.; Vienneau, T.; Ly, T., and Riddell, M. C. (2019). "Improved open-loop glucose control with basal insulin reduction 90 minutes before aerobic exercise in patients with type 1 diabetes on continuous subcutaneous insulin infusion". In: *Diabetes Care* 42.5, pp. 824–831. ISSN: 19355548. DOI: 10.2337/dc18-2204 (cit. on pp. 13, 14, 35).

Zaharieva, D. P.; Messer, L. H.; Paldus, B.; O'Neal, D. N.; Maahs, D. M., and Riddell, M. C. (2020). "Glucose Control During Physical Activity and Exercise Using Closed Loop Technology in Adults and Adolescents with Type 1 Diabetes". In: *Canadian Journal of Diabetes* 44.8, pp. 740–749. ISSN: 1499-2671. DOI: 10.1016/J.JCJD.2020.06.003 (cit. on pp. 6, 11, 13, 147, 152, 156).

Zak, S. H.; Chakrabarty, A., and Buzzard, G. T. (2017). "Robust state and unknown input estimation for nonlinear systems characterized by incremental multiplier matrices". In: *Proceedings of the American Control Conference*, pp. 3270–3275. ISSN: 07431619. DOI: 10.23919/ACC.2017.7963451 (cit. on p. 50).

Zeng, B.; Jia, H.; Gao, L.; Yang, Q.; Yu, K., and Sun, F. (2022). "Dual-hormone artificial pancreas for glucose control in type 1 diabetes: a meta-analysis". In: *Diabetes, Obesity and Metabolism*. ISSN: 1462-8902. DOI: 10.1111/dom.14781 (cit. on p. 36).

Zhang, Q. and Zhang, L. (2021). "Stability analysis of the Kalman predictor". In: *International Journal of Control* 94.5, pp. 1217–1224. ISSN: 0020-7179. DOI: 10.1080/00207179.2019.1638971 (cit. on pp. 46, 70).

Zheng, F.; Bonnet, S.; Villeneuve, E.; Doron, M.; Lepecq, A., and Forbes, F. (2020). "Unannounced Meal Detection for Artificial Pancreas Systems Using Extended Isolation Forest". In: *2020 42nd Annual International Conference of the IEEE Engineering in Medicine & Biology Society (EMBC)*. IEEE, pp. 5892–5895. ISBN: 978-1-7281-1990-8. DOI: 10.1109/EMBC44109.2020.9176856 (cit. on pp. 21, 51, 104).

Zheng, M.; Ni, B., and Kleinberg, S. (2019). "Automated meal detection from continuous glucose monitor data through simulation and explanation". In: *Journal of the American Medical Informatics Association* 26.12, pp. 1592–1599. ISSN: 1527974X. DOI: 10.1093/jamia/ocz159 (cit. on pp. 19, 20, 104).